Durham E-Theses

Palaeobiogeography of Crossbills (Loxia spp.) and their Food Plants

HOLLIDAY, PHYLLIDA,RACHEL

How to cite:

Use policy

Palaeobiogeography of Crossbills (*Loxia spp.*) and their Food Plants

Phyllida Rachel Holliday

Masters by Research

School of Biological and Biomedical Sciences

Durham University

2011

Illustrations of the Scottish Crossbill, *Loxia scotica* (left) and Parrot Crossbill, *Loxia pytyopsittacus* (right), created by P. R. Holliday.

Palaeobiogeography of Crossbills (*Loxia spp.*) and their Food Plants

Phyllida Rachel Holliday

Abstract

Crossbills (*Loxia* spp.) are members of the finch family (Fringillidae) and have a primarily granivorous diet, feeding on the seeds of conifers, specifically members of the family Pinaceae. Studies of the five extant crossbill species are abundant due to the distinctive evolution of their crossed mandibles, specifically adapted for a coniferous seed diet.   Many have attempted to understand their evolutionary origins and speciation but the complexity of *Loxia*'s phylogeography and movement patterns have made it difficult to gain an accurate understanding.   Although many hypotheses have been proposed, substantial evidence has yet to be found.

This study aims investigates the palaeobiogeography of the five species of crossbill, as well as their specific food trees, in order to better understand their past movements and the impacts of these on the evolutionary history of the genus.   By combining several different techniques of climate-based niche modelling with global palaeoclimatic simulations, potential ranges of crossbills and their food plants have been simulated for the last 120 thousand years.   These simulations have also been compared to available crossbill fossil records, pollen data and other palaeovegetation models.

The results indicate that significant species' specific population range shifts are likely to have occurred in response to climatic change throughout this period. The simulations have provided valuable insight into the evolution of *Loxia* taxa, particularly isolated island populations or races, supporting existing evolutionary theories in addition to introducing novel hypotheses.

Table of Contents

List of Tables

List of Figures

List of Figures cont.

List of Figures cont.

Chapter 4 – Discussion & Conclusions

List of Figures cont.

BLANK PAGE

Abbreviations

AET/PET	Annual ratio of actual to potential evapotranspiration
ANPP	Above-ground net primary productivity
AUC	Area under curve
B.P.	Before present
CRS	Climatic response surface
EPD	European pollen database
GAM	Generalised additive model
GDD5	Growing degree days above 5°C
K yr	Thousand years ago
LGM	Last glacial maximum
Maxent	Maximum entropy
MTCO	Mean temperature of the coldest month
Spp.	Species

Acknowledgements

Firstly I would like thank my supervisor, Prof. Brian Huntley; whose patience, support, encouragement and expertise were invaluable in the successful completion of this study.

Special thanks to Birdlife International for granting me permission to use their *Loxia* distribution data, particularly Stuart Butchart who dealt with all my queries and to Dr Aljos Farjon of the Royal Botanic Gardens, Kew, for providing me with a plethora of conifer distributions.   Without this data this study would not have been possible.

During this study, I was part of the Adaptation and Environment research group, many members of which provided me with much support and sacrificed their own time in helping me conduct this investigation.   Dr. Yvonne Collingham, particularly, provided much expertise and help in modelling and mapping, doing model runs for robustness and producing CRS plots.   Dr Judy Allen was a great support, particularly in helping me produce posters which have supplemented this research, sorting out computer glitches and also providing me with the ANPP data used in this thesis.   Dr Sean Twiss, Dr Robert Bagchi and Dr Steven Hancock also provided further help with GIS and modelling techniques.

A special mention for Dr Alan Knox as his paper "The Sympatric Breeding of Common and Scottish Crossbills *Loxia curvirostra* and *L. scotica* and the Evolution of crossbills" inspired this thesis and he has also been kind enough to answer many of my further queries.   I was lucky to also have the input of several crossbill experts including Prof. Craig Benkman and Dr Ron Summers, who were always willing to answer my questions and helped me develop my understanding of the fascinating *Loxia* genus.

Evaluating the sparse fossil record of the *Loxia* genus was a difficult task which was made much easier by the helpful contributions from Dr John Stewart, Dr Steve Emslie and Prof. Janusz Kozlowski.

On top of the tremendous amount of academic support I had, I was also lucky to be part of the supportive pastoral community of Collingwood College, Durham University.   I would like to thank particularly Nicky, Sarah, Suzy, Mike, Becky, Adam and Charlie for providing respite when the 'birds weren't behaving', help, patience and generally keeping me sane.

Lastly I would like to thank my parents, Nick and Marlene Holliday, who not only funded my quest for the 'Origins of the Scottish Crossbill', which I will forever be grateful for, but also sacrificed a dining room table, delayed Christmas and had a few sleepless nights to see its successful completion.   Without their love, support and encouragement this work could not have been completed.

CHAPTER 1

Palaeobiogeography of Crossbills (*Loxia* spp.) and their Food Plants

Crossbills (*Loxia* spp.) are members of the finch family (Fringillidae) and have a primarily granivorous diet, feeding on the cone-crop of conifers, specifically members of the family Pinaceae. *Loxia* has five extant species. Members of the genus are characterised by their crossed mandibles adapted for their coniferous cone diet; these are used to extract seeds from both open and closed cones by separating the scales in order to access the enclosed seeds (Benkman, 1988). All crossbills are sexually dimorphic; the males are orange to red in plumage colouration while females and juveniles are grey to olive. They also display species specific markings and morphology.

Crossbill distribution is limited to the northern hemisphere; the southern extreme of populations is observed in *Loxia curvirostra* (Common Crossbill) in Nicaragua, Vietnam and the Philippines (Fig. 1.1.1), while *L. leucoptera* (Two-Barred Crossbill) extends into the Northern Territories and Yukon in Canada and *L. pytyopsittacus* (Parrot Crossbill) breeds in the northern latitudes of Norway. In addition to these wide-spread crossbill species, there are two isolated island populations of *L. megaplaga* (Hispaniolan Crossbill) on the island of Hispaniola (Haiti and the Dominican Republic) and *L. scotica* (Scottish Crossbill) in the northern highlands of Scotland.

Studies of crossbills are abundant due to their distinctive evolution to utilise a specific food source and many have attempted to understand their evolutionary origins and speciation (Knox, 1990, Tyrberg, 1991). However, the complexity of *Loxia*'s phylogeography (Questiau *et al.*, 1999, Parchman *et al.*, 2006) and movement patterns (Marquiss & Rae, 1994) have made it difficult to gain an accurate understanding. Although many hypotheses have been proposed, substantial evidence to support these has yet to be found. This study aims to investigate the palaeobiogeography of the five distinct species of crossbill, as well as of their specific feeding trees, in order better to understand their past movements and potential impacts on the evolutionary history of the genus.

Section 1.1

Crossbill (*Loxia* genus) Range and Diet

Loxia curvirostra – Common Crossbill or Red Crossbill
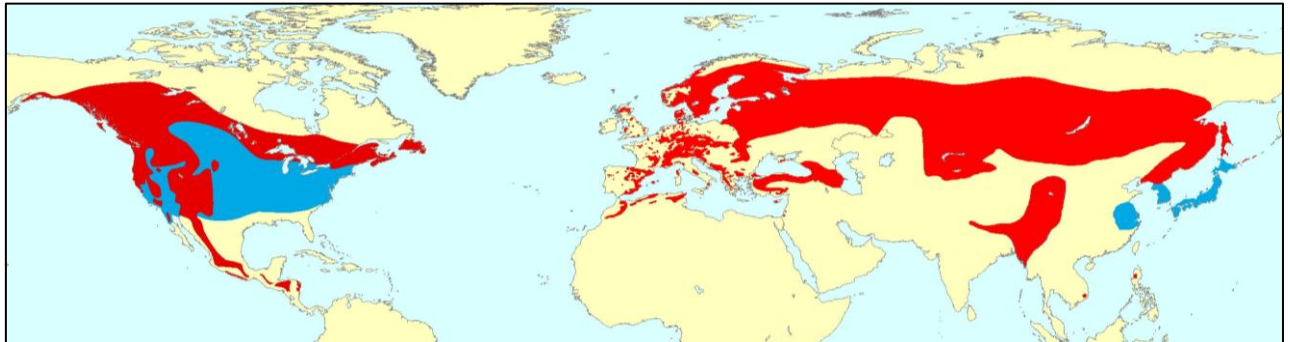
Figure 1.1.1:   Global distribution of *Loxia curvirostra*. Red – resident, Blue – non-breeding populations.
(Data provided by BirdLife International)

L. curvirostra, known as the Common Crossbill in Europe and the Red Crossbill in the Americas, due to the males' red colouration; is the most widespread and abundant of crossbill species, with estimates of between 30 and 100 million mature individuals globally (BirdLife International, 2010).   Its breeding range covers the west coast and northern states of the United States of America (USA) extending south into Mexico, Nicaragua and Guatemala (Fig. 1.1.1); non-breeding populations extend into the eastern states of the USA during the winter.   *L. curvirostra* populations are more sporadic across western and central Europe with records of resident birds also in North Africa (Payn, 1948, Smith, 1965).   Their breeding range covers most of southern Siberia, east to Japan and large areas of southern China, with isolated populations observed in the Philippines and Vietnam (Grant & Whitehead, 1898, Eames & Ericson, 1996).   There is sufficient isolation of many of the Common Crossbills' populations that they have been classified as subspecies (Table 1.1.1).

Table 1.1.1:   *Loxia curvirostra* (Common Crossbill) subspecies and distributions.

Subspecies	Distribution
L. c. curvirostra	Western, central & northern Europe from British Isles and Scandinavia, east through Siberia to eastern Russia (North Amurland), south to northern Spain, central Italy, Greece, Belarus, northern Ukraine, northern Kazakhstan, Sayan Mountains and northern Mongolia.
L. c. balearica	Central & southern Spain and Balearic Isles
L. c. corsicana	Corsica
L. c. poliogyna	Northeast Morocco, northern Algeria and northern Tunisia also (possibly this race) southern Italy and Sicily
L. c. guillemardi	Eastern Balkans, Turkey, Cyprus, southern Ukraine and Caucasus
L. c. japonica	Extreme south-eastern Russia (Ussuriland), Island of Sakhalin, southern Kuril Islands, northern & central Japan (Hokkaido, northern ,central & western Honshu), north-eastern & eastern China (Inner Mongolia and Heilongjiang south to Jiangsu) and North Korea; winters in south to eastern central China (southern Shaanxi and east to Jiangsu) and southern Japan

Table 1.1.1 cont.:   *Loxia curvirostra* (Common Crossbill) subspecies and distributions.

Subspecies	Distribution
L. c. altaiensis	North-eastern Kazakhstan, southern Russia (central & south Altai Mountains, Sayan Mountains and Tuva)
L. c. tianshanica	South-eastern Kazakhstan south to Tajikistan, and north-western China (north-western Xinjiang); winters to north-western & northern China
L. c. himalayensis	Himalayas from northern India (Himachal Pradesh) east to Bhutan, southern Tibetan Plateau (southern & eastern Xizang) and southern China (southern Qinghai and Gansu south to north-western Yunnan and western Sichuan); winters south to northern Myanmar
L. c. meridionalis	Southern Vietnam (southern Annam)
L. c. luzoniensis	Northern & western Luzon (Cordillera Mountains and Zambales Mountains) in northern Philippines
L. c. sitkensis	Southern & south-eastern Alaska, coastal western Canada and western USA (south to north-western California); winters to south to southern Canada and south-western USA
L. c. bendirei	South-western Canada (southern Yukon and central British Columbia east to south-western Saskatchewan) and north-western USA (south to Wyoming); winters south to southern USA
L. c. minor	South-eastern Canada (Ontario east to Nova Scotia) and north-eastern USA; winters south to east-central USA
L. c. pusilla	Eastern Canada (Newfoundland); winters south to north-eastern USA
L. c. benti	Central Rocky Mountains in west-central USA
L. c. grinnelli	California and Nevada in south-western USA; occasionally winters south to Arizona and north-western Mexico
L. c. stricklandi	Southern USA (Arizona and New Mexico) south to southern Mexico, possibly also Belize
L. c. mesamericana	Guatemala and Belize south to northern Nicaragua

Primarily, *L. curvirostra* is considered a specialist upon *Picea* (Spruce); however, it will readily take other conifer cones, especially because many *Picea* spp. fruit sporadically, leading to irregularities in food supply that mean other food sources must be used (Table. 1.1.2).   Sometimes the deficiency in food supply leads to whole populations of crossbills moving to new areas; these irruptive populations are often made up of fledglings and rarely breed in these new locations (Newton, 2006).   In North America, many Common Crossbills do not eat spruce at all, instead they have specialised upon particular *Pinus* species (Pine) (Siepielski & Benkman, 2004).   Similar feeding behaviours have been observed in Mediterranean subspecies, with *L. curvirostra balearica* specialising on *Pinus halepensis* (Aleppo Pine) (Mezquida & Benkman, 2005) and *L. curvirostra guillemardi* on *P. nigra* (Corsican/Austrian Pine) (Massa, 1987).

The North American population of *L. curvirostra* shows significant morphological variability, greater than that observed among most other passerine species, leading to early debate over whether morphologically divergent populations may be reproductively isolated (Monson & Phillips, 1981, Payne, 1987).   Early work conducted by Groth identified 9 different call-types of *L. curvirostra,* recognised by their distinctive vocalisations (Groth, 1993a in Benkman, 2003).   Studies of mate selection in relation to vocalisation and morphology

11

Table 1.1.2: Feeding tree species of *Loxia curvirostra* and subspecies.
Red indicates non-native introduced species to the region.

Species	Feeding Trees	Location	References
Loxia curvirostra	*Larix spp.*	The Netherlands	(Edelaar *et al.*, 2008)
	L. decidua *L. kaempferi*	Deeside, NE Scotland	(Marquiss & Rae, 1994)
	Picea abies	Scotland	(Marquiss & Rae, 1994, Summers & Buckland, 2010)
		Finland	(Watson *et al.*, 2009)
	Picea rubens	-	(Parchman *et al.*, 2006)
	Picea sitchensis	Deeside, NE Scotland The Netherlands	(Marquiss & Rae, 1994) (Edelaar *et al.*, 2008)
	Pinus contorta latifolia	Deeside, NE Scotland Idaho, USA - Colorado, USA The Netherlands	(Marquiss & Rae, 1994) (Benkman, 2003, Benkman *et al.*, 2005) (Parchman *et al.*, 2006) (Benkman, 2007) (Edelaar *et al.*, 2008)
	Pinus ponderosa scopulorum	Idaho, USA - Colorado, USA	(Benkman, 2003) (Parchman *et al.*, 2006) (Benkman, 2007)
	Pinus sylvestris	Deeside, NE Scotland The Netherlands	(Marquiss & Rae, 1994) (Edelaar & Terpstra, 2004, Edelaar *et al.*, 2008)
	Pseudotsuga menziesii menziesii	Deeside, NE Scotland Idaho, USA The Netherlands - Colorado, USA	(Marquiss & Rae, 1994) (Benkman, 2003) (Edelaar & Terpstra, 2004, Edelaar *et al.*, 2008) (Parchman *et al.*, 2006) (Benkman, 2007)
	Tsuga heterophylla	Idaho, USA - Colorado, USA	(Benkman, 2003) (Parchman *et al.*, 2006) (Benkman, 2007)
L. c. balearica	*Pinus halepensis*	Spain & Balearic Islands	(Edelaar *et al.*, 2003, Mezquida & Benkman, 2005, Alonso *et al.*, 2006)
L. c. himalayensis	*Larix griffithiana* *Larix otaninii* *Picea asperata* *Picea brachytyla* *Picea likiangensis* *Picea smithiana* *Picea spinulosa* *Pinus yunnanensis* *Tsuga chinensis* *Tsuga forrestii*	North-eastern India, Nepal, Bhutan, southern Tibet, south-western China	(Edelaar, 2008)
L. c. luzoniensis	*Pinus kesiya*	Vietnam	(Clouet & Goar, 1999)
L. c. meridionalis	*Pinus kesiya*	Philippines	(Clouet & Goar, 2001)
L. c. percna	*Picea mariana*	Newfoundland	(Benkman, 1989b, Parchman & Benkman, 2002)
L. c. tianshanica	*Pinus schrenkiana*	Central Asia	(Edelaar *et al.*, 2003)

among North American *L. curvirostra* in the Appalachian Mountains were consistent with the hypothesis that the distinctive forms of crossbill observed are reproductively isolated

(Groth, 1993b).   If treated as separate taxa, the conservation status would be of greater concern because of the individual populations' reliance on specific feeding trees and their relative isolation (Benkman, 1993).   With this in mind, studies continue in North America in particular by Benkman's research group, and several more subspecies have been found to be reproductively isolated; species status has been proposed for the population in Idaho (Benkman *et al.*, 2009).   Despite the ever growing argument for the recognition of these distinct populations as true species, the American Ornithologists' Union has, to date, not recognised them as such and so in this study they will be consider a single species.

Even though *L. curvirostra* has a vast range, research has primarily been focused in Europe and North America, with little known about Asian populations.   One study conducted on *L. c. luzoniensis*, the isolated population on the Philippine main-island of Luzon, found that birds were smaller than those of the closest neighbouring population in Vietnam, *L. c. meridionalis*, although both utilise the same pine species, *Pinus kesiya* (Khasi Pine) (Clouet & Goar, 2001).   Interestingly, the morphology of *L. c. luzoniensis* is most similar to the Himalayan subspecies, *L. c. himalayensis*, and it was hypothesised that the Philippine subspecies had migrated from the Himalayas with the Quaternary expansion of *P. kesiya* into the Philippines.   In fact the Vietnamese subspecies has beak morphology more suitable for the hard coned *P. kesiya*; *L. c. luzoniensis*' slender bill can only access open cones so it has altered its feeding behaviour, eating other seeds and even insects, yet another indication of the adaptability of *L. curvirostra* and the complexity of its history.

Figure 1.1.2:   Distribution of *Loxia leucoptera*.   Red – resident, Blue – non-breeding populations.   (Data provided by BirdLife International)

Loxia leucoptera – Two-Barred Crossbill or White-Winged Crossbill

The smallest of the crossbills, its common names are derived from the distinctive two white wing-panels all individuals of the species possess.   *L. leucoptera* has a slender, weaker mandible which limits its distribution to softer cones, primarily feeding on *Larix*, (Larch) (Cramp *et al.*, 1995) especially in Russia (Danilov *et al.*, 1984), although it will also consume *Picea* in Fennoscandia (Pulliainen, 1972) and America (Parchman *et al.*, 2006, Parchman *et*

Table 1.1.3:   Feeding tree species of *Loxia leucoptera*.

Species	Feeding Trees	Location	References
Loxia leucoptera	*Abies spp.*	-	(Harrison & Fisher, 1982)
	Larix spp.	Russia	(Danilov *et al.*, 1984, Cramp *et al.*, 1995)
	Picea abies	Fennoscandia	(Pulliainen, 1972)
	Picea engelmannii	Colorado, USA	(Benkman, 2007)
	Picea mariana	North America	(Parchman *et al.*, 2006, Parchman *et al.*, 2007)

al., 2007) (Table 1.1.3).   In depth studies on the feeding efficiency of crossbills have shown that *L. leucoptera*'s thin mandible is highly efficient at extracting seeds from the thin and short cone scales of larch and spruce (Benkman, 1987, 1989a).

Loxia leucoptera has an almost circum-polar distribution, with two subspecies (Table 1.1.4), one that extends throughout Canada and the northern USA and the other across Siberia; however, it is not found in Fennoscandia (Fig. 1.1.2).   Although it has successfully bred in central Europe, this is very rare (Fischer *et al.*, 1992).   All crossbills are restricted to the northern hemisphere due to their dietary reliance on conifers but, similar to *L. pytyopsittacus*, Two-Barred Crossbills have failed to colonise forests where food plants are abundant, especially in southern European mountainous regions.   *L. leucoptera*'s habitat selection has been suggested to be further restricted by climate; its northern distribution shows correlation with occupation of areas between July isotherms of 13-20°C (Voous, 1960, Cramp *et al.*, 1995).   Despite this limitation in distribution, *L. leucoptera*'s breeding grounds have been estimated to cover 15.7 million km^2 with 40 million adult birds occupying this area (BirdLife International, 2010).

Table 1.1.4:   *Loxia leucoptera* (Two-Barred Crossbill) subspecies and distributions.

Subspecies	Distribution
L. l. bifasciata	Eastern Finland, north-western & northern Russia (Kola Peninsula east in broad band through Siberia to Sea of Okhotsk, south to the central Urals, Baikal area, Yablonovy Mountains and western Amurland), probably also extreme north-eastern China (northern Heilongjiang); winters also southern to north-eastern Europe (irregular), north-eastern China (Liaoning & Hebei) and southern Siberia
L. l. leucoptera	Alaska and central & southern Canada east to central & eastern Quebec, Newfoundland and Nova Scotia, south into USA to northern Washington, western Wisconsin and southern Maine; in winter also south to southern Minnesota, northern Ohio, Pennysylvania and Massachusetts

Loxia pytyopsittacus – **Parrot Crossbill**
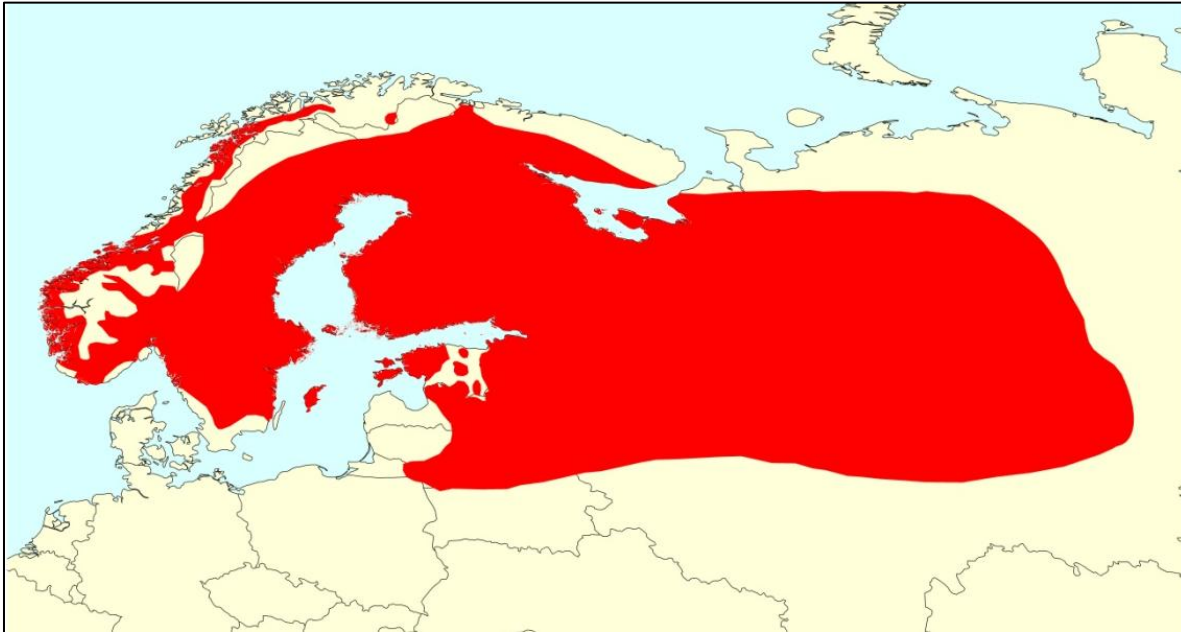
Figure 1.1.3:   Distribution of *Loxia pytyopsittacus* (Data provided by BirdLife International)

The Parrot Crossbill, the largest of the crossbills, possesses a deep bill which is the least crossed, giving it a parrot-beak appearance (Cramp *et al.*, 1995). *L. pytyopsittacus* is distributed in the boreal north-west Palaearctic (Fig. 1.1.3), with 95% of the estimated 780,000 to 3,300,000 mature individuals residing in Europe (BirdLife International, 2010). It is highly specialised to feed on pine, specifically *Pinus sylvestris* (Scots Pine) (Table. 1.1.5), its strong bill enabling it to access seeds even when the cones are closed. Research on this species is deficient primarily due to the difficulties in distinguishing it from *L. curvirostra* in the field; its limited distribution in north-western Eurasia thus has yet to be explained.   Competition between Parrot Crossbill and *L. leucoptera* to the east may account for the truncation observed, however there are extensive boreal pine forests lacking any competitor *Loxia* spp. that remain unoccupied (Newton, 1972).

Table 1.1.5: Feeding tree species of *Loxia pytyopsittacus* and *L. scotica*.
Red indicates non-native introduced species to the region.

Species	**Feeding Trees**	**Location**	**References**
Loxia pytyopsittacus	*Pinus sylvestris*	Scotland	(Summers & Buckland, 2010)
		Finland	(Watson *et al.*, 2009)
L. scotica	*Pinus sylvestris*	Scotland	(Marquiss & Rae, 1994, Summers & Buckland, 2010)
	Picea abies *Picea sitchensis* *Pinus contorta* *Pseudotsuga menziesii* *Larix decidua* *Larix kaempferi*	Scotland	(Marquiss & Rae, 1994)

Loxia scotica – **Scottish Crossbill**

Scottish Crossbills are considered Britain's only endemic bird, having a highly restricted population in natural stands and plantations of *P. sylvestris* (Scots Pine), its primary food source in the Scottish Highlands (Table. 1.1.5, Fig. 1.1.4). The Scottish Crossbill's morphology resembles that of an intermediate between *L. pytyopsittacus* and *L. curvirostra*, with plumage most similar to the Common Crossbill (Cramp *et al.*, 1995). Up until recent times the population of *L. scotica* has been isolated from other species; however, over the last few centuries the creation of non-native conifer plantations have established populations of *L. curvirostra* (Marquiss & Rae, 1994, Summers *et al.*, 2010) and sporadic sightings and occasional breeding of *L. pytyopsittacus* (Summers, 2002, 2004). Despite the more recent proximity of these other species of crossbill in Scotland, studies have shown that *L. scotica* occupies a feeding niche between the two more widely found species, and will diversify its diet on to the softer coned spruces and larches when competition is present (Marquiss & Rae, 2002).

Assessing the population size of *L. scotica* has been complicated due to the close likeness of *Loxia* spp. as well the birds generally feeding in the upper canopy of the forest making identification more complex. In the 1970's the population was estimated at around 1,500 adult birds, while a 1988 estimate placed it at between 300-1,250

Figure 1.1.4: Distribution of *Loxia scotica* (Data provided from Birdlife International)

breeding pairs (BirdLife International, 2010). Identification has improved by using vocal recordings to distinguish between species (Summers *et al.*, 2002), and the estimate has now risen to 13,600 adult individuals (Summers & Buckland, 2010).

16

Loxia megaplaga – **Hispaniolan Crossbill**

The Hispaniolan Crossbill was declared a separate species in 2003 by the American Ornithologists' Union.   Prior to this it was considered a subspecies of *L. leucoptera*; however, its isolated location on Hispaniola, the island occupied by Haiti and the Dominican Republic (Fig. 1.1.5) (Latta *et al.*, 2002), far from any other White-winged population, justified its new classification (Benkman, 1994).   It is confined primarily to the mountainous regions of the island and sightings outside Hispaniola are rare.   Several birds were observed in Jamaica in the 1970's but since then there have been no new sightings (Dod, 1978, 1992). It is estimated there are between 600 and 3,375 mature individuals presently, covering a range of 3,600 km^2; its small population and risks of further habitat destruction have seen it placed on the IUCN Red list of endangered species (BirdLife International, 2010).

Akin to its closest relative *L. leucoptera*, *L. megaplaga* has white wing-bars and a slender bill. It feeds almost exclusively on the, *Pinus occidentalis* (Hispaniolan Pine) (Table. 1.1.6). In observations of the birds feeding conducted by Latta, 98% of observed birds were feeding on *P. occidentalis*; however, when cone
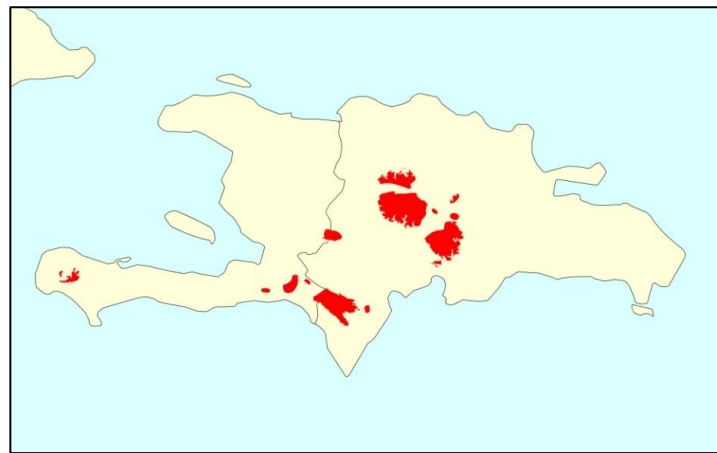
Figure 1.1.5:   Distribution of *Loxia megaplaga* (Data provided from Birdlife International)

crops are low it will feed on *Coocotrinax scoparia* (Palm Fruit) and *Arceuthobium bicarinatum* (Pine Mistletoe) (Latta *et al.*, 2000).   The cones of *P. occidentalis* are harder than *Larix* and *Picea*, the cones predated on by *Loxia leucoptera*.   This has resulted in a notable selection for larger bills in the Hispaniolan population, which are presently 25% deeper in the *L. megaplaga* and, in turn, populations of *Pinus occidentalis* have harder cones in the presence of the crossbills, an indication of a co-evolutionary process (Parchman *et al.*, 2007).

Table 1.1.6:   Feeding tree species of *Loxia megaplaga*.

Species	Feeding Trees	Location	References
L. megaplaga	*Pinus occidentalis*	Hispaniola	(Benkman, 1994, Latta *et al.*, 2000, Latta *et al.*, 2002, Parchman *et al.*, 2006, Parchman *et al.*, 2007)

Section 1.2

The Phylogenetics of the Crossbill

The progression in phylogenetics has been essential in defining evolutionary origin and relatedness of both extant and extinct species; it is therefore a good tool in attempting to understand the complex relations of the crossbills.   Within the finch family, *Loxia* spp. are observed to have very similar morphology and diet to *Pinicola enucleator* (Pine Grosbeak), both possessing strong bills and having a coniferous diet; however, genetic studies indicate that in fact crossbills are actually most closely related to the *Carduelis flammea* (Common Redpoll) and sister taxa (Arnaiz-Villena *et al.*, 2001).   Unfortunately, early studies indicated that phylogeography within *Loxia* spp. is far more complex, with very little genetic divergence observed between distinguished species (Piertney *et al.*, 1998, Piertney *et al.*, 2001) indicating a high amount of gene flow among species, which is not surprising due to nomadic and irruptive behaviour that crossbills exhibit (Questiau *et al.*, 1999).   In the case of the *L. scotica* (Scottish Crossbill) the absence of observed genetically separate clades among *Loxia* complicated the awarding of individual taxonomic status; instead, detailed behavioural observations noted that fidelity in breeding was maintained within mixed populations, warranting its species recognition (Summers *et al.*, 2007, BirdLife International, 2010).
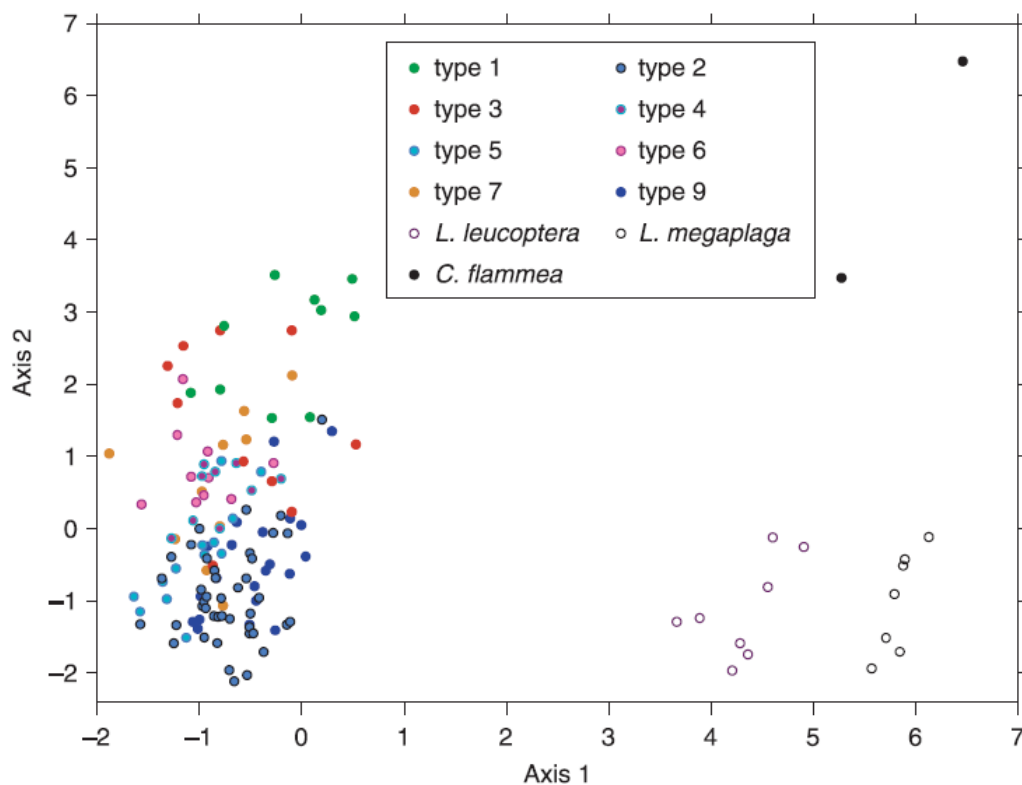
Figure 1.2.1:   Plot based on AFLP scores for individual *Loxia* specimens analysed in the study.   Key indicates the species they were allocated to before genetic analysis.   Note: Type 1-9 refer to different call types of North American *L. curvirostra*. (Fig. 2 in Parchman *et al.,* 2006)

Peirtney's and Questiau's studies had used mitochondrial DNA and microsatellite analysis to investigate Palaearctic crossbill phylogeography, a more recent study used AFLP marker variation with greater success in observable genetic differences (Parchman *et al.*, 2006). Parchman's study focused on New World crossbills, *L. leucoptera, L. megaplaga*, and the North American complex of *L. curvirostra* (Fig. 1.2.1); the principal coordinates analysis supports common theory that *L. leucoptera* and *L. megaplaga* are sister taxa.   However, the primary goal of this study was to ascertain whether different call-types of *L. curvirostra* were distinct species, a theory proposed for many years (Groth, 1993a, Benkman, 1999). Although genetic distances were sufficient to produce a phylogram showing the relatedness of each (see Fig. 4 in Parchman *et al.*, 2006), there was insufficient genetic divergence to allocate taxon status to any of the call-types studied (Fig. 1.2.1).   Parchman proposes that since the Old World studies showed similar genetic flow, the justification of species allocation based on call-type and behavioural observation remains; however, until AFLP genetic analysis is carried out on the Palaearctic populations, it is not truly comparable. Moreover call-type is a trait which is learnt, passed from parent to offspring (Groth, 1993b), and studies have showed no distinct morphology associated with populations of different call-types (Snowberg & Benkman, 2007).   Therefore it may not result in significant genetic divergence, as cultural isolation based on vocalisations may be open to frequent disruption, for example neighbouring birds may learn call-types.

Vietnamese Common Crossbill subspecies, *L. curvirostra meridionalis,* has also been subject to genetic analysis (Clouet & Goar, 1999).   It exhibits morphology most similar to that of the heavier built Palaearctic Parrot and Scottish Crossbill species and mitochondrial DNA showed that *L. c. meridionalis* genetics are very similar to those found in the western Palaearctic group rather than neighbouring populations in South Asia.   This further highlights the complexity of understanding phylogeography and the necessity for behavioural and evolutionary studies to be collated with genetic analysis to fully understand the phylogenetics of crossbills**.**

Section 1.3

The Fossil Record of the Crossbill

Passerine bones are of a highly delicate nature and the porosity of avian bones means their preservation is rare (Higgins, 1999).   In addition, many bones found remain unidentifiable to a particular genus, let alone a species, due to the fact they are often fragmented skeletal remains.   The most definable characteristic of *Loxia*, its bill, is rarely preserved due to its cartilaginous nature (Tyrberg, 1991), despite this, a number of fossils have been identified as crossbill species of varying age from 23-20 million years ago to the beginning of the Holocene, 10,000 years ago.

Crossbill fossils have been described primarily in Europe, (Fig. 1.3.1) dating from as early as early Miocene, 20-23 million years ago, (Mourer-Chauviré, 1995, Boev, 1999) until as recently as the early Holocene, (Harrison, 1980).   These fossils have been identified as the extant species *L. curvirostra, L. pytyopsittacus* and *L. leucoptera* as well as an extinct species *L. patevi* (Boev, 2002) and an as yet unknown ancestral fossil (Mourer-Chauviré, 1995). When comparing the collated fossil record (Fig. 7) with the present distributions (Fig. 1.1.2 & 1.1.3) it is evident that *L. leucoptera* and *L. pytyopsittacus* have in the past inhabited more
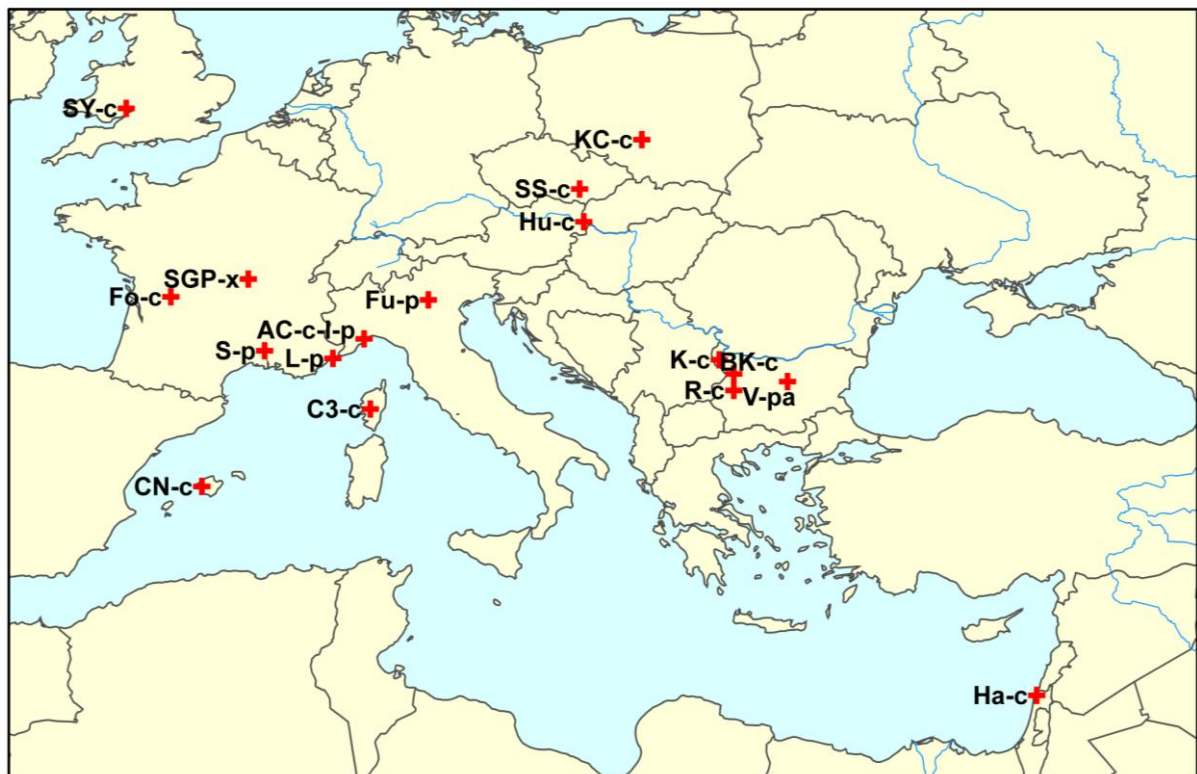
Figure 1.3.1:   Locations of fossil records of crossbills (*Loxia* spp.) in Europe. ✚ denotes the site of the fossil discovery. Labels start with an abbreviation of location (Table 1.3.1) followed by an indication of the species found: "c" – *L. curvirostra* (Common Crossbill), "p" – *L. pytyopsittacus* (Parrot Crossbill), "l" – L. leucoptera (Two-Barred Crossbill), "pa" – *L. patevi* (Extinct crossbill), "x" – Unknown species of crossbill

Table 1.3.1: Locations of *Loxia* genus fossil sites listed in chronological order/by the date of the fossil/layer it was found in.

Abbrev.	Location	Date (years B.P.)	Species	Reference
SGP	Saint-Gérand-le-Puy, France	23-20,000,000	*L. spp.?*	(Mourer-Chauviré, 1995) *in* *(Mlíkovský, 2002)*
V	Varshets, Bulgaria	2,000,000	*L. patevi*	(Boev, 2000)
SS	Stránská skála, Brno, Czech Republic	900-850,000	*L. curvirostra*	(Jánossy, 1972) *in* (Mlíkovský, 2002)
Hu	Hundsheim, Austria	850-700,000	*L. curvirostra*	(Mlíkovský, 2009)
C3	Castiglione 3, North Corsica	350,000	*L. curvirostra*	(Salotti *et al.*, 2000) *in* (Marco, 2004)
Fo	Fontéchevade, Montbron, France	300-200,000	*L. curvirostra*	(Mourer-Chauviré, 1975) *in* (Marco, 2004)
L	Lazaret, Boron Mountain, Nice, France	150-125,000	*L. pytyopsittacus*	(Vilette, 1993) *in* (Marco, 2004)
CN	Cova Nova, Capdepera, Mallorca Island	128-100,000	*L. curvirostra*	(Florit & Alcover, 1987) *in* (Marco, 2004)
KC	Komarowa Cave, Częstochowa, Poland	80,000 35,500-28,500 9,900-present	*L. curvirostra*	(Tomek & Bocheński, 2005)
BK	Bacho Kiro, Dryanovo, Bulgaria	47-43,000	*L. curvirostra*	(Bochenski, 1982)
Fu	Fumane, Vento, Italy	28,000	*L. pytyopsittacus*	(Bartolomei *et al.*, 1994, Cassoli & Tagliacozzo, 1994) *in* (Marco, 2004)
S	Salpêtrière, Remoulins, France	28,000	*L. pytyopsittacus*	(Vilette, 1983) *in* (Marco, 2004)
K	Kozarnika, Belogradchik, Bulgaria	26-19,000	*L. curvirostra*	(Boev, 2001)
AC	Arene Candide, Savona, Italy	13,400	*L. curvirostra* *L. leucoptera* *L. pytyopsittacus*	(Cassoli, 1980) *in* (Marco, 2004)
Ha	Hayonim Cave, Galilee, Israel	12,400-10,700	*L. curvirostra*	(Tchernov, 1979) *in* (Tyrberg, 1998)
R	Razhishkata, Lakatnik, Sofia, Bulgaria	11,000	*L. curvirostra*	(Boev, 2000)
SY	Symond's Yat, Herefordshire, United Kingdom	10,000	*L. curvirostra*	(Harrison, 1980)

southerly locations. This conclusion was also found in a comprehensive fossil study of avian zoogeography during the Quaternary in the Mediterranean, a trend also observed in twenty-six boreal bird species including the closely related *Carduelis flammea* (Common Redpoll) and *Pinicola enucleator* (Pine Grosbeak) (Marco, 2004).

Records for the Americas are even far more infrequent, but two fossils of *Loxia curvirostra* have been discovered in the Southern state of New Mexico (Schultz & Howard, 1935) and on the west coast in California (Miller, 1932). Both are dated from the Upper Pleistocene, around 100 thousand years ago. Although at first glance these fossils provide little evidence of past changes in distribution, as they are both located in regions where *L. curvirostra* is still present, one must not assume the species has always been present in this location, rather that

the conditions have been suitable in the past, in addition to the present day, to support this species.

In addition to the sparseness of the fossil record, Dr John Stewart, an avian palaeontology expert, highlights the major issues in identification of the remains (Stewart, 2002). Most species are distinguished by their plumage and song, which are not preserved in the fossil record; therefore classification of skeletal remains is often flawed and debatable. The present extant species are often used to classify avian archaeological remains (Stewart, 2004). The relevance of present taxa is valid but this may limit interpretation of records, especially when one takes into account past climatic, zoogeographical and ecosystem shifts as well as anthropogenic alterations which have greatly affected avian distribution. The characteristic irruptive nature of crossbills (Marquiss & Rae, 1994) further complicates the interpretation of the fossil record, due to the fact *Loxia* may have reached areas during irruptions but not established breeding colonies.

Although there are many issues with the avifauna fossil record, discoveries can be crucial for re-evaluating our understanding of evolutionary origins. For example the discovery of the earliest known fossil of passerines in Australia dating from the early Eocene (55 million years old) and 25 million years older than any find previously unearthed, challenged the common theory that passerines evolved in the Northern Hemisphere (Boles, 1997). However, fossil evidence alone was not sufficient to sway a commonly accepted theory of a Northern evolutionary origin. A combination with phylogenetic studies on extant species *Acanthisitta* spp. (New Zealand wrens), (Ericson *et al.*, 2002) established a now widely accepted theory that modern-day perching birds (Passeriformes) had a southern Cretaceous origin (Edwards & Boles, 2002). This highlights the importance when investigating evolutionary origins not to study zoogeography, palaeontology and phylogeny in isolation but rather consolidate and compare such data in order to establish a strong hypothesis.

Section 1.4

Evolution of the Crossbill

The acclaimed ornithologist Professor Ian Newton theorised that after the glaciations there was massive expansion in conifers, especially across the Palaearctic, the result being that a great amount of biome nutrients was stored in the hard Pinaceae cones (Newton, 1972).   This provided a new niche for a strong, cross-billed bird to establish, and variation in cones resulted in the ideal environment for distinct species to evolve.   Since then, the debate over the evolutionary origins of crossbills has continued, Tommy Tyrberg analysed the European fossil record and came up with two alternative hypotheses dependent on whether the larger fossil crossbills, resembling *L. pytyopsittacus*, found in the Alps were a distinct species or in fact a highly variable ancestral population (Tyrberg, 1991).

Tyrberg suggests that if the two fossil morphs of crossbill resembling *L. pytyopsittacus* and *L. curvirostra* were distinct species, they must have both followed the pine population northwards at the end of the glaciations and that one of the species then became extinct in Scotland and South Europe.   If the fossils are simply samples from a single phenotypically variable species then all of the larger-billed crossbills, *L. pytyopsittacus, L. scotica* and Mediterranean subspecies are descended from this ancestral pine crossbill and moved northwards with the pines getting isolated in Fennoscandia and Scotland followed by a later colonisation of *L. curvirostra* coming westwards into Europe following the progression of *Picea*.   Tyrberg also comments on the evolution of *L. leucoptera*, stating that its origins are probably outside Europe, in the eastern Palaearctic or Nearctic, due to the fact it subsists on *Larix* primarily.   However, it may have had ranges in Europe during previous interglacials and early interstadials when *Larix* populations were present (Huntley & Birks, 1983).

The *Loxia scotica* (Scottish Crossbill) has also been the subject of evolutionary investigation; Dr Alan Knox proposed that it could have evolved as recently as the beginning of the Holocene from *L. pytyopsittacus*, sharing similar morphology and diet of *Pinus sylvestris* (Knox, 1990).   It is hypothesised that a population of *L. pytyopsittacus* could have survived on the western coast of Ireland, on the edge of ice sheets, becoming reproductively isolated long enough for a new species to establish.   Pollen studies (Birks, 1989), as well as climate-based simulations (Holliday, 2010, Huntley *et al.*, In Press),   indicate that populations of *Pinus sylvestris* may have been present in western Ireland during the last glaciation. Similarly, it has long been hypothesised that the *L. megaplaga* (Hispaniolan Crossbill) originates from a population of *L. leucoptera* that were isolated on Hispaniola during the last

glaciation (Bond, 1948, Benkman, 1994) when the extent of *Pinus* and *Picea* spp. was much further south at that time (Davis & Shaw, 2001).

The presence of the Vietnamese heavier billed Common Crossbill subspecies, *L. c. meridionalis*, in such an isolated location is yet another conundrum in the evolution of crossbills, especially with neighbouring populations in the Philippines and Himalayas having more standard *L. curvirostra* morphology (Clouet & Goar, 1999). Clouet & Goar proposed two hypotheses that these Vietnamese Crossbills are the ancestors of large-billed crossbills present in south-east Asia, like those in Europe from the mid-late Pleistocene or that there was later colonisation of the thin beaked *L. curvirostra* with a rapid phenotypic evolution of the heavier beak in the Vietnamese population.

A similar large billed form of *L. curvirostra* was studied in Newfoundland, *L. c. percna*, feeding on *Picea mariana* (Black Spruce) (Griscom, 1937 in Benkman, 1989b), a feeding tree species that thin-billed *L. leucoptera* also predates on the mainland. Initial explanations for this large-billed morph focused on its isolated island location and its inability to escape cone failures (Benkman, 1989b) and therefore bill morphology has adapted to be able to exploit unopened and tougher cones when necessary. This is a theory already found to be exhibited in other avian island populations, most notably Darwin's finches, whose bill morphology changes according to the availability of the food (Grant & Grant, 2009). A more recent study proposed that in fact *Picea mariana* cones had become tougher in the presence of the resident *L. c. percna* and in turn this had resulted in selection of deeper bills among the population, a classic "co-evolutionary arms race" between predator and prey (Parchman & Benkman, 2002).

This is not an isolated case; further research by Benkman's research group has found the *Pinus occidentalis* (Hispaniolan Pine) in Hispaniola (Parchman *et al.*, 2007) and *P. nigra* (Corsican/Austrian Pine) in the Mediterranean (Benkman & Parchman, 2009) and *P. contorta* (Lodgepole Pine) in Idaho (Benkman, 1999) have all adapted defences in the presence of their respective crossbill species. Interestingly neighbouring populations of *L. curvirostra* in Idaho also feeding on the *P. contorta* show no increased bill depth; this is due to the presence of an ectoparasite which results in higher fatality rates among heavier billed individuals preventing this adaptive peak in bill morphology (Benkman *et al.*, 2005). In addition, there are evident effects in range and morphological adaptation of *L. curvirostra* in the presence of competitive species, such as squirrels, which may need to be accounted for when addressing evolutionary history (Siepielski & Benkman, 2004, Parchman & Benkman, 2008).

It is evident the evolution of crossbills is linked to past climatic shifts and its effects on the distribution of their feeding trees, more so than for many other bird species. *Loxia* species' ability to disperse rapidly and adapt to new tree species has made for many interpretations of crossbill origins. Thus there are many parameters which must be investigated in order to gain a comprehensive understanding including palaeoclimate, past biome shifts and dispersal ability of crossbills.

Section 1.5

Anthropogenic Impacts on Species' Distribution

When simulating species' distributions it is important to take into account anthropogenic alterations to the species' current ranges being used in the models. This is relevant in assessing whether the climatic niche observed today is actually a true reflection of their full potential. This relates back to the long debated fundamental versus realised ecological niche, where in general it is only possible for species' distribution models to simulate based on realised niches. However, the inclusion of our knowledge of human-driven changes to species' distributions will undoubtedly improve the model outputs and their interpretation.

In many cases, anthropogenic effects have limited species' distributions, isolating communities and restricting ranges. Although these alterations are relevant in modelling future distributions of these residual populations, they can evidently present a vast problem when simulating past species' distribution in time periods when human activity is unlikely to have had the significant effects observed today. To effectively model past range shifts, the models would need to be fully informed through historical and fossil records to incorporate the most complete species' ecological niche. Due to the relatively new development of retrodicting species' distributions, there are few studies addressing this directly, but there is a growing consensus that the palaeobiology may be integral in truly gaining a full understanding of ecological modelling (Dietl & Flessa, 2011).

Notably, though, the majority crossbill populations appear to be robust to human expansion, showing no recently observable population declines (Burfield & van Bommel, 2004). However the small isolated island population of *L. megaplaga*, the Hispaniolan Crossbill, is listed as 'endangered' (IUCN, 2011). Due to the risk of logging it is consider a species in threat of decline, limited to mountainous regions of Hispaniola (Dávalos & Brooks, 2001). Although the population does naturally fluctuate in size due to conifer productivity (Benkman, 1994) it has been considered more stable since the late 1970's after being unrecorded in Hispaniola between 1930-1970 (Dod, 1978).

However, on the contrary, some populations of crossbill have benefited from human activity. The creation of conifer plantations for the timber industry has generally been perceived to result in a decline in local bird species (Newton, 1983), primarily as high diversity grassland and deciduous woodland is replaced by monocultures of boreal coniferous species. Yet, other studies have found no significant change in the local bird populations (Avery, 1989). In fact, conifer plantations have been shown to attract a greater diversity and abundance of

avian populations than would have been supported by the native habitat they replaced (Moss *et al.*, 1979), mainly through attraction of boreal bird species such as Red Polls, *Carduelis flammea*, and Siskin, *Carduelis spinus*, and crossbills.

These conifer plantations provide Crossbills with an increase in food resources and allowed the establishment of active breeding populations in regions where conifers are not naturally found, such as East Anglia in England (Nethersole-Thompson, 1975).   This presents a new problem for effective retrodiction of their distributions; evidently the climatic conditions at these sites are suitable for the established crossbills, however many of these conifer plantations are situated in areas that would not maintain such boreal plant types and it is only with human intervention that their introduction and persistence occurs.   This highlights that the realised climatic niche of crossbills is restricted primarily by habitat and indirectly by climate.

With this in mind, it was important to establish the impact of conifer plantations on the present crossbills' ranges.   The formation of these fast-growing soft-wood conifer plantations, containing both native and non-native species of *Pinus*, pine, *Larix*, larch and *Picea*, spruce, has been most prolific in the United Kingdom (UK) and began on a large-scale in the 1920's and 30's to fulfil the growing consumer need for timber.   The British introduction of non-native conifer species, specifically *Picea*, has provided abundant food resources for *Loxia curvirostra*, generally considered a non-native vagrant in the UK (Cramp *et al.*, 1995), and there have been recordings of population irruptions since the 1840's and breeding since the 1920's (Nethersole-Thompson, 1975).   In fact irruptions starting in 1838 may have resulted in the establishment of a resident population in Ireland until the early 20th Century, supported by conifer plantation in the southeast and midland counties of Ireland (Holloway, 1996) which went extinct for many years with few occurrences in the 1960's (Sharrock, 1976) but have more recently, late 1980's, been observed again breeding in plantations in Ireland (Gibbons *et al.*, 1993).   Although irruptive populations are typical in crossbills' life-history it is notable the establishment of *Loxia curvirostra* breeding colonies in the United Kingdom corresponds with the expanding Victorian botanic collections and the progressive establishment of timber plantations introducing *Picea* throughout the country.

Evidence of Breeding: ·   Possible   •   Probable   ●   Confirmed
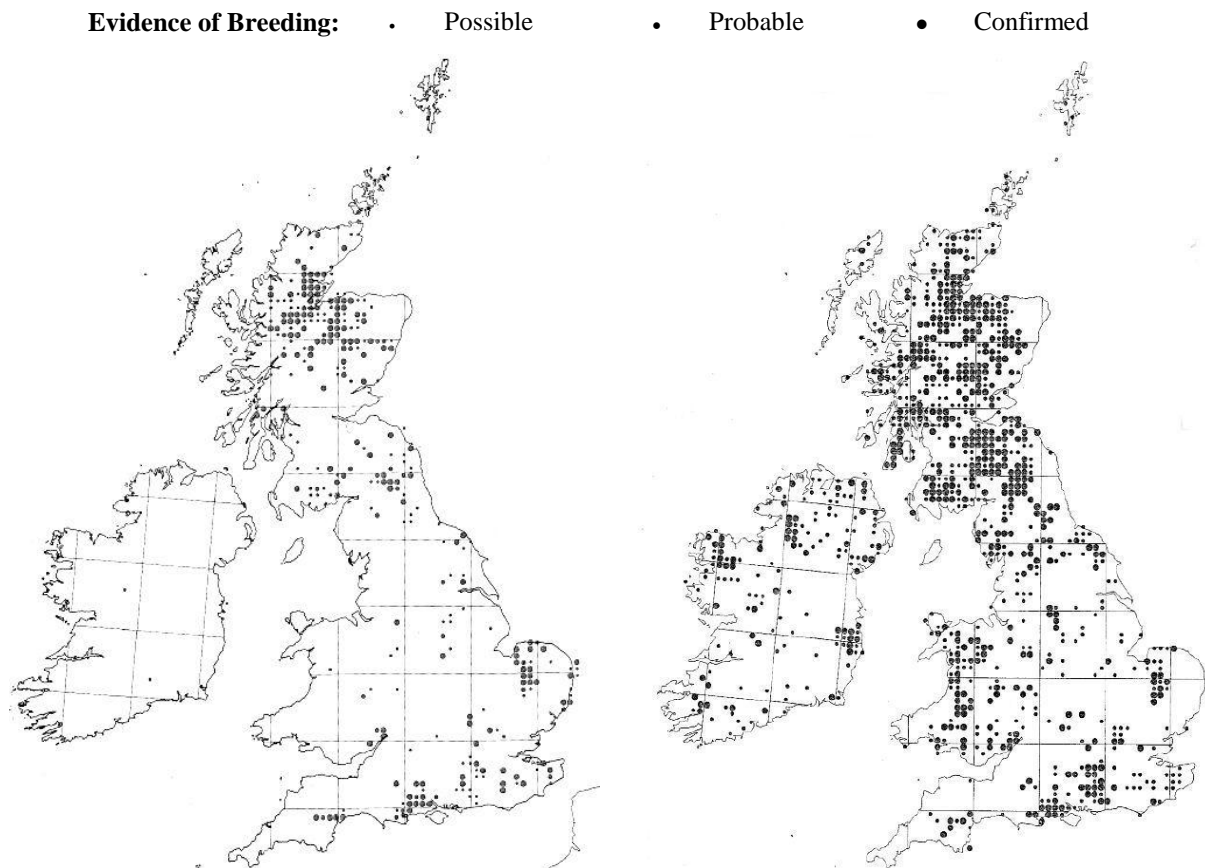
Figure 1.5.1:   Breeding records for *Loxia curvirostra* and *L. scotica* (grouped together) between 1968 and 1972 in Britain and Ireland recorded at 10km square scale (Sharrock, 1976).

Figure 1.5.2:   Breeding records for *Loxia curvirostra* and *L. scotica* (grouped together) between 1988 and 1991 in Britain and Ireland recorded at 10km square scale (Gibbons *et al.*, 1993).

Years	Present, No Breeding Evidence		Breeding Evidence		All Records	
	Britain	Ireland	Britain	Ireland	Britain	Ireland
1968-72	128	3	174	0	302	3
1988-91	337	100	406	56	763	156
				% Change	152.6	5100.0

Table 1.5.1:   A comparison of the presence and breeding records for *Loxia curvirostra* and *L. scotica* (grouped together) collected in 1968-72 and 1988-91 in Britain and Ireland recorded on a 10km square scale as well as the percentage change in number of records observed published by Gibbons *et al.* (1993).

Bird breeding records collated for the British Isles show an increase in the number of observed Crossbills breeding in the UK and Ireland (Table 1.5.1) from 1968-72 (Fig. 1.5.1) to those records from 1988-91 (Fig. 1.5.2) highlighting the varying occurrences of *L. curvirostra*.   Although in both these studies *L. curvirostra* and *L. scotica* were not differentiated in the field, as no recorded breeding of *L.* scotica has been noted outside Scotland, the records in Ireland, England and Wales are of *L. curvirostra*.

The breeding distributions for *L. curvirostra,* provided by Birdlife International, includes many of these more modern establishments of breeding populations in the UK and Ireland (Fig. 1.5.3).   However, further investigation of these sites established the presence of conifer plantations, either as private or national park aforestation schemes (Table 1.5.2).   Having established that these populations were likely as a result of an anthropogenic habitat alteration, there exclusion from the modelling was deemed appropriate to avoid inaccurate representations of *L. curvirostra*'s climatic niche.
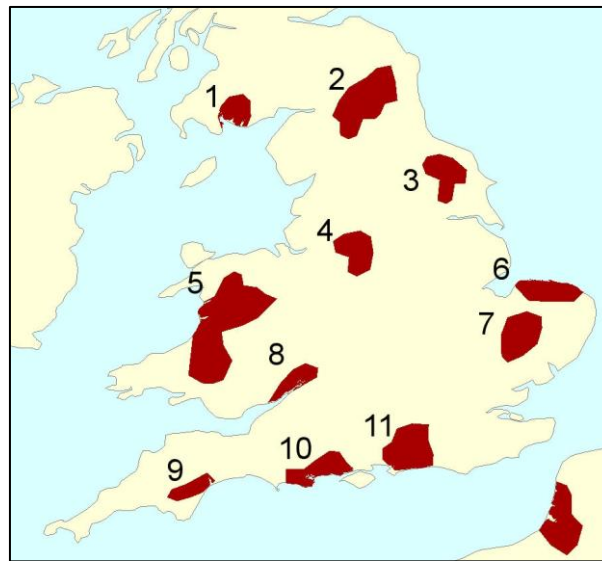
Figure 1.5.3:   The distributions of *Loxia curvirostra* breeding populations in the United Kingdom according to the Birdlife International Data.

ID	Location	Notes
	Fleet Forest	
1	Galloway Forrest Park	http://www.forestry.gov.uk/gallowayforestpark
	Dalbeattie Forest	Established in 1920's
2	Northumbria National Park	http://www.northumberlandnationalpark.org.uk/
	Kielder Forest	Established in 1930's. Species include: *Picea sitchensis, P. abies, Pinus contorta*
	North York Moors	http://www.northyorkmoors.org.uk/
3	Dalby Forest	http://www.forestry.gov.uk/dalbyforest
	Howardian Hills	Managed woodland
4	Peak District	http://www.peakdistrict.gov.uk/
5	Snowdonia	http://www.snowdoniaguide.com/
	Brechfa Forest	Established in 1930's
6	Sheringham Woods	Establish in the early 20th Century.
7	The Brecks	Evidence of *Pinus sylvestris* from 1668. Established plantations in the mid 18th Century. http://www.brecks.org/
8	Forest of Dean	Evidence from 1781.Species today include: *Picea*, *Pseudotsuga* and *Larix*. http://www.visitforestofdean.co.uk/
9	Dartmoor Forest	3,900 hectares of conifer plantation (Dartmoor National Park Authority, 2010) http://www.dartmoor-npa.gov.uk
10	New Forest	17th & 18th Century Timber Production http://www.newforestnpa.gov.uk
11	South Downs	http://www.southdowns.gov.uk

Table 1.5.2:   ID localities of breeding records for *Loxia curvirostra* (Fig. 1.5.3) and the particular regions/woods where conifer plantations have been established which provide food for these crossbills.   Notes include date establishment, species and source of further information.

Section 1.6

Quaternary Climate and Species' response

The Quaternary Period, from *ca.* 2.5 million years ago to present day, incorporating both the Pleistocene and Holocene epochs, is characterised as having a varying climate with a series of long cold glaciations followed by relatively short warm interglacials (Fig. 1.6.1) (Petit *et al.*, 1999).   In order to measure palaeoclimatic change, a variety of techniques are utilised including ice core analysis which is able to yield data on air composition, ice accumulation, precipitation levels and ocean temperatures (Petit *et al.*, 1999, Isaksson *et al.*, 2003).   Lake sediment (Allen *et al.*, 1999) can yield well-preserved stratified pollen records which can be used to determine vegetation composition and in turn climatic conditions (Seppä & Bennett, 2003, Seppä *et al.*, 2004).   Dendrochronology, the measuring of tree rings, is also a useful tool in assessing climatic fluctuations especially applicable for finer scale investigation of regional variation in temperature and growth season (Zech *et al.*, 2003, Martinelli, 2004).
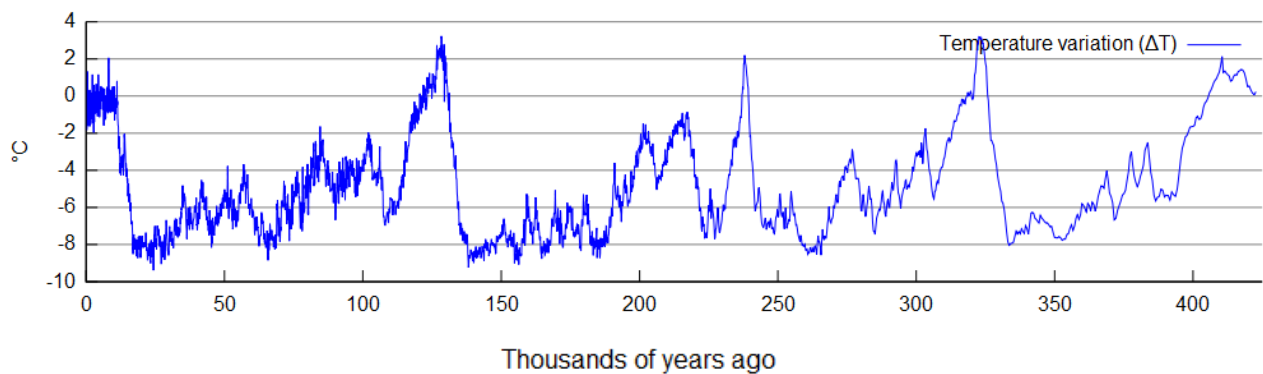
Figure 1.6.1: The variation in temperature compared to present day. Data measured using ice cores from Vostok, Antarctica dating back to 420 thousand years ago.(Petit *et al.*, 1999).

By integrating these techniques and consolidating results, a common understanding of global and regional climatic change over the Quaternary period has been ascertained and more recently modelled using global climate models (Kutzbach *et al.*, 1998, Singarayer & Valdes, 2010).   In the case of Singarayer & Valdes, they produced simulations at one thousand year intervals until 120 thousand years ago using an existing general circulation model combined with known changes in the Earth's orbit, greenhouse gases and ice sheet evolution in order to produce regionally gridded palaeoclimatic simulations.

The variation in climate prior to the Holocene triggered major shifts in the ranges of many species and in turn in the compositions of ecological communities, such as the changes in deciduous forest composition and extent throughout the Quaternary (Davis, 1983) and in some cases extinctions of both flora (Wolfe, 1978, Jackson & Weng, 1999) and fauna (Koch & Barnosky, 2006).   It is generally accepted that it is the individual species' responses to

climatic variation that are behind the observable range shifts in communities (Stewart, 2008). As vegetation composition is often characteristic of particular biomes, pollen records are a valuable tool in understanding past biome movement (Williams *et al.*, 2000, Williams *et al.*, 2004). The limitations of the fossil record mean there are few studies on Quaternary shifts in faunal distributions; a comprehensive project mapping Quaternary mammal fossil records of North America has been conducted (Graham *et al.*, 1996) but few studies of this scale have been carried out. However, it is apparent that past climatic fluctuations and the resultant shifts in plant species have resulted in faunal range shifts; this relationship also had implications in the context of future climatic change (Huntley, 1995). For example, changes in vegetation potentially had a role in the extinction of mega-fauna during the latter stages of the Last Glacial Maximum (LGM) and simulation of past flora ranges and productivity has given insight into probable causes (Allen *et al.*, 2010). It is interesting to note that this latter study shows that boreal evergreens, the conifers that most crossbills feed on, had a southern European distribution during the last glacial from 42 to 21 thousand years ago, a correlation with the observed fossil record of boreal crossbills in the Mediterranean (Fig. 1.3.1).

Many evolutionary theories of crossbill speciation have alluded to the importance of glaciations forcing population movements and separation (Knox, 1990, Tyrberg, 1991). In the midst of the Pleistocene glaciations, sporadic regional refugia would have been able to maintain some populations, in turn affecting the present observed phylogeography and distribution of species (Hewitt, 1996, 1999, Stewart & Lister, 2001). Thus the Pleistocene is often characterised as a time of dynamic populations and significant ecological change (Hofreiter & Stewart, 2009). In Europe, the presence of many refugia may have resulted in the genetic diversity observed, such as the high species richness of temperate forests (Huntley, 1993). Mitochondrial DNA analysis of avifauna indicated that many speciations were initiated or completed during the Pleistocene (Avise & Walker, 1998); however, other studies indicate that the more recent glaciations did not accelerate speciation; a phylogenetic study on North America passerines indicated that speciation rates appear relatively constant throughout the last 2.4 million years (Klicka & Zink, 1997). It is widely accepted that the glaciation of the Quaternary affected the present distributions of taxa but whether speciations could have resulted from these isolations has yet to be fully established.

Section 1.7

Species' Distribution Modelling

Modelling distributions of flora and fauna rely on the assumption that species occupy a specific niche (Soberón, 2007); some propose that modelling is an approximation of a species' fundamental niche (Soberón & Peterson, 2005), others conclude it is a spatial representation of the realised niche (Pearson & Dawson, 2003). Models based on recorded presence distributions are only able to model realised niches due to various interacting factors that have already dictated the presence or absence of the organism. As well as this, the accuracy of the model output is fundamentally reliant on the sampling of data, selection of parameters and the specific model which are used to generate it (Araújo & Guisan, 2006).

For large scale distribution studies, climate-based models of species have been developed and reviewed thoroughly (Thuiller, 2003, Araújo *et al.*, 2005, Pearson *et al.*, 2006) and have proved effective, specifically in modelling future impacts of climatic change on range shifts (Huntley, 1995, Thuiller *et al.*, 2005b, Huntley *et al.*, 2006, Huntley *et al.*, 2007, Settele *et al.*, 2008), and also have been utilised in the modelling of palaeovegetation (Harrison & Prentice, 2003, Huntley *et al.*, 2003, Miller *et al.*, 2008, Allen *et al.*, 2010). There are, as of yet, only a few examples of faunal palaeogeographical simulations, these include the now extinct mammoth (Nogués-Bravo *et al.*, 2008) and Aphelocoma jays (Peterson *et al.*, 2004). Overall climate based models have proved to be effective in modelling a range of taxa independent of their respective trophic level (Huntley *et al.*, 2004). However, Beale argues that in the case of birds, an association with climate may be by chance and that avian sensitivity to climate varies (Beale *et al.*, 2008) but this appears unlikely in the context of crossbills' high dependence on specific tree species, whose distribution is in turn dictated by climate.

Climate response surface models use predefined parameters to produce a climatic envelope in which the species is presently observed to exist (Huntley *et al.*, 1995). The parameters generally used include a measure of coldness, mean temperature of the coldest month, moisture availability, evapotranspiration rates, and growth season, growth degree days and have been shown effective to model present and future distributions (Huntley *et al.*, 1995, Huntley *et al.*, 2004, Huntley *et al.*, 2007). Generalised additive models (GAMs) (Hastie & Tibshirani, 1990), a combination of additive models and general linear models, can also be applied to assess the environmental parameters controlling species' distribution without assuming a parametric relationship, so the data, rather than the model, often determines the

relationship between the variables and the response (Guisan *et al.*, 2002). In addition, GAMs are highly adaptable enabling the incorporation of biotic factors into the climate envelope model, with significant improvement seen in the fine scale (10km grid resolution) model predictions of boreal owl distribution when woodpecker presence was factored into the model (Heikkinen *et al.*, 2007).

Climate response surface modelling and GAMs are most precise when applied to distributional data where both presences and absences are known to produce an accurate probability distribution, however many species' distributions are documented by presence-only. Assumptions of an un-recorded presence denoting absence is potentially dangerous so the maximum entropy method (Maxent), a statistical model similar to GAM, was developed in order to model presence only data (Phillips *et al.*, 2006). It is based on the maximum entropy principle that the approximation should satisfy all constraints in the indefinite distribution (Jaynes, 1957), combining this rule with machine learning methods to aid predictions of distributions.

If there is a wide range of data available and the parameters affecting the distributions are unclear, then machine learning methods may be applied, such as genetic algorithms and decision trees, to define the best modelling parameters. The Genetic Algorithm for Rule-Set Prediction (GARP) modelling system was developed as an automated model for predicting species' distributions working with presence-only data too (Stockwell & Peters, 1999). It combines climatic envelope, artificial neural network (ANN), an adaptive computational model, and general linear models using environment conditions as limits for the population, generating multiple models using mathematical rules exploring and recombining these to investigate potential distributions and was used to establish parameters for modelling the palaeobiogeography of Aphelocoma jays (Peterson *et al.*, 2004).

Classification and regression tree analysis (CART) is a non-parametric decision tree learning technique which analyses data using selected criteria to separate the data recursively into terminal nodes (De'ath & Fabricius, 2000). Primarily used in clinical research (Lewis, 2000), the best "rules" for separation infer the variables which account for the patterns in the data observed but it also has applications in ecological modelling such as defining variables for simulating forest canopy (Herold *et al.*, 2003) and assessing the success of introduction programmes (Kolar & Lodge, 2002).

In a study that combined both Maxent and GARP to establish the range of the recently discovered Bugun Liocichla, *Liocichla bugunorum*, which has very limited records from

north-eastern India, they produced very different results, with the Maxent simulating distribution suitability over the expanse of the study area and the GARP simulation predicting a significantly sparse distribution (Peterson & Papeş, 2006).   This highlights the differences in simulation output from the same data set just using a different model, and the relevance of constructing several species' distribution models.

Thuiller developed biodiversity modelling (BIOMOD), which simultaneously combined general linear and additive models with CART and ANN in order to maximise the predictive accuracy of species' distribution simulations (Thuiller, 2003).   Thuiller applied the model to 61 European tree species and yielded predicted distributions which were of good correlation to the observed; however the techniques employed performed with varying efficiency depending on the taxa being modelling.   On evaluation it was suggested that it should be common practice to conduct multiple model projections, specifically to account for differential species specificity of modelling techniques. Although Thuiller suggests averaging multiple models, it may be more informative to compare and contrast the different model outputs in order to evaluate both the similarities and the alternative simulations.

Section 1.8

Aims and Objectives

The overall aim of this project is to investigate the palaeobiogeography of *Loxia* species and their feeding trees using species' distribution models and simulated palaeoclimatic conditions to provide potential insights into past range shifts, regions of climatic stability and the life history of this complex genus.   Given this aim, and with background knowledge in mind, three specific objectives were established for the project, each of which had a number of associated subsidiary objectives which also would be addressed.   The three principal objectives, and the subsidiary objectives associated with each, are outlined below:

- To obtain the best performing and most robust distribution model for each species.
  - Identify the best performing species' distribution model for each species by fitting a selection of those most commonly used in the literature (Section 3.1).
  - In the case of more limited distributed species, test whether grid extent affects the performance of the model (Section 3.1).
  - Assess some of the common differences in the simulated outputs between the modelling techniques used (Section 3.2 & 3.3).

- To simulate past and present distributions of *Loxia* species and their feeding trees and compare these with available evidence.
  - Using palaeoclimate simulations at regular intervals throughout the last glacial period, from 120 thousand years to the present day, apply the species' distribution models to simulate species' distributions (Section 3.4 & 3.5).
  - Compare the simulated range extents to available fossil records of similar ages (fossil remains of crossbills (Section 4.2) and pollen and macrofossil records of conifers (Section 4.3)), as well as to the results from other palaeobiogeography modelling projects (Section 4.3).

- To identify regions of climatic stability, specific scenarios where a species' range is most restricted and potential links these may have with species' history and evolution (Section 4.6).
  - Examine the simulated range changes for *Loxia* species and their feeding trees through the last glacial (Section 3.5).

- o Supplement existing understanding of *Loxia* species and sub-species' conifer feeding specificity by comparing simulated distributions of the *Loxia* species and of their potential feeding trees (Section 4.4).
- o Investigate the origins of the island populations of crossbills¸ *Loxia scotica* and *L. megaplaga*, by examining the simulated range movements and determining whether these may indicate the origin of their ancestral population and the timing of its subsequent isolation (Section 4.6).

CHAPTER 2 – Data Collection & Methods

Section 2.1

Species' Distribution Data

The *Loxia* distribution data were provided by Birdlife International (2010) as digitised polygons of both observed non-breeding and breeding ranges.   For modelling purposes the breeding ranges were used, as for *Loxia* this best represents the resident populations.   Only *L. curvirostra* and *L. leucoptera* show non-breeding range shifts, and these ranges only represented the observed southern limits and not the complete non-breeding distribution and therefore could not be used in isolation as modelling data.   In the particular case of the Scottish Crossbill, these data were supplemented with European Bird Census Council (EBCC) (Hagemeijer & Blair, 1997) recorded breeding data based on primary observations of species' presence.

Larix spp.	Location	Distribution Source
L. decidua	Central Europe, Alps & Carpathians	(EUFORGEN, 2009)
L. gmelinii	Russia, Mongolia, China & North Korea	(Bard *et al.*, 1990, Farjon, 1990)
L. griffithii	Nepal, Sikkim, Bhutan & China	(Farjon, 1990)
L. kaempferi	Japan	(Farjon, 1990)
L. laricina	Northern USA & Canada	(Little, 1971)
L. potaninii	China & Nepal	(Farjon, 1990)
L. sibirica (russica)	Russia	(Farjon, 1990)
Picea spp.		
P. abies	Across Europe & Russia	(EUFORGEN, 2009)
P. alcoquiana	Japan	(Farjon, 1990)
P. asperata	China	(Farjon, 1990)
P. aurantiaca	China	(Farjon, 1990)
P. brachytyla	China	(Farjon, 1990)
P. glauca	Eastern USA	(Little, 1971)
P. glehnii	Russia & Japan	(Farjon, 1990)
P. jezoensis	Japan, Korea &Russia	(Farjon, 1990)
P. koraiensis	Korean	(Farjon, 1990)
P. koyamae	Japan	(Farjon, 1990)
P. likiangensis	Bhutan & China	(Farjon, 1990)
P. mariana	Northern USA & Canada	(Little, 1971)
P. meyeri	China	(Farjon, 1990)
P. neoveitchii	China	(Farjon, 1990)
P. orientalis	Caucasus & Turkey	(Farjon, 1990)
P. reteroflexa	China	(Farjon, 1990)
P. rubens	North America & Canada	(Little, 1971)
P. schrenkiana	China, Kazakhstan, Kyrgyzstan & Pakistan	(Farjon, 1990)
P. sitchensis	Western USA & Canada	(Little, 1971)
P. smithiana	Afghanistan & Nepal	(Farjon, 1990)
P. spinulosa	Sikkim & Bhutan	(Farjon, 1990)
P. torano	Japan	(Farjon, 1990)

Table 2.1.1:   The selection of *Larix* & *Picea* species used as potential feeding trees of Crossbills, their location in the world and the distribution source from which they were obtained.   Species highlighted in grey were later eliminated from further modelling due to their limited distribution or rarity.

The conifer species' distributions were obtained from various sources (Tables: 2.1.1 & 2.1.2). The North American conifers were sourced from digitised representations of the tree species' ranges in Little's "Atlas of American Trees" (Little, 1971) and in an earlier Critchfield and Little publication "Geographic Distribution of the Pines of the World" provided by U.S. Geological Survey (USGS) as digitised polygons (USGS, 2006). The digitised conifer ranges for European tree species were produced by the European Forest Genetic Resources Programme (EUFORGEN, 2009). For all the Asian conifers, and some other ranges access was granted to original drawings produced by Farjon published in "Pinaceae" (Farjon, 1990). These were manually digitised using Arc (ESRI, 1998).

Pinus species	Location	Distribution source
P. ayacahuite	Mexico & Western Central America	(Critchfield & Little, 1966)
P. caribaea	Cuba, Jamaica, Bahamas & Central America	(Critchfield & Little, 1966)
P. contorta	Western USA & Canada	(Little, 1971)
P. cooperi	Mexico	(Critchfield & Little, 1966)
P. douglasiana	Mexico	(Critchfield & Little, 1966)
P. durangensis	Mexico	(Critchfield & Little, 1966)
P. engelmannii	Southern USA & Mexico	(Little, 1971)
P. halepensis	Mediterranean, South European & North African coastline.	(EUFORGEN, 2009)
P. hartwegii	Mexico, Central America to Honduras	(Critchfield & Little, 1966)
P. kesiya	Thailand, Myanmar, Laos, China, Vietnam & the Philippines	(Farjon, 1990)
P. latteri	Myanmar, Thailand, Laos, Cambodia, Vietnam & Hainan	(Farjon, 1990)
P. lawsonii	Mexico	(Critchfield & Little, 1966)
P. leiophylla	Southern USA & Mexico	(Critchfield & Little, 1966, Little, 1971)
P. lumholtzii	Mexico	(New *et al.*, 2003)
P. merkusii	Indonesia & Sumatra	(Farjon, 1990)
P. michoacana	Mexico & Guatemala	(Critchfield & Little, 1966)
P. montezumae	Mexico & Central America	(Critchfield & Little, 1966)
P. nigra	South European coastline of Mediterranean	(EUFORGEN, 2009)
P. occidentalis	Haiti & Dominican Republic	(Critchfield & Little, 1966)
P. ponderosa	Western USA	(Little, 1971)
P. pseudostrobus	Mexico	(Critchfield & Little, 1966)
P. strobus	Eastern USA & Canada	(Little, 1971)
P. strobiformes	South western USA	(Little, 1971)
P. sylvestris	Europe, Scandinavia to Caucasus Mountains & Central Russia	(EUFORGEN, 2009)
P. teocote	Mexico	(Critchfield & Little, 1966)
P. yunnanensis	China	(Farjon, 1990)
** **		
***Pseudotsuga* spp.**		
P. japonica	Japan	(Farjon, 1990)
P. menziesii	Western USA & Canada	(Little, 1971)
P. sinensis	China & Taiwan	(Farjon, 1990)
** **		
***Tsuga* spp.**		
T. canadensis	Eastern USA & Canada	(Little, 1971)
T. chinensis	China, Taiwan, Tibet & Vietnam	(Farjon, 1990)
T. dumosa	India, Myanmar, Vietnam, Tibet & China	(Farjon, 1990)
T. forrestii	China	(Farjon, 1990)
T. heterophylla	Western USA & Canada	(Little, 1971)

Table 2.1.2: The selection of *Pinus*, *Pseudotsuga* and *Tsuga* species used as potential feeding trees of Crossbills, their location in the world and the distribution source from which they were obtained. Species highlighted in grey were later eliminated from further modelling due to their limited distribution or rarity.

All the species' digitised polygon distributions were intersected with a 0.5° x 0.5° grid spanning most of the northern hemisphere to encompass the entirety of both the Crossbill and feeding tree distributions, from the equator (0°N) to 85°N and spanning the complete longitudinal range of from 180°W to 180°E using ArcMap (ESRI, 1998).   The presence or absence of the species was automatically recorded for each 0.5^o x 0.5^o grid square and exported as a data table.   By default Arc attributes '1' to a presence, while '0' signifies an absence of intersection with polygons.   However, if polygons are grouped within a dataset, for example breeding and non-breeding ranges, the numerical complexity of labelling will automatically increase or can be specifically tailored to accommodate the categories required.

Some manual additions of presences and absences had to be made using ArcMap (ESRI, 1998), specifically for the EBCC data, transferring these from their 50km^2 grid resolution, as well as adding supplementary tree species' presence data points provided by EUFORGEN and the selective elimination of *Loxia curvirostra* breeding sites in exotic conifer plantations (Section 1.5).   In each case, manual alterations were made by identifying the relevant unique grid ID in ArcMap and making the necessary modifications to the exported data table.

Notably some of the conifer species selected, although likely to be a food source for local *Loxia* spp., were considered rare or had very restricted distributions, often having more wide-spread species also present in the area.   Unless specified in the literature as being a primary food source, such as the limited distributions of *Pinus occidentalis*, the rare species were eliminated from further modelling due to their negligible impact and overlapping presence. In addition, once initial species' distribution modelling had been done (Section 2.4) it was evident from the low 'goodness of fit' measures obtained (Section 2.5, Appendix: Table 1) that some of the conifer species' distributions were not representative of distinct bioclimatic niches, rather range restrictions are possible as a result of other factors, such as geographical isolation, on islands, for example *Pinus occidentalis*, and mountains, *Larix deciduas*, as well as interspecific competition, such as in the Alps between *Larix decidua*, *Picea abies* and *Pinus mugo* (Dullinger et al., 2005) which limits the species from occupying all the locations which are climatically suitable.   The 'goodness of fit' was significantly increased when species were combined within a genus (Section 3.1, Table 3.1.2), thus all species listed in Tables 2.1.1 & 2.1.2, barring those excluded due to their limited range or rarity, were merged into larger generic groups for further modelling process.   *Picea abies* and *Pinus sylvestris*, however, had high goodness of fit, reflecting their wide-spanning distributions in Eurasia, enabling them to be modelled individually, as well as their inclusion in the relevant generic models.

Section 2.2

Bioclimatic Data

The bioclimatic variables to which the species' distribution models were fitted were derived from climatic variable values in the CRU CL 1.0 dataset; averages from 1961-1990 first published at a 0.5^o x 0.5^o resolution by New *et al*. (1999), with regional meteorological-station data used to interpolate the average climate to this high resolution.   From this climate dataset, bioclimatic variables were calculated which best represent the key constraints on the bird and plant species being modelled, whether through direct or indirection interactions.   In the high latitudes the most constraining variables are a combination of the cold minimum, the length of the growing season and the moisture availability (Huntley *et al.*, 2006).   Hence the following bioclimatic variables were used; the coldest month mean temperature, the annual thermal sum above a 5°C and the annual ratio of actual to potential evapotranspiration, a combination of variables which has been used effectively in other species modelling studies (Huntley, 1995, Huntley *et al.*, 1995, Thuiller *et al.*, 2005a, Huntley *et al.*, 2006).

The mean temperature of the coldest month (MTCO), measured in °C, is a measure of the winter coldness to which many species are sensitive and acts as a limit to species' range. The monthly mean temperature for each month is computed and then the month with the lowest average is selected for the MTCO value.   This is used preferentially to absolute minimum annual temperature as records of this variable are not as extensive in global climate compilations and the two variables are observed to be highly correlated (Müller, 1982, Prentice *et al.*, 1992).

Growing-degree days above 5°C (GDD5 degree days (d°)) is the annual temperature sum above 5°C, a measure of 'growing season' or the overall cumulative warmth.   Growing degree days are calculated by taking the daily-temperature average degrees that exceed 5°C and totalling these to produce an annual sum.   Temperate plants often have a threshold temperature for metabolic activity of around 5°C; under this value their growth is limited. The cumulative warmth above 5°C has been shown to restrict tree-lines of cold environment boreal conifers such as *Picea* and *Larix* (Tuhkanen, 1984, Prentice *et al.*, 1992).   This parameter is favoured over other measures of warmth such as maximum annual temperature and mean temperature of the warmest month.   Primarily the thermal sum is selected as it determines whether the location is suitable for species to complete annual growth or reproductive cycle, especially in higher latitudes, processes which are not wholly linked to summer extremes in temperature.   It is important to note that gradients of continentality of

sites across the northern hemisphere mean that there are significant differences in spatial patterns of warm extremes and thermal sum. Comparisons of these climatic variable patterns with major taxonomic groups in Europe, including plants and birds, have indicated that GDD5 has a greater frequency of alignment with the Northern limits of species' distributions (Huntley *et al.*, 1995, Huntley *et al.*, 2006).

The annual ratio of actual to potential evapotranspiration (AET/PET), also known as Priestley-Taylor's α (Priestley & Taylor, 1972), is a moisture availability index calculated in this case using a bucket model developed by Cramer & Prentice (1988). The bucket model combines estimates of the 'daily' temperature, precipitation and cloudiness from the monthly variable averages, with a measure of potential insolation, calculated from latitude and Julian day, and soil-water capacity, sourced from a 0.5^o gridded world dataset first developed by Prentice *et al*. (1992). This index includes both precipitation rates, the input into the system, and the evaporative and transpirational demands, outputs from the system, to produce a measure of regional moisture availability. This index represents the limitations of moisture supply directly experienced by the organisms much more effectively than a simple precipitation measure. In addition, previous studies have shown that species' distribution patterns are more correlated with AET/PET patterns than those of seasonal precipitation (Huntley *et al.*, 2006).

Section 2.3

Palaeobioclimatic Data

Palaeoclimatic data was sourced from a series of general circulation model (GCM) simulations made by Singarayer and Valdes (2010). The series of 52 palaeoclimatic simulations selected, which spans the past 120 thousand years, was produced using the Hadley Centre Unified Model (HadCM3), a fully-coupled atmosphere-ocean GCM (Gordon *et al.*, 2000, Pope *et al.*, 2000). The atmosphere was simulated at 2.5° x 3.75° x 19 levels spatial resolution, while the ocean was at 1.25° x 1.25° x 20 levels. The palaeoclimate simulations were formulated by collating available data from ice cores (The Vostok record; Petit *et al.*, 1999, Loulergue *et al.*, 2008), ice-sheet simulations, orbital calculations and sea-level change derived from ice-volume evidence, and using these to prescribe for each scenario the atmospheric composition, ice sheet altitude and extent, orbital forcing and land-sea mask. Each of the prescribed GCM palaeo-simulations was run for 500 years until they reached quasi-equilibrium (Singarayer & Valdes, 2010). The GCM output scenarios were processed using the methods outlined in Allen *et al.* (2010). First the climatic anomalies were calculated as the difference, for monthly mean temperature, or, in the case of both monthly precipitation and mean percentage cloud cover, the ratio between the palaeoclimate simulation and a control pre-industrial climate simulation. Using thin-plat splines (Hutchinson, 1989), the palaeoclimate simulated scenario anomalies were interpolated to the centre of each respective 0.5° x 0.5° grid square and applied to the CRU 1961-90 average climate. From each of these regionalised palaeoclimatic scenarios the bioclimatic variables could then be calculated using the same methods used for the present climate.

However, in this study, values were also calculated for the continental shelf exposed by sea level depression from present during the glaciations. As described in Huntley *et al*. (In Press), the potential present climate, the average of 1961-1990, was calculated for the areas exposed at maximum sea depression during the last glacial, approximately 120 metres below current sea-level. The grid cell altitudes were derived by calculating the mean values from the GEBCO 1′ (IOC *et al.*, 2003) resolution global bathymetric and altitudinal grid. To generate climate for the grid-cells exposed at maximum sea-level depression, thin-plate spline surfaces (Hutchinson, 1989) were fitted to relate the selected 36 climatic variables, monthly means of temperature, precipitation and percentage cloud cover, to the longitude, latitude and altitude. For each of the palaeoclimate scenarios, the interpolated anomalies were applied to the present average climate values estimated for the exposed continental shelf, and from these the bioclimatic variable values ware then calculated.

There were 53 palaeoclimatic scenarios simulated spanning from 120 thousand years ago to present day.   Scenarios are for every thousand years from present day to 22 thousand years ago, spanning the Holocene, beginning around 10 thousand years ago, to the LGM, *circa* 21 thousand years ago.   Palaeoclimatic scenarios are then for every two thousand years from 24 to 60 thousand years before present, spanning the most recent glacial.   From 100 to 120 thousand years ago, simulations are every four thousand years, spanning into the Eemian interglacial.   In addition to these simulations there are also the five of the latest Heinrich events, at 17, 24, 32, 38, 46 thousand years ago, when temperature dropped significantly due to the ice sheet melting causing an influx of cold water into sea resulting in a significant by short-lived drop in global temperature.

From these simulations the bioclimatic data for the models was simulated and gridded at the 0.5° x 0.5° scale; the average bioclimatic variables across the northern hemisphere grid for each scenario are shown in Figure 2.3.1.   Simulations are absent between 60 and 100 thousand years before present due to lack of knowledge and debate over climate
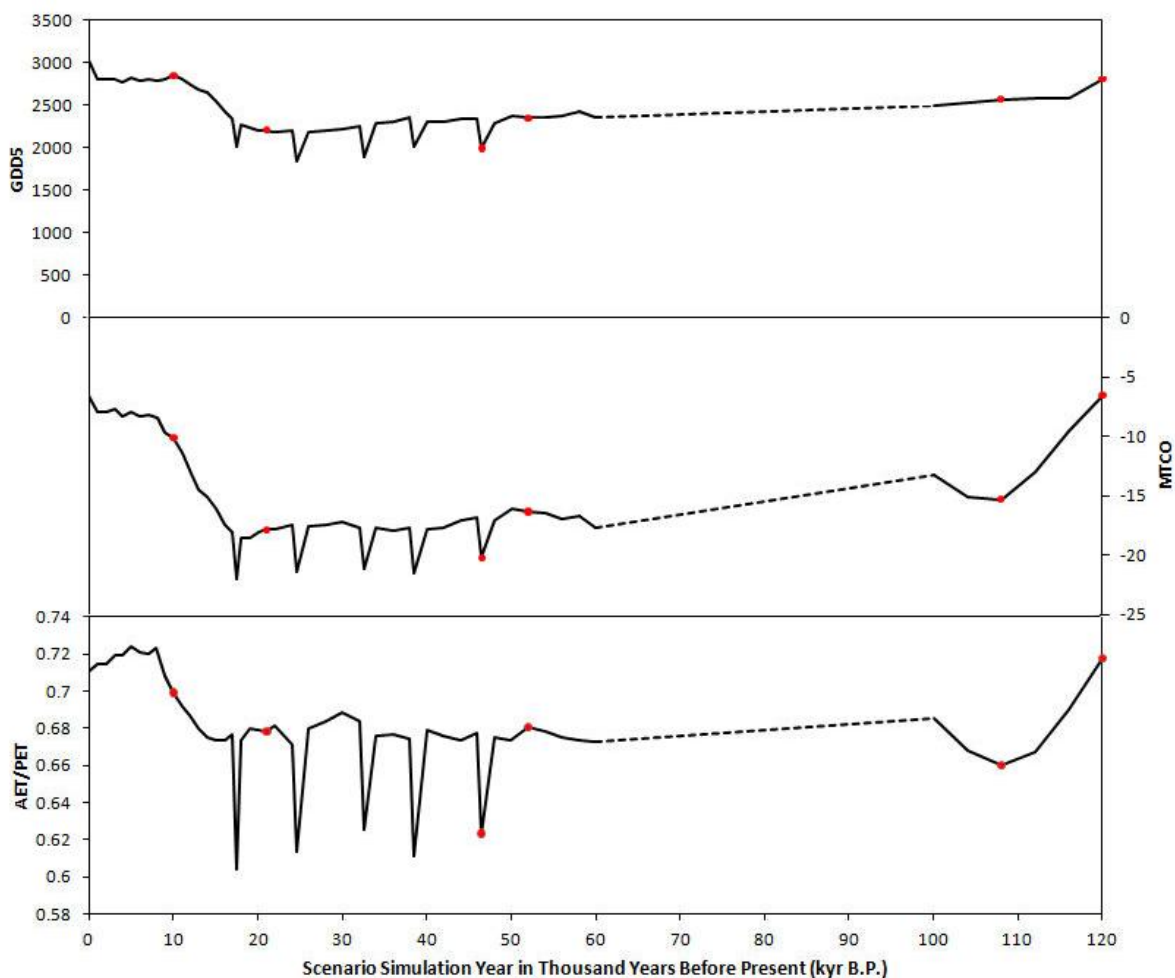
Figure 2.3.1:   The mean bioclimatic values for the palaeoclimatic scenarios calculated for the northern hemisphere extensive grid, including the growing degree days above 5°C (GDD5), mean temperature of the coldest month (MTCO in °C) and moisture availability index (AET/PET). Red dots indicate the scenarios selected for inclusion in the thesis.

reconstructions over this time period so no assumptions are made of these climates.   Maps were produced for all scenarios using all three modelling techniques (CD ROM Appendix), however in regards to the write up a selection of scenarios were generated (red dots in Fig. 2.3.1) by the best performing model for each species (Section 3.1) in all cases this was the climatic response surface model.

The earliest scenario selected, 120 thousand years ago, represents the previous interglacial conditions, known as the Eemian interglacial and similar in climate to the present interglacial, a significant length of warmer and wetter climatic conditions where the ice sheets in the northern hemisphere were limited to ranges similar to those observed today.   The scenario generated for 108 thousand years ago was selected to represent a stadial, a colder and drier period within the warmer interglacial, this one in particular is referred to as the Melisey 1 stadial.   During the most recent glacial from approximately 100 to 10 thousand years ago, the bioclimatic scenario of 52 thousand years ago was selected as a representative of interstadial conditions during the glaciations, a short period of warmer wetter conditions.   A Heinrich Event scenario, specifically HE5 which occurred approximately 46 thousand years ago, was also selected for inclusion.   Heinrich Events occurred during the last glacial when icebergs broke away from the glaciers and melted releasing large amounts of cold water into the North Atlantic having an effect on the thermohaline circulation and causing a drop in temperature and decreased moisture availability.   It is important to note that these events are unlikely to have been long-lived lasting about 750 years maximum (Maslin *et al.*, 2001). The glacial maximum, 21 thousand years ago, when the ice sheet reached its greatest extent, was also selected for inclusion as a representative of the glacial conditions.   The beginning of the Holocene, 10 thousand years ago, was selected as a representation of the warmer and wetter climate at the beginning of the present interglacial.

The previous Eemian interglacial scenario was from around 120 thousand years before present.   The interglacial is the warm period between the glacial when the ice sheets have receded, conditions very similar today.   There was a long growing season, an average of 2810 GDD5, just lower than the current 3035 GDD5 (Fig. 2.3.1).   The average northern hemisphere MTCO is just -6.6°C, significantly warmer than glacial temperatures.   It is also wetter, with a moisture availability average of 0.717 AET/PET, in fact fractionally wetter than the present day, 0.710 AET/PET.   These warmer, wetter interglacial conditions, similar to the present, are likely to result in species' distributions similar to the observed ranges seen today.

The stadial is a period during the interglacial, the warm period between glaciations, when temperatures are lower but of insufficient length for the formation of glaciers. There have been a number in the current glacial, including the Older Dryas, Younger Dryas and Little Ice Age but in this case an example has been selected from the previous Eemian interglacial of the Melisey 1 stadial which occurred around 108 thousand years ago. During this colder period the growing season shortens to an average of 2568 GDD5, shorter than the normal interglacial conditions, which are generally greater than 2700 GDD5 (Fig. 2.3.1). The MTCO also dips below -10°C the cold maximum average of the most recent interglacial conditions, to -15.3°C during this stadial. It is also drier, with a moisture availability of just 0.660 AET/PET compared to the normal interglacial, approximately 0.700 AET/PET. The sea-level during the interglacial and stadial is simulated as being the same as the current sea-level, as, even though it was colder during this period, there was no significant ice formation.

The interstadial was a period during the glacial epoch when the temperatures were warmer, the result being that glaciers either ceased growing or retreated in their overall extent. During the last glacial there was several interstadials but the one selected here was close to the Heinrich Event, at around 50-52 thousand years ago, in this case the scenario at 52 thousand years before present has been selected. The growth season at this time was greater, measuring on average 2353 GDD5, than at later periods of the glaciation, from 34-19 thousand years ago where the GDD5 measure less than 2250 on average. Temperatures were higher, the MTCO is -16.3°C on average, compared to later glacial averages, from 44 thousand years ago to the LGM where were under -17°C (Fig. 2.3.1). There was also increased moisture availability, with a mean of 0.680 AET/PET across the northern hemisphere, similarly high moisture availability is not observed until 32 thousand years before present. This warmer and wetter climatic scenario in the midst of the glaciation is likely to have had an effect on the availability of suitable climate for the species being modelled. During both these scenarios the sea-level is 80 metres below current due to the substantial amount of water locked up in the ice-sheet during the glaciation.

Heinrich Events occurred throughout the last glaciation and were caused by the breaking away and melting of icebergs from the Northern hemisphere ice sheets releasing large quantities of cold water into the North Atlantic Ocean, this is thought to have altered the thermohaline circulation patterns of the ocean and coincided with global reduction in temperature. In total five of these events were modelled, and here the Heinrich Event 5 has been selected which occurred around 45-46 thousand years ago. The cold freshwater influx into the ocean system lead to the growing season being dramatically shorter throughout the

northern hemisphere, only 1995 GDD5, compared to the scenarios preceding, 2292 GDD5, and post, 2338 GDD5, the Event (Fig. 2.3.1). There was also a drop in the mean northern hemisphere temperate to just -20.2°C MTCO compared to the scenarios before (-17.1°C) and after (-16.8°C) the ice sheet melt water influx. The moisture availability also reduced significantly during the Heinrich Event, to just 0.623 AET/PET, the normal glacial conditions range between was 0.67 and 0.68. Although the Heinrich Events resulted in an extreme reduction in growing season, precipitation and temperature, it is important to note that they were temporally short lived lasting around 750 years maximum (Maslin *et al.*, 2001).

The Last Glacial Maximum (LGM) conditions were selected as the scenario at 21 thousand years before present and marks the time of maximum ice sheet extent in the most recent glacial, when temperatures were significantly cooler than present, approximately 11.4°C lower, with a MTCO of -17.9°C on average in the Northern hemisphere (Fig. 2.3.1). The growth season was also shorter on average being 2209 GDD5, over 800 degree days lower than the present average. It was also drier than present day with the moisture availability averaged at 0.678 AET/PET. At this time, the substantial ice sheets in the Northern hemisphere, the Laurentide ice sheet covering much of North America and the Weichselian ice sheet in northern Europe, also meant that sea-levels were at their lowest during the last glaciation, at 120 metres lower than the current sea-level.

The scenario selected for the beginning of the Holocene was that attributed to 10 thousand years before present. At this time the climatic conditions were beginning to warm post-glacial but were still cooler and drier than present day. The average growing season in the northern hemisphere was 2852 GDD5, shorter than the present day (3035 GDD5), and the MTCO was -10.1°C significantly cooler than the post-industrial present minimum temperature of -6.5°C (Fig. 2.3.1). The average moisture availability was 0.699 AET/PET, lower than the present day value by 0.011 (0.710 AET/PET) indicating overall drier conditions at the beginning of the Holocene compared to present day. The ice sheets were significantly larger at the beginning of the Holocene than the current size of the ice sheets so the sea-level was 38 metres lower than the present sea-level.

Section 2.4

Modelling Approaches

Three different approaches were used for modelling the species' distributions based on their bioclimatic niche; maximum entropy (Maxent), generalised additive (GAM) and climatic response surface (CRS) models. Each of the models related the gridded distributions of species (or aggregated species groups) and the bioclimatic data to produce the modelled species' specific niches which could then be applied to re-simulate present day distributions as well as for retrodiction using the palaeoclimate datasets.

Maxent (Phillips & Schapire, 2005) was developed as an approach for modelling habitat suitability with presence-only records (Phillips *et al.*, 2004), such as Natural History museum collections, where specimens only denote presence at those locations, or for establishing the extent to which a species with few observations may potentially be found, where modelling of this kind offers the most valuable insight into habitat suitability and future conservation (Papeş & Gaubert, 2007, Kumar & Stohlgren, 2009, Thorn *et al.*, 2009). Maxent's origins lie in the statistical mechanism, maximum entropy, first explained by Jaynes (1957); the principle is based on an axiom that states that the best representative probability distribution for current knowledge, taking into account known constraints, is the one with the highest entropy.

The species' distribution modelling programme Maxent uses the presence data and the background covariates, in this case based on the bioclimate data, (Elith *et al.*, 2011) to estimate the ratio of probability densities for covariates where the species is present, compared to background covariate probability densities. This ratio is the primary output generated by Maxent for the extent of the background data; in essence it is a measure of the likelihood of presence in relation to a completely random species' distribution. During this process the relationship of the species to the inputted climatic data is assessed, but as the species' response to environmental variables is generally of greater complexity than a simple linear relationship, it is often desirable to fit nonlinear functions (Austin, 2002). Maxent's model matrix is augmented with a number of fitting function features including; linear, quadratic, product, which takes into account interactions between variables: threshold, which establishes values above or below which conditions were unsuitable; and categorical, the constraints of classed data on species presence (not relevant in the datasets used for this study) (Phillips *et al.*, 2006).

In both the case of the data used for *Loxia* and that of the aggregated conifer distributions, they denote species range, therefore representing a described presence based on a combination of records and generalised understanding of habitat suitability and so can be effectively treated as presence-only data.   Based on this assumption, the use of Maxent as a modelling tool seems acceptable, especially when this data compilation is compared with more stringent data sets used for such modelling, for example the EBCC data, which are based on direct observation of presence and absence in each specified region as well as 'no-data' locations, where sampling has yet to occur.   However, for the other two modelling techniques, GAMs and CRSs, presence and absence were needed to inform the models, and although the bird and conifer distributions were only records of presence ranges, they were considered to be of suitable accuracy, the product of aggregated expertise and encompassing of their full range limits, that, for the case of these models, the lack of ascribed range potential was inferred as an absence.

A java-based interface Maxent package (ver. 3.3.3e) developed by Phillips and Schapire (2005) was used in this study to model the distributions of all the species and genera.   The precise method by which the Maxent modelling was conducted and examples of data input can be found in the Appendix: Maxent.

Generalised additive models (GAMs) are semi-parametric extensions of generalised linear models (GLMs) (Guisan *et al.*, 2002), their underlying assumptions being that the functions are additive and all the components are smooth.   GAMs, like GLMs, allow for non-linearity and inconsistency in data structural variance, thus avoiding forcing the data into unnatural scales like simplistic linear models might (Hastie & Tibshirani, 1990).   The flexibility of GAMs and GLMs means they are considered more suitable for modelling and analysis of complex ecological relationships than the classical Gaussian distributions (Austin, 1987). GAMs assume a relationship, often referred to as a 'link function', between the response variable mean and a 'smoothed' function for the set of explanatory variables.   There is a range of assumed probability distributions that can be fitted to the data including normal, (negative) binomial, Poisson or gamma distribution, often producing a better fit for the non-normal errors observed in ecological data (Guisan *et al.*, 2002).   The ability of GAMs to deal with responses that have non-linear and non-monotonic relationships to the effecting variables is their great strength and has lead to GAMs often being referred to as "data-driven" rather than model-driven.

R (version 2.12.1) (R Development Core Team, 2011) was used for fitting the GAMs for this study and a particular integrated package called mgcv was used to run the GAMs. Mgcv (Wood, 2000, 2003, 2006, 2011) package provides the tools to run GAMs with an inbuilt model selection methodology, where the degrees of freedom for each smoother term fitted in the model are simultaneously selected by a process of minimising the generalised cross validation (mgcv) across the whole model rather than the components individually (Wood, 2001), and uses penalised regression splines in its model selection process (Wood & Augustin, 2002). With the package providing a competent selection process for modelling the relationship observed between the species presence/absence and the bioclimatic data, the user is required only to define the probability distribution expected for the environmental variables; in the case of the bioclimatic data being used, this was defined as a binomial probability distribution. The package also contains an inbuilt prediction model, which takes the fitted GAM and produces predictions based on a new (or same) set of environmental values, in this case the output was specified as "response", rather than just producing the linear predictor (positive values denoting greater likelihood of presence, negative denoting absence), the output is automatically transformed to probability of presence values between 1 and 0 (similar to the outputs of Maxent and CRS). This transformation was carried out by taking the exponential (to the base e) of the linear predictor and dividing this by the total of the exponential of the linear predictor plus 1 (Equation 2.4.1). Details of method and date input format and examples can be found in Appendix: GAM.

Equation 2.4.1:

$$\frac{e^{\,linear\,predictor}}{1 \;+\; e^{\,linear\,predictor}}$$

Climatic response surface (CRS) model uses both the presences and absences of the species to fit a three-dimensional response surface based on the bioclimatic values related to the presence/absence data (Huntley *et al.*, 1995, Huntley *et al.*, 2006). The models use locally-weighted regression (Cleveland & Devlin, 1988) to fit the response surface, with the fitted values representing the probability of species' occurrence at a location with that particular combination of climatic variable values (Huntley, 1995). Fitted values were evaluated in climatic space using regularly spaced 'nodes' in a 64 x 58 x 41 grid (GDD5 x MTCO x AET/PET), with the intervals between grid points being 150 degree days (GDD5), 1.5°C (MTCO) and 0.025 (AET/PET) respectively. The fitting was evaluated at each of the individual nodes on the bioclimatic axis using a moving window, with dimensions of

300 degree days (GDD5), 3°C (MTCO) and 0.1 (AET/PET) (Huntley, 1995, Huntley *et al.*, 2006).   The probability of species occurrence was evaluated at each of the nodes; this was calculated using the inverse distance weighted means of the observed species' occurrence probabilities for all cells falling within the nodal fitting window.   These distance weightings used a combination of Euclidean distance of the climatic variables in three-dimensional space (Huntley *et al.*, 2007), along with weights calculated using the tricube function (Huntley *et al.*, 1989).   In this way, data points closest to the node were given a stronger weighting than those on the periphery of the fitting window.   Probabilities of occurrence at each of the nodes were, as with Maxent and GAMs, scaled with '1.0' denoting certainty of presence and '0.0' an absence, or climatic unsuitability.

Simulations of present and past occurrence probability were established by applying the fitted response surface to the bioclimatic datasets for each scenario.   For any given combination of the three bioclimatic variables, the probability of species' occurrence is obtained through interpolating between the response surface nodal probability values surrounding the target location in the three-dimensional bioclimatic space (Huntley *et al.*, 2007).   This interpolation was carried out in a similar manner to the surface fitting, using inverse distance tricubic weighting, applied to all the nodal points that fall within the defined fitting window centred on the target bioclimatic locality.

CRSs were fitted using a FORTRAN programme, written originally by P.J. Bartlein and modified by B. Huntley, running in a Unix environment.   Further details on the method, date input and examples can be found in Appendix: CRS.

The fitted models produced are three-dimensional, as they are based upon three bioclimatic variables, and thus are difficult to visually represent on paper.   If there were only two variables, then the fitted model could be relatively easily represented on a square grid map with the two variables along the vertical and horizontal axes, and differential shading of the grid squares according to the probability of occurrence associated with the two specific variable values to represent the species' 'bioclimatic space'.   To represent the three dimensional fitted model, sections can be taken set at thresholds of the third variable and displayed as a series of panels.   In the case of the CRS model, the panels are set for specific AET/PET values, in this study 8 intervals were taken between 1.000 and 0.400, and each panel has axes represent increasing MTCO and GDD5, with differential shading representing the probability of occurrence.   Note, no shading means no present climate in the models exists with these variable conditions.   These 'bioclimatic space' representation have been

used to illustrate the CRS fitted model in previous studies by Huntley *et al.* (2007) and were produced in this study from the CRS model fits by Y.C. Collingham.

All three modelling techniques fit the climatic niche in relation to the present climate; however many of the palaeoclimatic scenarios will have conditions, or combinations of climatic variables, which do not occur today, known as non-analogous conditions. In cases of non-analogous climatic conditions the species' distribution model has to be extrapolated to produce predictions in these novel scenarios. Each of the models in this study uses a different method of extrapolating (Fig. 2.4.2). Maxent extrapolation method is dependent on fitting function selected for the bioclimatic variable which is often down automatically, for instance a quadratic fitting

Figure 2.4.2: A summary of the different methods of extrapolation in 'no-analogue' environmental conditions used by maximum entropy (Maxent – BLUE), generalised additive models (GAM - YELLOW) and climatic response surface (CRS - RED) model.

function (Fig. 2.4.2) may result in an extrapolation which could predict a decline initially in probability of occurrence into novel conditions but then an increase without any data to drive this prediction. Maxent, but more commonly GAM, can extrapolate in a linear fashion, but this too has the risk of assuming that the relationship observed between the species and the environmental variable continues relative to increasing or decreasing conditions. CRS extrapolates using the same probability threshold of the closest variable conditions to the new novel climate, which is a more conservative method of predicting into novel environments. The differing methods of extrapolation are likely to have an effect on the simulated distributions produced by each of the modelling techniques.

In all cases, the three species' distribution models produce a species' probability of occurrence, rather than a definitive absence or presence. In order to determine presence/absence, a probability threshold had to be established for each individual species and model used, where probability values greater than the threshold infer a predicted presence and those below the threshold value, an absence.

Section 2.5

Model Thresholds and Evaluation

Until recent times, many of the species' distribution studies used an arbitrary threshold of 0.5 for the probability of occurrence, although there is little technical justification for this. Huntley *et al*. (1995) developed a method where the 'goodness of fit' is used to establish a threshold value. This approach involves using the present probabilities of occurrence, simulated with the same bioclimatic data used to drive the initial model, and comparing them with observed presences and absences originally inputted into the model (Huntley *et al.*, 2004, Huntley *et al.*, 2007). This is tested by experimentally setting the threshold at 1000 step intervals (of 0.001) from 0.0 to 1.0, with each of these probability thresholds and their inferred presence/absences being tested against the source observed data.

To assess the '**goodness of fit'**, and thus determine the best probability threshold for the distribution model, a measure needed to be used that would take into account each of the experimental thresholds of predicted presence and absence and evaluate their similarity to the observed data. Most of these 'goodness of fit' measures are based on a 'confusion matrix' (Table 2.5.1); from these values there are a selection of measures which may be derived and Manel *et al*. (2001) assessed their varying advantages and disadvantages. The Cohen's κ (Cohen, 1960, Equation 2.5.1) was selected as the most appropriate measure of this and has been used with great success in a number of species' distribution studies (Prentice *et al.*, 1992, Huntley, 1995, Loiselle *et al.*, 2003, Petit *et al.*, 2003, Segurado & Araújo, 2004, Huntley *et al.*, 2006, Huntley *et al.*, 2007, Huntley *et al.*, 2008).

Model Predictions	Observations	
	Present	Absence
Present	*a*	*b*
Absent	*c*	*d*

Table 2.5.1: A confusion matrix for evaluation the 'Goodness of fit' for a model compared to the observed data.

Equation 2.5.1: (Sourced from Huntley *et al.*, 2007)

$$\kappa = \frac{(\varphi_o - \varphi_e)}{(1 - \varphi_e)}$$

Where:

$$\varphi_o = a + d$$
$$\varphi_e = ((a+c) \times (a+b)) + ((b+d) \times (c+d))$$

Cohen's κ has several advantages; most crucially it takes into account the possibility that the predictions are correct by mere chance alone, and thus measures the extent to which the model outperforms a random assignment of the same proportions of presence and absences for the grid cells being mapped. The κ values were compared across all the one thousand 0.001 intervals of probability and the threshold with the maximum κ value was selected. In the case of ties, where thresholds gave the same maximum κ value, the lowest of these probability thresholds was taken (Huntley *et al.*, 2007). These probability values were then used to set the presence/absence thresholds for mapping of the simulated distributions.

The precise method, data input formats and examples of how the maximum κ values were calculated can be found in the Appendix: Maximum κ value. The 'goodness of fit' and performance of the model in relation to the maximum κ value obtained, were reviewed using assessment criteria based on the work of Monserud (1990; Table 2.5.2).

Maximum κ value	Model Performance
$\kappa \geq 0.85$	excellent
$0.7 \leq \kappa < 0.85$	very good
$0.55 \leq \kappa < 0.7$	good
$0.4 \leq \kappa < 0.55$	fair
$\kappa < 0.4$	poor / very poor

Table 2.5.2: Assessment criteria for the model performance based on the maximum κ value obtained when simulated present probabilities of occurrence were compared to the 'real' observed presences. (Monserud, 1990)

However, although Cohen's κ value is good for establishing the probability threshold to produce the 'best' simulation, it is not the most accurate value to establish the 'goodness of the fit' as it is strongly affected by the prevalence of the species being modelled. Another measure which is less sensitive to the species' prevalence, is a calculation of the area under the curve (AUC) for a receiver operating characteristic (ROC) plot of sensitivity against 1-specificity generated for all threshold probability intervals (Metz, 1978). When generating the ROC plot, sensitivity is termed as the proportion of true positives correctly predicted, and specificity as the proportion of true negatives accurately predicted. In terms of the confusion matrix; sensitivity is *a/(a+c)* and specificity is *d/(b+d)*. The performance of the model in relation to the AUC measure was established in work published by Swets (1988; Table 2.5.3).

AUC	Model Performance
AUC > 0.9	high
0.7 < AUC ≤ 0.9	useful
0.5 < AUC ≤ 0.7	low

Table 2.5.3: Assessment criteria for the model performance based on the area under curve (AUC) value from a ROC plot obtained when simulated present probabilities of occurrence were compared to the 'real' observed presences (Swets, 1988).

In this study AUC was calculated by deriving the specificity and sensitivity from the same output file used to generate the κ and other 'goodness of fit' measures. The ROC plots were then calculated from these gleaned values in a specifically developed C programme run in an Unix environment and the AUC values outputted. In addition, the left-most portion of the area under the curve (LAUC) (Zhang *et al.*, 2010), which sometimes reports better performances for models with highly specific rule sets, was also reported but in the case of this study the difference between LAUC and AUC was nominal (0.000001) if any variance between values was observed at all.

To assess the **robustness** of the models, there are several techniques commonly used in species' distribution modelling. In each case, the process involves the omitting of a selection of the original observed species' dataset in the generation of the niche-model and assessment of difference and variance in goodness of fit of the simulation produced from this more limited dataset. The use of these approaches is meant to account for the autocorrelation that may occur from neighbouring grid cells sharing greater similarity in the data values observed and thus having a greater weighting in model fitting. One of the methods frequently used is the 'leave one out' approach, which, as entitled, involves the removal of a single item from the dataset and then the simulation of this point using the model fitted to the rest of the dataset.

However, this technique is highly computationally intensive with large datasets and is relatively weak, with very few of the individual data points not actually being rendered redundant in relation to neighbouring autocorrelation. The other commonly used method is split datasets, to form one dataset for model fitting and another for evaluation, to assess the predictive ability of the limited 'training set' used. This splitting is often done sequentially or at random and so is considered to produce 'optimistic' results as it is likely that autocorrelation will still have an effect. Although regionally splitting may overcome some of the autocorrelation issues, it may in fact produce overly 'pessimistic' assessments of the model robustness as not all the climatic niche may be included in the sample as climates are

unique to a region.   In rigorous studies a combination of these robustness test methods is used to best reflect the size of the distributions being modelling and to minimise effects of autocorrelation (Huntley *et al.*, 2012).

In this study, a data splitting approach was undertaken where at random 70% of both presences and absences from the dataset, the 'training set', were used to form the model. This 'training set' model was then used to simulate the range of the 30% of climatic data excluded from the initial model, the 'evaluation set'.   The simulation of the 'evaluation set' was then compared to the observed data of the species' presence and absence to determine how well the model had performed.   These comparisons were made in the same way that the present day simulations made using 'complete' models were assessed, using their maximum κ value and AUC scores.   Data splitting replicated a hundred times for each species and model type so that a mean and variance of maximum κ value and AUC could be estimated allowing comparison between models and with the original species' 'full model' 'Goodness of fit' measures to ascertain the model robustness.   This method was carried out on all the species and genera extensively modelled in this study, even on the more limited distributed species and across all modelling techniques so that direct comparisons could be made.

Section 2.6

Modelling Grid Extent

The model grid extent can evidently have a great effect on the ability of the species' distribution niche-models produced. The model resolution (Guisan & Thuiller, 2005, Austin, 2007), as well as species range size (McPherson *et al.*, 2004), have been noted to affect performance of species' distribution models. *Loxia curvirostra* and *L. leucoptera* have ranges that span the whole of the Northern hemisphere; however, the other three recognised Crossbill species have much more limited distributions. *L. pytyopsittacus* is found only in northern Europe, while *L. scotica* is found only in Scotland, and *L. megaplaga* only on Hispaniola. It is likely that these restrictions are not just climate driven but also geographically constrained; there is also the possibility of competition with the other extant species limiting their range size. With this in mind, it may not be suitable to use such an extensive grid, comprising the majority of the Northern hemisphere, for modelling those species with more restricted distributions. It is likely that climatic conditions in other regions, especially at similar latitudes on neighbouring continents, are just as suitable for the species but are inaccessible due to hostility of climate or habitat between the regions.

This is important to bear in mind for the GAM and CRS models, which use the (inferred) species absences to form the fitted model and therefore could be incorrectly restricting the modelled species bioclimatic-niche. This is a lesser issue for the Maxent models, as this works primarily with the presence-only data to form the fitted model for the bioclimatic variables. Nevertheless this is an important factor for all the modelling procedures when the goodness of fit and probability thresholds are established, as the simulated probability of presences are highly likely to attribute high values to climates which are analogous to those where the species is found but have restricted colonisation potential, known as an error of 'commission'. As such, the 'goodness of fit' measures will define these as false positives which in turn will affect the allocation of probability thresholds and the assessment of overall model performance.

There is also a likelihood of omission errors, where the model simulates a low probability of occurrence when in fact the species is present. This often occurs when the species has a restricted distribution that occupies a climatic niche which is found abundantly elsewhere but is absent of the species due to geographical or other reasons. In these cases the larger number of absences results in a dilution of the presences and therefore a lower simulated probability of occurrences. In both the cases of errors of 'commission' and 'omission' the

net effect is poor 'goodness of fit' and usually a low threshold probability of occurrence. Indeed, the latter is often considered a diagnostic of a restrict distribution which has been fitted to too extensive a dataset.

In order to reduce the risk of this and in turn improve the models produced, a grid of smaller extent were also generated, encompassing the distributions of the species with more limited range but still including a range of unoccupied regions, so that a suitable gradient of bioclimatic variables is sampled.   For *L. scotica* and *L. pytyopsittacus*, a grid was used that was restricted to Europe, spanning from 30°N to 75°N and 30°W to 75°E to include the full ranges of both species.   For the Hispaniolan resident, *L. megaplaga*, the grid encompassed much of the Caribbean and areas of Central America, extending from 10°N to 30°N and 90°W to 60°W, again encompassing the entire range of *L. megaplaga.*

The models were run as described above, but using these smaller grids for presence/absences and climatic values, as well as for simulating the past distributions of these three species. 'Goodness of fit' and robustness were also tested for comparison with the more extensive grid models generated for the same species using the methods outlined above.

Section 2.7

Mapping

Producing maps of the predicted distributions was not only essential in determining how well the model had performed in its re-simulation of the present day range but, more importantly, for observing and interpreting the past movements of Crossbills and their feeding trees and the insight this may provide into their evolutionary history.   In order to generate visually the simulated distributions, the probability of occurrences for each scenario were mapped using ArcGIS (ESRI, 1998), with the model probability thresholds used to determine whether the species is mapped as present or absent.   Further information on the methods, data input and examples of the way in which the distributions were mapped can be found in Appendix: Mapping.

As mentioned above, the sea level has changed significantly throughout the palaeoclimatic interval being studied.   In order to map the distributions effectively, this had to be taken into account.   The sea-level estimates are based primarily on data published by the INTegration of Ice core, MArine and TErrestrial records (INTIMATE) group (Walker *et al.*, 1999, Lowe *et al.*, 2008) (Table 2.7.1).   These changes in sea-level were mapped using GEBCO (IOC *et al.*, 2003) to define an overlay 'sea' which was placed on top of the simulated output in order to mask any distributions which would have been unfeasible.

Age (cal. kyr BP)	Sea level (metres below present)
0-4	0
5	7
6	8
7	11
8	16
9	26
10	38
11	56
12	66
13	70
14-15	88
16-18 (Heinrich 1)	104
19-20	115
21-22	120
24 (Heinrich 2)	112
26	100
28-60 (Heinrich 3-5)	80
100-120	0

Table 2.7.1: The estimated sea-levels below present day for present day to 120,000 years before present (BP) (Fairbanks, 1989, Bard *et al.*, 1990, Walker *et al.*, 1999, Lowe *et al.*, 2008)

This sea-level change was as a result of the glaciation that occurred during the course of the palaeo-interval being investigated. The glaciation also placed constraints on the population due to the large ice sheets covering many northerly latitudes. It was therefore important to include these ice sheets, where the likelihood of presence was low even if climate may have been suitable, mainly on the edges. The ice sheets used in the mapping were provided by Ehlers and Gibbard (2007) and were overlaid on top of both the simulated distribution and sea, to produce a realistic representation. Unfortunately, these ice sheet maps are available only for a limited number of intervals. The 'Younger Dryas' ice extent therefore was used to represent ice sheets from 12 to 20 thousand years before present and the 'Last Glacial Maximum' ice extent used for 21 to 60 thousand years ago.

The manual mapping in ArcMap produced high resolution outputs, primarily for inclusion in write-up and therefore it was not practical to apply this intensive and time-consuming process to all the simulations produced. Instead, automapping was conducted in Arc's Grid package to produce simple representations of the large quantity of simulated distributions (+1000). Methods are outlined in the Appendix: Automapping.

CHAPTER 3 – Results

Section 3.1

Species' Distribution Model Performance

'Goodness of Fit'

The maximum κ values obtained for *Loxia* species using the three different species' distributions modelling techniques varied greatly in value with the species modelled, however across the three modelling techniques, the climatic response surface (CRS) models produced the highest maximum κ values for all the *Loxia* species compared to the values calculated for the generalised additive models (GAM) and maximum entropy (Maxent) model simulation (Table 3.1.1). *Loxia* species all achieved 'fair' or higher assessments for their maximum κ values (Methods: Table 2.5.2).

| | No. of grid cells from which | 'Goodness of Fit' Measure | | | | | |
| | | Maximum κ value | | | AUC value | | |
Species	**recorded**	**Maxent**	**GAM**	**CRS**	**Maxent**	**GAM**	**CRS**
Loxia curvirostra	14963	0.641	0.658	**0.790**	0.923	0.923	**0.970**
L. leucoptera	10548	0.713	0.703	**0.767**	0.953	0.949	**0.972**
L. pytyopsittacus	2409	0.612	0.602	**0.680**	0.977	0.976	**0.985**
L. scotica	23	0.550	0.171	**0.591**	**0.999**	0.997	**0.999**
L. megaplaga	10	0.022	0.047	**0.476**	0.986	0.993	**0.999**

Table 3.1.1:   The 'Goodness of Fit' measures for the *Loxia* species.   The number of 0.5° by 0.5° grid cells the *Loxia* species is recorded in and the maximum κ and Area Under Curve (AUC) values, obtained for the species modelled using the three different species' distribution modelling techniques: maximum entropy (Maxent), generalised additive model (GAM) and Climatic response surface (CRS) using the north hemisphere bioclimatic grid.   **Bold highlights the highest maximum κ and AUC values attained for that species.**

Initial modelling of the feeding tree species individually using CRS, already identified as the best performing of the models by7 previous work with *Loxia*, indicated that the 'goodness of fit' varied greatly within conifer genera (Appendix: Table 1), the maximum κ values for *Larix* ranged between 0.386-0.818, *Picea*; 0.189-0.714, *Pinus*; 0.213-0.768, *Pseudotsuga*; 0.285-0.596, *Tsuga*; 0.470-0.634.   The high incidence of scores for CRS which are considered 'poor' would either necessitate the exclusion of those species that demonstrate low 'goodness of fit' or a merging of the species into their genus.   In this case genus conifer grouping was selected as the low 'goodness of fit' measures obtained for individual species are likely to be a result of analogous climates elsewhere in the world, which may in fact be occupied by other closely related but geographically isolated species from the same genus.   Having just five

genera of conifers is less labour intensive than modelling over 60 species and the genera models produced maximum κ values which were all at least 'good' fit.   In addition, the specialism of crossbills on conifers is often only discussed at a genus level or their feeding trees span a wide variety of species (Tables: 1.1.2, 1.1.3 & 1.1.4).   The exceptions of sole specialism are *Loxia scotica* and *L. pytyopsittacus* on *Pinus sylvestris*, and *L. megaplaga* on *P. occidentalis*.   So in addition to these *Pinus* species inclusion in their genus model, they were also modelled separately. *Picea abies*, which is the most common and widely spread of Spruces in Eurasia, was also modelled separately due to the high individual maximum κ value it achieved.

The CRS models for *Loxia* and the refined tree species/genera produced maximum κ values ranging between 0.476-0.828 (Table 3.1.1 & 3.1.2), while both Maxent and GAM were significantly lower.   Therefore from these results the CRS model appeared the most successful at producing a bioclimatic niche, simulating the present ranges of greatest similarity to the observed.   The CRS model produced maximum κ values of a 'very good' fit between 0.7 and 0.85 for *Loxia curvirostra*, *L. leucoptera*, and the genera of *Larix*, *Picea* and *Pinus*.   These all have large ranges spanning across the northern hemisphere and are recorded in over 10,000 grid cells, generating climatic niche models which produced simulations of greatest similarity to the observed distributions.   In addition to these, the

| Species | No. of grid cells from which recorded | 'Goodness of Fit' Measure | | | | | |
| | | Maximum κ value | | | AUC value | | |
		Maxent	GAM	CRS	Maxent	GAM	CRS
Larix spp.	13202	0.770	0.777	**0.828**	0.936	0.964	**0.981**
Picea spp.	14962	0.746	0.742	**0.805**	0.701	0.948	**0.975**
Pinus spp.	11405	0.574	0.551	**0.707**	0.896	0.886	**0.953**
Pseudotsuga spp.	1322	0.352	0.313	**0.578**	0.946	0.930	**0.982**
Tsuga spp.	2379	0.385	0.393	**0.612**	0.945	0.944	**0.980**
Picea abies	8478	0.653	0.640	**0.714**	0.947	0.945	**0.966**
Pinus sylvestris	6723	0.603	0.584	**0.675**	0.936	0.931	**0.964**
Pinus occidentalis	23	-	-	0.264	-	-	0.997

Table 3.1.2:   The 'Goodness of Fit' measures for the tree genera/species.   The number of 0.5° by 0.5° grid cells the tree genera/species is recorded in and the maximum κ and Area Under Curve (AUC) values, obtained for the tree species/genera modelled using the three different species' distribution modelling techniques: maximum entropy (Maxent), generalised additive models (GAM) and climatic response surface (CRS) model using the north hemisphere bioclimatic grid.   **Bold highlights the highest maximum κ and AUC values attained for that species**.   Highlighted in grey is a species which was modelled using CRS on the northern hemisphere climatic grid which had such a low maximum κ value, 'very poor', that the other modelling techniques at this dimension were not carried out due to the likely continued poor performance.

Eurasia-restricted *Picea abies* also had a maximum κ value of 'very good' fit, 0.714, but it was recorded in 8,478 grid cells, the greatest range of the more restricted species.

The remaining species or aggregated genera had maximum κ values of a 'good' fit between 0.55 and 0.7, due in part to their more restricted distributions and the presence of analogous or similar climates resulting in increased simulations of pseudo-presences.   The only exceptions are *Loxia megaplaga* and *Pinus occidentalis,* both of which are constrained ranges on Caribbean islands, produced the lowest maximum κ values of 0.476 and 0.264 respectively, with *L. megaplaga* being considered as having a 'fair' fit and *P. occidentalis* exceedingly low value evaluated as 'very poor'.

It is widely discussed in the literature that maximum κ values are affected by the prevalence of the species (Guisan & Zimmermann, 2000).   Similarly in this study, the maximum κ values increase with the increase in the number of grid cells the species is recorded in (Fig. 3.1.1).   All the modelling techniques demonstrated this correlation, however CRS did not only produce higher maximum κ values, it also showed the lowest effect of species' range size on maximum κ values, the trend line having a gradient of just 0.0831 compared to Maxent's 0.1463 and GAM's 0.1997.   This indicates a lower effect of species' distribution
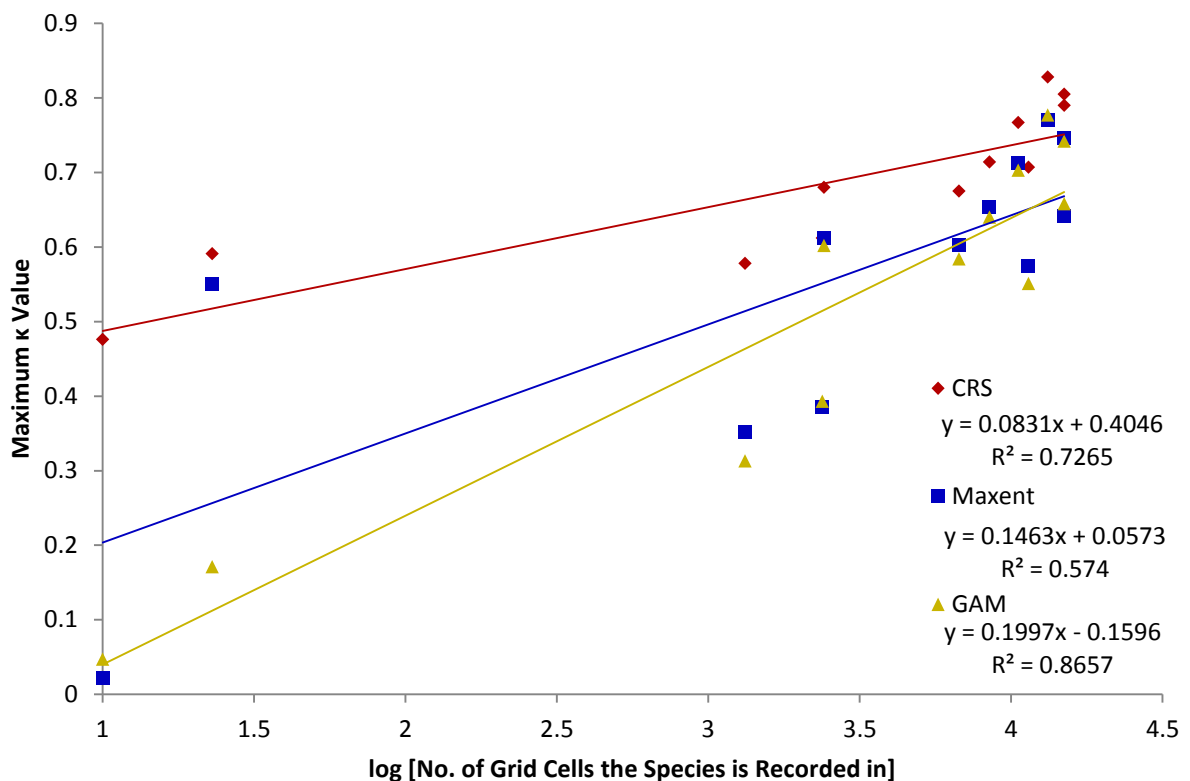
Figure 3.1.1:   The effect of species' range size, the number of 0.5° x 0.5° grid cells the species is recorded in, on the calculated maximum κ values for the three species' distribution modelling techniques; climatic response surface (CRS), maximum entropy (Maxent) and generalised additive model (GAM).
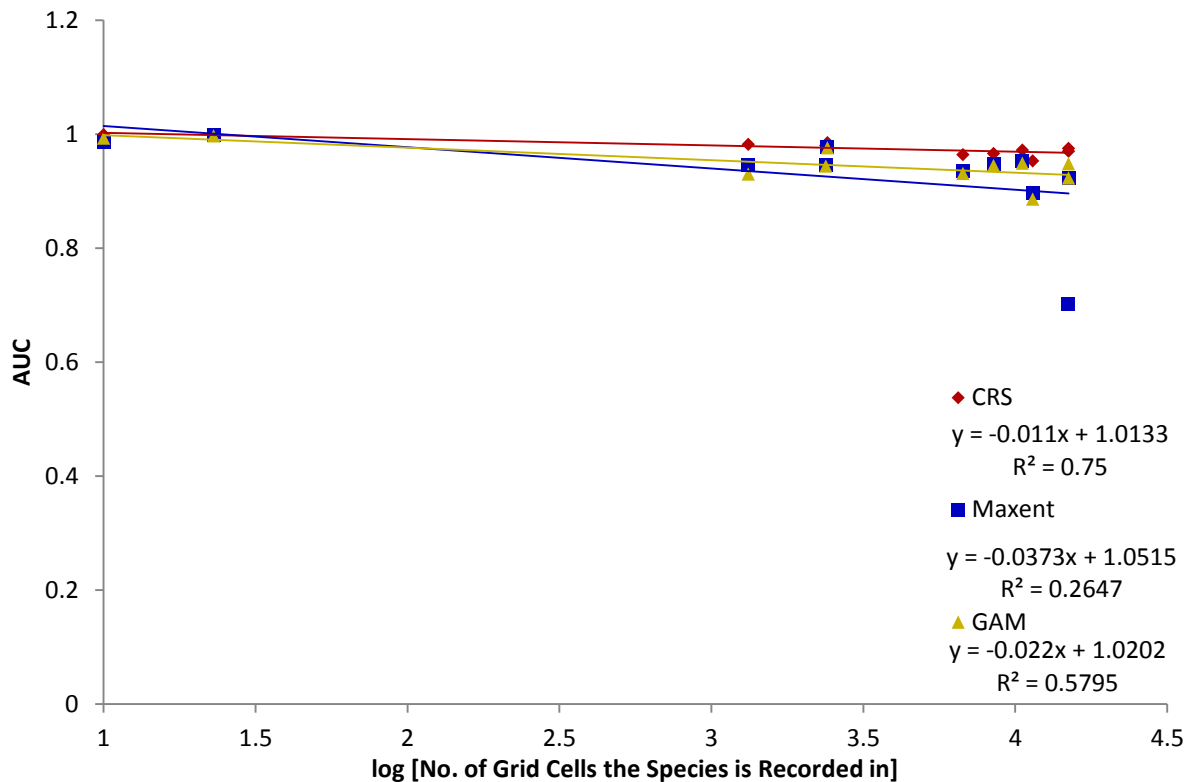
Figure 3.1.2:   The effect of species' range size, the number of 0.5° x 0.5° grid cells the species is recorded in, on the calculated Area Under Curve (AUC) values for the three species' distribution modelling techniques; climatic response surface (CRS), maximum entropy (Maxent) and generalised additive model (GAM).

size on the assessed maximum κ value than is observed for the other two modelling techniques.

The Area Under Curve (AUC) is a measure of 'goodness of fit' considered to be independent of species' distribution size, and this study demonstrated a similarly independent relationship (Fig. 3.1.2).   The correlation between AUC and species' record numbers was negative for all the species' distribution models, an increasing species' distribution resulted in a lower AUC but the gradients were negligible, –0.011 (CRS), -0.0373 (Maxent) and -0.022 (GAM), when compared to those observed from maximum κ values, indicating little or no effect of range size.   The AUC values obtained for all the species and genera modelled and across the three different modelling technique were all considered greater than 0.7 (Table 3.1.1 & 3.1.2) and thus considered 'useful' but the majority showed high model performance (Methods: Table 2.5.3), great than 0.9.   The highest AUC values were obtained for the CRS model across all species and genera.   Maxent also obtained the same value for one species, *L. scotica*, but did produce a value 0.274 lower than that obtained for CRS model (*Picea* spp.), while GAM produced AUC values which were between 0.002 and 0.067 lower than CRS.

In order to improve 'goodness of fit' of the bioclimatic niche models for the more limited distributed species, such as the Caribbean residents, *Loxia megaplaga* and *Pinus occidentalis*, and the European-restricted *L. pytyopsittacus* and *L. scotica*, models were applied to the smaller dimensioned grids for reasons discussed above (Section 2.6). In so doing this reduced the constraints of the climatic niche models produced by CRS and GAM, which use the absences to form the model and so the smaller grid excludes climates that may in fact be suitable but are geographically isolated. This also reduces the incidence of pseudo-presence simulations in these areas of analogous climates when using the model to predict the present range. This should increase the 'goodness of fit' measures obtained and in turn provide more reliable probability thresholds used to define the presence/absence of the species. The

		'Goodness of Fit' Measure					
		Maximum κ value			**AUC value**		
Grid	**Species**	**Maxent**	**GAM**	**CRS**	**Maxent**	**GAM**	**CRS**
European	*Loxia pytyopsittacus*	0.800	0.822	**0.861**	0.976	0.978	**0.987**
	L. scotica	0.682	0.680	**0.702**	**0.999**	**0.999**	**0.999**
Caribbean	*L. megaplaga*	0.305	0.393	**0.690**	0.931	0.950	**0.992**
	Pinus occidentalis	0.264	0.253	**0.594**	0.844	0.854	**0.951**

Table 3.1.3: The 'Goodness of Fit' measures, maximum κ and Area Under Curve (AUC) values, obtained for the European and Caribbean restricted species modelled using the three different species' distribution modelling techniques: maximum entropy (Maxent), generalised additive models (GAM) and climatic response surface (CRS) using the smaller dimensioned European and Caribbean grids.
Bold highlights the highest maximum κ and AUC values attained for that species.

resulting maximum κ values from these smaller grids were much improved from the initial values obtained using the northern hemisphere grid (Table. 3.1.3).

In the case of the European species, across all the modelling techniques, both the maximum κ and AUC values improved and CRS again was the best performing of the models. The CRS maximum κ values for both *Loxia pytyopsittacus* and *L: scotica* improved from 'good' values, of 0.680 and 0.591 respectively, to 0.861 and 0.702, measurements for a 'very good' fit. AUC values, which were high for the original larger grid, were also 'high' but improved in value for smaller grids, and in fact Maxent, CRS and GAMs produced AUC values of 0.999, indicating a very good fit of model.

The Caribbean grid improved the maximum κ value of *Loxia megaplaga* across all three modelling techniques, similarly CRS outperformed the other two models which only achieved 'poor' scores and improved *L. megaplaga* model's 'fair' fit with the large grid to a 'good' for the smaller. In a similar manner, *Pinus occidentalis*, although not modelled using all three

techniques on the larger grid, obtained a 'good' maximum κ value for the smaller dimensioned bioclimatic grid using the CRS model, a significant improvement on the 'very poor' initial value from the large grid model, while Maxent and GAM produced 'poor' values even for the smaller grid. From these results it appears the climatic niche model is significantly improved when the Caribbean species are modelled on the more restricted grid. However, the AUC values are lower for *L. megaplaga* and *Pinus occidentalis* on this smaller grid but all models still produce values of a 'high' assessment and again CRS outperforms the two other modelling techniques.

In all cases, when 'goodness of fit' was tested for all three modelling techniques, the simulations that performed the best were produced by CRS. In addition the model performance improved when species with more limited distributions were modelled on the smaller grids specific to their ranges. Therefore, although all the species and genera were simulated using all three modelling techniques and grid sizes (except *Pinus occidentalis* which is only modelled on the smaller Caribbean grid with all three modelling techniques), the CRS and smaller relevant grid simulations were selected for description and analysis in the study.

Robustness

Initial assumptions prior to testing were that Maxent, which is designed for projecting into areas which have yet to be sampled similar to the test scenario, would perform the best out of the models and that it would be likely that the CRS would have a low robustness due to its propensity to over-fit to the distribution data provided resulting in it not being as capable to predict in unsampled climates, although there is no previous work that compares these three modelling techniques to affirm these assumptions. However, the k-cross validation tests for robustness indicate that CRS is a surprisingly robust model compared to the other two modelling techniques.

When the *Loxia* species are modelled on the larger northern hemisphere grid extent, the maximum κ values obtained for the tests were higher on average for the CRS model than the other modelling techniques, and the difference of these values from those attained for the original models was the smallest in two of the cases, *L. curvirostra* and *L. leucoptera*. For *L. pytyopsittacus* the CRS model had the second lowest difference with Maxent showing no difference in its average robustness maximum κ value to value attained for complete model (Table 3.1.4). The other two species where CRS had high differences in maximum κ values calculated, were the more limited *L. scotica* and *L. megaplaga* where performance improved

| Species | Model | 'Goodness of Fit' Measure | | | | | |
| | | Maximum κ value | | | AUC value | | |
		Average	Difference	Standard Deviation	Average	Difference	Standard Deviation
Loxia curvirostra	Maxent	0.693	-0.052	0.009	0.927	**0.004**	0.003
	GAM	0.598	-0.060	0.014	0.874	-0.049	0.008
	CRS	**0.754**	**-0.036**	**0.005**	**0.959**	-0.011	**0.001**
L. leucoptera	Maxent	0.454	-0.259	**0.004**	0.822	-0.131	0.003
	GAM	0.412	-0.291	**0.004**	0.785	-0.164	0.003
	CRS	**0.756**	**-0.011**	0.006	**0.969**	**-0.003**	**0.001**
L. pytyopsittacus	Maxent	0.612	**0.000**	0.012	0.978	**0.001**	**0.001**
	GAM	0.611	0.009	0.012	0.977	**0.001**	**0.001**
	CRS	**0.676**	-0.004	**0.010**	**0.984**	**-0.001**	**0.001**
L. scotica	Maxent	0.575	0.025	0.130	**0.999**	0.002	**0.000**
	GAM	0.175	**0.004**	**0.045**	0.997	-0.002	0.001
	CRS	**0.627**	0.140	0.121	**0.999**	**0.000**	**0.000**
L. megaplaga	Maxent	0.006	-0.016	**0.002**	**0.946**	**-0.040**	**0.007**
	GAM	0.054	**0.007**	0.036	0.881	-0.122	0.156
	CRS	**0.120**	-0.356	0.120	0.738	-0.261	0.107

Table 3.1.4:   The average 'Goodness of Fit' measures obtained by k-cross validation tests of robustness for *Loxia* species   The average maximum κ and Area Under Curve (AUC) values for the 100 samples taken, the difference between these values and the complete species' distribution model value and the standard deviation of the measures across the 100 tests.   K-cross validation was conducted for the three different species' distribution modelling techniques: maximum entropy (Maxent), generalised additive models (GAM) and climatic response surface (CRS).   **Bold highlights the highest maximum κ and AUC values attained for that species, smallest differences and standard deviations**.

significantly in terms of the maximum κ value obtained for *L. scotica* CRS robustness models compared to that calculated for the full model, and dropped significantly for *L. megaplaga*. For both these species GAM demonstrated the least change in 'goodness of fit' of maximum κ value among the models but it should be noted its performance to begin was poorer than that of CRS.   The standard deviation for maximum κ values found across the 100 samples of k-cross validation conducted was lowest for CRS in two of the cases, *L. curvirostra* and *L. pytyopsittacus*, once for GAM solely, *L. scotica*, and Maxent, *L. megaplaga*, and both GAM and Maxent share the lowest value of standard deviation for *L. leucoptera*.

The AUC values also remain highest on average for the CRS model across all the species apart from *L. megaplaga*, which Maxent also achieves the same mean value and it also matches the CRS average AUC value in the case of *L. scotica*.   All three models produce the same difference between values attained in the testing stage to the complete model for *L. pytyopsittacus*, while CRS, for *L. leucoptera* and *L. scotica*, and Maxent, for *L. curvirostra* and *L. megaplaga*, both attain the smallest change in AUC values.   In the case of the standard deviation in the AUC values ascertained for the 100 replicates, CRS has the lowest for both *L. curvirostra* and *L. leucoptera*, and is equal in value to Maxent for *L. scotica*.

Both Maxent and GAM have the same standard deviation for *L. pytyopsittacus*, with Maxent producing the lowest variance solely in the case of *L. megaplaga*.

Overall it appears that the robustness of CRS is often greater than that of the other two models, and certainly the model performs better in a test scenario on average for *Loxia* species attaining the higher maximum κ values and AUC values in 9 out of 10 cases.   The more limited species appear to cause the greatest variation in performance of CRS compared with other species and this is also the case for the tree genus *Pseudotsuga*, attaining both the highest difference, for maximum κ and AUC values and largest standard deviation for maximum κ value (Table°3.1.5).   Despite this, across all the tree species and genera modelled on the large northern hemisphere spanning grid, CRS produces the highest average maximum κ value and AUC values and is not matched by the other models.   In four out of the seven tree species/genera CRS attains the lowest difference in maximum κ value and also the AUC, with GAM producing the least difference for both these measures of 'goodness of

| | | 'Goodness of Fit' Measure | | | | | |
| | | Maximum κ value | | | AUC value | | |
Species	**Model**	**Average**	**Difference**	**Standard Deviation**	**Average**	**Difference**	**Standard Deviation**
Larix spp.	Maxent	0.693	-0.077	0.009	0.927	-0.009	0.003
	GAM	0.598	-0.179	0.014	0.874	-0.090	0.008
	CRS	**0.815**	**-0.013**	**0.005**	**0.976**	**-0.005**	**0.001**
Picea spp.	Maxent	0.542	-0.204	0.007	0.833	-0.132	0.006
	GAM	0.387	-0.355	0.009	0.690	-0.258	0.009
	CRS	**0.784**	**-0.021**	**0.004**	**0.969**	**-0.006**	**0.001**
Pinus spp.	Maxent	0.538	**-0.036**	0.011	0.887	**-0.009**	0.004
	GAM	0.451	-0.100	0.014	0.852	-0.036	0.005
	CRS	**0.668**	-0.039	**0.005**	**0.938**	-0.015	**0.002**
Pseudotsuga spp.	Maxent	0.340	-0.012	**0.014**	0.944	-0.002	**0.003**
	GAM	0.317	**0.004**	0.015	0.930	**0.000**	**0.003**
	CRS	**0.459**	-0.119	0.017	**0.961**	-0.021	**0.003**
Tsuga spp.	Maxent	0.340	-0.045	**0.011**	0.948	0.004	**0.002**
	GAM	0.401	**-0.008**	**0.011**	0.948	**0.003**	**0.002**
	CRS	**0.579**	-0.033	**0.011**	**0.971**	-0.009	**0.002**
Picea abies	Maxent	0.574	-0.079	0.006	0.920	-0.027	**0.001**
	GAM	0.528	-0.112	**0.004**	0.907	-0.038	0.006
	CRS	**0.702**	**-0.033**	0.006	**0.962**	**-0.004**	**0.001**
Pinus sylvestris	Maxent	0.580	-0.023	**0.007**	0.928	-0.008	0.002
	GAM	0.560	-0.024	0.008	0.924	-0.007	0.002
	CRS	**0.658**	**-0.017**	**0.007**	**0.959**	**-0.005**	**0.001**

Table 3.1.5:   The average 'Goodness of Fit' measures obtained by k-cross validation tests of robustness for the tree species/genera   The average maximum κ and Area Under Curve (AUC) values for the 100 samples taken, the difference between these values and the complete species' distribution model value and the standard deviation of the measures across the 100 tests.   K-cross validation was conducted for the three different species' distribution modelling techniques: maximum entropy (Maxent), generalised additive models (GAM) and climatic response surface (CRS).   **Bold highlights the highest maximum κ and AUC values attained for that species, smallest differences and standard deviations**.

fit' for the two more limited distributed genera of *Tsuga* and *Pseudotsuga*, and Maxent, *Pinus* species, although CRS is a close second in both cases.   In five of the seven tree species/genera, the standard deviation of maximum κ values and all seven of the AUC values for the 100 replicates are lowest for CRS, with the other two models matching these values for *Tsuga* and *Pseudotsuga*.   Maxent matches the CRS *Picea abies'* standard deviation for AUC, with GAM achieving the lowest standard deviation for this species' maximum κ values. This analysis suggests that CRS is the most consistently robust as well as the best at performing in test conditions of the three modelling techniques utilised.

K-cross validation tests undertaken on the smaller bioclimatic grids, which improved 'goodness of fit' measures for the overall model performance, showed some differing levels of robustness across the modelling techniques (Table 3.1.6).   The European-gridded species, *L. pytyopsittacus* is modelled best across all robustness measures by the CRS model.   While in the case of *L.* scotica, CRS produced the highest averaged maximum κ value and the lowest standard deviation but not the smallest difference, that accolade goes to the GAM.   CRS also achieved the highest AUC for *L. scotica* and smallest difference, equalled by Maxent, which also has the lowest standard deviation.   For *L. megaplaga*, modelled on the smaller Caribbean grid, the highest robustness average maximum κ value is produced by the CRS model, but this is substantially lower than the value obtained for the full model.   The AUC averages obtained for *L. megaplaga* were highest in the case of GAM which also had the

Species	Model	'Goodness of fit' Measure					
		Maximum κ value			AUC value		
		Average	Difference	Standard Deviation	Average	Difference	Standard Deviation
Loxia pytyopsittacus	Maxent	0.609	-0.191	0.036	0.894	-0.082	0.021
	GAM	0.694	-0.128	0.030	0.929	-0.049	0.015
	CRS	**0.861**	**0.000**	**0.008**	**0.986**	**-0.001**	**0.001**
L. scotica	Maxent	0.693	0.011	0.117	**0.998**	**-0.001**	**0.001**
	GAM	0.682	**0.002**	0.116	0.997	-0.002	0.008
	CRS	**0.714**	0.012	**0.113**	0.998	-0.001	0.009
L. megaplaga	Maxent	0.240	**-0.065**	0.217	0.815	-0.116	**0.091**
	GAM	0.282	-0.099	**0.173**	**0.842**	**-0.108**	0.174
	CRS	**0.311**	-0.379	0.203	0.594	-0.357	0.155
Pinus occidentalis	Maxent	0.220	-0.044	0.097	0.741	-0.103	0.107
	GAM	**0.227**	**-0.026**	**0.080**	**0.789**	**-0.065**	**0.085**
	CRS	0.211	-0.383	0.104	0.639	-0.312	0.104

Table 3.1.6:   The average 'Goodness of Fit' measures obtained by k-cross validation tests of robustness for species modelled on the European and Caribbean bioclimatic grids   The average maximum κ and Area Under Curve (AUC) values for the 100 samples taken, the difference between these values and the complete species' distribution model value and the standard deviation of the measures across the 100 tests.   K-cross validation was conducted for the three different species' distribution modelling techniques: maximum entropy (Maxent), generalised additive models (GAM) and climatic response surface (CRS).   **Bold highlights the highest maximum κ and AUC values attained for that species, smallest differences and standard deviations**.

smallest difference although it had the highest standard deviation, while Maxent had the lowest. Finally the pine species native to the Caribbean, *Pinus occidentalis*, was the only species to achieve for which CRS did not achieve the highest maximum κ value, instead GAM produced the highest average for both maximum κ value and AUC, smallest difference and least standard deviation for the replicates.

In summary, the indications are that CRS is the most robust of the models however in certain cases the other models perform better, specifically in the case of smaller distributed species. The lower performance of CRS on these smaller grids, specifically the Caribbean, is likely to be due to the limited numbers of records being handled (10 to 23 grid cells) and the greater likelihood of pseudo-replicates being present in the 100 replications. It is interesting that Maxent does not perform significantly better than the other models, despite its wide application in projecting potential species' distribution into un-sampled environments.

The 'Goodness of Fit' and robustness measures suggest that CRS is the most frequently the best performing and consistent of the models and therefore has been selected to be used in simulations of species and genera distributions discussed comprehensively in this study.

Section 3.2

Comparison of the Model Simulations of Species' Distribution

As the three species' distribution modelling techniques; climatic response surface (CRS), maximum entropy (Maxent) and generalised additive models (GAM) have different fitting functions and extrapolation methods into novel climates (Section 2.4), their model predictions are subject to variation.   Although CRS was selected as the best performing of these modelling techniques, here the simulations generated by CRS, Maxent and GAM are compared for *Loxia curvirostra* for all the key scenarios described in the previous chapters:

- Present day

- The beginning of the Holocene, 10 thousand years ago

- The Last Glacial Maximum (LGM), 21 thousand years ago

- Heinrich Event 5, 46 thousand years ago

- Interstadial,52 thousand years ago

- Stadial, 108 thousand years ago

- Eemian interglacial, 120 thousand years ago

Loxia curvirostra was selected as the example species due to its extensive distribution in both Eurasia and North America, enabling comparison of model performances in these latitudinal similar but geomorphologically distinct regions.   In addition to mapped comparisons (Fig. 3.2.1-7), totals were made of the number of grid cells predicted to be climatically suitable by the models, in various combinations as well as individually (Table 3.2.1).

No. of Grid Cells Simulated as Suitable for *Loxia curvirostra*

Scenario Date (kyr B.P.)	Only CRS	Only Maxent	Only GAM	Only CRS & Maxent	Only GAM & Maxent	Only CRS & GAM	CRS, GAM & Maxent
0	2,356	137	301	239	1,866	494	12,387
10	3,444	906	644	673	1,444	1,712	11,102
21	2,786	1,135	815	441	930	1,182	7,049
46 (Heinrich)	3,485	1,241	352	1,329	648	2,662	4,309
52	2,842	1,139	724	664	1,209	1,533	8,598
108	3,195	738	568	552	962	3,683	6, 364
120	3,088	1,037	454	524	2,272	973	11,874

Table 3.2.1:   The total number of grid cells the models individually or combined simulated as suitable for *Loxia curvirostra* in each of the scenarios.   The species' distribution models used being; climatic response surface (CRS), maximum entropy (Maxent) and generalised additive model (GAM) for the present (0 kyr B.P.), beginning of the Holocene (10 kyr B.P.), last glacial maximum (21 kyr B.P.), Heinrich Event 5 (46 kyr B.P.), interstadial (52 kyr B.P.), stadial (108 kyr B.P.) and Eemian interglacial (120 kyr B.P.).

Colours correspond to the maps (Fig. 3.2.1-7).

Present Simulation

The predicted distributions produced by the three models utilised in this study share a significant amount of overlap, 12,397 grid cells (Table 3.2.1).   These shared sites (grey) are found in Eurasia from the Scottish Highland and southern England across central Europe and southern Fennoscandia, through central and southern Russia to the south-eastern coastline and northern Japan, as well as the eastern Himalayas and Tibetan plateau and the Caucasus Mountains (Fig. 3.2.1).   In North America, all three models predict that the climate is suitable throughout southern Canada, along the western coast of the USA and through the Rocky Mountains with some locations in Alaska.   There are many areas in Eurasia and North America that are only simulated as suitable by the CRS model (red), totalling 2,356 grid cells, such as Turkey, Spain, the central Himalayas, further north and south along the eastern coast of Russia, south in the American Rocky Mountains and along the western coast into Mexico.

However, there are also a number of sites, 1,866 grid cells, where both Maxent and GAM (green), and not CRS, predict that the climate is suitable for *L. curvirostra* in areas such as northern China, along the southern and northern fringes of the Russian and Canadian ranges where all three concurred, the remainder are in Poland, throughout the rest of the UK, South America and western Alaska.   There are some sites in Fennoscandia and northern France where GAM and CRS (orange) both simulate that climate is suitable and other sporadic locations totalling 494 grid cells, but few where just Maxent (blue, 137 grid cells) or GAM (yellow, 301 grid cells), or CRS and Maxent combined (purple, 239 grid cells) predict sites that are not simulated by any of the other models.
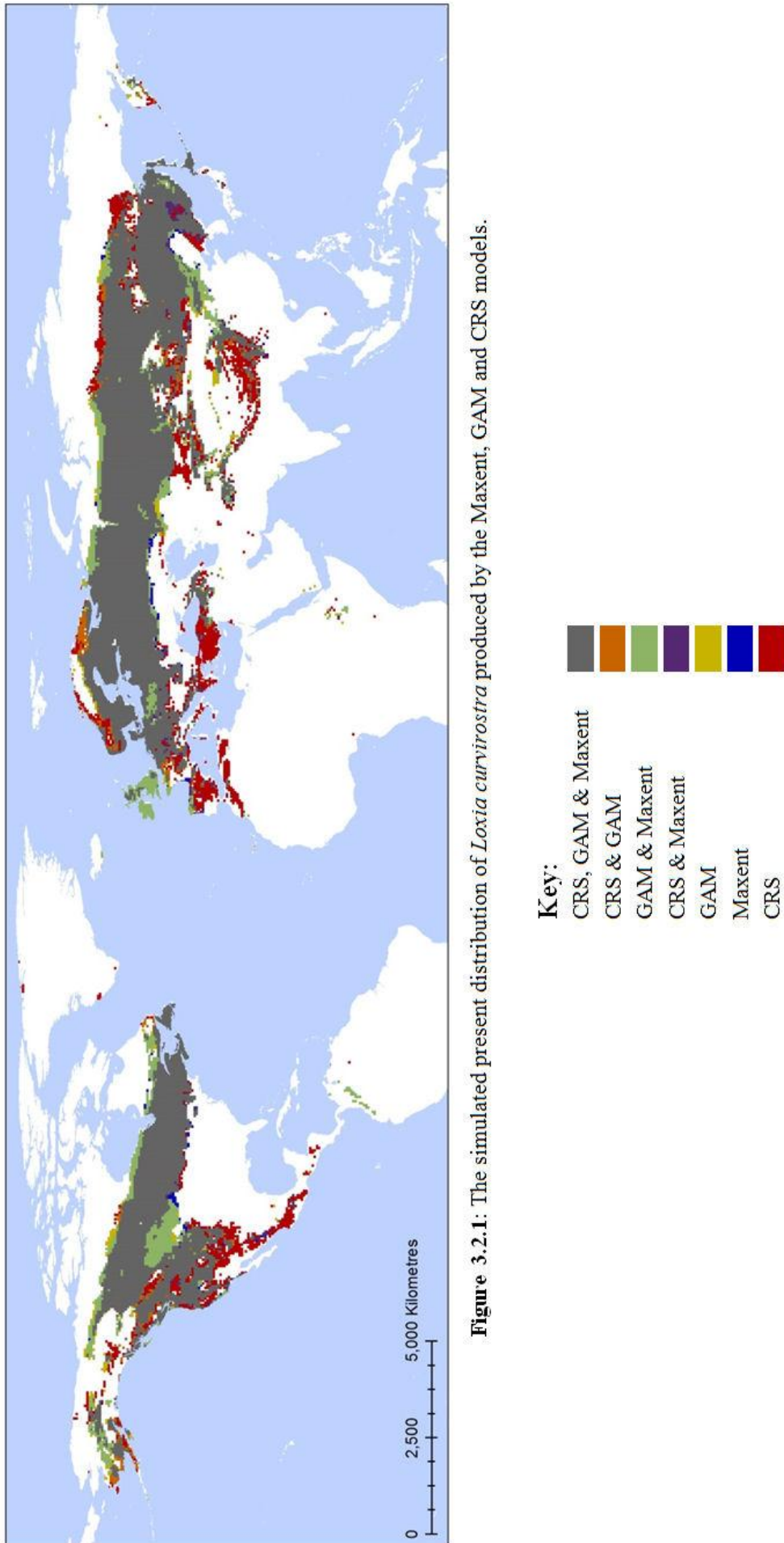
Figure 3.2.1: The simulated present distribution of *Loxia curvirostra* produced by the Maxent, GAM and CRS models.

Key:
CRS, GAM & Maxent
CRS & GAM
GAM & Maxent
CRS & Maxent
GAM
Maxent
CRS

The Beginning of the Holocene

The three models all simulate (grey) that the climate 10 thousand years ago was suitable from Scotland and northern to south-eastern England, central Europe and southern Fennoscandia and across from north-western Russia into central and southern regions of Siberia and along the east coast, northern Japan and in Kamchatka peninsula, as well as areas in the Asian mountain ranges and Caucasus Mountains (Fig.°3.2.2).   In North America, all three models predict that the climate is suitable from Newfoundland on the east coast through southern Canada and into the north-west, into Alaska and south into the mountain of western North America, totalling 11,102 grid cells across the northern hemisphere (Table 3.2.1).   There is a vast expanse in southern Siberia where Maxent does not simulate suitability but both GAM and CRS do (orange) as well as some areas along the Arctic coastline of Canada (1,712 grid cells).   There are some areas where both GAM and Maxent (green) predict climate suitable for *L. curvirostra* which CRS does not, in Ireland, south-western England and southern Alberta and in middle and fringes of the shared simulated range of all three models, with 1,444 grid cells being simulated in total.   Many fewer sites have just Maxent and CRS simulated together (purple), just 673 grid cells mainly in the Rocky Mountains and northern Spain.

There are many areas which only the CRS model (red) simulates as being suitable, 3,444 grid cells, which are found mainly in the Himalayas, Tibetan Plateau, southern Russia, Kazahstan southern regions of Siberia as well as expanses in Canada south of the Hudson Bay and in the south into the Mexican mountains.   Although the other two models also simulate some uniquely areas of suitability, for instances Maxent's site identifications (blue, 906 grid cells) are found throughout the Rocky Mountains, Mexico, north into Alaska, the Bering Strait and northern Canada, and in Eurasia, western France, the coast of the Barents Sea and south in the Himalayas, Turkey and eastern central Africa.   GAM has the least unique sites, 644 grid cells, mainly in Russia, fringing the concurring ranges and in northern Canada.
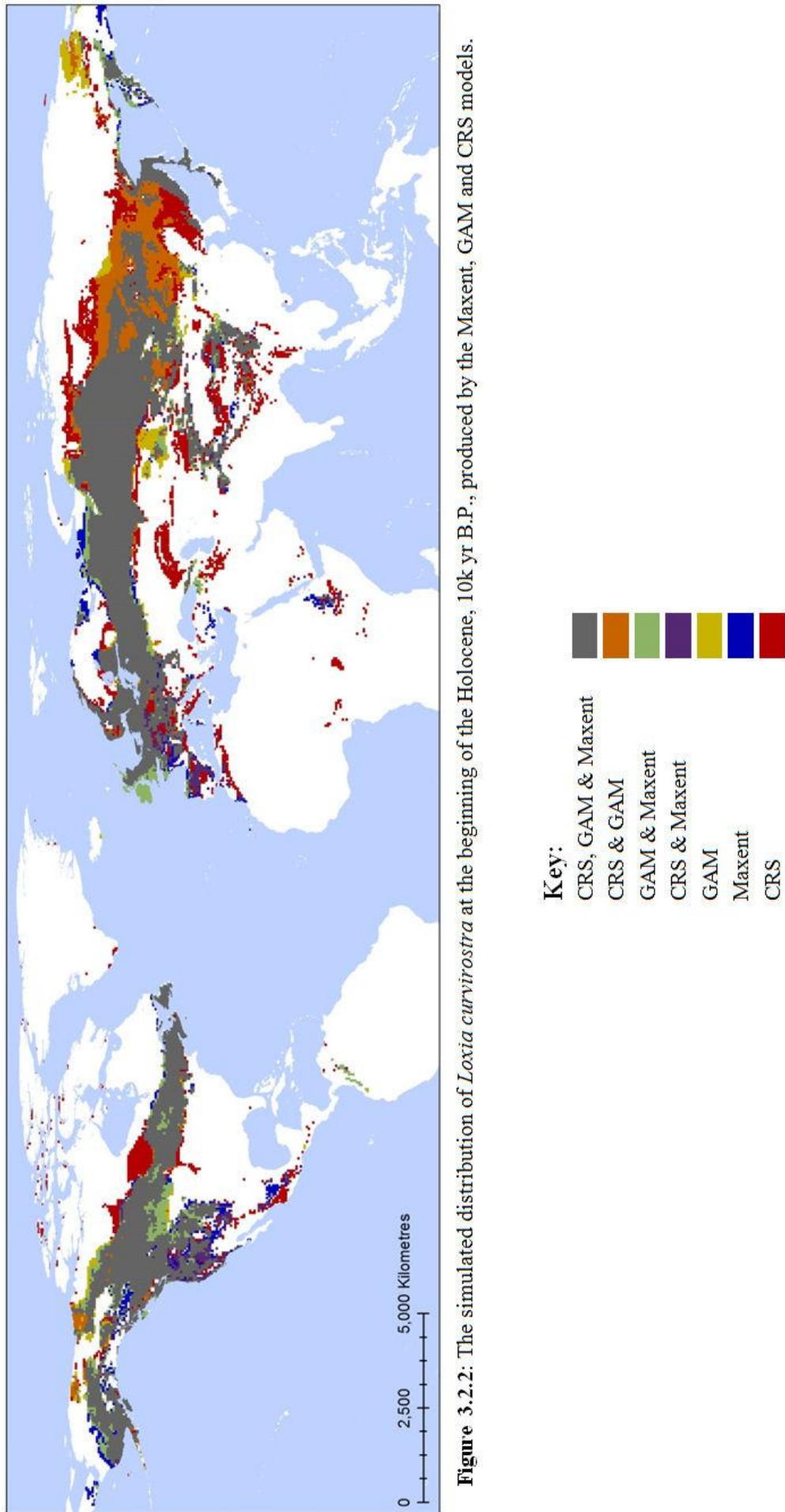
Figure 3.2.2: The simulated distribution of *Loxia curvirostra* at the beginning of the Holocene, 10k yr B.P., produced by the Maxent, GAM and CRS models.

Key:
CRS, GAM & Maxent
CRS & GAM
GAM & Maxent
CRS & Maxent
GAM
Maxent
CRS

The Last Glacial Maximum

The conditions 21 thousand years ago provide many sites where all three models simulate that the climate is suitable for *L. curvirostra* (grey), all suggesting the range was more southerly restricted that present day, primarily in central Europe and south-western Russia and to the east of the mountains of southern Siberia, to Japan and through the mountains of China into the Himalayas and in North America south of the Laurentide ice sheet and to the west in southern Alaska (Fig. 3.2.3).   In total there were 7,049 grid cells identified by all three of the models (Table 3.2.1), a further 1,182 grid cell sites have climate which both CRS and GAM simulate to be suitable (orange) and there are found north of the combined south-west Russian bloc and north in Alaska.   Areas where just GAM and Maxent find climate suitable (green, 930) are mainly south of those areas which all three found climate suitable.   A far fewer number of sites have an overlap between CRS and Maxent (purple, 441 grid cells), mainly in western Spain, the Himalayas and western North America.

CRS again predicts a vast number of sites, 2,786 grid cells, of unique suitability (red) for the model; further north into central Russia, northern Britain, southern Spain, south of the Himalaya, central Africa, southern North America, the Rockies and Mexico and west of the Laurentide ice sheet.   However, Maxent also predicts a significant number of sites (blue, 1,135 grid cells) in western North America southern Russia and Japan, all south of the shared range, and more easterly into south-east coastline of Siberia, Kamchatka peninsula and further into central China.   GAMs unique sites of climatic suitability (yellow, 815 grid cells) are situated primarily in north-western Alaska and the southern Siberia mountains.   Despite the discrepancies in model outputs all the models suggest that vast expanses of northern Russia were inhospitable for *L. curvirostra* during the glacial conditions.

Figure 3.2.3: The simulated distribution of *Loxia curvirostra* at the Last Glacial Maximum, 21k yr B.P., produced by the Maxent, GAM and CRS models.

Key:
CRS, GAM & Maxent
CRS & GAM
GAM & Maxent
CRS & Maxent
GAM
Maxent
CRS

Heinrich Event 5

The Heinrich Event 5 conditions resulted in a lower level of corroboration between the models, with just 4,309 grid cells (Table 3.2.1) having climate which all three models predict as being suitable for *L. curvirostra*, mainly found south of the Laurentide ice sheet in North America, in central and southern Europe, northern coastline of Africa, western areas of Russia and the south-eastern coast of Russia and southern Japan (Fig. 3.2.4).   Maxent produces the most limited range simulation, and thus there are vast areas of central and southern Russia where just CRS and GAM are predicting climate available (orange, 2,662 grid cells).   There are some areas in Eastern Europe, northern Middle East and China where CRS does not indicate climate is suitable but both GAM and Maxent do (green, 648 grid cells).   Fringes of the North America core range, Alaska and northern China as well as the Himalayas are areas which Maxent and CRS both corroborate on as being suitable (purple, 1,329).

CRS uniquely predicts (red) 3,485 grid cells, with the simulations indicating distributions of *L. curvirostra* that stretch further west into north Spain; south into northern Africa and Middle East, areas of south-east Asia as well as much of Central America; and north into central Russia.   GAM only simulates a few unique locations (yellow) in northern Alaska and central Russia totalling just 352 grid cells.   There are numerous exclusive locations simulated by Maxent (blue, 1,241 grid cells) which suggest *L. curvirostra* could have ranged further north-west into the Netherlands and southern England, east along the Siberian coastline and throughout Japan and the south in the mountains of the Himalayas as well as a broader range both north and south in central North America and to the west of the Laurentide in Alaska. It is most interesting that Maxent's distribution in Eurasia is split between the west and east where it finds more climatically suitable locations than the other models but nothing in central areas of Russia, where the other two models suggest there is abundant climate.   This highlights one of the difficulties of just using a single modelling technique as it may by-pass large areas of climate that other models may determine as suitable.

Figure 3.2.4: The simulated distribution of *Loxia curvirostra* at Heinrich Event 5, 46 k yr B.P, produced by the Maxent, GAM and CRS models.

Key:
CRS, GAM & Maxent
CRS & GAM
GAM & Maxent
CRS & Maxent
GAM
Maxent
CRS

Interstadial

The warmer conditions of the interstadial, 52 thousand years ago, provide a distribution of climate suitable for all three models (grey) for *L. curvirostra* from the western coast of Ireland through central Europe and southern Russia as far east as the south-eastern coastline and areas of Japan, with additional suitability in the Kamchatka peninsula, Chinese and Middle Eastern mountain ranges as well as across central North America and southern Alaska (Fig.°3.2.5). The corroborating range is of similar expanse, of 6,364 grid cells (Table 3.2.1), to that observed at the glacial maximum but more northerly areas are suitable during the warmer conditions, however GAM and CRS (orange) and CRS alone (red) suggest that climate was suitable further north into Russia than Maxent indicates.   In addition to the substantial region into north Russia where both CRS and GAM (3,683 grid cells) concur, there are regions of central Alaska.   There are more northerly parts of Alaska and the Bering Strait where only GAM (yellow, 568 grid cells) simulates the climate as suitable, with further locations in central Mexico and southern Finland.   Areas south of the overlapping range of three models in Russia, Turkey and China and to the west, coastline of France and south-west England and of the Laurentide ice sheet are all regions where GAM and Maxent (green, 962 grid cells) both find suitable climate for *L. curvirostra*.   There are even less sites which have just Maxent and CRS (purple, 552 grid cells) simulating presence of *L. curvirostra*, mainly in the Himalayas, Spain and north-west America, where Maxent and CRS simulations extend further south than the GAM simulations.

3,195 grid cells have climate which only CRS (red) indicates are suitable for *L. curvirostra*, patchily through the southern mountains of North America, further north than the other models in Russia, south into northern coast and central Africa and in the southern Asian regions of Indic and Myanmar.   Maxent (blue) suggests climate is more suitable north and south of corroborating ranges in eastern North America, central Europe and eastern Siberia totalling 738 grid cells.   It is interesting to note in this climatic scenario that Maxent is more southerly orientated in Eurasia and GAM more northerly while CRS encompasses many different latitudes.

Figure 3.2.5: The simulated distribution of *Loxia curvirostra* during interstadial conditions, 52k yr B.P., produced by the Maxent, GAM and CRS models.

Key:
CRS, GAM & Maxent
CRS & GAM
GAM & Maxent
CRS & Maxent
GAM
Maxent
CRS

Melisey 1 Stadial

Maxent's distribution during the stadial colder conditions is dramatically restricted, resulting in corroborating areas being geographically constrained to central Europe, north of the Caspian Sea, south-central Russia and the south-eastern coastline, Japan, the mountains of the Himalayas, China and Middle East, central Alaska and central North America with more abundance in the western mountains (Fig. 3.2.6). Overall this corroborating simulated range includes 8,598 grid cells, similar in size and range to the later Heinrich Event conditions and likewise there is an area in central Russia which only simulated as suitable by GAM and CRS (orange, 3,683 grid cells). There are a number locations where CRS does not simulate but the other two models find suitable climate (green, 962 grid cells), these include southern areas of Russia, Kazakhstan, northern Turkey and central North America, the Rocky Mountains and southern Canada as well as sporadic locations in southern Alaska, isolated sites have climate which is found to be suitable by just CRS and Maxent (purple, 552 grid cells) in locations like the Himalayas, northern Spain and Italy, northern China and the Aleutian Islands.

Once again CRS has a large abundance of unique simulated suitable location (red, 3,195 grid cells), further north than the other models in Russia as well as areas of the Tibetan Plateau, southern Asia, southern Spain, north coast of Africa and American mountain ranges of Sierra Nevada and Sierra Madres. Maxent only produces 738 unique simulated grid cells (blue), mainly in the Himalayas, Eastern Europe, Scotland, southern Canada and Alaska while GAM simulates just 568 grid cells that none of the other models identify (yellow), on the Arctic Canadian coastline, central North America and south-western Russia.
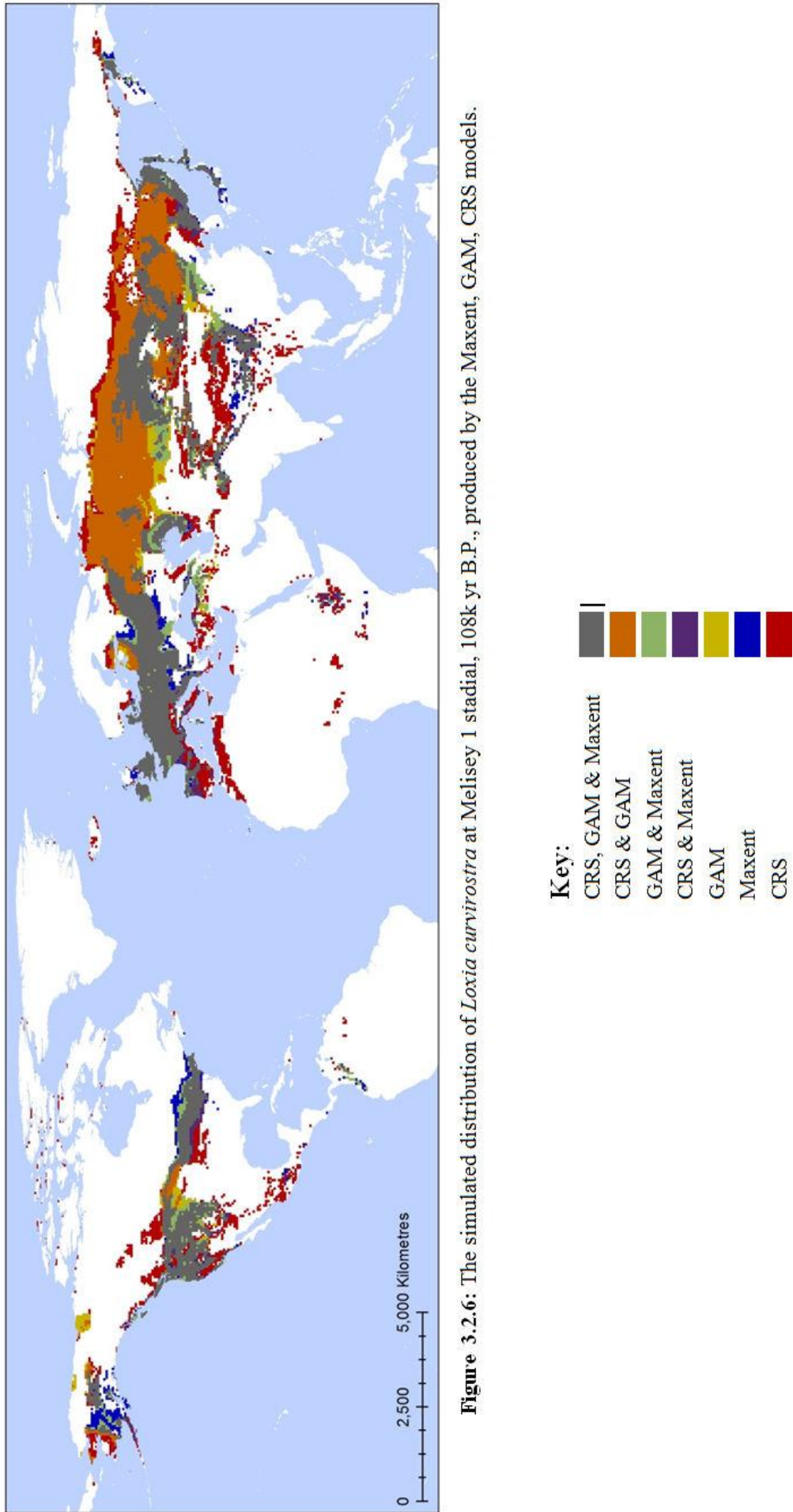
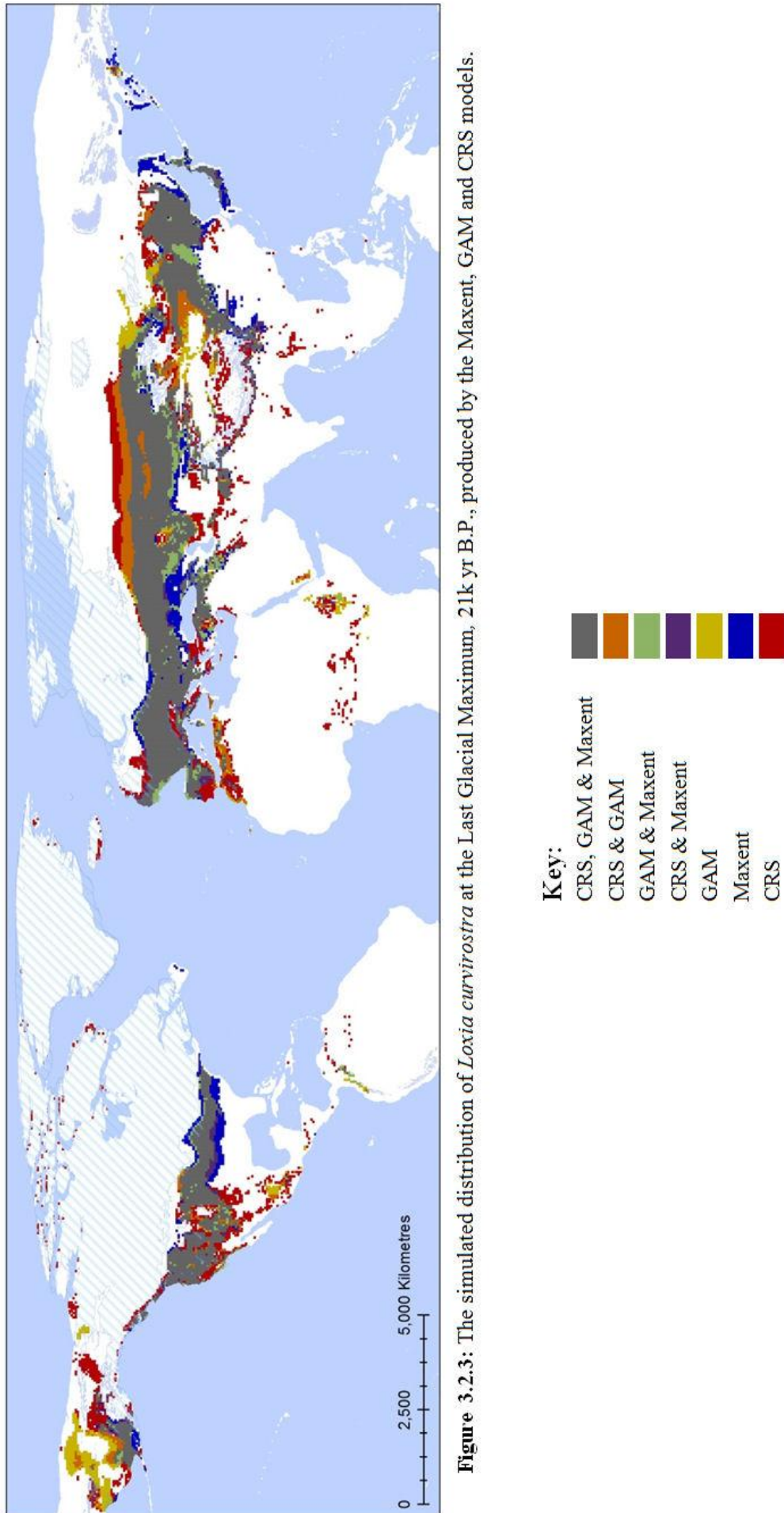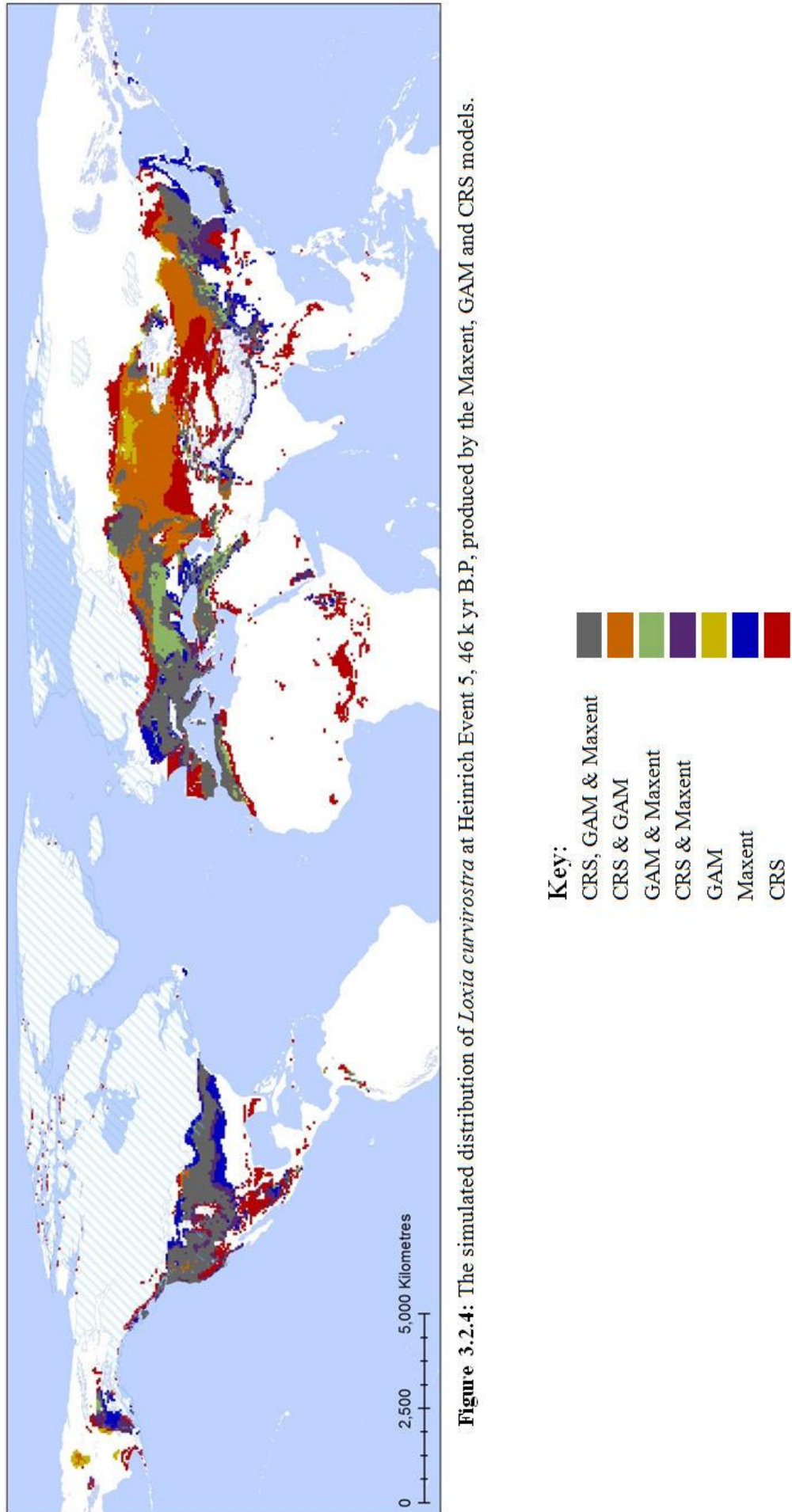**Figure 3.2.6:** The simulated distribution of *Loxia curvirostra* at Melisey 1 stadial, 108k yr B.P., produced by the Maxent, GAM, CRS models.

Key:
CRS, GAM & Maxent
CRS & GAM
GAM & Maxent
CRS & Maxent
GAM
Maxent
CRS

Eemian Interglacial

The corroborating model simulated sites (grey) for the Eemian interglacial of 120 thousand years ago, have a similar distribution to the present day range from central Europe across Russia to the south-east coastline and northern Japan, mountain ranges such as those found in China, the Middle East and the Caucasus mountains and throughout south-eastern Canada to the north-west and along the western mountain ranges of North America (Fig. 3.2.8); a similarly expansive range of 11,874 grid cells (Table 3.2.1).   There is a substantial quantity of sites which are not simulated by CRS as being suitable but are by the other two models (green), a total of 2,272 grid cells, which are found in the British Isles, regions of central and southern Russia, and southern Canada.   There are far fewer location where CRS and GAM only predict climate is suitable (orange, 973 grid cells), mainly in Germany, northern Fennoscandia, southern Alaska and the Rocky Mountains.   CRS and Maxent have even less corresponding locations (purple, 524 grid cells) mainly in southern Canada, western Span and north-eastern fringes of the combined range limit in Siberia.

CRS produces many more exclusive predictions (red) than the other two models, with 3,088 grid cells solely identified by this model as being suitable for *L. curvirostra* mainly found in southern Europe, northern Africa, northern Fennoscandia, the Himalayans and neighbouring Tibetan Plateau and the southern mountains of North America.   GAM solely predicts just 454 grid cells (yellow), in south-eastern England and northern coast of France, north-west Russia and sporadic locations in Alaska and Newfoundland whilst Maxent produces a number of locations (blue, 1,037 grid cells).   These are more southerly than the other models predict in central and south-eastern Canada, Kazahstan and northern Russia and well as some further into north-eastern Siberia than GAM and CRS suggest.
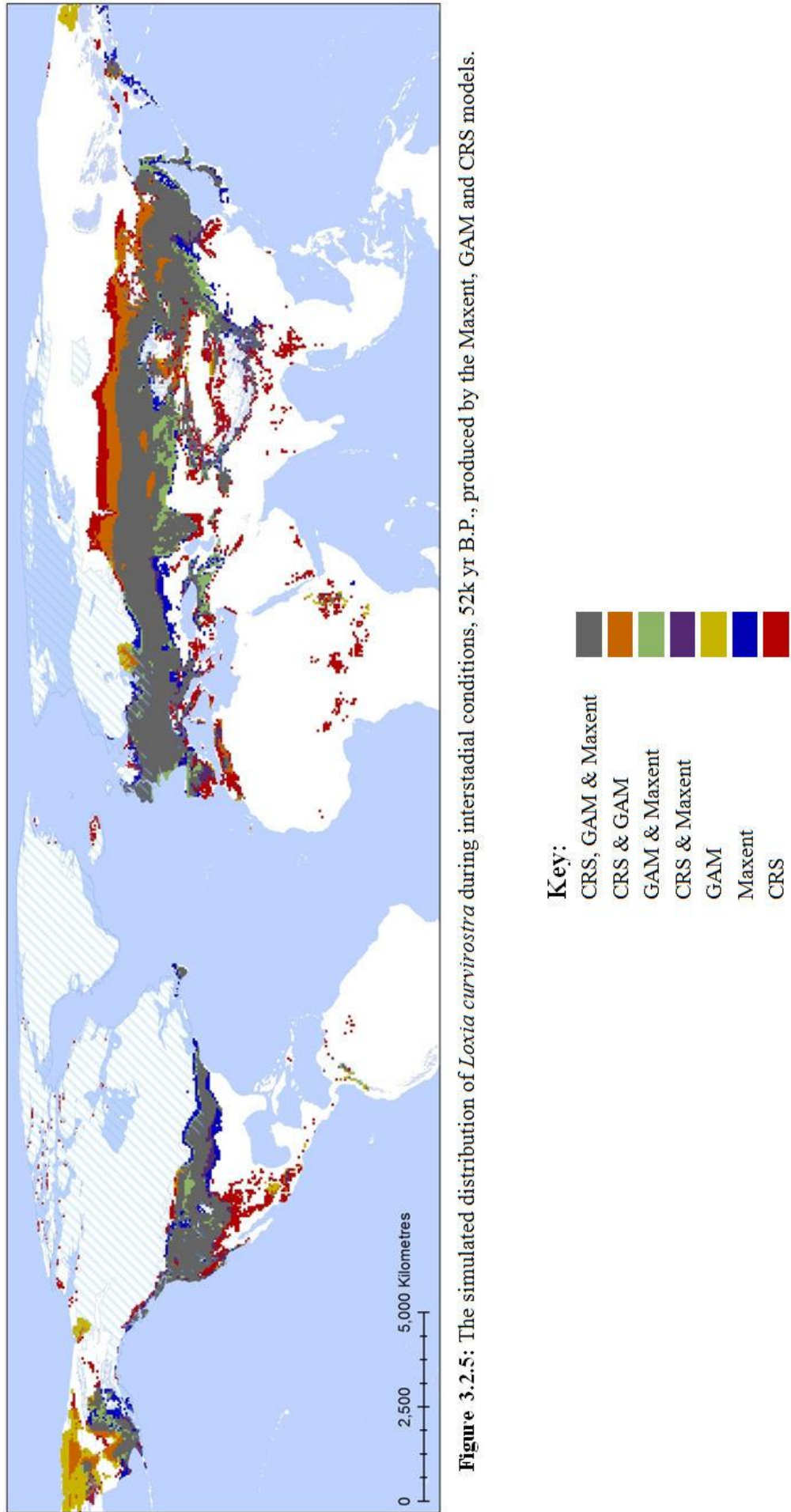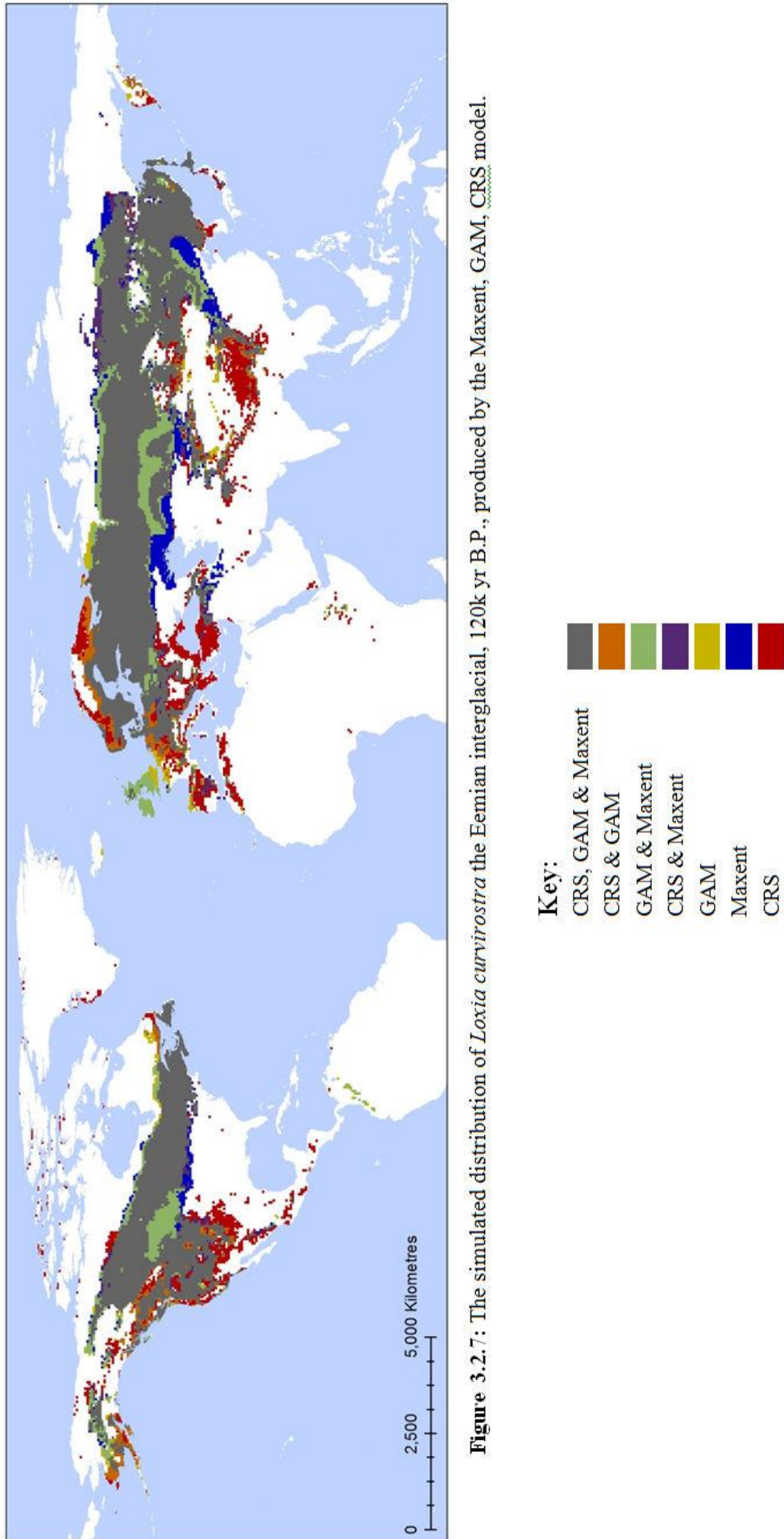
Figure 3.2.7: The simulated distribution of *Loxia curvirostra* the Eemian interglacial, 120k yr B.P., produced by the Maxent, GAM, CRS model.

Key:
CRS, GAM & Maxent
CRS & GAM
GAM & Maxent
CRS & Maxent
GAM
Maxent
CRS

Section 3.3

Comparison of Model Simulations of Species' and Genera's Range Size

In addition to the disparities in the distribution of the climatically suitable ranges generated for each of the species/genera by the different models, the overall size of range also varies and can be used as an indicator of model performance. By studying the difference in overall grid cell coverage of the simulations it may be possible to ascertain whether some models produce more conservative estimates of range size potential based on climate than others, noting any corroborative results which may affirm the validity of the simulations based on climate. Here the three modelling techniques utilised in this study are compared, climatic response surface (CRS), maximum entropy (Maxent) and generalised additive model (GAM) to note the similarities and discrepancies between the climatic niche models.

Loxia curvirostra

The range sizes simulated for *Loxia curvirostra* fluctuate throughout the last 120 thousand years. All three modelling techniques identify the interglacials as having the greatest abundance of climatically suitable locations and the Heinrich Events and late glacial stages,
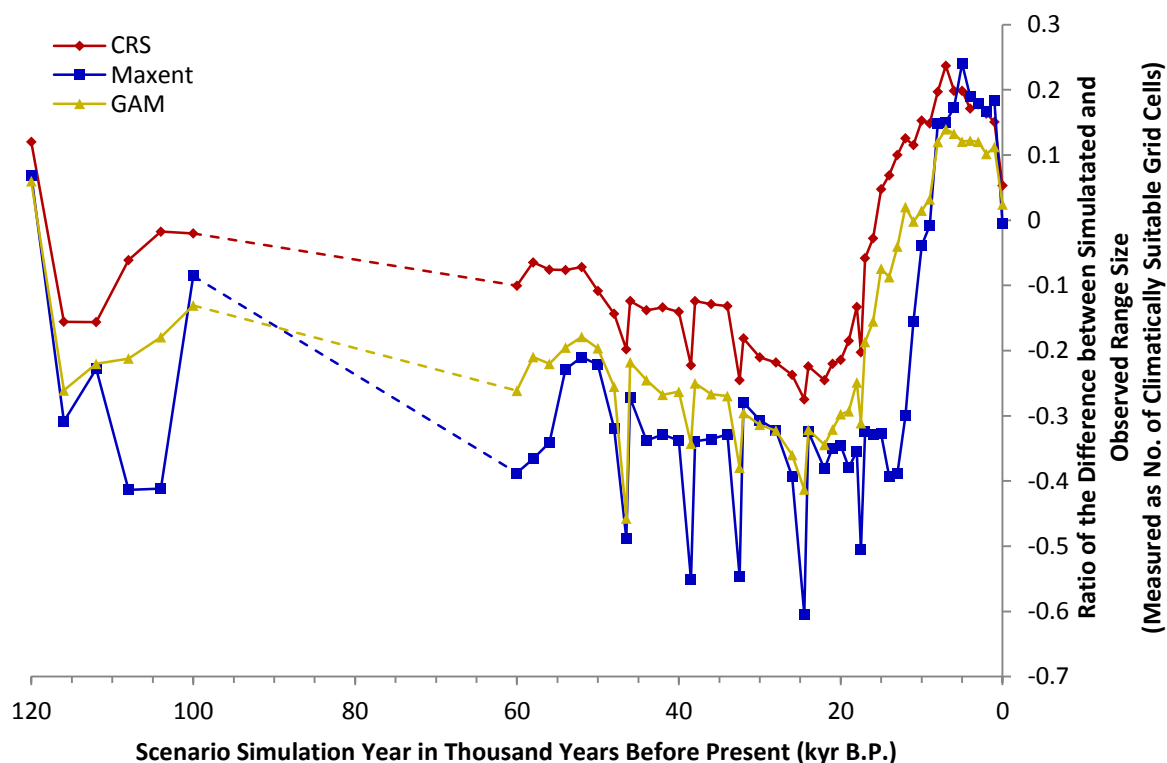
Figure 3.3.1: The difference in simulated range size from observed for *Loxia curvirostra* calculated as a ratio of the difference between the simulated and the observed distribution (total number of grid cells occupied) divided by the observed. Simulation were made for each of the 52 palaeoclimatic scenarios and present day using the climatic response surface model (CRS), maximum entropy (Maxent) and generalised additive model (GAM).

Note: The dashed line represents the period, 100 to 60 kyr B.P, when no simulations were modelled.

the most limited (Fig. 3.3.1).   CRS identifies the greatest range sizes throughout the glacial and previous interglacial conditions.   During the Holocene conditions, CRS and Maxent generate similar abundances, while the GAM model produces less.   However, during the glacial, from 60 to 10 thousand years ago, the Maxent model produces smaller climatically suitable ranges than both the CRS and GAM.   The Maxent model also predicts the most dramatic restriction in population size during the Heinrich Events.   All the models concur that *L. curvirostra*'s climatic range is more constrained during the Eemian interglacial and glacial conditions compared to the later Holocene.

Loxia leucoptera

All three models suggest that potential range of *L. leucoptera* was of a similar or larger extent in relation to the observed populations during the earlier Holocene scenarios (Fig. 3.3.2). The glacial conditions cause a reduction in overall distribution size for all three of the models, however the GAM model appears to recover from this low sooner than the other models, generating its greatest abundance of climate suitability around 17 thousand years ago, prior to the onset of the Holocene.   Overall, the GAM predicts larger ranges for all the scenarios, and Maxent generates the lowest, with CRS having a very similar range to Maxent at a slightly

Figure 3.3.2:   The difference in simulated range size from observed for *Loxia leucoptera* calculated as a ratio of the difference between the simulated and the observed distribution (total number of grid cells occupied) divided by the observed.   Simulation were made for each of the 52 palaeoclimatic scenarios and present day using the climatic response surface model (CRS), maximum entropy (Maxent) and generalised additive model (GAM).

Note: The dashed line represents the period, 100 to 60 kyr B.P, when no simulations were modelled.

higher level.   For both the Maxent and CRS, the Heinrich Events produce the most restricted climatic range; this is not the case for GAM simulations, rather the greatest decline is during stadial conditions in the previous Eemian interglacial.   Both Maxent and CRS models consistently suggest that *L. leucoptera*'s climatic range is more constrained during the Eemian interglacial and glacial conditions compared to the later Holocene.

Loxia pytyopsittacus

In the case of *L. pytyopsittacus*, all three models produce strikingly similar relative changes in climatic abundance between the different palaeoclimatic scenarios, with Maxent generating the greatest abundance and GAM the lowest during the Eemian interglacial and glacial conditions, while during the later Holocene, GAM's generate higher abundance than the other two modelling techniques which perform similarly (Fig. 3.3.3).   There is a significantly smaller predicted range size during the stadial and glacial conditions than during the warmer Eemian and Holocene interglacial across all modelling techniques and Heinrich Events result in the most constrained suitable climatic abundance.
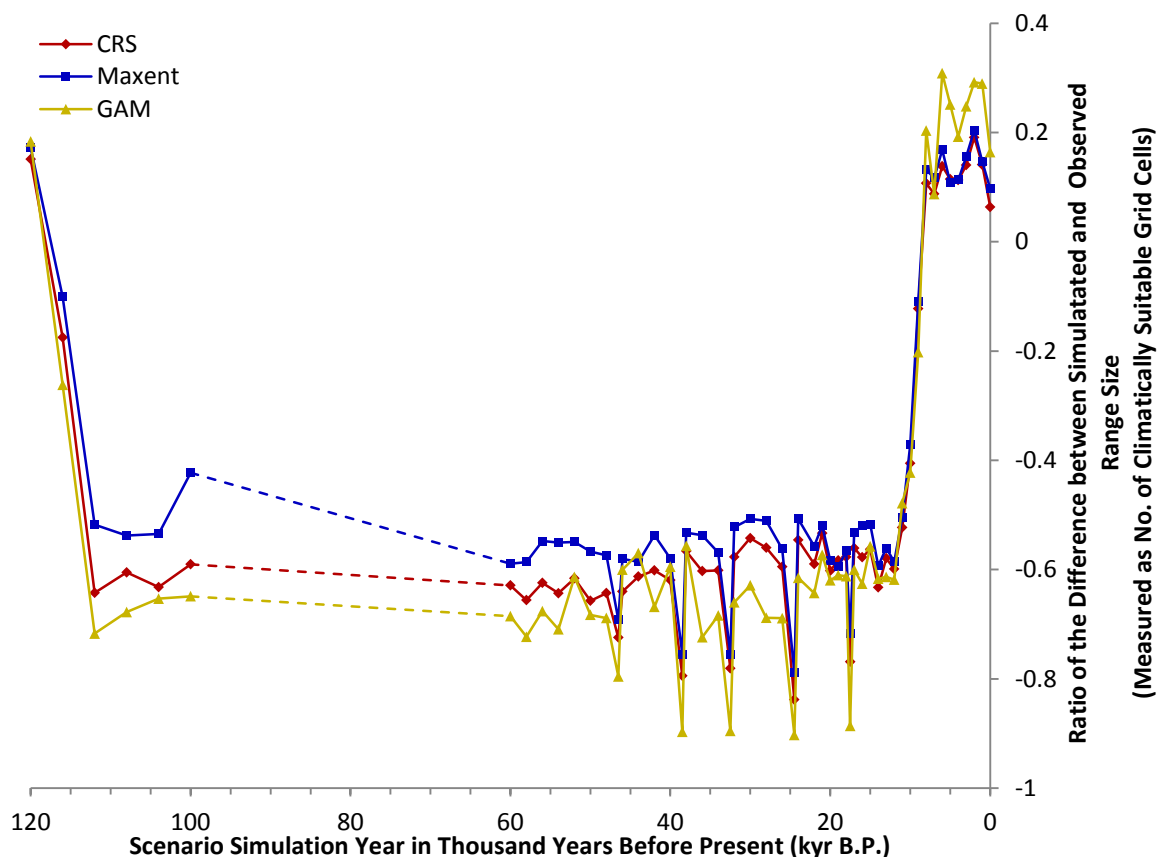
Figure 3.3.3:   The difference in simulated range size from observed for *Loxia pytyopsittacus* calculated as a ratio of the difference between the simulated and the observed distribution (total number of grid cells occupied) divided by the observed.   Simulations were made for each of the 52 palaeoclimatic scenarios and present day using the climatic response surface model (CRS), maximum entropy (Maxent) and generalised additive model (GAM) using the European bioclimatic grid.

Note: The dashed line represents the period, 100 to 60 kyr B.P, when no simulations were modelled.

Loxia scotica

Unlike the other *Loxia* species, for *L. scotica* there appears to be no close association between the abundance of climatically suitable locations and it is a glacial or interglacial stage across all three of the modelling techniques (Fig. 3.3.4).   The abundance of potential sites fluctuates between scenarios to varying degrees of magnitude dependent on the model, with the GAM demonstrating the greatest changes in simulated climatic range.   However, all the models suggest that the Heinrich Events had no climate suitable for *L. scotica* and that glacial conditions provided varying conditions of suitability, while the warming conditions of the Holocene result in a gradual increase in the quantity of locations suitable for *L. scotica* and the models converge to observe similar range changes.   This highlights the instability of the climatic niche for *L. scotica* throughout the last 120 thousand years.

Figure 3.3.4:   The difference in simulated range size from observed for *Loxia scotica* calculated as a ratio of the difference between the simulated and the observed distribution (total number of grid cells occupied) divided by the observed.   Simulations were made for each of the 52 palaeoclimatic scenarios and present day using the climatic response surface model (CRS), maximum entropy (Maxent) and generalised additive model (GAM) using the European bioclimatic grid.
Note: The dashed line represents the period, 100 to 60 kyr B.P, when no simulations were modelled.

Loxia megaplaga

The models for *L. megaplaga* produce very different simulations of range size over the last 120 thousand years (Fig. 3.3.5).   The CRS model suggests that climatic conditions were significantly more suitable in a great number of areas during the glacial than during the interglacial, while both Maxent and GAM predict that there are fewer climatically suitable locations available during the glacial in comparison to interglacial conditions, with GAM simulations producing the lowest potential range sizes.   However, there are some similarities in range size response to the climate scenarios, from 120 to 100 thousand years ago; there is an initial decline in predicted range size and an increase into the onset of a glacial. Interestingly the GAM and Maxent simulations suggest that there is no climate suitable for *L. megaplaga* during Heinrich Event conditions, while CRS model simulations predict that these events have no consistent effect on range size, with both increases and decreases relative to previous and later scenarios.   These significant differences in model predicting performance are probably as a result of the restricted present day climatic conditions of *L. megaplaga* combined with the models' different approaches to extrapolation into novel climates, with CRS producing a more expansive potential climatic niche for *L. megaplaga*

Figure 3.3.5:   The difference in simulated range size from observed for *Loxia megaplaga* calculated as a ratio of the difference between the simulated and the observed distribution (total number of grid cells occupied) divided by the observed.   Simulations were made for each of the 52 palaeoclimatic scenarios and present day using the climatic response surface model (CRS), maximum entropy (Maxent) and generalised additive model (GAM) using the Caribbean bioclimatic grid.

Note: The dashed line represents the period, 100 to 60 kyr B.P, when no simulations were modelled.

compared to the more conservative Maxent and GAM.

Larix species

Unlike the other conifer genera modelled, both GAM and CRS model predictions indicate that the climate during the glacial, from around 56 thousand years ago, to the early Holocene, provided more potential sites for *Larix* species than the interglacial conditions preceding and succeeding it (Fig. 3.3.6).   All three models show similar changes in the predicted range size, with more restricted predictions of climatically suitable ranges for *Larix* species during stadial, 108 thousand years ago, interstadial, 52 thousand years ago, and around the glacial maximum 25-17 thousand years ago.   Most interestingly the cold Heinrich Events of 1-4 result in little or no significant decline in the range size of *Larix* species across all three modelling techniques.   GAM produces the most consistently larger predictions as well as having the most variance in range size simulations, while Maxent produces the most restricted simulations and CRS falls between these.   The consensus among the three modelling techniques suggests that the bioclimatic niche that *Larix* species is found living in today was of greater abundance during the middle stages of the glacial, unsurprising since it is the
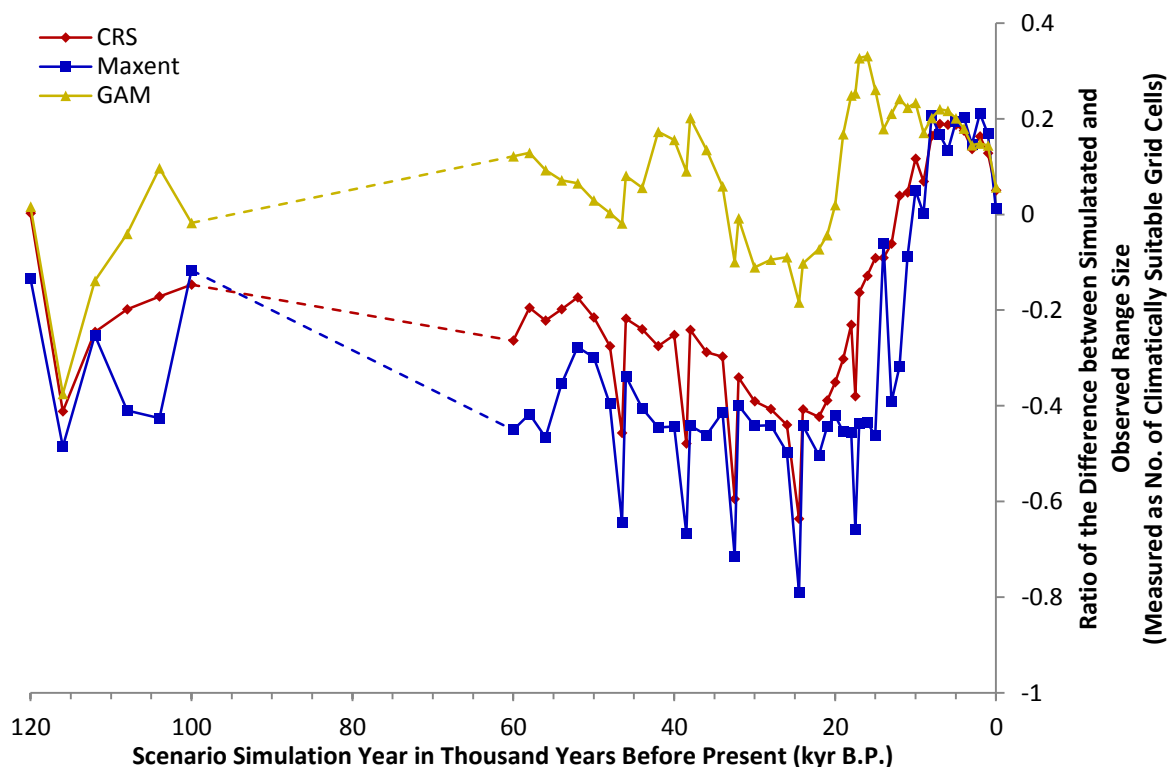

Figure 3.3.6:   The difference in simulated range size from observed for *Larix* spp. calculated as a ratio of the difference between the simulated and the observed distribution (total number of grid cells occupied) divided by the observed.   Simulations were made for each of the 52 palaeoclimatic scenarios and present day using the climatic response surface model (CRS), maximum entropy (Maxent) and generalised additive model (GAM).

Note: The dashed line represents the period, 100 to 60 kyr B.P, when no simulations were modelled.

dominant species of the present boreal zones in Russia and Canada and obviously thrives in colder climes, such as the glacial provided.

Picea species

There are many similarities between the three different modelling techniques used to model *Picea* species when the predicted range sizes are compared, with CRS producing the greatest predictions of range size throughout the last 120 thousand years (Fig. 3.3.7). Maxent predicts the more limited ranges during the glacial conditions and has the greatest variation. All three suggest that the Eemian interglacial had a similar number of climatically suitable locations to the present day, with reduced availability during the approach of the glacial and throughout the glacial until post-glacial maximum when conditions improve becoming more favourable to the genus by the onset of the Holocene, with greater potential range sizes than the present.   The Heinrich Events produce the most restricted availability of predicted range size for *Picea* species consistently across the three models.   There is also an additional decline in cumulative suitability from the Eemian to the palaeoclimate scenario at 116 thousand years ago despite the average climate not being as cold or dry as later conditions

Figure 3.3.7:   The difference in simulated range size from observed for *Picea* spp. calculated as a ratio of the difference between the simulated and the observed distribution (total number of grid cells occupied) divided by the observed.   Simulations were made for each of the 52 palaeoclimatic scenarios and present day using the climatic response surface model (CRS), maximum entropy (Maxent) and generalised additive model (GAM).

Note: The dashed line represents the period, 100 to 60 kyr B.P, when no simulations were modelled.

(Fig. 2.3.1). This highlights that the average climate conditions may not represent the local conditions where *Pic*ea species is found and small average change in growth season and temperature may mask more dramatic localised changes in simulated conditions.

Pinus **species**

The three modelling techniques all predict a similar relative response to the changing climate scenarios for the *Pinus* species, the CRS model produces consistently higher predictions of range size, with GAM being similar or fractionally lower and Maxent simulating the lowest predictions with the greatest variance (Fig: 3.3.8). Akin to *Picea, Pinus* species are modelled to have initial conditions at the Eemian being similar in range size to present day with fewer climatically suitable locations during the pre-glaciation and glacial period with conditions improved towards the onset of the Holocene to support range sizes larger than observed today. Heinrich Events also cause the most dramatic reductions in potential climatic range across all three of the modelling types.

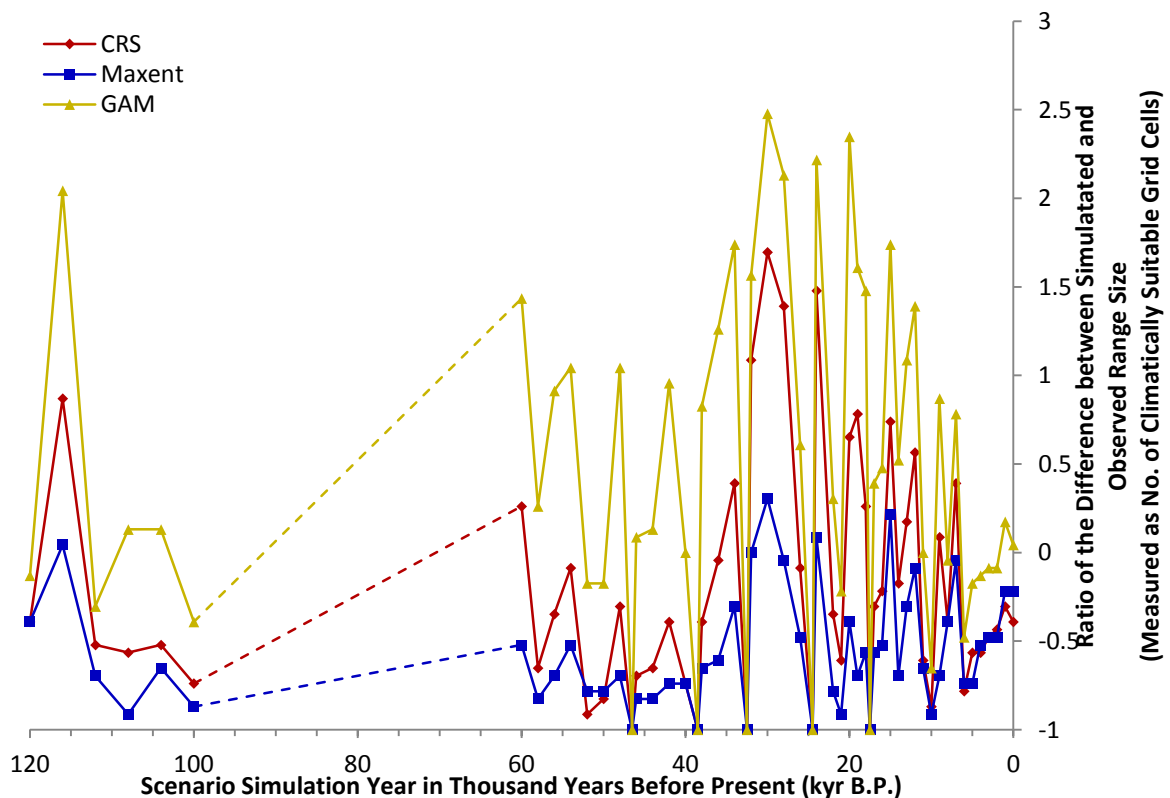**Figure 3.3.8:**   The difference in simulated range size from observed for *Pinus* spp. calculated as a ratio of the difference between the simulated and the observed distribution (total number of grid cells occupied) divided by the observed.   Simulations were made for each of the 52 palaeoclimatic scenarios and present day using the climatic response surface model (CRS), maximum entropy (Maxent) and generalised additive model (GAM).

Note: The dashed line represents the period, 100 to 60 kyr B.P, when no simulations were modelled.

Pseudotsuga **species**

GAM and CRS model predict larger range sizes than present of *Pseudotsuga* species throughout the simulated scenarios, including present day, due to areas of Europe also having suitable climate for the genus although not occupied (Fig. 3.3.9). Both models suggest indicate a high variance in the size of the climate range suitable for the genus during the last 120 thousand years. Maxent simulations suggest that the range size than the present range during late Eemian and into the glacial. Maxent and GAM both predict that the Heinrich Events produce their lowest relative range sizes during modelled scenarios, while CRS shows no such association. However CRS does produce the highest variance in range size predictions, the greatest prediction being the climatic conditions of 116 thousand years ago and the lowest being around 13 thousand years ago prior to the onset of the Holocene. This great variance in the range size observed both between models and the scenario simulations of *Pseudotsuga* species is likely due to the small size of the current range and the significant geographic isolation of many of the species from other members of the genus resulting in presence of climate that is suitable but remains unoccupied by *Pseudotsuga* species. It is interesting to note that Maxent is exceedingly conservative in its estimations of range size.
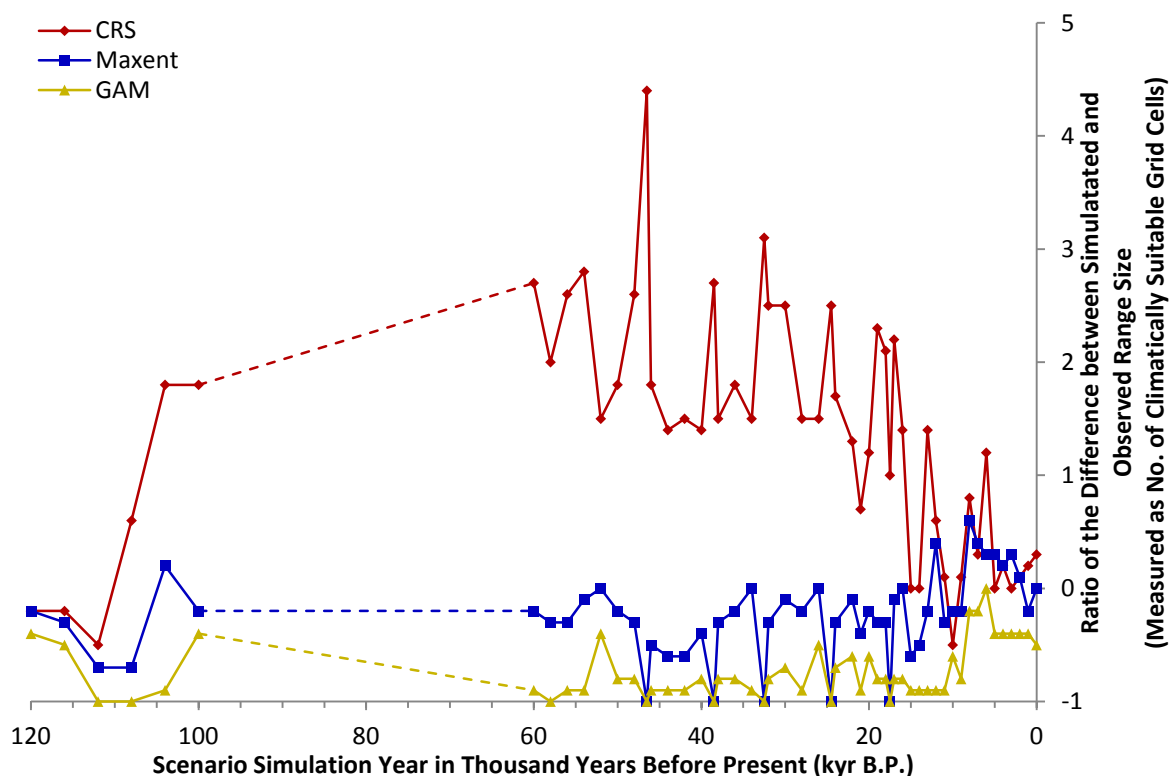

Figure 3.3.9: The difference in simulated range size from observed for *Pseudotsuga* spp. calculated as a ratio of the difference between the simulated and the observed distribution (total number of grid cells occupied) divided by the observed. Simulations were made for each of the 52 palaeoclimatic scenarios and present day using the climatic response surface model (CRS), maximum entropy (Maxent) and generalised additive model (GAM).

Note: The dashed line represents the period, 100 to 60 kyr B.P. when no simulations were modelled.

Tsuga species

There are many similarities among all three models when simulating the range size of *Tsuga* species and at some points there is overlap of predicted size (Fig. 3.3.10).   All three suggest that there are fewer climatically suitable areas available for *Tsuga* species during the colder glacial and stadial condition compared to the warmer interglacial, both the Eemian and the Holocene.   Both Maxent and GAM show the decline in climate availability during Heinrich Events observed across many of the other species and genera but the CRS model suggest that *Tsuga* species may have been resilient to these colder events with little or no change in the range size for scenarios chronologically adjacent.   The GAM model frequently produces the most 'optimistic' estimates of range size for *Tsuga* species, while CRS is generally the most conservative and Maxent shows the most variation in predictions of range size of all the models.
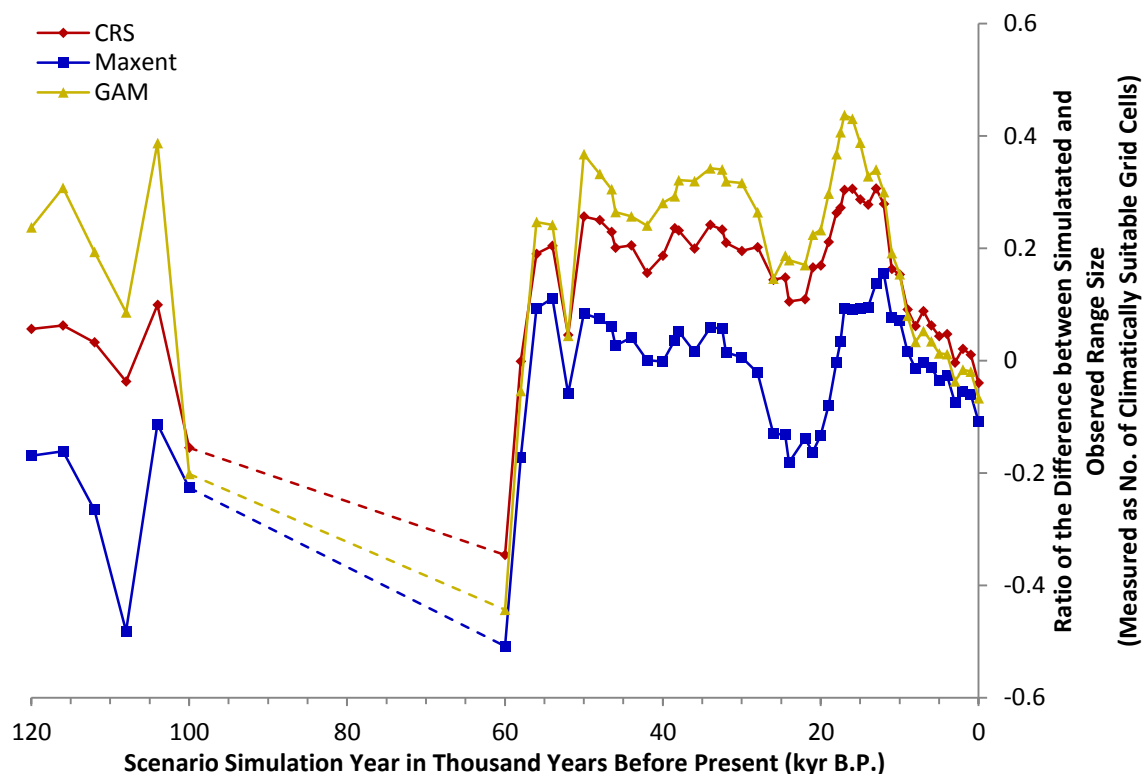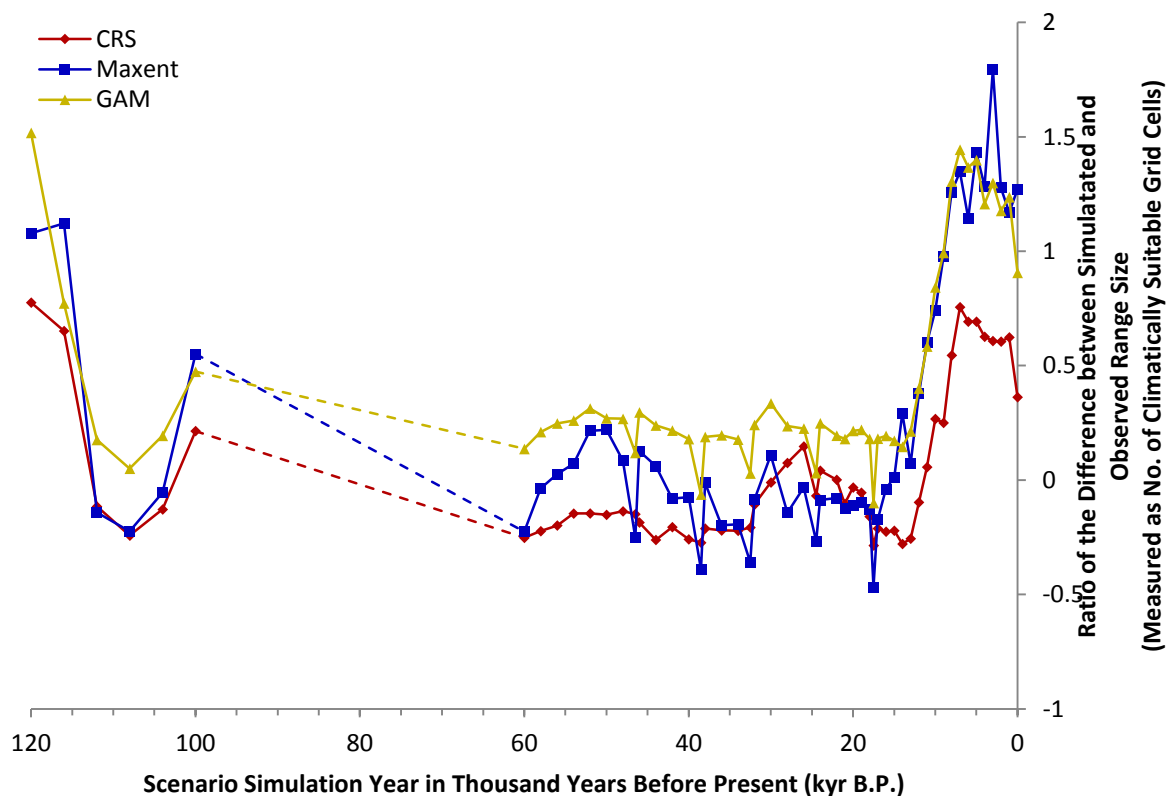

Figure 3.3.10:   The difference in simulated range size from observed for *Tsuga* spp. calculated as a ratio of the difference between the simulated and the observed distribution (total number of grid cells occupied) divided by the observed.   Simulations were made for each of the 52 palaeoclimatic scenarios and present day using the climatic response surface model (CRS), maximum entropy (Maxent) and generalised additive model (GAM).

Note: The dashed line represents the period, 100 to 60 kyr B.P, when no simulations were modelled.

Picea abies

The relative change in range size modelled by CRS, Maxent and GAM for *Picea abies* is highly correlated across the 120 thousand years investigated, with CRS and GAM producing comparable values for the cumulative range extent during the Eemian interglacial, prior to the glacial onset, and the latter stages of warming before the beginning of the Holocene (Fig. 3.3.11). The Maxent model for *Picea abies* identifies the fewest sites of climatic suitability during the glaciation, but simulates the most during the Holocene conditions resulting in the highest variance of range size predictions. GAM and CRS maintain their close association in simulated range size, with GAM producing a slightly higher range size prediction during the glacial and CRS being more 'optimistic' during the Holocene. Heinrich Events are observed to be the most constraining climatic scenarios across all the modelling techniques and *Picea abies*, like the models produced for the genus of *Picea*, is more limited in range size during the glacial than the later warmer Holocene, but it also appears to have been more restricted during the previous interglacial too.
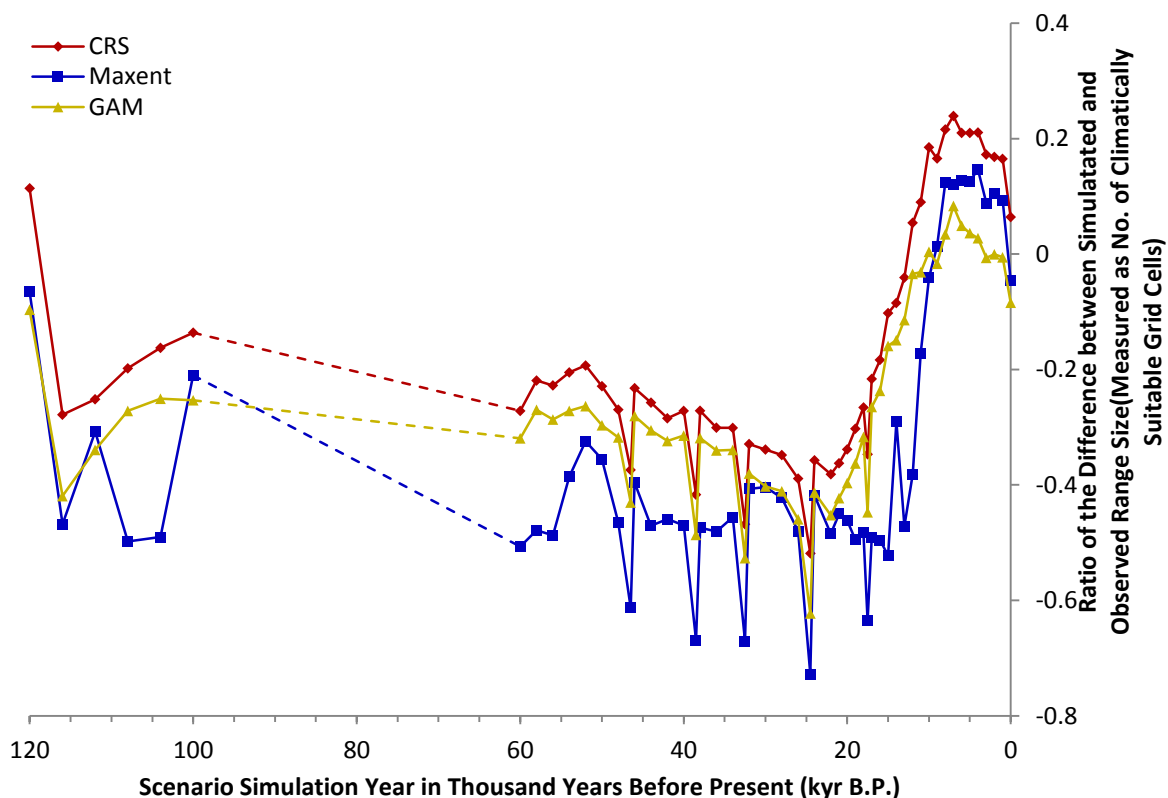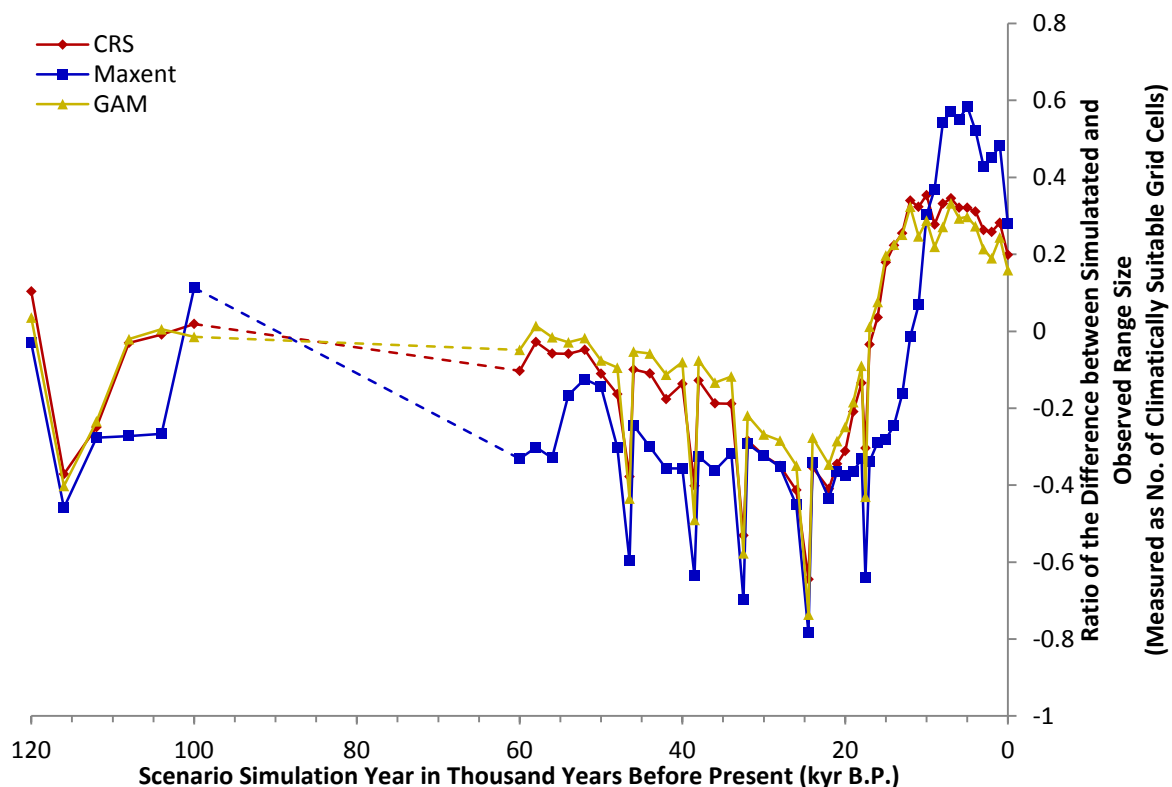

Figure 3.3.11:   The difference in simulated range size from observed for *Picea abies* calculated as a ratio of the difference between the simulated and the observed distribution (total number of grid cells occupied) divided by the observed.   Simulations were made for each of the 52 palaeoclimatic scenarios and present day using the climatic response surface model (CRS), maximum entropy (Maxent) and generalised additive model (GAM).

Note: The dashed line represents the period, 100 to 60 kyr B.P, when no simulations were modelled.

Pinus sylvestris

Overall the range size change for *Pinus sylvestris* throughout the last 120 thousand years correlate with those modelled for its collated genus (Fig. 3.3.8), with there being fewer areas of climatic suitability during the colder glacial compared to the interglacial conditions of 120 thousand years ago and the Holocene (Fig. 3.3.12). All three models demonstrate similar corresponding changes in range size across all the simulations, with Maxent yet again producing the most conservative estimates while the GAM indentifies the most sites suitable at each scenario as well as having the greatest variance in range size predictions across the scenarios. There is also a decline in the climatically suitable range during the colder Heinrich Events of the glacial exhibited across all the modelling techniques, and a rapid increase in climate available post the last Heinrich Event (17 thousand years ago) to a peak around 9-7 thousand years ago with a slight decrease since.
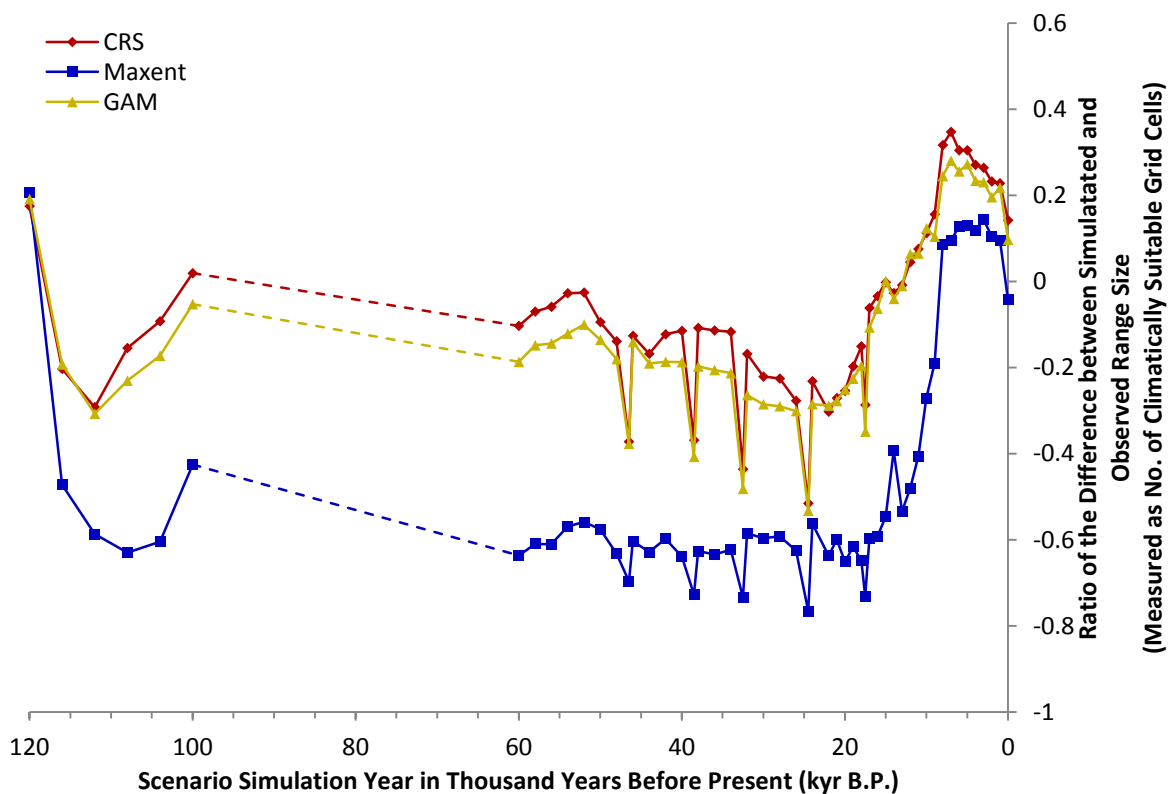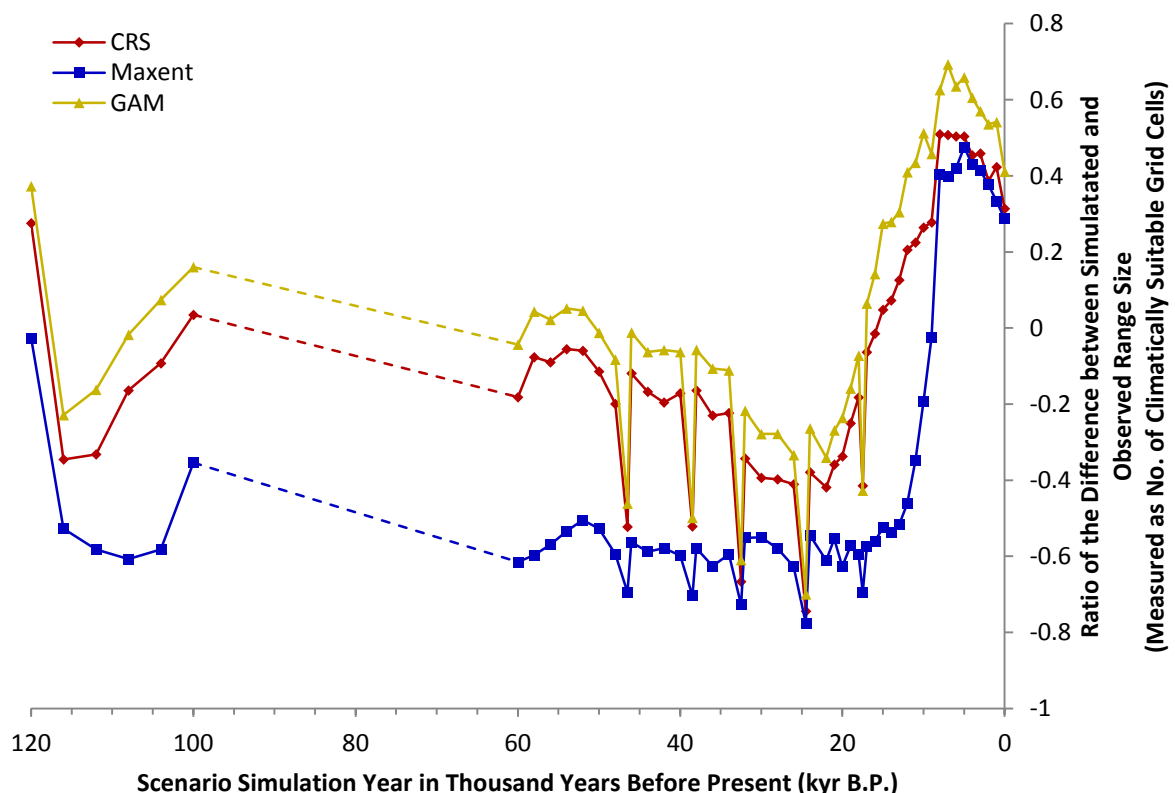

Figure 3.3.12:   The difference in simulated range size from observed for *Pinus sylvestris* calculated as a ratio of the difference between the simulated and the observed distribution (total number of grid cells occupied) divided by the observed.   Simulations were made for each of the 52 palaeoclimatic scenarios and present day using the climatic response surface model (CRS), maximum entropy (Maxent) and generalised additive model (GAM).

Note: The dashed line represents the period, 100 to 60 kyr B.P, when no simulations were modelled.

Pinus occidentalis

The other Caribbean modelled species, *Pinus occidentalis*, the food-plant of *L. megaplaga,* shows some similarities in the model predictions. All the models similarly suggest significant constraints during the stadial conditions, 112-108 thousand years ago, compared to the earlier Eemian glacial conditions, and there is an increase in climatically suitable range post the stadial (Fig. 3.3.13). Similarly GAM and Maxent range size predictions demonstrate a similar change through the glacial, with interstadial conditions being more favourable and Heinrich Events having no suitable climate for *P. occidentalis*, like *L. megaplaga*. The CRS model simulations do not show consistency in response in relation to described climate events during the glacial. However, there is a consensus among all three models that the earlier conditions of the Holocene, 10 thousand years ago were more suitable with a decline in suitability to present day. Maxent is the most conservative of the range size predictors, while GAM and CRS both have significantly larger range size predictions and GAM shows the greatest variation in range size predictions.
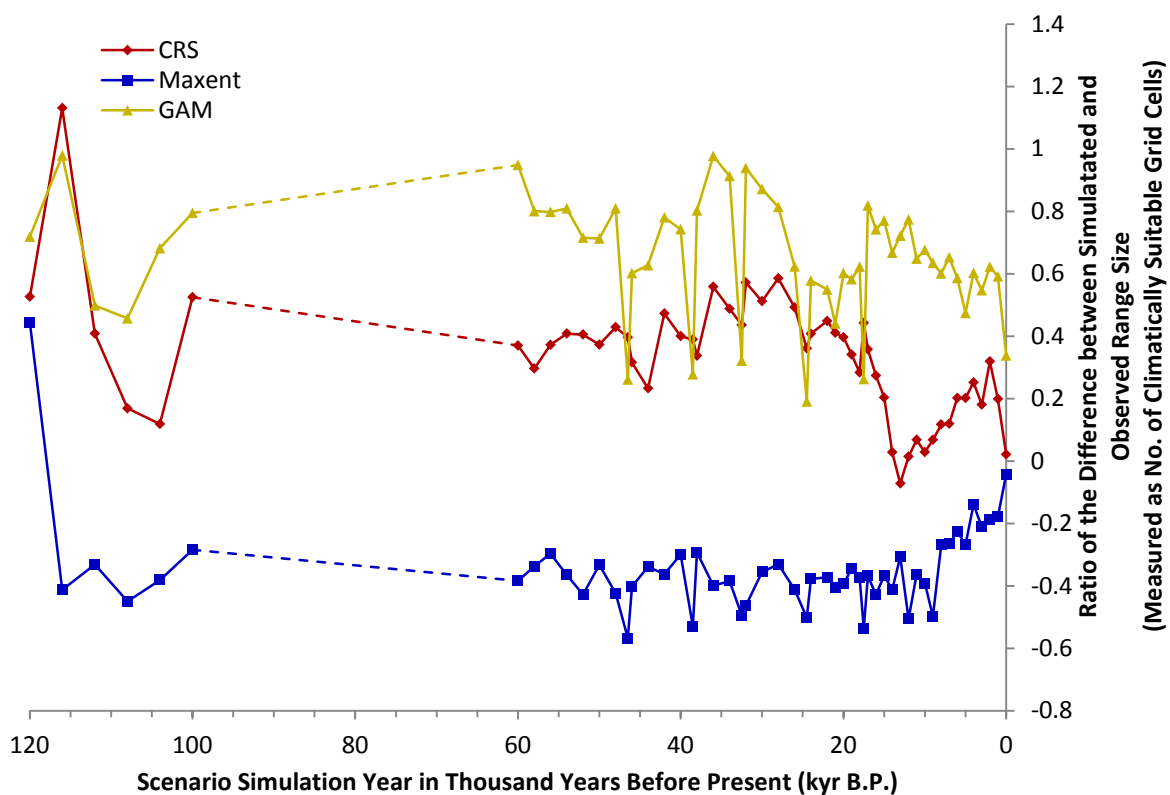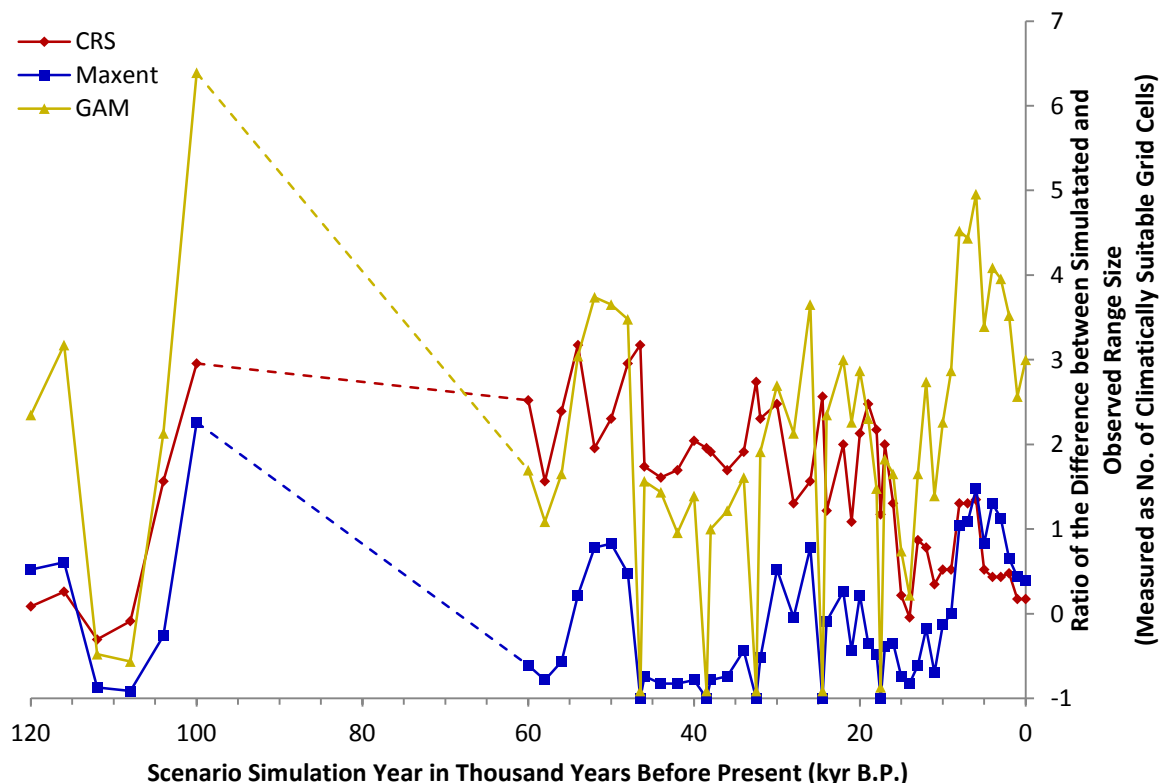

Figure 3.3.13:   The difference in simulated range size from observed for *Pinus occidentalis* calculated as a ratio of the difference between the simulated and the observed distribution (total number of grid cells occupied) divided by the observed. Simulations were made for each of the 52 palaeoclimatic scenarios and present day using the climatic response surface model (CRS), maximum entropy (Maxent) and generalised additive model (GAM) using the Caribbean bioclimatic grid.
Note: The dashed line represents the period, 100 to 60 kyr B.P, when no simulations were modelled.

Section 3.4

Observed Compared with Simulated Range

Loxia curvirostra

The CRS model for *Loxia curvirostra* produced 'goodness of fit' measures of very good and high assessment values respectively for maximum κ value (0.790) and AUC (0.970), with the best performing probability threshold being at 0.454.   The CRS (Fig. 3.4.1) indicates a broad climatic niche within the available present climatic range with a large proportion of probabilities of occurrence greater than 0.900 probability threshold. Most suitable bioclimatic conditions ranged between approximately -25°C and 8°C MTCO, up to 6,500 GDD5 and there is still prevalence of suitability at the lowest moisture availability of 0.400 AET/PET cut off shown in the diagram, indicating this broad tolerance of temperature and moisture availability in habitat selection.
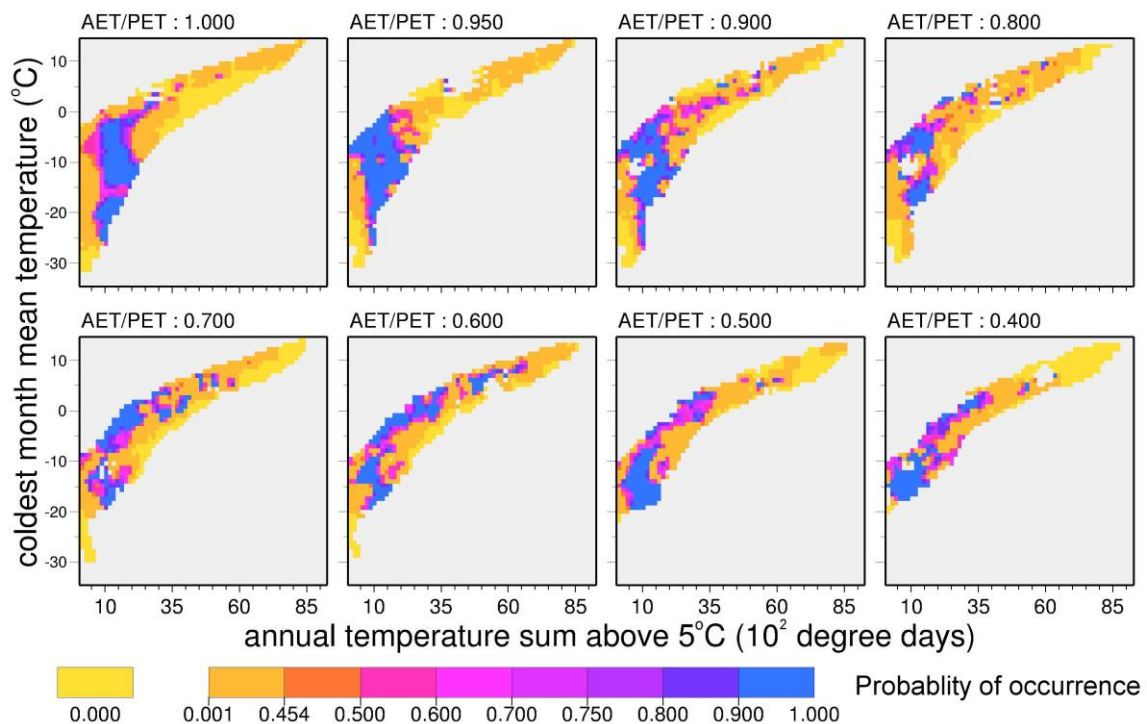
Figure 3.4.1: Climatic response surface for *Loxia curvirostra*.

The simulated range (Fig. 3.4.3) is generally very similar to the observed (Figure 3.4.2) distribution, spanning across the northern hemisphere throughout Eurasia and northern North America, along the west coast of North America and the Himalayas.   In many areas the simulated distribution is patchier than the observed, but it is important to note that the observed data is providing only an overall indication of range extent and so the simulation may be accurate in identifying areas within the overall range which may not be suitable for *L. curvirostra* to persist.

Figure 3.4.2: The gridded observed distribution of *Loxia curvirostra*.
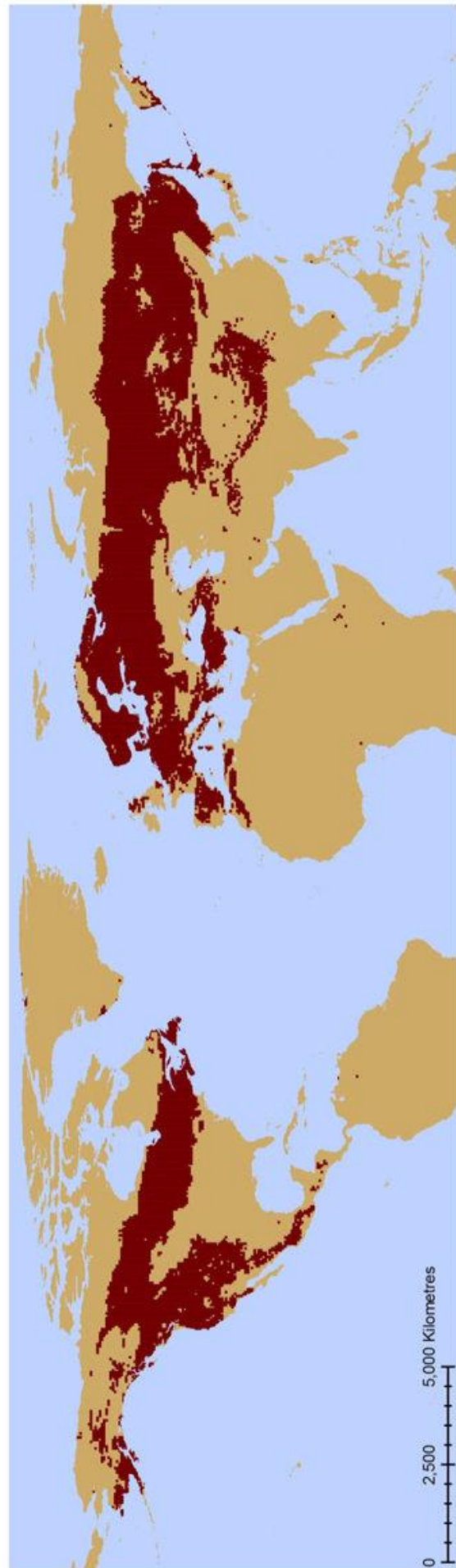
Figure 3.4.3: The simulated present distribution of *Loxia curvirostra* produced by the CRS model. κ = 0.790 AUC = 0.970

However, in other cases, the simulated range does indicate climatically suitable areas where the species is not recorded, such as in southern Alaska, sporadic incidence in eastern Africa and into far-eastern Siberian Kamchatka Peninsula. Notably, areas in the UK are also simulated as being suitable for breeding, especially Scotland, even though, following consultations with the literature; observances of *L. curvirostra* were eliminated as they were identified as being recent and of anthropogenic origins (Section 1.5). However, it may actually be that climate in recent times, post industrialisation, has indeed become suitable for this species and conifer plantations are a secondary contribution to the establishment of breeding in the British Isles. In addition, the CRS model also simulates the small isolated populations in the Philippines and Vietnam. Although simulated as smaller than the observed ranges in these regions, the fact the model correctly predicts this small range is important as it indicates the model represents the broad *Loxia curvirostra* climatic niche. Overall the model identifies 15,476 climatically suitable grid cells, this is substantially greater number than those occupied, which is 14,963 grid cells, but this demonstrates the climatic response surface model is very effective at representing the distribution of *L. curvirostra*.

Loxia leucoptera

The *L. leucoptera* model has a 'very good' maximum κ value (0.767) at the probability threshold of 0.439 and a 'high' AUC (0.972) measure of 'goodness of fit' for the CRS model. The CRS (Fig. 3.4.4) produced indicates that *Loxia leucoptera* occupies environments of moisture abundance, ideally greater than 0.500 AET/PET and colder climes, less than -25°C to -2°C MTCO and shorter growing seasons, lower than 2,000 GDD5.
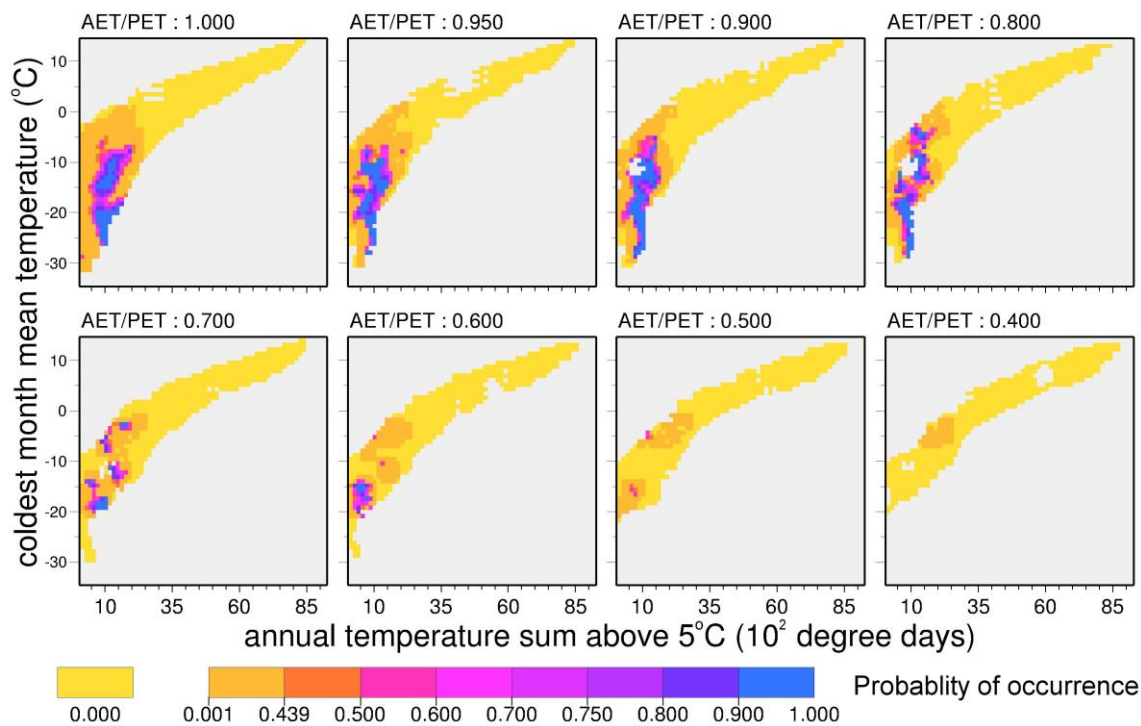
Figure 3.4.4: Climatic response surface for *Loxia leucoptera*.

The simulated range (Fig. 3.4.6) resembles the observed (Fig. 3.4.5) distribution of *L. leucoptera* most accurately in North America, where discrepancies are mainly the patchiness in mid-range, which may be accurate due to the observations being primarily of range extent, and the model does not simulate as far east as is observed, into Newfoundland and Labrador. The Eurasian simulation diverges more from the observed distribution, showing climate suitable in the Siberian Kamchatka Peninsula and northern Japan as well as in the Caucasus Mountains. Interestingly, climate is also highlighted as being suitable across Fennoscandia, a region which many researchers have wondered why *L. leucoptera* has not occupied, its absence being explained by a combination of the absence of *Larix* species and possible competition with *L. pytyopsittacus* which is native to Fennoscandia. The model simulates 11,080 grid cells of suitable climate only around 500 cells greater than the observed ranges of 10,548.

Figure 3.4.5: The gridded observed distribution of *Loxia leucoptera*.

Figure 3.4.6: The simulated present distribution of *Loxia leucoptera* produced by the CRS model. κ = 0.767 AUC = 0.972

Loxia pytyopsittacus

L. pytyopsittacus was modelled using the smaller European climatic grid, producing a simulation of 'excellent' maximum κ value (0.861) fit at the probability threshold of 0.508 and 'high' AUC (0.987).   The CRS (Fig. 3.4.7) indicates that within the climate of Europe, *Loxia pytyopsittacus* has a select niche, breeding in areas of high moisture availability, 0.800 or higher AET/PET, between -13°C and -2°C MTCO and growth season remains less than 2,000 GDD5.
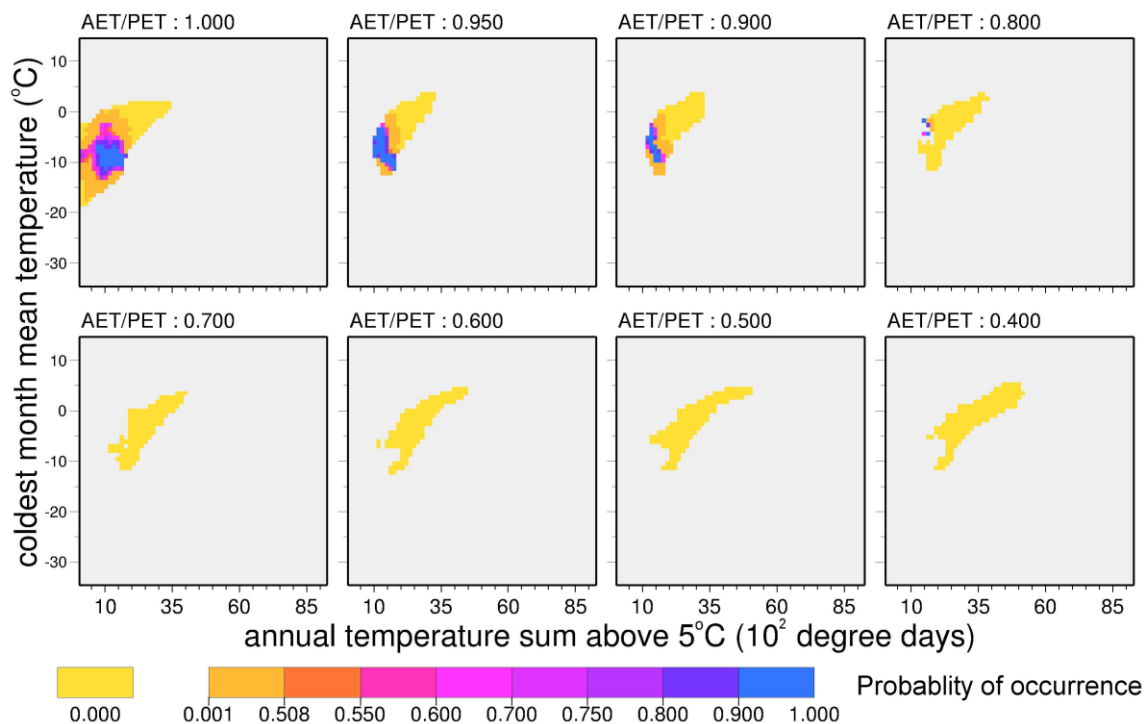
Figure 3.4.7: Climatic response surface for *Loxia pytyopsittacus.*

The main simulated range (Fig. 3.4.9) extent is of great similarity to the observed (Fig. 3.4.8), although the simulations suggest climate is suitable to the northern coast of Russian Murmansk Oblast, the species' absence there may be accounted for by their feeding tree, *Pinus sylvestris* not being native to this northerly region.   The model also indicates that the climate of mountainous regions in central Europe, such as the Alps, the Pyrenees and also the Caucasus Mountains in Eastern Europe as suitable for *L. pytyopsittacus.*   These mountain ranges, although climatically suitable, are geographically isolated from the present day population so they are unlikely to be colonised and being rather sporadically spread may not be able to sustain a population of *L. pytyopsittacus.*   Overall, the simulation produces a total of 2,562 grid cells that are climatically suitable, this is only slightly greater than the 2,409 it is observed in, indicating that the model simulates a similar sized range to the observed.
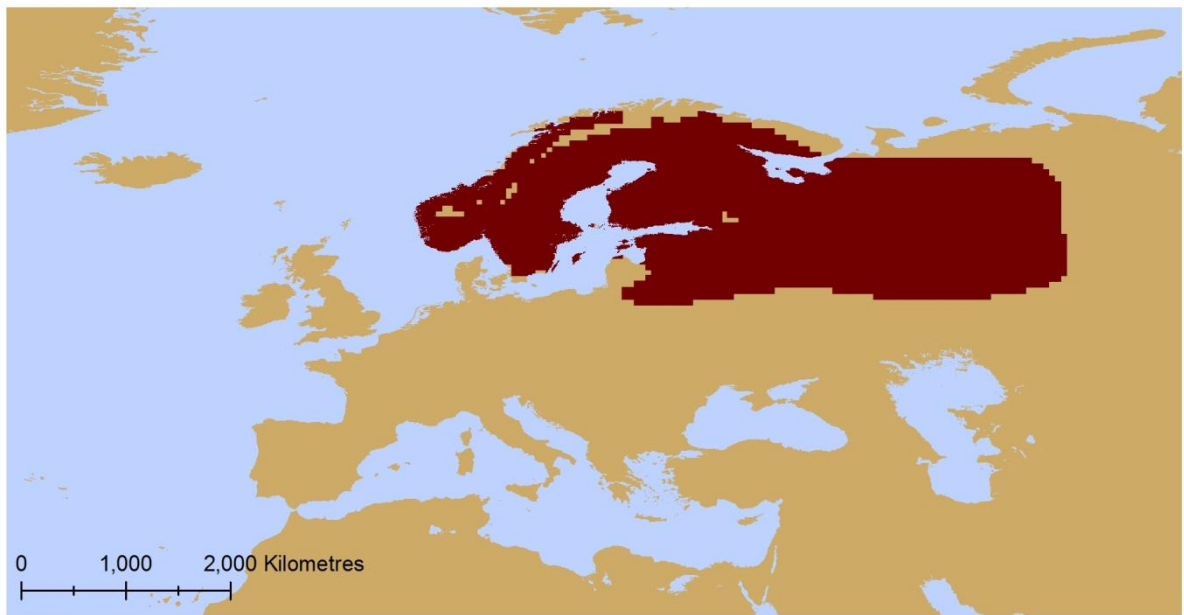
Figure 3.4.8: The gridded observed distribution of *Loxia pytyopsittacus*.
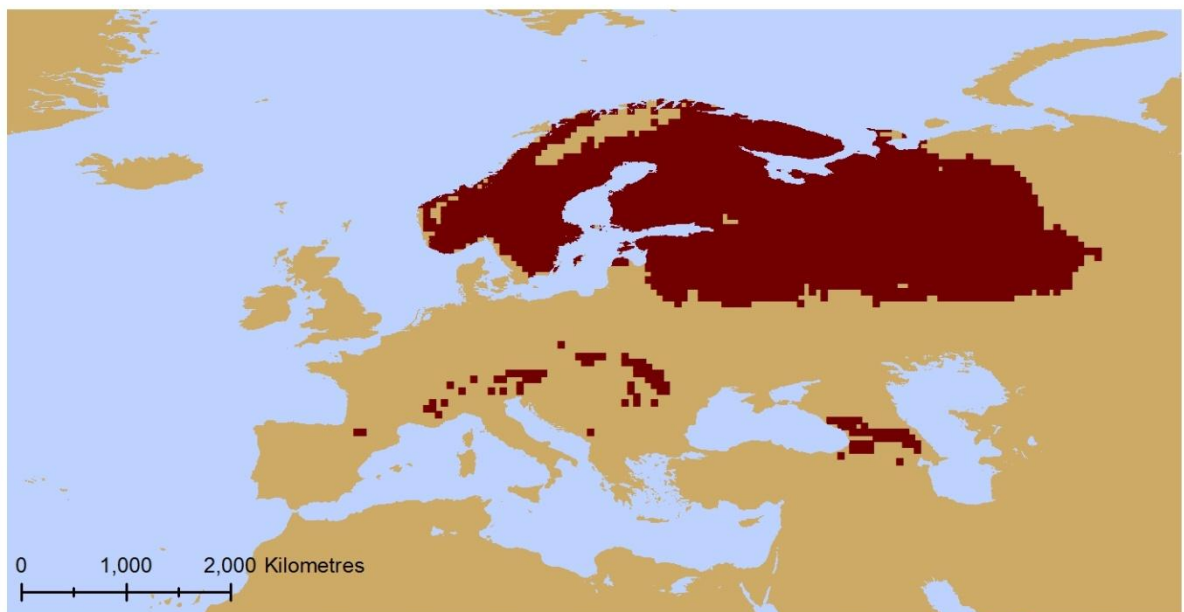
Figure 3.4.9: The simulated present distribution of *Loxia pytyopsittacus* produced by the CRS model and the European grid. $\kappa = 0.861$ AUC $= 0.987$

Loxia scotica

Also modelled using the European bioclimate, the CRS model produced for *L. scotica* is of a 'very good' fit for the maximum κ value (0.702) achieved at the probability threshold of 0.352 and a 'high' model performance as ascertained from the AUC (0.999). The climatic response surface (Fig. 3.4.10) indicates that the range of *L. scotica* has a very specific climatic niche; the MTCO is between -2°C and 0°C, moisture availability at 1.000 AET/PET and a growth season between 500-1,000 GDD5.
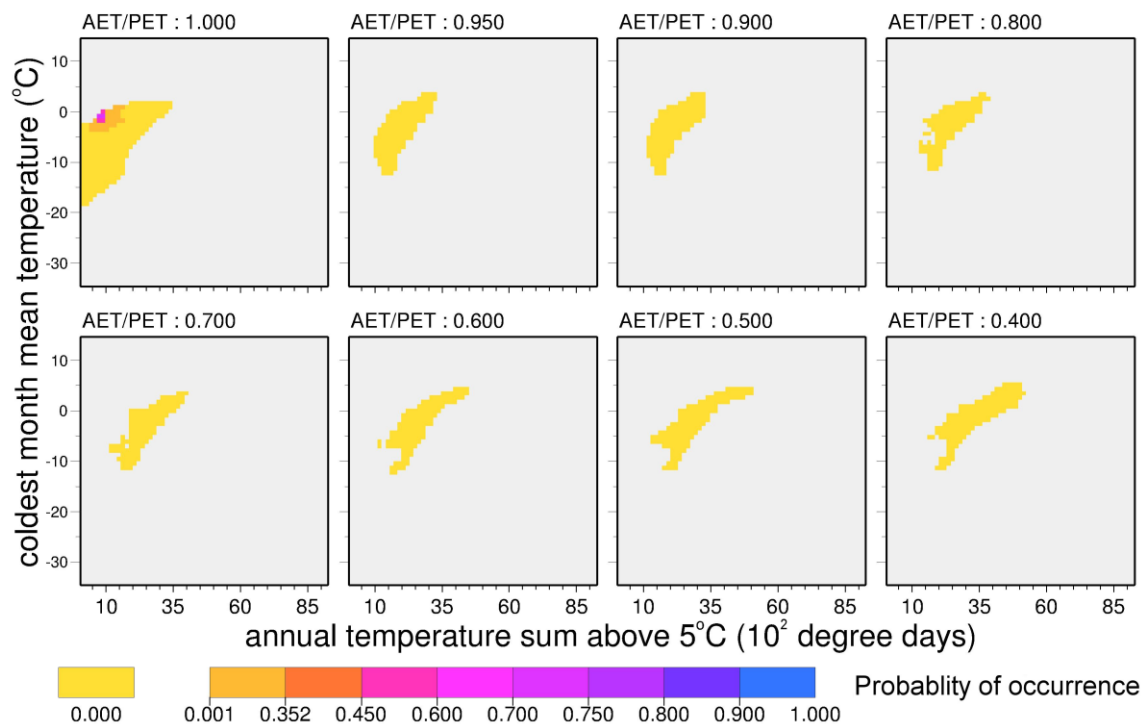
Figure 3.4.10: Climatic response surface for *Loxia scotica.*

The simulated climatically suitable range (Fig. 3.4.12) is slightly smaller than the observed (Fig. 3.4.11), specifically not finding the climate suitable to the east of the range, in North-eastern Scotland, Aberdeenshire and Angus. However, when compared to the original range outline (Fig. 1.1.4), prior to gridding, the records of breeding in North-eastern Scotland do not reach the coastline and in fact the presence is based on some spurs of occupation from the core breeding range in central and northern Scotland. On this basis it might be postulated that the average climatic conditions across eastern regions of Aberdeenshire and Angus are not suitable for *L. scotica*, except in isolated areas. In addition the simulated present distribution indicates that breeding should be climatically viable further south than the species currently occurs, but it may be that this range is not achievable due to deforestation or other anthropogenic changes to the habitat. Overall the model simulation is of great resemblance, although the simulation is more limited in range generating just 14 suitable grid cells only

nine less than the observed of 23, it does not suggest that any climate outside of Scotland is currently suitable for *L. scotica*, it occupies a unique climatic niche.
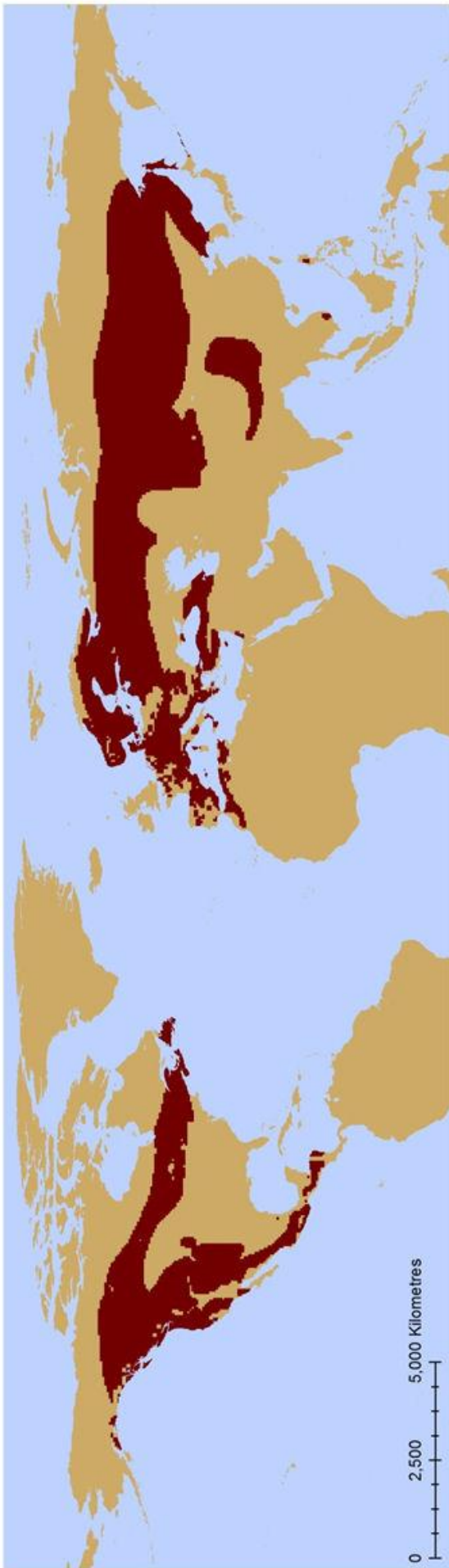

Figure 3.4.11: The gridded observed distribution of *Loxia scotica.*
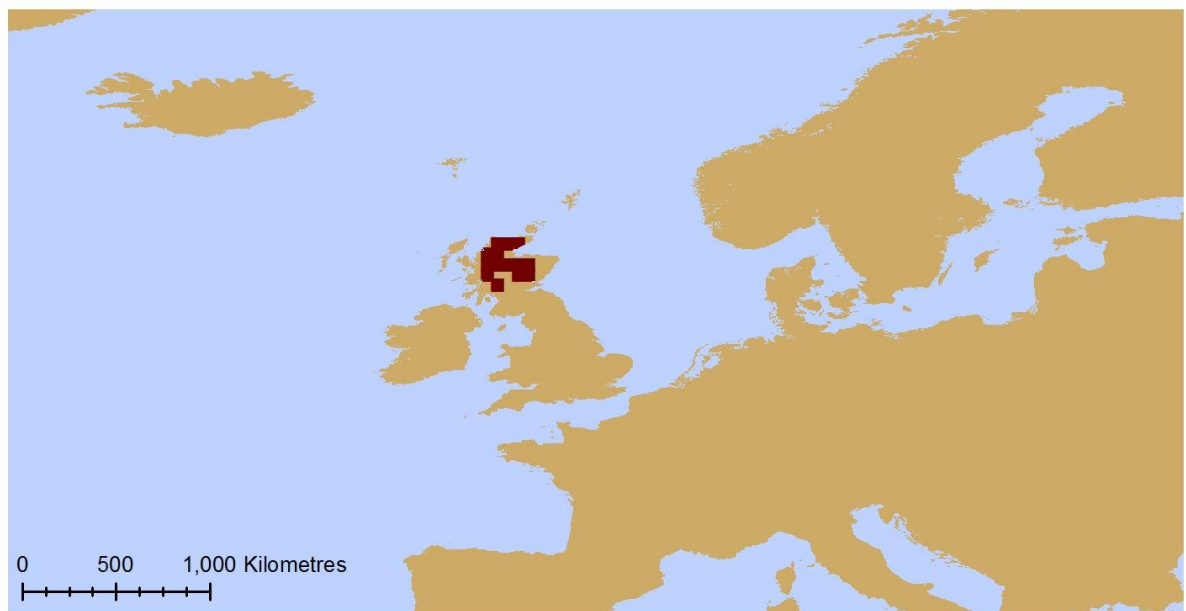
Figure 3.4.12: The simulated present distribution of *Loxia scotica* produced by the CRS model and the European grid. $\kappa = 0.702$ AUC $= 0.999$.

Loxia megaplaga

The smallest population, both in individual numbers and range coverage, of *Loxia*, *L. megaplaga*, native to Hispaniola, was modelled using climate data just from the Caribbean region, and produced a 'high' AUC (0.992) performance and a 'good' maximum κ value (0.690) 'goodness of fit' at the probability threshold of 0.312. The CRS (Fig. 3.4.13) indicates a very small climatic niche in the Caribbean for *L. megaplaga*, unsurprisingly when considering the limited range size. *L. megaplaga* is found in significantly hotter more tropical conditions than other crossbill species, moisture availability between 0.900 and 0.950 AET/PET, the MTCO is constrained between 7°C and 12°C and growing season between 4,500 and 7,000 GDD5. However, within this already very narrow climatic niche of the Caribbean, there is a unique climatic condition which is generated as most suited (blue), at 0.950 AET/PET, *ca*. 7°C MTCO and 4,500 GDD5, and is an outlier to rest of the Caribbean climate. This scenario is likely to represent the climatic conditions in the mountainous regions of Hispaniola where the *L. megaplaga* is found.
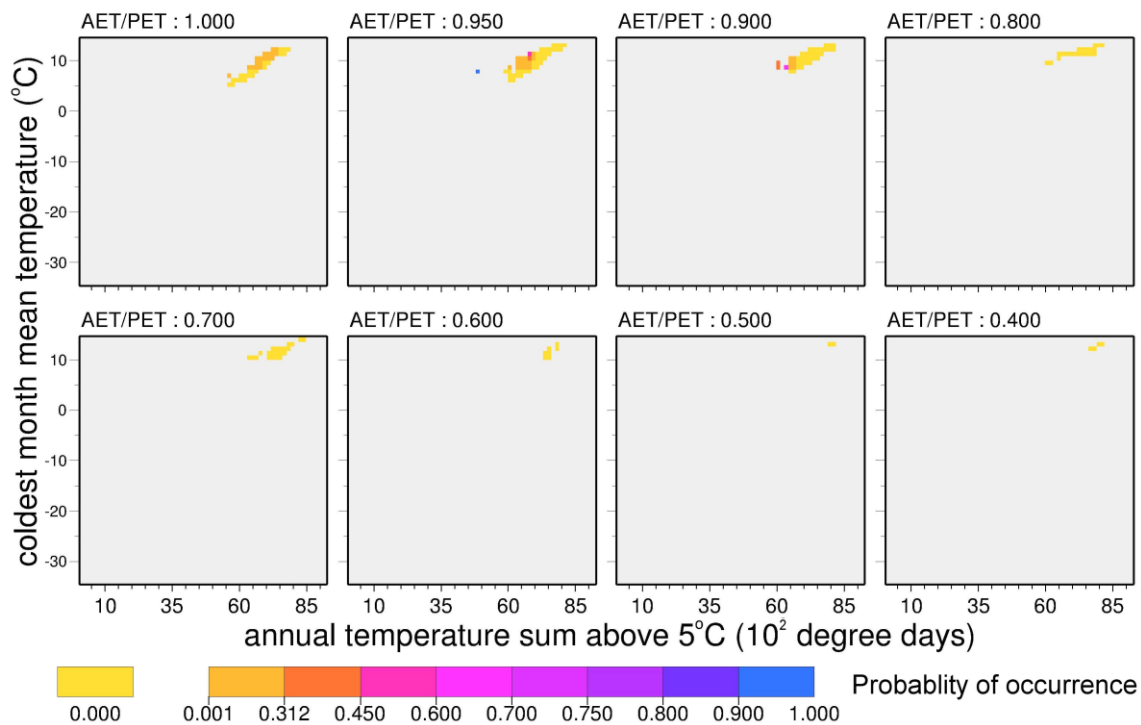
Figure 3.4.13: Climatic response surface for *Loxia megaplaga*.

At the best threshold (0.312), the CRS model accurately predicts the distributions of *L. megaplaga* in central Hispaniola (Fig. 3.4.15); however it does not simulate the isolated occurrence in the mountain range Massif de la Hotte in the Sud and Grand'Anse department of Haiti seen in the observed distribution (Fig. 3.4.14). This is probably due in part to the difference in climate this maritime location would have from the central mountainous region the species primarily occupies and the likelihood that this microclimate a smaller region of is

not represented at this coarse grid-scale.   Overall this resembles a good fit, but the model also produces a number of false-presence simulations in northern South America (Colombia: 2 simulated grid cells) and Central American (Honduras: 1 cell and Nicaragua: 2 cells).
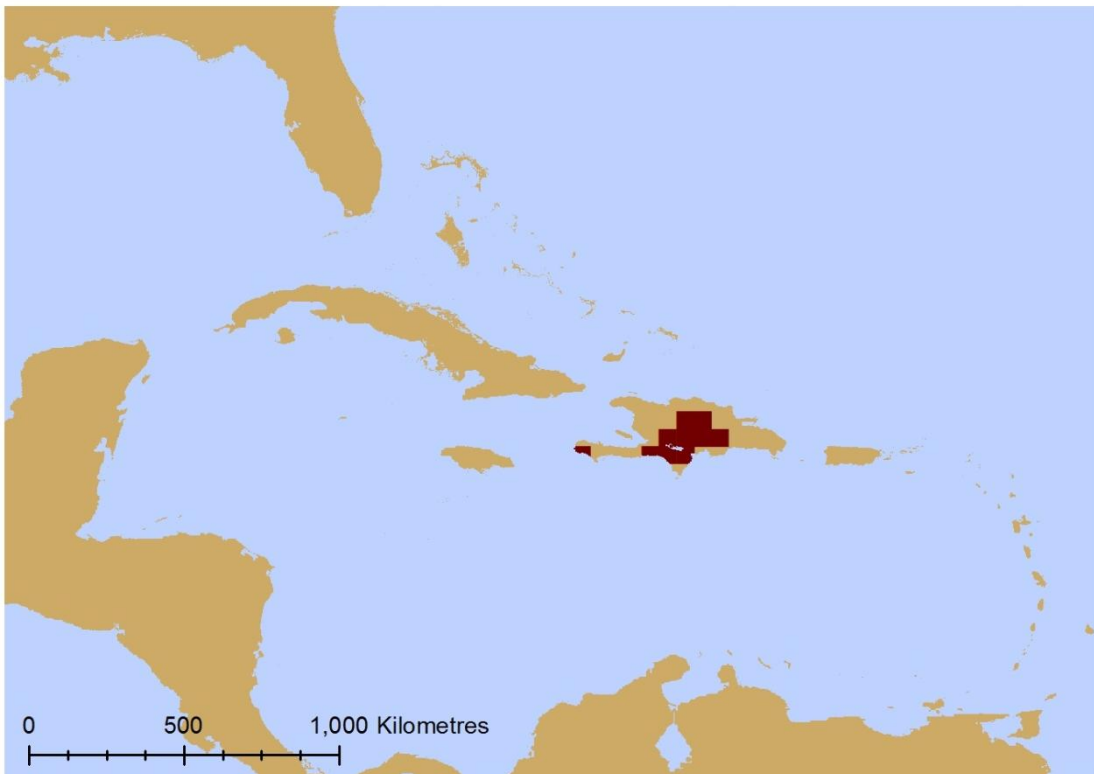
Figure 3.4.14: The gridded observed distribution of *Loxia megaplaga*.
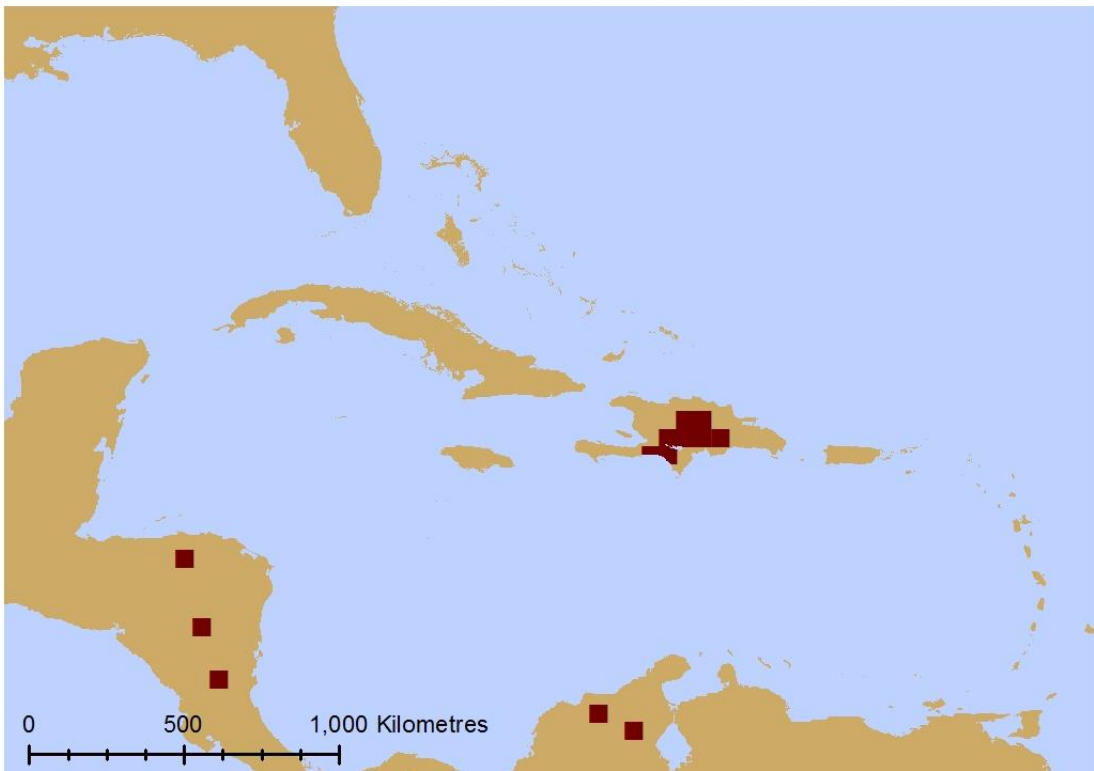
Figure 3.4.15: The simulated present distribution of *Loxia megaplaga* produced by the CRS model using the Caribbean grid. $\kappa = 0.690$ AUC $= 0.992$.

Larix **species**

The CRS model for *Larix* species produced a 'very good' maximum κ value of 0.828 at the threshold of 0.488 and a 'useful' AUC value of 0.972.   The CRS (Fig. 3.4.16) indicates that *Larix* species can be found in two distinct climatic niches.   The larger is represented by cooler temperatures between -32°C and -5°C MTCO and moisture availability of 0.500 or greater AET/PET and growth season lower than 2,500 GDD5.   The other, smaller climatic niche has a longer growing season and warmer minimum temperatures, present in conditions of moisture indices ranging between 0.700 to 0.950 AET/PET, a MTCO between 0°C and 7°C and growing seasons of 3,000 to 7,500 GDD5.
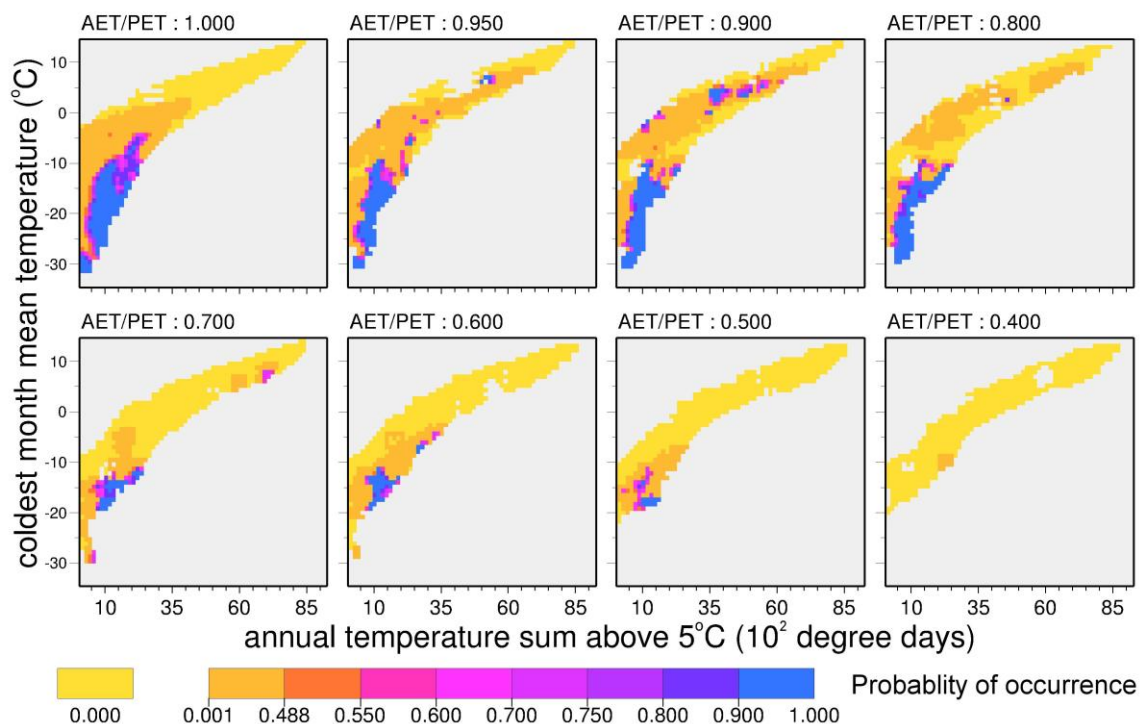
Figure 3.4.16: Climatic response surface for *Larix* species.

The simulated distribution of *Larix* species (Fig. 3.4.18) closely resembles that of the observed (Fig. 3.4.17).   The greatest discrepancy is the absence of simulations in Europe of the *Larix decidua* whose observed range is in the Alps.   Although there are some climatically suitable areas generated in the Polish Carpathian Mountains and the Caucasus Mountains; evidently the climatic space *Larix decidua* is found in is distinctly different from the rest of the observed ranges and its small size means it is not defined in the niche model generated.   Its lack of simulation has no marked significance on the calculated maximum κ value the AUC values.

Figure 3.4.17: The gridded observed distribution of *Larix* species used as feeding trees for *Loxia* species.

Figure 3.4.18: The simulated present distribution of *Larix* spp. produced by the CRS model. κ = 0.828 AUC = 0.981

Despite the lack of *Larix decidua*, the rest of the distributions are represented using the climate based model.   The core Eurasian range throughout Siberia and into northern China and Japan is very similar to the observed, with a minor difference in the eastern extent to the range, 'false' presences simulated in the Russian region of Chukotka and northern Kamchatka peninsula.   The Himalayan *Larix* species were simulated more sporadically than the observed ranges had indicated, although the climate is not indicated as suitable as far north as ranges have indicated species are found.   In Northern America, the range simulations are similar to the observed especially in Alaska and Canada; however, there are some areas highlighted as climatically unsuitable which in fact are occupied to the east in Newfoundland and Quebec.   Overall the simulation generates less climatically suitable grid cells, 12,677, than the observed range (13,202) highlighting that the not all the ranges lie within a similar climatic niche, such as that of *Larix decidua*.

BLANK PAGE

Picea species

For the *Picea* species, the CRS model produced a present simulation of a 'very good' maximum κ value (0.805) at the best performing probability threshold (0.431) and a 'high' AUC (0.956) fit to the observed.   The CRS (Fig. 3.4.19) shows that the primary climatic niche *Picea* species occupy is colder, -30°C to 2°C MTCO and has a shorter growing season, less than 2,500 GDD5 with moisture availability not being significantly restricting to the 0.400 AET/PET assessed here.   In warmer climes, between 2°C and 5°C MTCO and longer growing seasons, 3,500 and 6,000 GDD5 there are also conditions which are suitable for some *Picea* species in areas with moisture availability between 0.600 and 0.900 AET/PET.
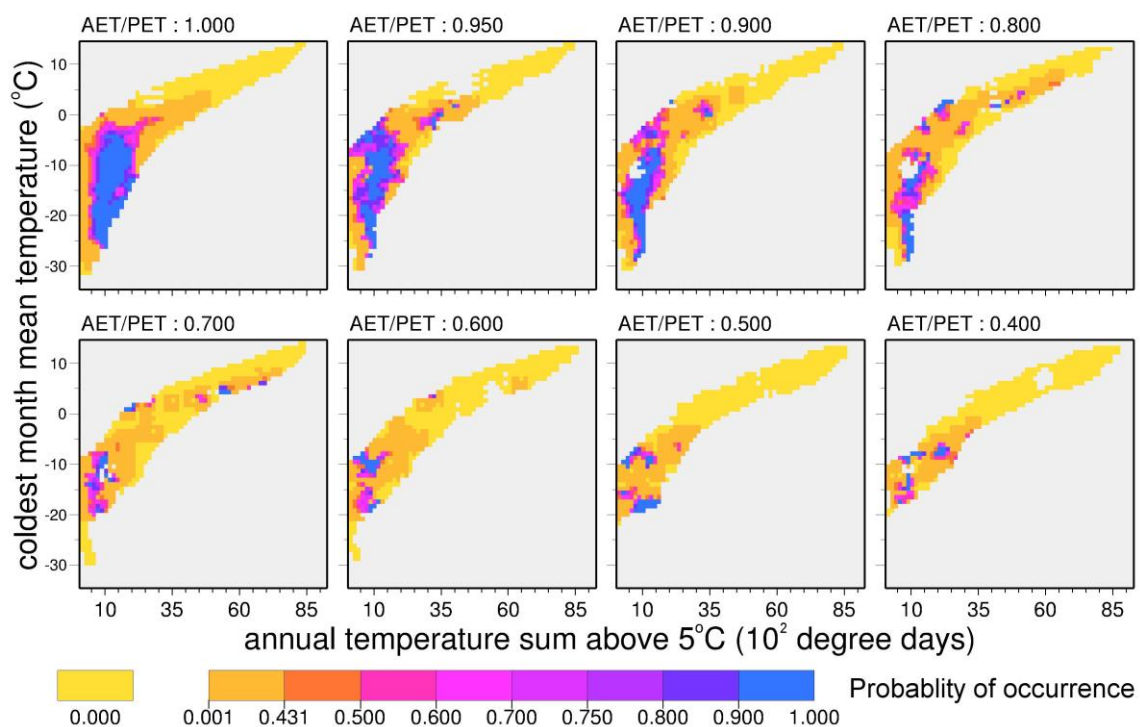
Figure 3.4.19: Climatic response surface for *Picea* species.

Comparison of the observed (Fig. 3.4.20) and simulated ranges (Fig. 3.4.21) in North America highlights a high-degree of similarity, although there are a numerous false-presences simulated making the range simulation less 'patchy'.   These areas may not be colonised for reasons other than climatic conditions, such a soil or substrate type.   The Eurasian simulation indicates a greater range of climatically suitable areas than are observed; further into the eastern Siberian Chukotka district and the coastline of Kamchatka peninsula; westerly, Scotland and northern Spain; and northerly, the Fennoscandian coastline and northern Russia. In central Asia, the simulations in the Himalayas are similar in extent but patchier than observed.   However, the overall fit of the CRS modelled range shows a great similarity to the observed.   The climatically suitable range totals 15,922 grid cells, greater than the observed (14,962), indicating that *Picea* does not exploit all the climatically suitable regions.

Figure 3.4.20: The gridded observed distribution of *Picea* species used as feeding trees for *Loxia* species.

Figure 3.4.21: The simulated present distribution of *Picea* spp. produced by the CRS model. κ = 0.805 AUC = 0.956

5,000 Kilometres

2,500

0

5,000 Kilometres

2,500

0

Pinus species

The consolidated *Pinus* species CRS model produced a present simulation of a 'good' maximum κ value (0.707) fit and 'high' AUC (0.953) measurement.   The CRS (Fig. 3.4.22) indicates that *Pinus* species occupy a wide spanning climatic niche and their tolerance of temperature appears linked with moisture availability.   In moisture rich environments, between 0.900 and 1.000 AET/PET, the MTCO can span between *ca*. -26°C and 1°C with a growing season of 2,500 GDD5.   Under 0.800 AET/PET value of moisture availability there is still a residual of this colder tolerating niche and a warmer thriving niche dominates, from around -7°C to 12°C MTCO and a larger range of growth season from 500 to 7,500 GDD5. *Pinus* species show a greater tolerance to temperature and moisture availability than the other conifer species, having a numerous species which occupy varying niches from the tropics to the boreal regions.
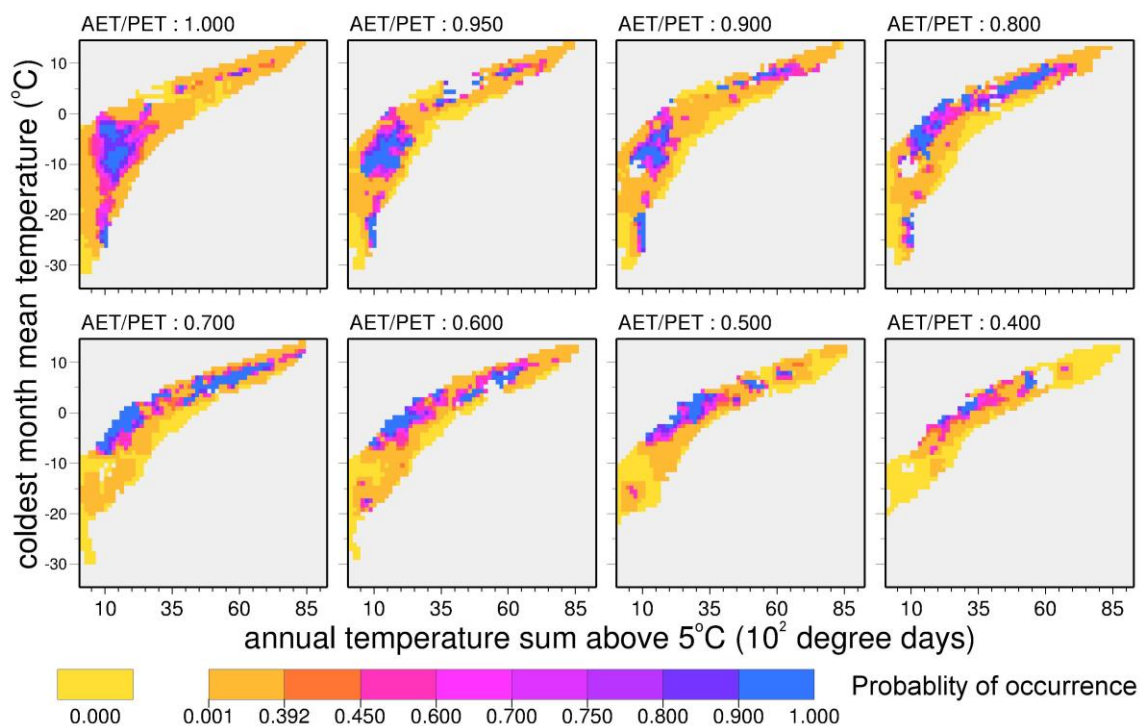
Figure 3.4.22: Climatic response surface for *Pinus* species.

Comparison of the simulated *Pinus* species range (Fig. 3.4.24) at the best performing probability threshold (0.392) with the observed (Fig. 3.4.23) indicates similarity between the North American western populations, although there are unoccupied modelled climatically suitable regions in Alaska.   In eastern North American the simulation suggests more climatically viable land to the west of the range, into other regions of Canada; Saskatchewan, and northerly into Ontario, Manitoba and Quebec, but the range is not simulated as southerly as it occurs into northern USA.   Simulation in Central America are similar, albeit a little sparser than the observed ranges might suggest, with some notable differences, for instance

Figure 3.4.23: The gridded observed distribution of *Pinus* species used as feeding trees for *Loxia* species.

Figure 3.4.24: The simulated present distribution of *Pinus* spp. produced by the CRS model. κ = 0.707 AUC =0.953

5,000 Kilometres

2,500

0

the modelled absence in Cuba and apparent climate suitable in south Florida and northern Colombia.

The simulations of the *Pinus* species in Eurasia show a many similarities, specifically across Siberia and Europe. Northern areas of Fennoscandia are incorrectly identified as inhospitable by the model, while the climate in western Spain is identified as suitable when in fact there are no current native *Pinus* species. In Great Britain, the CRS model correctly simulates the Scottish range of *Pinus sylvestris*, but it indicates that climate further north and south is also suitable as well as in south-eastern England. This is actually highly interesting given the great number of exotic conifers, many of which are *Pinus* species that have been introduced in these areas (Section 1.5) and the resulting establishment of *Loxia curvirostra* breeding colonies in the UK. Notably there are also presence simulations to the east, in the Russian region of Khabarovsk and the Sakhalin island into parts of northern China and Japan, these areas do have the kind of habitat pines could thrive in however the species selected that *Loxia* are known to consume do not have ranges in these areas (Section 2.1). The CRS model generates a substantially larger cumulative range spanning 13,022 grid cells compared to the 11,405 *Pinus* species are observed in. Compared to *Picea*, the simulation of *Pinus* species shows a lot more discrepancies, also reflected in the lower, although still good, maximum κ value. Interestingly this difference is not observed so greatly in the AUC value difference, only 0.003 lower than the *Picea*.

BLANK PAGE

Pseudotsuga species

The selection of *Pseudotsuga* species used with the CRS model produced a low 'good' maximum κ value (0.578) but a 'high' AUC (0.982). The climatic response surface (Fig. 3.4.25) indicates that the climatic niche of *Pseudotsuga* species is split, in a climate of full moisture saturation, a 1.000 AET/PET value, the MTCO occupied 0°C to 8°C mean temperature of the coldest month and a growing season between 3,000 and 6,000 GDD5. In more moisture restricted environments, below 0.950 AET/PET value, the climatic niche expands to include growth seasons as low as 500 GDD5 and tolerating -10°C MTCO.
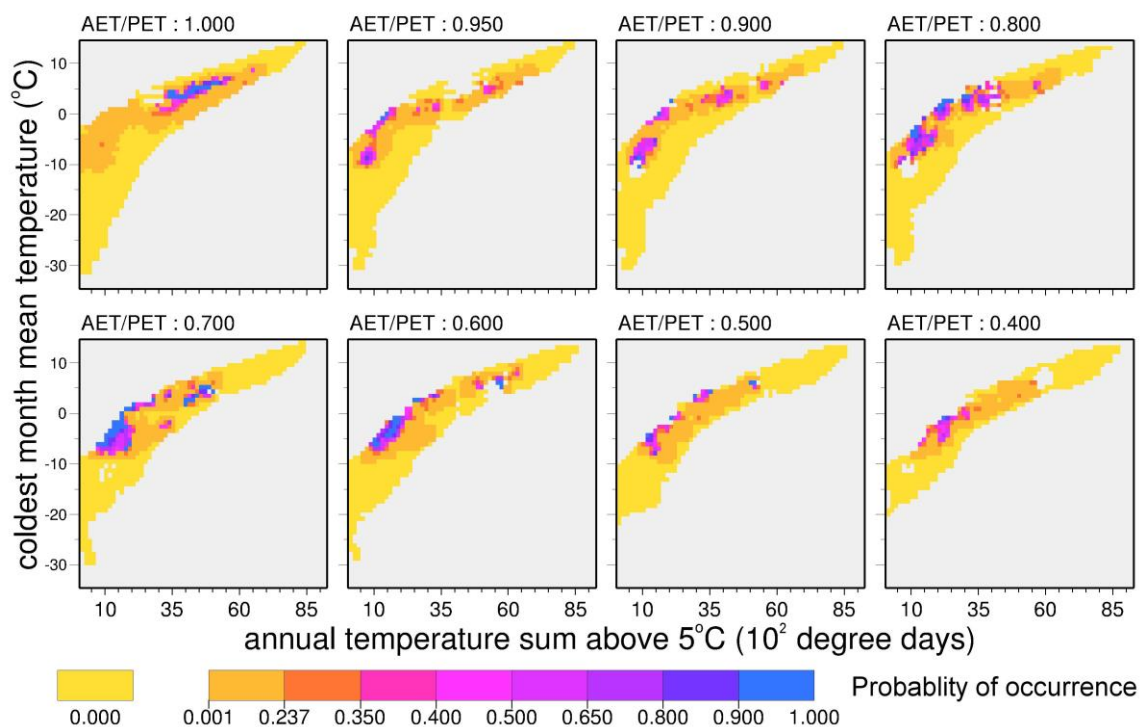
Figure 3.4.25: Climatic Response surface for *Pseudotsuga* species.

The simulated range of *Pseudotsuga* species (Fig. 3.4.27) at the best performing probability threshold (0.237) looks markedly similar to the observed range of *Pseudotsuga* (Fig. 3.4.26) in western North America. In Asia simulations are sparser than the observed ranges, although this may be more reflective of actual suitable habitat within the range outline. The model falsely simulates in the Himalayas, Turkey and also northern Spain and some dispersed locations across Europe. Interestingly the climate is indicated as suitable in south-eastern England, an area which has been exploited with a number of plantations of *Pseudotsuga* species. The simulation generates 1,350 grid cell presences, very close t o the observed (1,322), but many of these are found in different locations. The model performance appears weak from the statistics, and the genus' limited prevalence has likely affected its evaluation. Interestingly the model identifies areas which are suitable but unoccupied by naturally occurring species but which have been demonstrated to be ideal for introduced species.

Figure 3.4.26: The gridded observed distribution of *Pseudotsuga* species used as feeding trees for *Loxia* species.
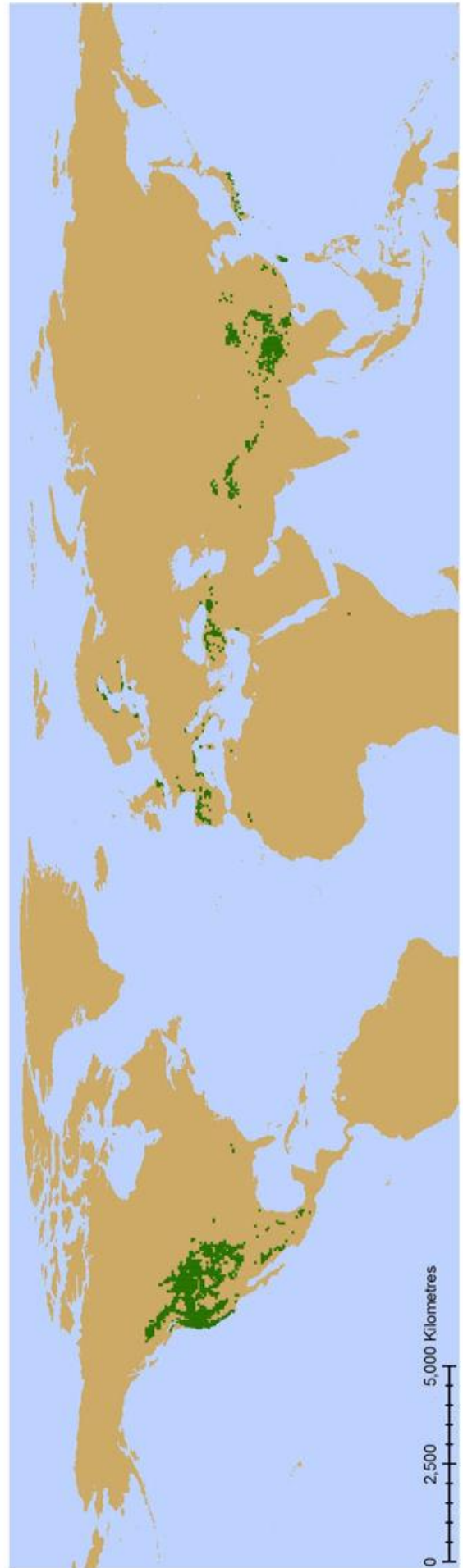
Figure 3.4.27: The simulated present distribution of *Pseudotsuga* spp. produced by the CRS model. κ = 0.578 AUC = 0.982

Tsuga species

The CRS model generates a present-day simulation of the selection of *Tsuga* species which is a 'good' maximum κ value (0.602) fit and 'high' AUC (0.980). The CRS (Fig. 3.4.28) for *Tsuga* species highlights that the present ranges are restricted by moisture availability, with suitable conditions above 0.600 AET/PET. Within this moisture niche, the growing season can vary greatly up to 6,500 GDD5 and MTCO tolerances can range between -10°C and 5°C.
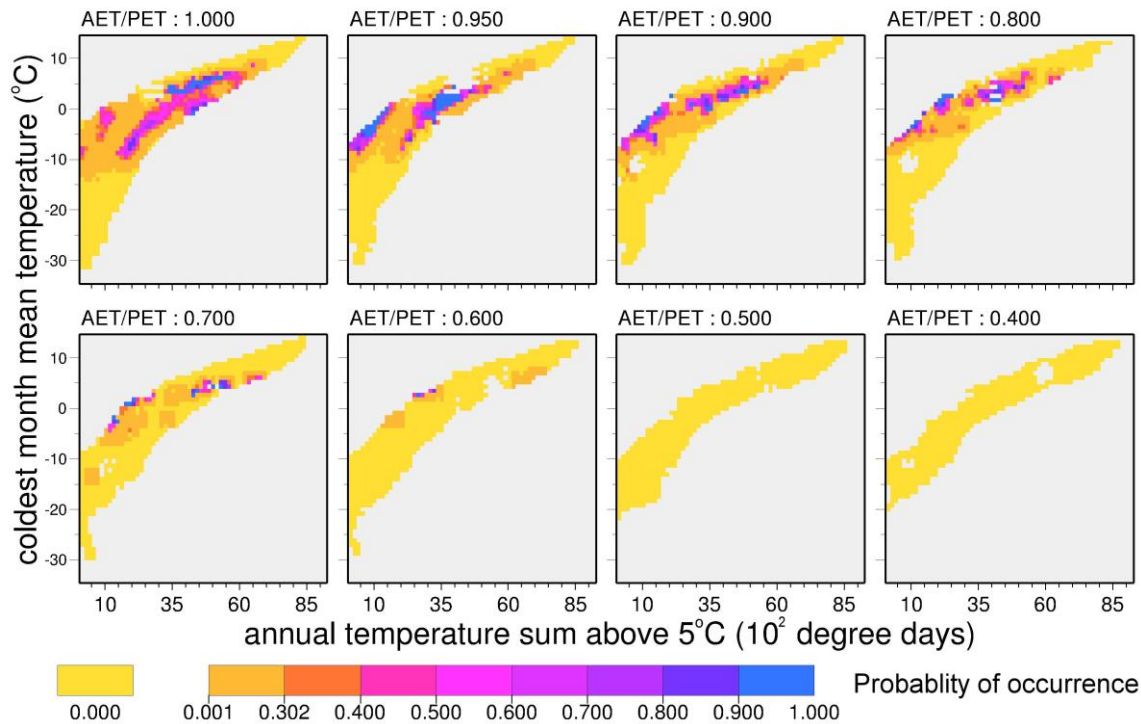
Figure 3.4.28: Climatic response surface for *Tsuga* species.

At the best performing probability threshold (0.302), the simulated distribution of *Tsuga* (Fig. 3.4.30) on the western-coast of North America is sparser but of similar range to the observed (Fig. 3.4.29), while eastern populations are simulated as viable further south than the observed into Florida. The model also simulates in north-western Mexico and southern Greenland, where no *Tsuga* species are observed. In Asia, simulated presences in China and the Himalayas resemble the observed. There are 'false-presences' in Japan, however *Tsuga* species are native to this region, Southern and Northern Japanese Hemlock, *T. sieboldii* and *T. diversifolia*, which are not species *Loxia* species feed upon. This indicates that the genus *Tsuga* has a similar climatic niche for all species. There are incorrect simulations of *Tsuga* in Europe, however previous work on a species *Tsuga* is associated with in North America, *Fagus* (Beech), has demonstrated a similar climatic niche between its observed North American and European populations (Huntley *et al.*, 1989) potentially explaining this simulation inaccuracy. The cumulative range of grid cells reflects this over simulation in Europe, with 3,241 grid cells simulated, larger than the observed (2,379).

Figure 3.4.29: The gridded observed distribution of *Tsuga* species used as feeding trees for *Loxia* species.

Figure 3.4.30: The simulated present distribution of *Tsuga* spp. produced by the CRS model. $\kappa = 0.612$ AUC $= 0.980$

Picea abies

The CRS model for *Picea abies* (Fig. 3.4.31), which has a broad distribution across Eastern Europe and Siberia (Fig. 3.4.32), produced a 'good' maximum κ value (0.714) and a 'high' AUC (0.966) and is most similar at the 0.413 probability threshold.   The CRS generated indicates that *Picea abies* is found in cooler conditions with short growing seasons, archetypal of the boreal conditions it is associated with.   It is found in areas with -27°C to -2°C MTCO and growing seasons of approximately or lower than 1,500 GDD5, but in lower moisture availability (0.700-0.400 AET/PET values) their MTCO tolerance narrows to -20°C to -15°C.
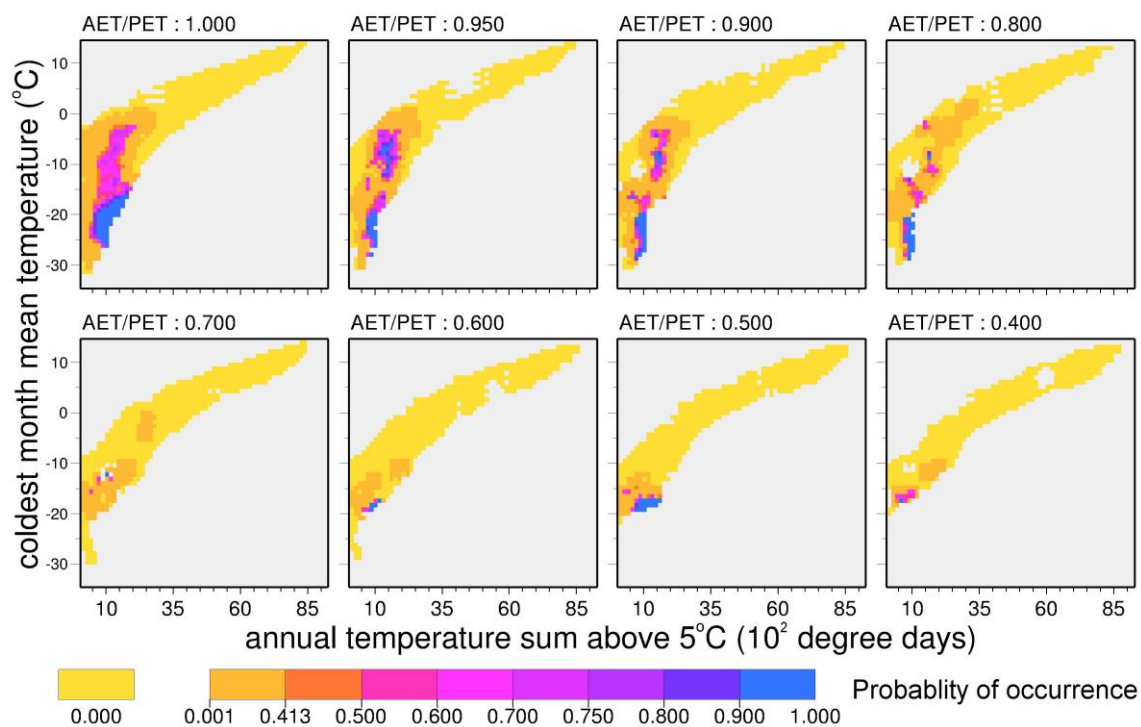
Figure 3.4.31: Climatic response surface for *Picea abies*.

Although the model was created using the complete global grid, comparison will only be made between the observed (Fig. 3.4.32) and simulated range (Fig. 3.4.33) in Eurasia as this is where the species is native.   There were some indications of suitable locations on the North American continent, however evidently this is significantly geographically isolated from the present range.

The model simulated the core observed distribution effectively, with discrepancies mainly at the edges, for example in central Europe where the model simulate presence as far west as the species is observed.   Similarly the simulated range is not as far north as the observed in Fennoscandia and eastern Russia; or south, in Siberia.   There are areas of simulated suitability that are unoccupied, to the north of observed; northern Russian, Krasnoyarsk; easterly, Magadan and Kamchatka peninsula, the Sakhalin Isle and northern Japan.
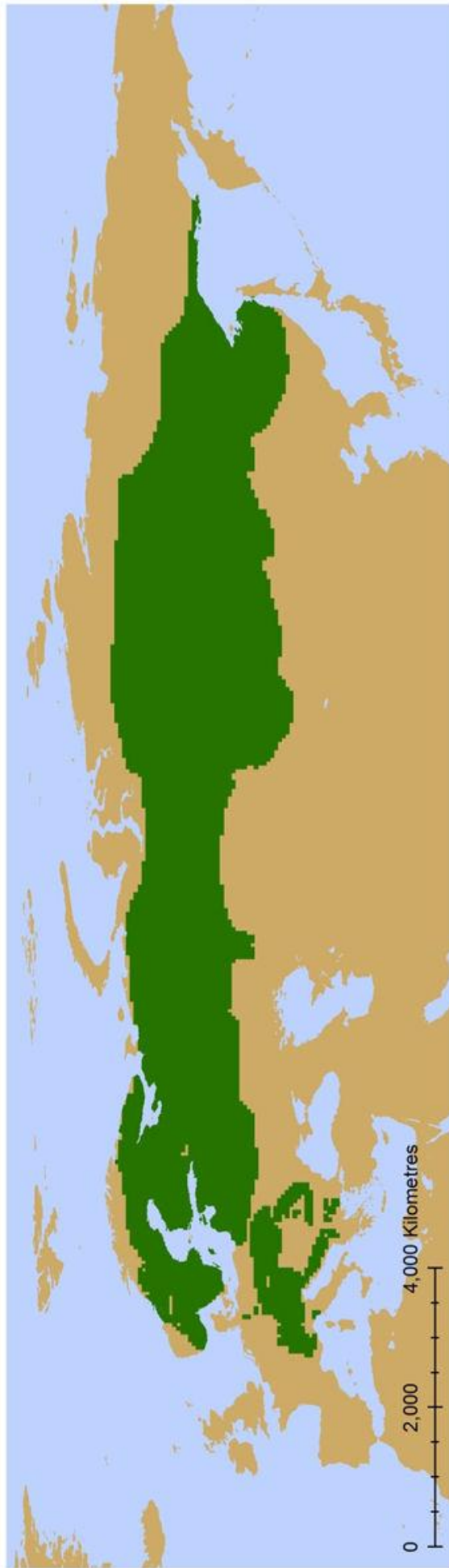
Figure 3.4.32: The gridded observed distribution of *Picea abies* used as a feeding tree for *Loxia* species.
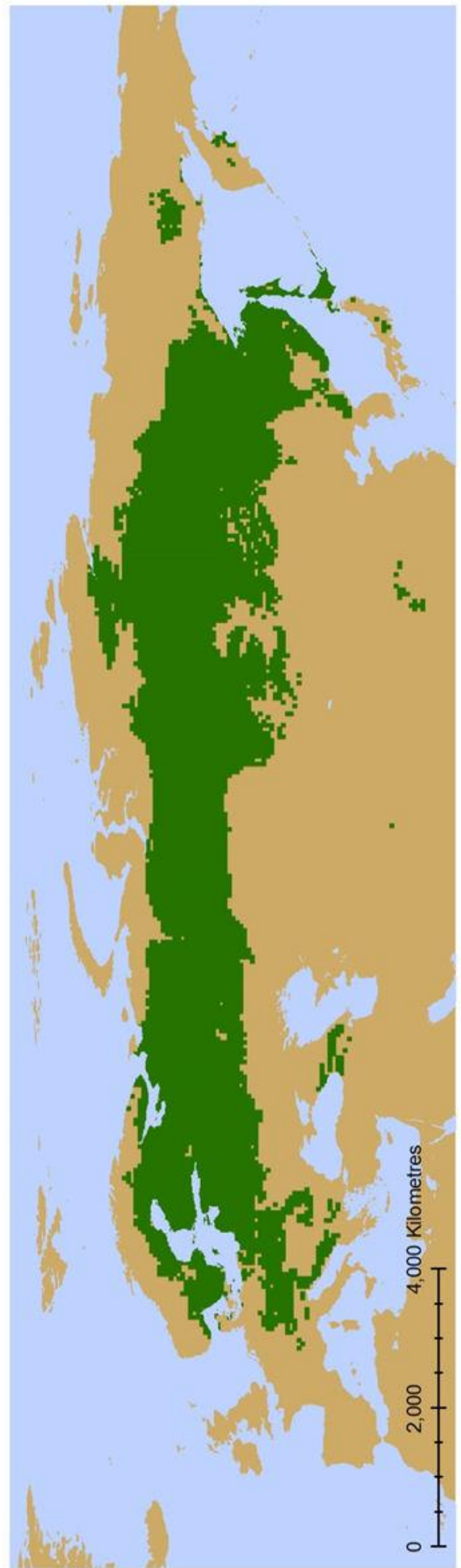
Figure 3.4.33: The simulated present distribution of *Picea abies* produced by the CRS model. κ = 0.714 AUC = 0.966

There are additional false-presences simulated in the Caucasus Mountain and Himalayas, which due to their regional isolation, may be suitable but are unlikely to be occupied. However, on the whole as an individual feeding tree species, *Picea abies* produced the best simulation compared to the other trees included in this study.   Despite the fact the CRS model finds climate suitable in Northern America, the cumulative grid cell coverage generated by the climatic niche model is 10,162 grid cells, compared with the observed, which is 8,478, indicating the majority of climatic space *Picea abies* is found in is unique to Eurasia as much of the range has been correctly simulated.

Pinus sylvestris

For *Pinus sylvestris*, the next most abundant feeding-tree species consumed by *Loxia*, the CRS model produces a 'good' maximum κ value (0.675) of fitness and a 'high' AUC (0.964). The CRS (Fig. 3.4.34) for *Pinus sylvestris* indicates this boreal species has an unsurprisingly cold climatic niche, ranging between -27°C to 1°C MTCO, a short growing season of less than 2,500 GDD5.   *P. sylvestris* has a moisture availability threshold of 0.600 AET/PET, below which it is not found.   There is an evident shifting to warmer and longer growing season for its climatic niche when the moisture availability is restricted (<0.800 AET/PET).
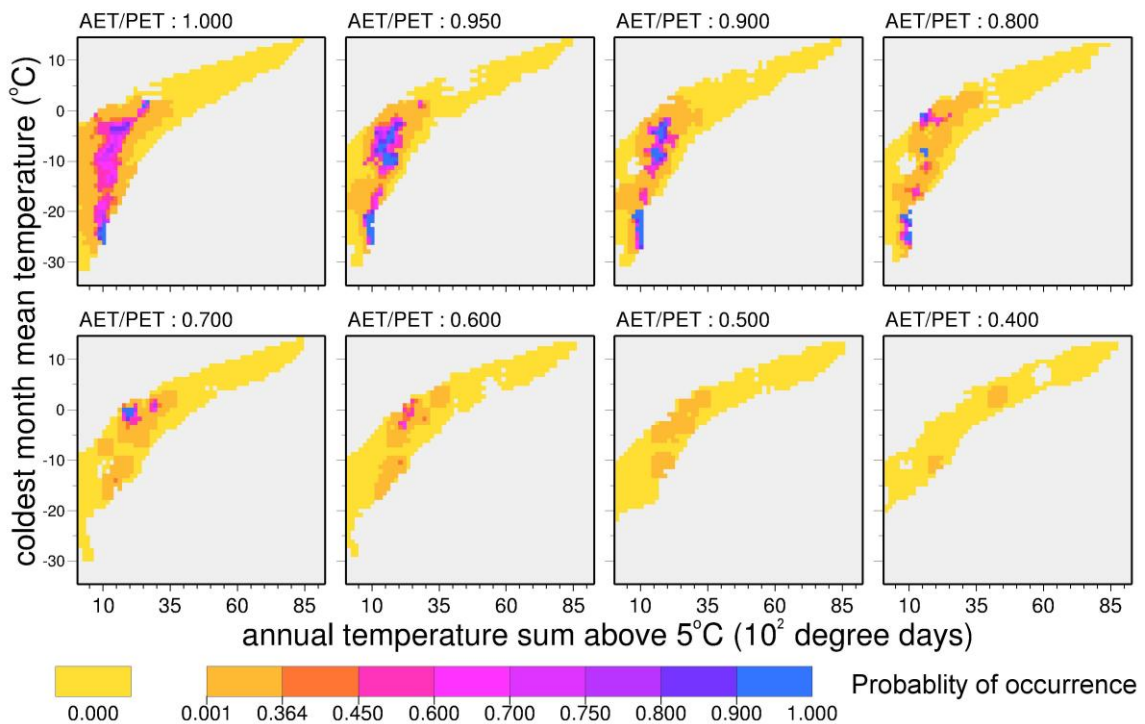
Figure 3.4.34: Climatic response surface for *Pinus sylvestris*.

Again, like *Picea* abies, the distribution in Eurasia, where the species is native, is considered here but there are also false-simulations in North America (CD ROM Appendix: *Pinus sylvestris*- CRS).   The simulated distribution (Fig. 3.4.36) at the probability threshold of 0.364 shows many similarities with observed (Fig. 3.4.35), simulating the core distributions and identifying climate suitable for smaller isolated populations in Scotland, northern Spain and Turkey and Caucasus mountains.   Discrepancies arise where the model simulates no climate suitability in the northern Fennoscandia, where *P. sylvestris* is in fact abundant. There are also sites which are apparently suitable which are not colonised in eastern Russia, the eastern coast of Kamchatka peninsula, throughout the Sakhalin Isle and northern Japan. Within these climates, although colonisation may be it is achievable likely to be outcompeted by other native *Pinus* species such as *P. densiflora* (Japanese Red Pine), *P. thunbergii* (Japanese Black Pine) and *P. koraiensis* (Korean Pine).
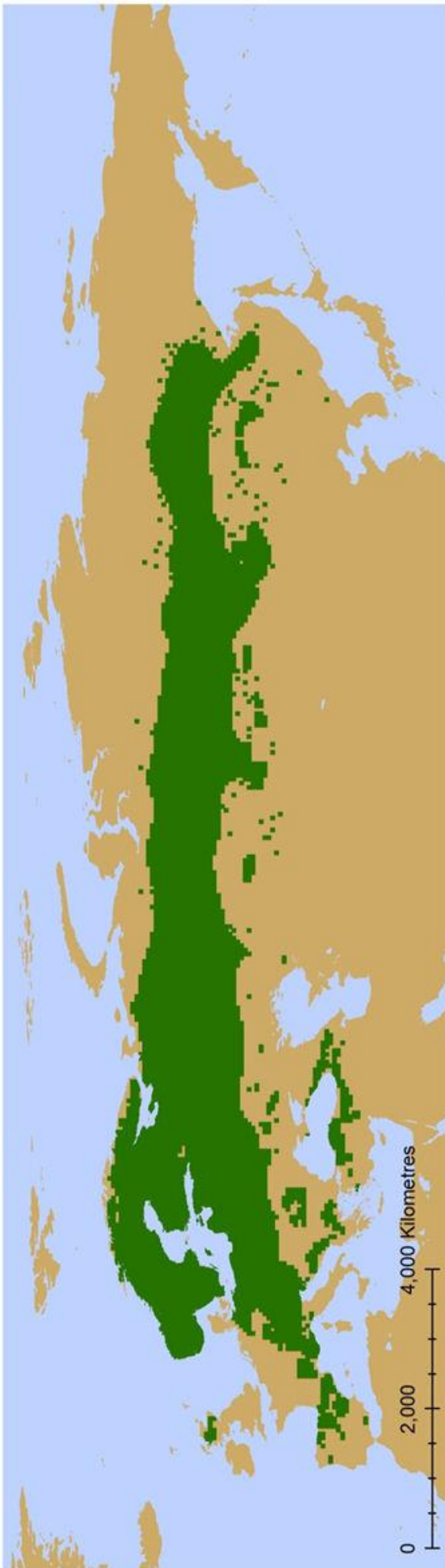
Figure 3.4.35: The gridded observed distribution of *Pinus sylvestris* used as a feeding tree for *Loxia* species.
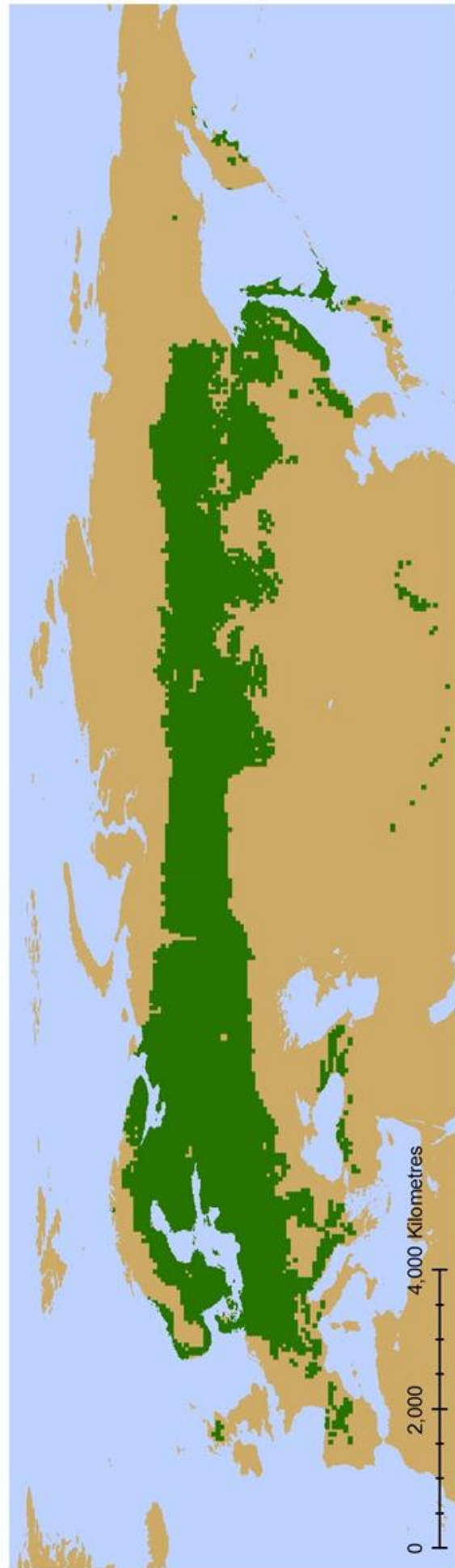
Figure 3.4.36: The simulated present distribution of *Pinus sylvestris* produced by the CRS model. κ = 0.675 AUC = 0.964

Additionally, the simulations of suitable climate in the Himalayas are geographically isolated, even though the bioclimate may be suitable.   The CRS model produces a total of 8,478 grid cell simulated presences, which is substantially larger than the observed (6,723), however when one considers the inclusion of North America and the similar climates it possesses to regions of Eurasia, this figure seems to affirm that the model is performing at a suitable level of accuracy.

Pinus occidentalis

The CRS model *Pinus occidentalis* produced using the climate limited to the Caribbean, where the species is native, had a 'good' maximum κ value (0.584) at the probability threshold of 0.187 and a 'high' AUC (0.952).   The CRS (Fig. 3.4.37) generated shows that *Pinus occidentalis* has a small niche, which has a growth season between 6,000 and 7,000 GDD5, MTCO between 9°C and 11°C and moisture availability between 0.900 and 0.950 AET/PET.   However, in addition to this, like *L. megaplaga*, the species of Crossbill that consumes this tree, it has greatest likelihood in an outlier of the Caribbean climate niche, at 0.950 AET/PET, *ca.* 7°C MTCO and 4,500 GDD5, and a likely representative of the mountainous regions in Hispaniola, indicating both the bird and the tree may be occupying a rare climatic niche in the Caribbean.
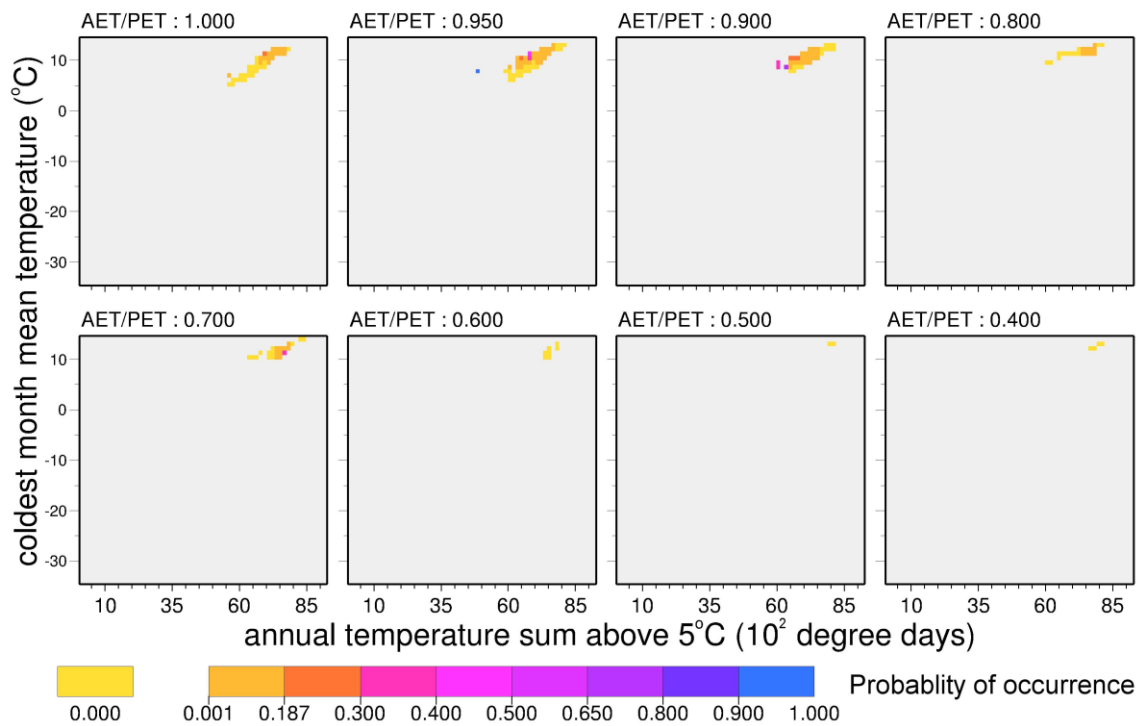
Figure 3.4.37: Climatic response surface for *Pinus occidentalis.*

A comparison of the observed (Fig. 3.4.38) and the simulated (Fig. 3.4.39) shows a great number of similarities in the range in Hispaniola, although the simulation incorrectly identifies areas in the centre which are not part of the range and does not simulate as far north and east as the observed range.   It correctly simulates parts of the range in southern Cuba, although not to the complete northerly extent that is found.   The inaccuracy of simulated presences may be due in part to the climate at this coarse scale not representing the regionally limited microclimates it utilises.   There are also incorrect predictions in Nicaragua, Honduras and Colombia in similarly mountainous regions.   Overall the model performed well, simulating much of the observed range accurately.

Figure 3.4.38: The gridded observed distribution of *Pinus occidentalis* used as a feeding tree for *Loxia megaplaga.*
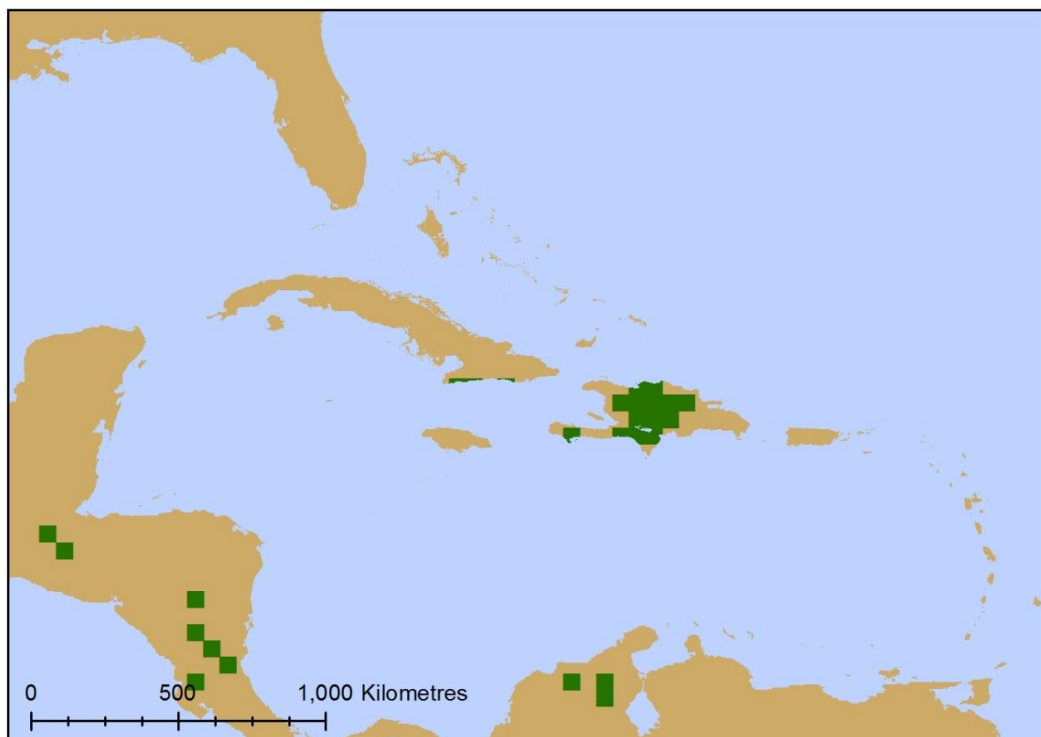
Figure 3.4.39: The simulated present distribution of *Pinus occidentalis* produced by the CRS model and the Caribbean grid. $\kappa = 0.584$ AUC $= 0.952$

Section 3.5

Species' Palaeo-Simulations and Duration of Occupation

In addition to individually analysing the palaeo-simulations, the results can also be aggregated for each grid cell to see how frequently in that location the climatic scenarios were suitable for the species or genus.   In so doing, a crude measure of the 'duration' of cell climatic suitability and potential length of occupation can be generated in terms of number of scenarios, rather than precise years. This novel information can be both mapped (Fig. 3.7.odd numbers), to identify regions of climate stability through the last 120 thousand years, and also numerically investigated (Table 3.5.1), by looking at total abundance of grid cells with similar duration lengths, an insight into the potential size of these areas of similar simulated duration.

In total there are 53 climatic scenarios collated for each species, spanning from present day to 120 thousand years ago, with all the simulations produced using the best performing species' distribution model CRS (Section 3.1).   The 11 classes used in the mapping, with each covering five 'frequency of simulation totals', with the last class only spanning three, from 51-53.   This highest class will be considered a stable climatic niche, as it includes at least two Heinrich Event scenarios, when the climatic availability for most species/genus was at its most limited.   Overall there are:

- 11 scenarios representing the present interglacial, the Holocene, spanning 10 thousand years ago to present day.
- 31 scenarios representing 49 thousand years of glacial conditions from 60 thousand years ago to 11 thousand years ago.
- 5 scenarios of the individual intermittent Heinrich Events during the last glacial.
- 6 scenarios representing conditions pre-glaciation, the Eemian interglacial, spanning a total of 20 thousand years from 100 to 120 thousand years ago.

Therefore there are 36 simulated scenarios representing roughly 60 thousand years of cooler glacial temperatures, represented by a total of, and 17 scenarios represent 30 thousand years of warmer interglacial conditions.   Note there no reliable data for the period between 60 and 100 thousand years ago so this is excluded from this study.

Duration of Simulation

(No. of Climatic Scenarios the Grid Cell was Modelled as Climatically Suitable)

Species/Genus	>0	1-5	6-10	11-15	16-20	21-25	26-30	31-35	36-40	41-45	46-50	51-53
					The Total Number of 0.5°x 0.5° Grid Cells							
Loxia curvirostra	32,857	6,618	3,858	4,943	2,792	1,827	1,747	1,976	1,999	1,752	2,822	2,523
L. leucoptera	24,845	6,254	3,563	4,311	2,169	1,406	1,198	1,163	1,176	1,274	1,783	548
L. pytyopsittacus	5,937	1,446	1,386	1,938	364	208	279	202	63	26	18	7
L. scotica	230	173	33	15	8	1	0	0	0	0	0	0
L. megaplaga	180	122	19	16	5	7	7	1	1	1	0	1
Pinus occidentalis	411	259	57	33	25	17	13	4	0	2	0	1
Larix spp.	27,612	5,196	2,019	2,122	1,410	1,270	1,442	1,664	2,242	2,474	2,233	5,540
Picea spp.	31,708	6,942	3,871	5,625	2,715	1,849	1,388	1,469	1,402	1,557	2,259	2,631
Pinus spp.	29,421	6980	3841	4333	2842	1996	1777	1827	2091	1583	1287	864
Pseudotsuga spp.	9,208	4,905	1,362	832	527	420	337	286	256	126	71	86
Tsuga spp.	10,588	4496	1867	1314	766	434	375	327	348	321	222	118
Picea abies	23,469	6,806	3,941	3,183	1,490	1,180	1,099	951	1,257	1,139	1,258	1,165
Pinus sylvestris	19,668	5,358	3,326	2,813	1,747	1,170	1,120	1,032	1,403	889	745	65

Table 3.5.1:   The total number of 0.5°x 0.5° grid cells grouped by the species/genus' duration of simulation, calculated as the number of modelled climatic scenarios when an occurrence in the grid cell was simulated, grouped into the classes, of at least 1 simulation through to the maximum of 51 to 53 simulations which span from 120 thousand years ago to present day.   The colours relate to the map colour coded class ranges.

Loxia curvirostra

Loxia curvirostra, the widest ranging of the Crossbill species, had an expansive range throughout central and northern Eurasia and across the north and west of North America during the Eemian interglacial, 120 thousand years ago (Fig. 3.5.1 A).   The cooling climate of the stadials (Fig. 3.5.1 B) followed by the onset of the glaciation (Fig. 3.5.1 C, D & E) saw a southerly shift in the climatic range of *L. curvirostra*, with areas such as Fennoscandia becoming inhospitable and the North American climatically suitable regions being split by the Laurentide ice sheet, isolating the Alaska potential populations from the rest of North America.   At the onset of the Holocene (Fig. 3.5.1 F), as the climate warmed and the glaciers receded, the climatic range of *L. curvirostra* shifted northwards again, colonising Fennoscandia and progressing northwards through Canada reconnecting with the Alaskan climatically suitable region forming the distribution observed today (Fig. 3.4.2).   However, this isolation of the Alaskan region may in fact explain why, although the climate is suitable in Alaska today, the present day populations of *L. curvirostra* do not utilise these regions. Isolated populations are more likely to go extinct and once this occurs the region may not be re-colonised because of it lack of suitability due to geographical isolation, competitors or low food abundance.

There are a number of regions in the northern hemisphere which have climatic conditions which have remained relatively stable for *Loxia curvirostra* (Fig. 3.5.2).   In North America these areas are found in the west, in southern Alaska and along the Canadian coastline into the USA, and throughout the western mountains of the Cascades, Sierra Nevada, the Rocky Mountains and some areas as far south as the Mexican Sierra Madres.   This suggests that the present day range in the east is relatively novel and it was an unstable climatic area during the glacial compared to the western mountainous regions.

In Eurasia, there is a greater abundance of stable suitable climate found mainly in southern Europe, as far north as Germany, into the Ukraine and central western Russia as far as the Ural Mountains.   Further the east; there is high frequency of climatic suitability in the southern Sayan and south-eastern Stanovor Mountains, northern China and northern Japan as well as the central Asian mountain ranges of the Himalayas and other mountainous regions in Afghanistan and Mongolia.   Most notably there are number of regions, where presently there are designated subspecies of *L. curvirostra* (Table 1.1.1), which have had climatic conditions which remained stable throughout the previous interglacial and glacial to present day, these include; Corsica and its sub-species, *L. c. corsicana*; northeast Morocco and northern Algeria,
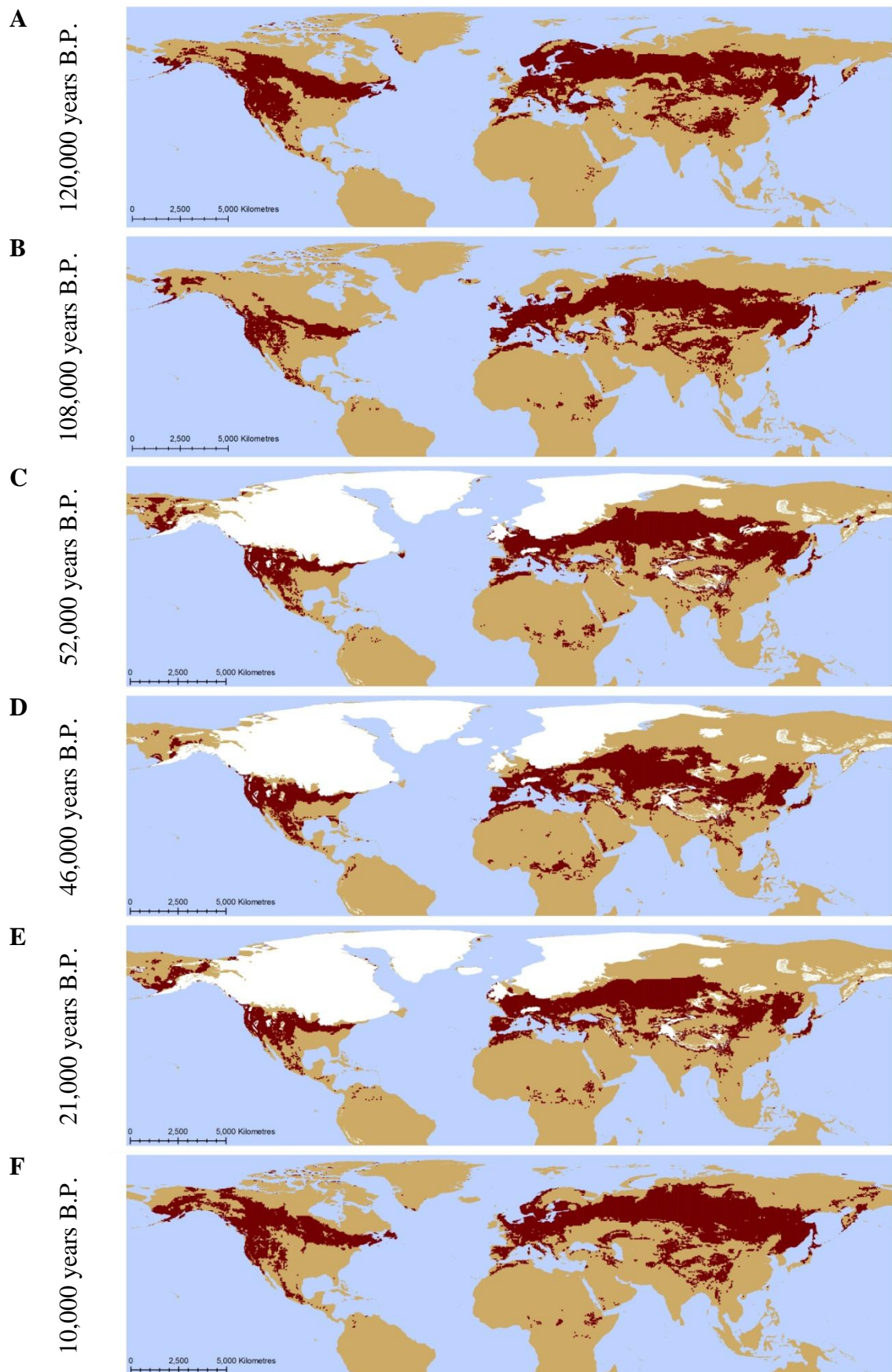
Figure 3.5.1: The simulated distribution of *Loxia curvirostra* (red) during the Eemian interglacial (A); at the Meisley 1 stadial (B); during interstadial conditions (C); at Heinrich Event 5 (D); at the Last Glacial Maximum (E) and the beginning of the Holocene (F), all produced by the CRS model.
See Appendix: Results – *Loxia curvirostra* for full descriptions of the simulated distributions.
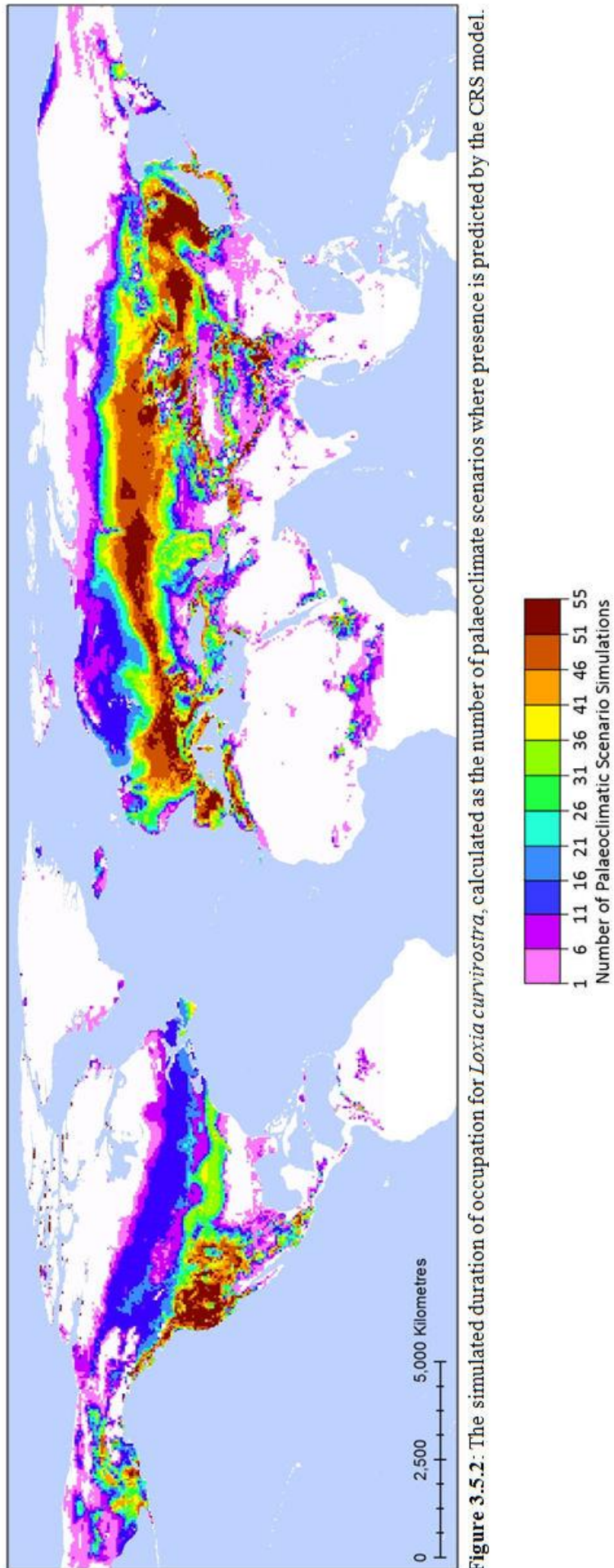
Figure 3.5.2: The simulated duration of occupation for *Loxia curvirostra*, calculated as the number of palaeoclimate scenarios where presence is predicted by the CRS model.
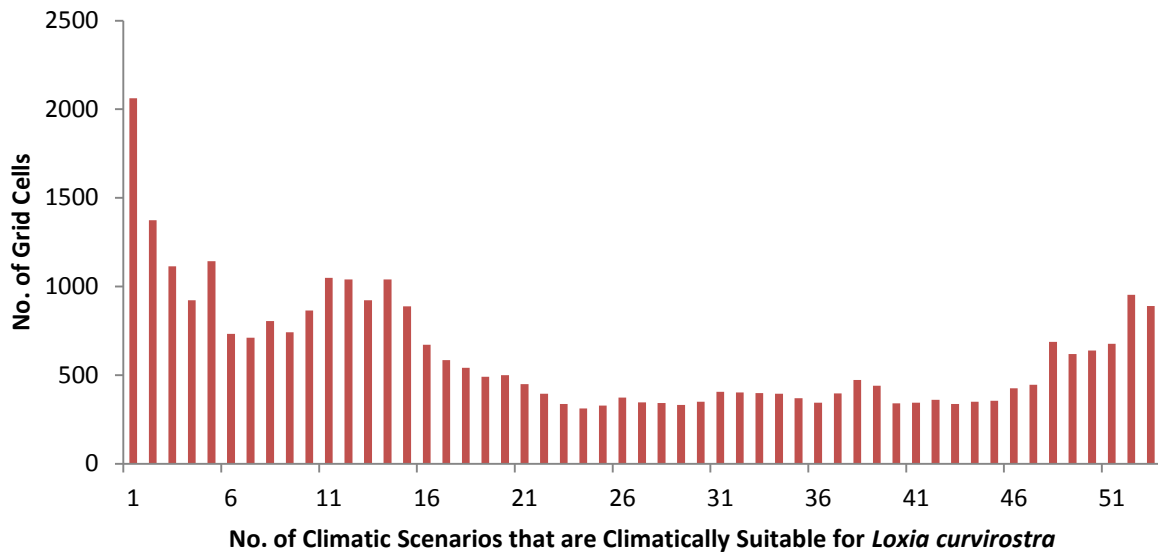
Figure 3.5.3: The quantified durations of climatic suitability for *Loxia curvirostra*. The number of 0.5° x 0.5° grid cells that have the same duration of occupation for *L. curvirostra*. Duration of occupation is calculated as the number of scenarios the grid cell is predicted to have climatic conditions suitable for the species.

L. c. poliogyna; central and southern Spain, *L. c. balearica*; and the south Altai and Sayan Mountains, *L. c. altaiensis*. On the contrary, the climatic conditions in the Philippines and Vietnam result in no locations in this region exceeding 20 scenarios of suitability. This indicates that the respective present-day sub-species, *L. c. luzoniensis* and *L. c. meridionalis* are either a relatively new colonisation or have different climatic necessities than the broader species' climatic niche.

Overall there are 2,523 grid cells that have stable climatic conditions where over 51 climatic scenarios are suitable for *L. curvirostra's* modelled niche (Table 3.5.1). This is a larger range than the other *Loxia* species, unsurprisingly since its present range is the largest. When you take into account the total number of grid cells that are simulated as climatically suitable in at least one of the climate scenarios for *L. curvirostra*, the stable climate range accounts for 7.68%, the highest percentage attained for a *Loxia* species. This highlights that many locations are only climatically suitable for shorter periods with a majority being only suitable for less than 16 scenarios, with over 2,000 sites only simulated once by the model (Fig. 3.5.3).

Loxia leucoptera

The interglacial conditions of the Eemian, at around 120 thousand years ago, are simulated to produce a range for *L. leucoptera* that spans across Siberia into southern parts of Fennoscandia and across Canada, from Newfoundland to Alaska (Fig. 3.5.4 A).   The cooling climates initialised in the stadial (Fig. 3.5.4 B) but then maintained throughout the glaciation (Fig. 3.5.4 C, D & E), lead to a southerly shift in the range into central regions of Eurasia, into southern Siberia and central Europe, France and Germany.   In North America, the colder climes and growing Laurentide ice sheet made much of Canada inhospitable, leading to a splitting of climatically suitable regions, with Alaska maintaining the larger and most consistent range potential during the glaciation than the southerly potential population bordering the ice sheet.

The warming climate that began around 11,000 years ago, triggering the onset of the Holocene (Fig. 3.5.4 F), resulted in the range of *L. leucoptera* shifting north-easterly in Eurasia, out of central Europe into north-west and central Siberia.   In North America, the progression of the southern ice sheet population northwards with the retreating ice sheet results in the conjoining of the east and western populations by the beginning of the Holocene and some further expansion during the interglacial results in the distribution observed today (Fig. 3.4.5).

A 120,000 years B.P.

B 108,000 years B.P.

C 52,000 years B.P.

D 46,000 years B.P.

E 21,000 years B.P.

F 10,000 years B.P.

Figure 3.5.4: The simulated distribution of *Loxia leucoptera* (red) during the Eemian interglacial (A); at the Meisley 1 stadial (B); during interstadial conditions (C); at Heinrich Event 5 (D); at the Last Glacial Maximum (E) and the beginning of the Holocene (F), all produced by the CRS model.
See Appendix: Results – *Loxia leucoptera* for full descriptions of the simulated distributions.
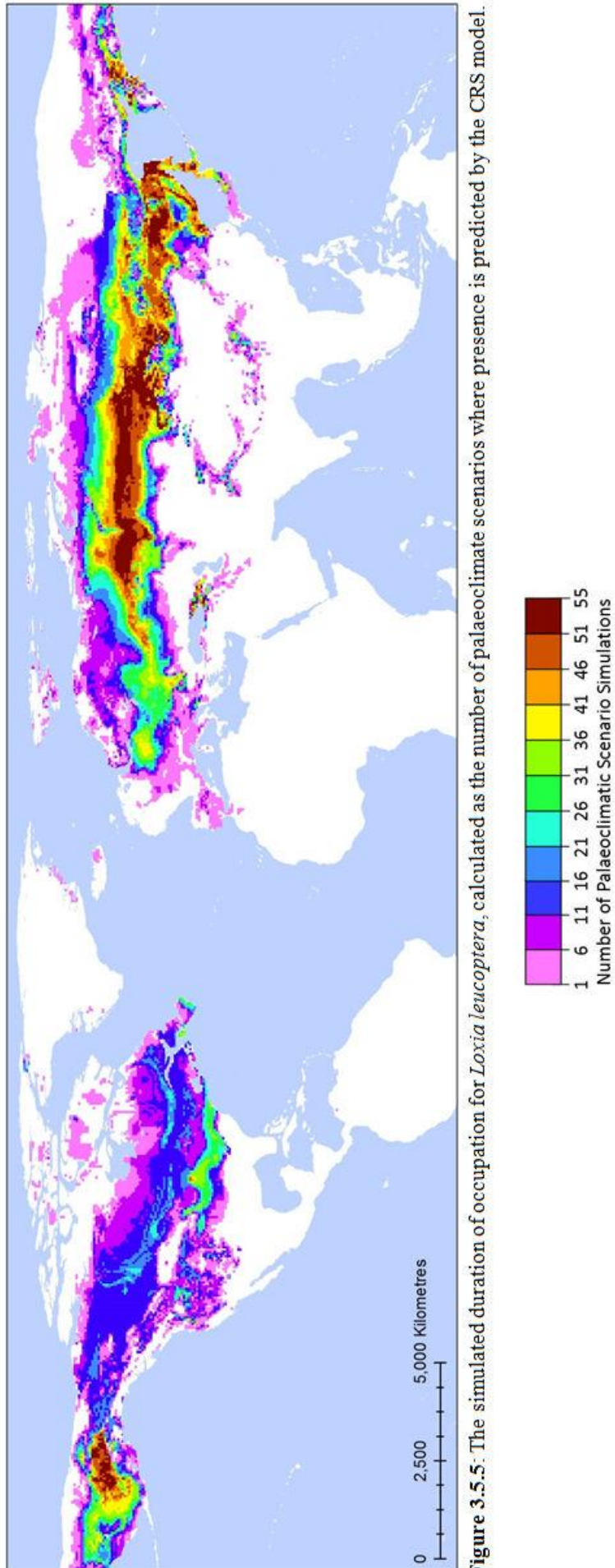
Figure 3.5.5: The simulated duration of occupation for *Loxia leucoptera*, calculated as the number of palaeoclimate scenarios where presence is predicted by the CRS model.

Number of Palaeoclimatic Scenario Simulations
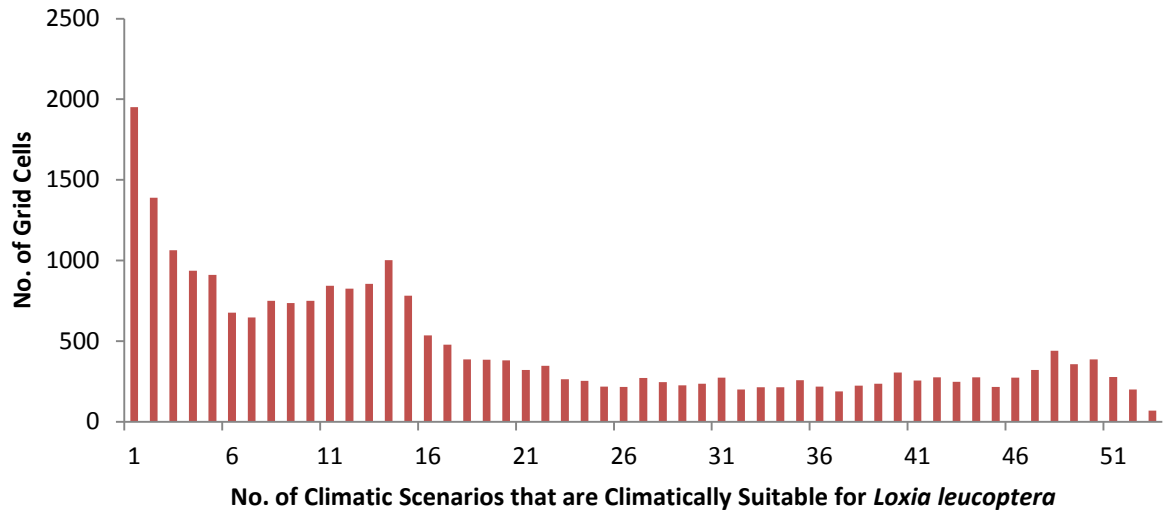
Figure 3.5.6:   The quantified durations of climatic suitability for *Loxia leucoptera*.   The number of 0.5° x 0.5° grid cells that have the same duration of occupation for *L. leucoptera*.   Duration of occupation is calculated as the number of scenarios the grid cell is predicted to have climatic conditions suitable for the species.

The regions with the longest duration of climatic suitability simulated for *L. leucoptera* are throughout central and south-eastern Russia and along the south-eastern Siberian coastline, the island of Sakhalin and northern Japan as well as the Kamchatka peninsula.   This substantial area is much the same as the present range suggesting that the populations in Eurasia have maintained a core range in Russia throughout the last 120 thousand years, potentially expanding into Europe when the climate was more suitable during the glacial (Fig. 3.5.5).   In North America, the most consistent climatic range is in Alaska and a small area in the central-east near the Great Lakes, with much of the rest of North America having sites which are suitable for just 35 or less of the scenarios modelled.   This suggests that during the glacial expansion, *L. leucoptera* populations had to significantly shift their range southerly although Alaska remained a consistent climatic refuge for the species throughout the fluctuating conditions.

There are only 548 locations in the northern hemisphere which have climatic conditions which are suitable for more than 51 of the scenarios modelled (Table. 3.5.1).   This 'long' duration class accounts for just 2.21% of the grid cells which have climate suitable during at least once of the reconstructions, with the majority of grid cells actually having less than 16 simulations at that location (Fig. 3.5.6), of which 1,952 grid cell locations are only suitable in a single simulation and just 70 grid cells being suitable for all of the 53 present and palaeoclimatic scenarios.

Loxia pytyopsittacus

L. pytyopsittacus was at its most expansive climatic range during the warmer interglacial periods, such as the Eemian, 120 thousand years ago (Fig. 3.5.7 A), where it could have potentially been found throughout Fennoscandia and into western Russia.   During the glaciation (Fig. 3.5.7 C, D & E) its distribution was limited more southerly in central Europe, bordering the Weichselian ice sheet covering much of northern Europe, where climate for the species persisted throughout the simulations of glacial conditions (CD ROM Appendix: *Loxia pytyopsittacus* - CRS).   At the end of the last glaciation and the beginning of the Holocene (Fig. 3.5.7 F), the warming climate and receding ice sheets resulted in *L. pytyopsittacus* colonising northern Europe as far north as the Arctic Sea coastline and establishing the

A   120,000 years B.P.   **B**   108,000 years B.P.
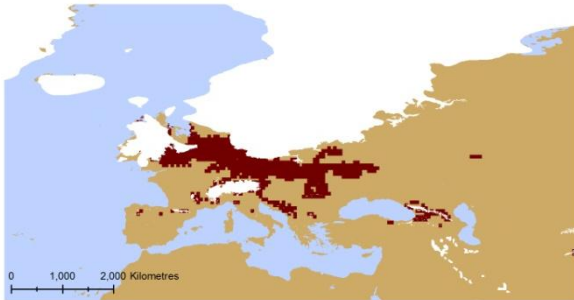
C   52,000 years B.P.   **D**   46,000 years B.P.
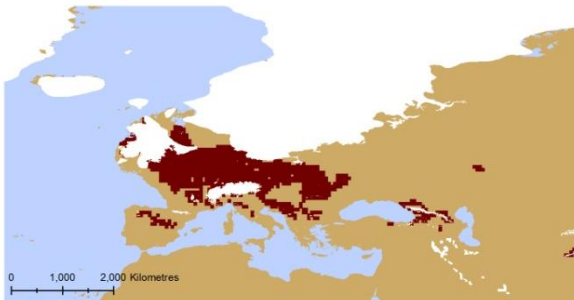
E   21,000 years B.P.   **F**   10,000 years B.P.
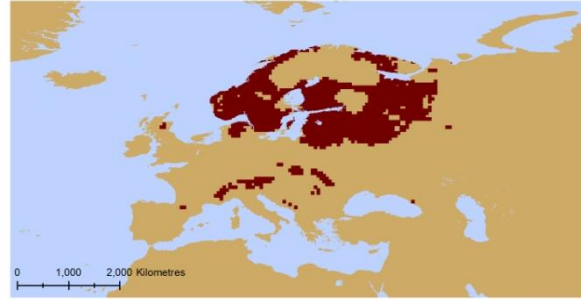
Figure 3.5.7: The simulated distribution of *Loxia pytyopsittacus* (red) during the Eemian interglacial (A); at the Meisley 1 stadial (B); during interstadial conditions (C); at Heinrich Event 5 (D); at the Last Glacial Maximum (E) and the beginning of the Holocene (F), all produced by the CRS model.
See Appendix: Results – *Loxia pytyopsittacus* for full descriptions of the simulated distributions.
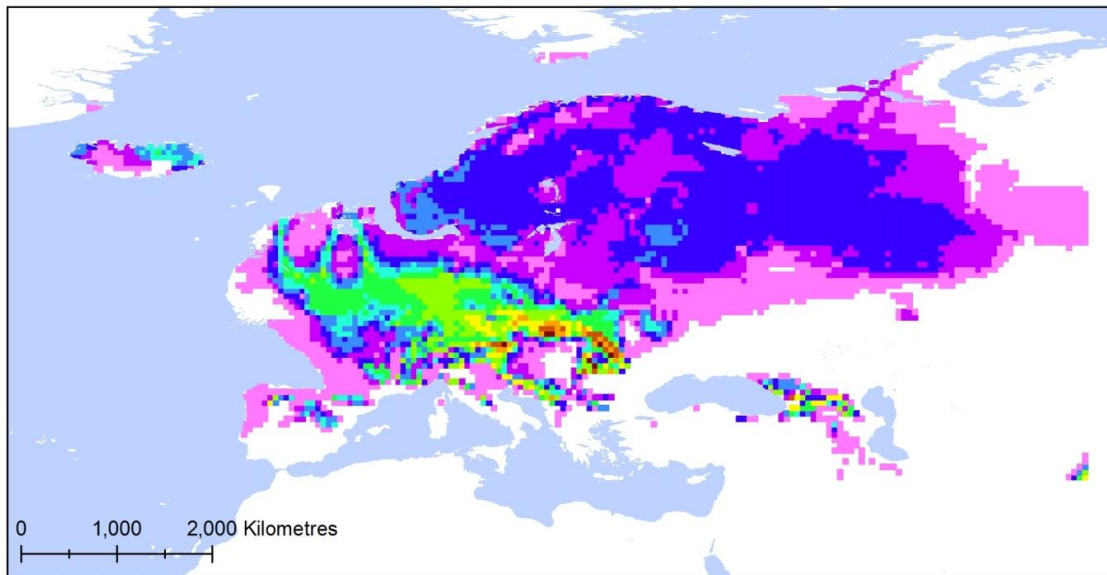
Figure 3.5.8: The simulated duration of occupation for *Loxia pytyopsittacus*, calculated as the number of palaeoclimate scenarios where presence is predicted by the CRS model.
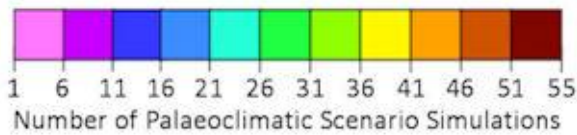
distribution observed today (Fig. 3.4.8).

Unlike the broad ranging *L. curvirostra* and *L. leucoptera*, *L. pytyopsittacus* has only 7 sites (Table 3.5.1) which have climate that is suitable in 51 or more of the modelled scenarios and these sites are actually situated in the Alps, where although the climate is suitable, present populations of *L. pytyopsittacus* are not found (Fig. 3.5.8).   This implied a significant shift in
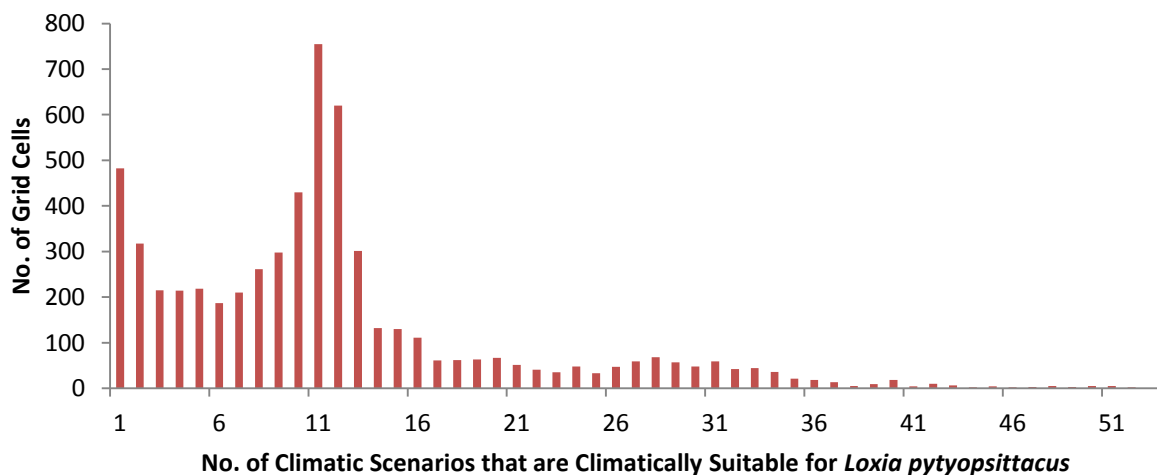
Figure 3.5.9:   The quantified durations of climatic suitability for *Loxia pytyopsittacus*.   The number of 0.5° x 0.5° grid cells that have the same duration of occupation for *L. pytyopsittacus*.   Duration of occupation is calculated as the number of scenarios the grid cell is predicted to have climatic conditions suitable for the species.

range given that much of *L. pytyopsittacus* current distribution is in areas of Fennoscandia which were covered by the Weichselian ice sheet for much of the glacial.   The longevity of the glaciation also reveals that the UK, France, Germany and mountainous regions such as the Alps, Dinaric Alps and Carpathian Mountains actually had longer periods of climatic suitability than the areas of Fennoscandia where they are observed today.

The small range of climatic stability accounts for just 0.12% of the total number of grid cells which have climate suitable at some point during the last 120 thousand years.   The majority of the locations in fact have a total of less than 15 scenarios being climatically suitable, highlighting the significant shift in range that *L. pytyopsittacus* must have undertaken during the glacial (Fig. 3.5.9).

Loxia scotica

At 120 thousand years ago, the interglacial simulations of *Loxia scotica* suggest its primary range was in the Scottish Highlands (Fig. 3.5.10 A), where it is found today (Fig. 3.4.11). However, the cooling temperatures of the stadial (Fig. 3.5.10 B) followed by the glaciation (Fig. 3.5.10 C & E) resulted in its climatically suitable range shifting into Ireland, along the continental shelf exposed on the west coast of the expanding Devensian ice sheets. Although there are also sporadic simulations of climate suitability in Spain during the glaciation it is unlikely that these regions were colonised due to their isolation. As the climate warmed into the most recent interglacial, the Holocene (Fig. 3.5.10 F), the climate suitability range followed the shrinking British ice sheets northwards through Northern

A   120,000 years B.P.

B   108,000 years B.P.

C   52,000 years B.P.

D   46,000 years B.P.

E   21,000 years B.P.

F   10,000 years B.P.

Figure 3.5.10: The simulated distribution of *Loxia scotica* (red) during the Eemian interglacial (A); at the Meisley 1 stadial (B); during interstadial conditions (C); at Heinrich Event 5 (D); at the Last Glacial Maximum (E) and the beginning of the Holocene (F), all produced by the CRS model.
See Appendix: Results – *Loxia scotica* for full descriptions of the simulated distributions.
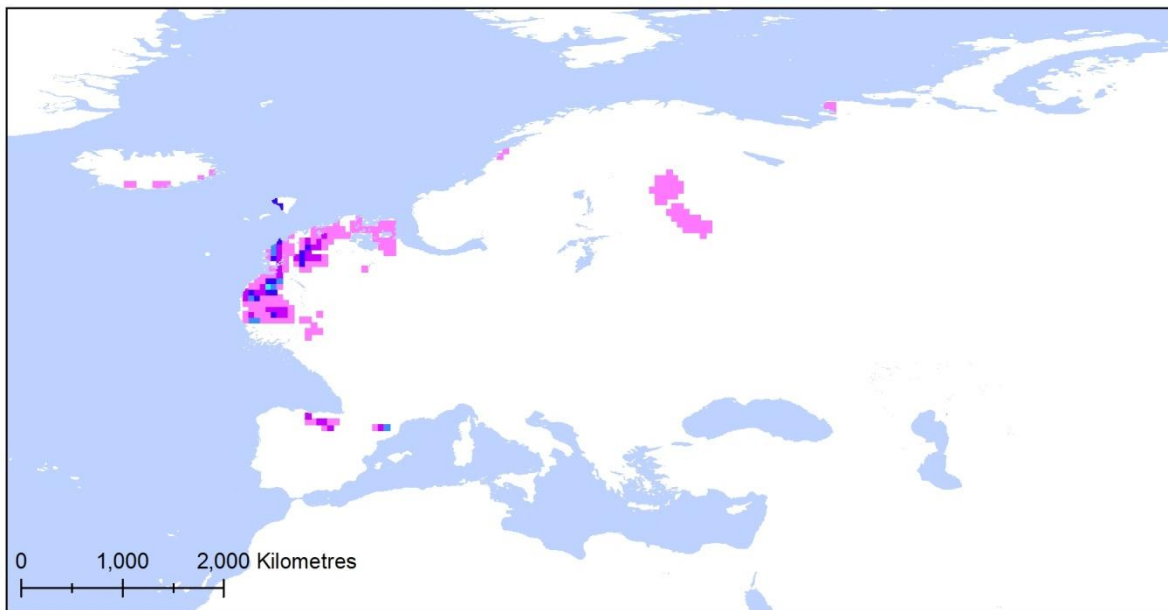
Figure 3.5.11: The simulated duration of occupation for *Loxia scotica,* calculated as the number of palaeoclimate scenarios where presence is predicted by the CRS model.

Number of Palaeoclimatic Scenario Simulations
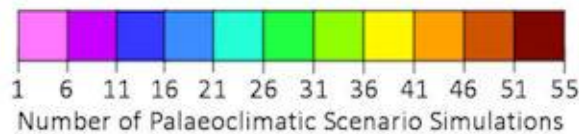
Ireland and into Scotland, establishing the characterised range known today. However, it is important to note that the cold but relatively temporally short Heinrich Events produce completely inhospitable conditions for *L. scotica*'s climatic niche (Fig. 3.5.10 D), highlighting that it may not have in fact persisted as a species throughout the glaciation and could instead be a relatively new species with its unique niche.

Loxia scotica has a significantly restricted climatic range, with just 230 grid cells having
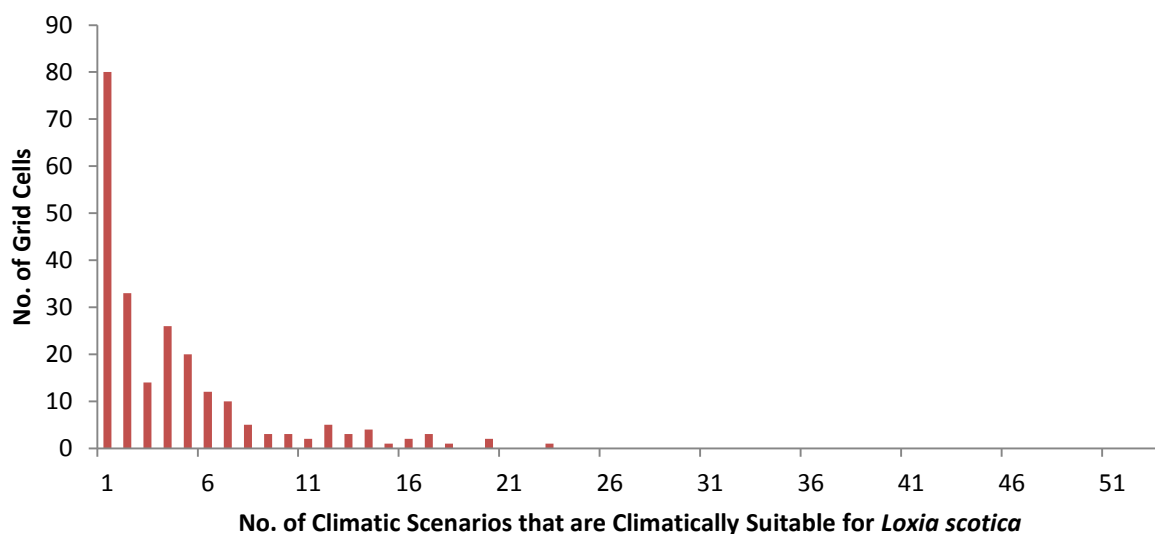
Figure 3.5.12: The quantified durations of climatic suitability for *Loxia scotica*. The number of 0.5° x 0.5° grid cell that have the same duration of occupation for *L. scotica*. Duration of occupation is calculated as the number of scenarios the grid cell is predicted to have climatic conditions suitable for the species.
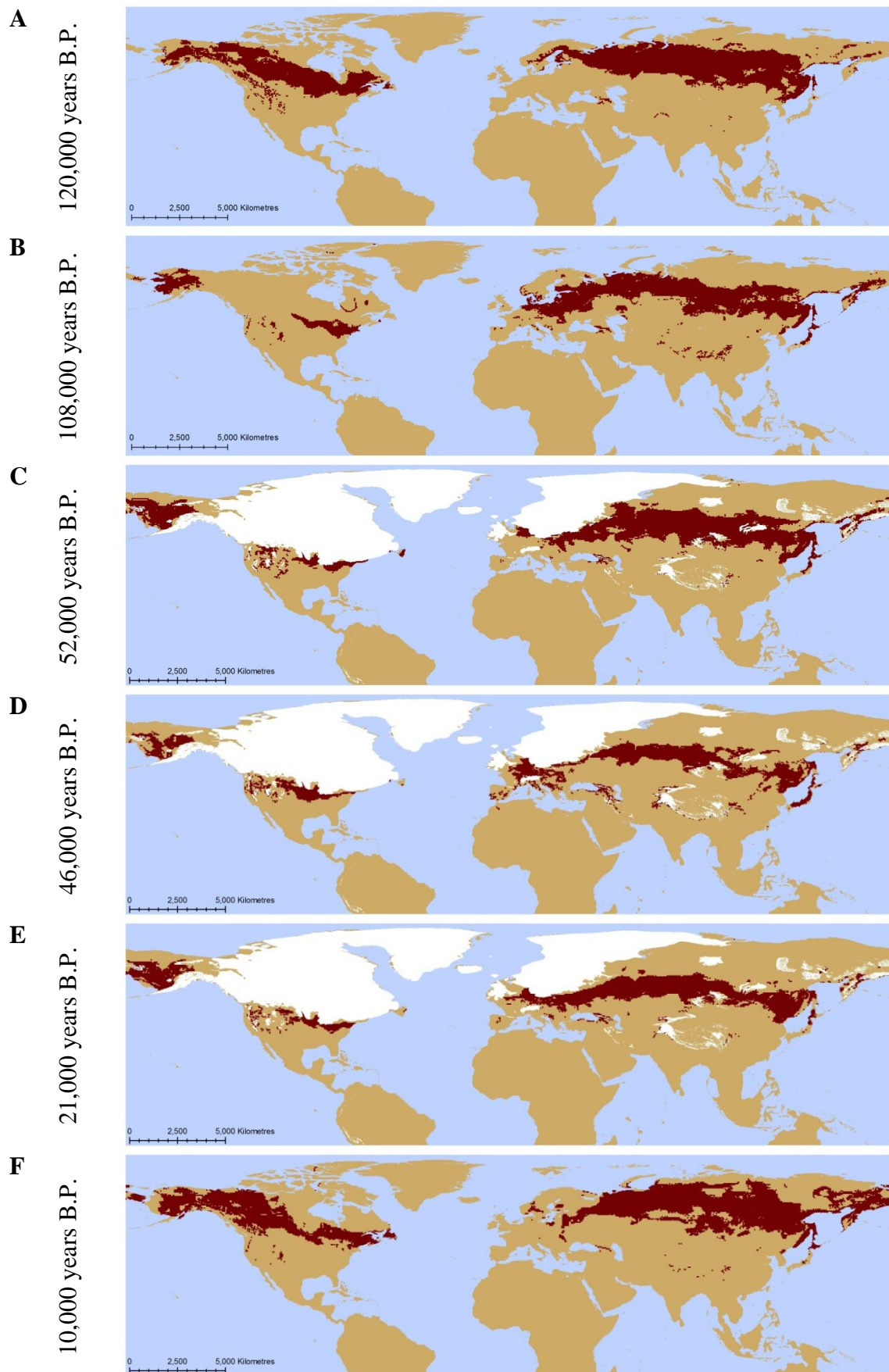
climate suitable across all the scenarios, and none of the locations have a duration greater than 25 scenarios (Table. 3.5.1). These areas are found mainly in Scotland, Ireland and the continental shelf surrounding these countries, exposed by the lower glacial sea levels (Fig. 3.5.11), with some other isolated locations in the Faroe Islands, Iceland, the coastline of Norway, northern Spain and Finland. The majority of these sites do not exceed six climatically suitable scenarios (Fig. 3.5.12); indicating that *L. scotica* had very little climatic stability throughout the glacial compared to the other *Loxia* species with broader ranges. During the glaciations, areas of ice-free Ireland provide potential locations where these species may have survived the colder conditions.

Loxia megaplaga

L. megaplaga has the potential to have been a resident of Hispaniola from 120 thousand years ago (Fig. 3.5.13 A) and in fact, this could have been maintained throughout the interglacial (to 100 thousand years ago) (CD ROM Appendix: *Loxia megaplaga* - CRS); however, during stadial scenarios (112 & 108 thousand years ago) (Fig. 3.5.13 B), conditions in the Caribbean

A   120,000 years B.P.   **B**   108,000 years B.P.

C   52,000 years B.P.   **D**   46,000 years B.P.

E   21,000 years B.P.   **F**   10,000 years B.P.
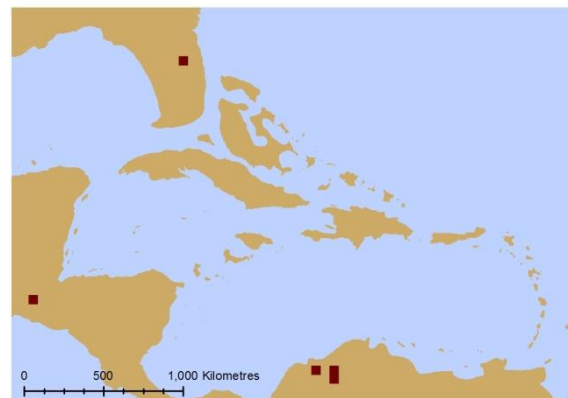
**Figure 3.5.13:** The simulated distribution of *Loxia megaplaga* (red) during the Eemian interglacial (A); at the Meisley 1 stadial (B); during interstadial conditions (C); at Heinrich Event 5 (D); at the Last Glacial Maximum (E) and the beginning of the Holocene (F), all produced by the CRS model.
See Appendix: Results – *Loxia megaplaga* for full descriptions of the simulated distributions.

were inhospitable.   During the glaciation (Fig. 3.5.13 C & E), from 60 to 44, 34 to 26 and 13 to 11 thousand years ago, there was climate suitable for *L. megaplaga* on the Hispaniolan Island, but in between these simulations up until the beginning of the Holocene (Fig. 3.5.13 F), there were periods simulated to have been climactically unsuitable on this island.   In some scenarios the climate on adjacent islands, such as Cuba and Jamaica, was suitable for *L. megaplaga* and specifically during Heinrich Events (Fig. 3.5.13 D), when Cuba harbours climates similar to those of its present-day niche.   Since the beginning of the Holocene (Fig. 3.5.13 F), from nine thousand years ago, simulations suggest that the climate of Hispaniola has been suitable for *L. megaplaga*.

It is evident that, unlike the other Crossbill species there are no obvious observable patterns of movement in response to climate and the simulations at this resolution may not reflect the stability of the climatic niche this small isolated population utilises.   In addition, the unknown temporal origins of this isolated off-shoot colony of *L. megaplaga* from their closest relative *L. leucoptera*, means there is still speculation over the precise time of establishment of this species in the Caribbean.   It is also important to note that this species has suffered reductions in distributions due to deforestation and in fact it is speculated that there were once
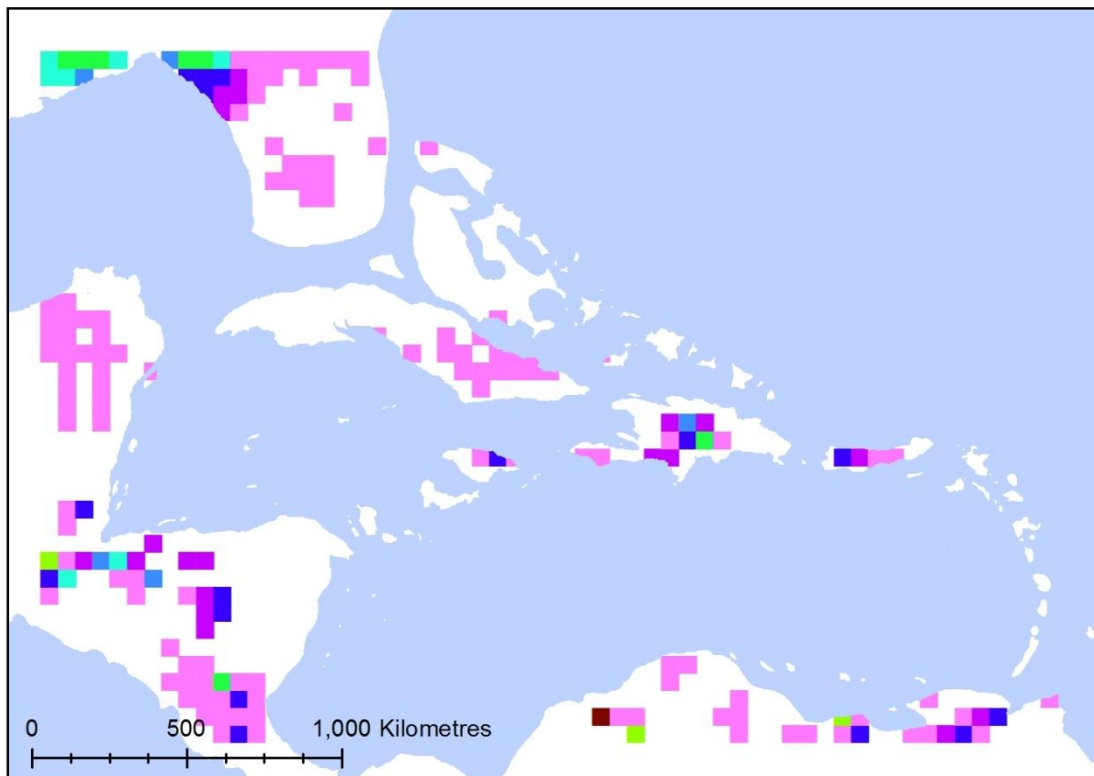
Figure 3.5.14:   The simulated duration of occupation for *Loxia megaplaga*, calculated as the number of palaeoclimate scenarios where presence is predicted by the CRS model.
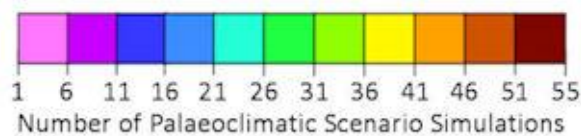
populations in Cuba which are now extinct.

In the case of *L. megaplaga*, it has the smallest present range size of the *Loxia* species and it also has the fewest sites of climatic suitability throughout the 120 thousand years of climatic simulations with just 180 individual sites identified (Table 3.5.1).   Only one of the sites, located in northern Colombia (Fig. 3.5.14) had a frequency of simulations that had suitability in climate for all 53 of the climate scenarios.   However this site, like many of the other sites where climate is suitable, is on the mainland surrounding the Caribbean Sea, significantly isolated from island of Hispaniola the only location where the species is found today.

The duration of climate suitability on Hispaniola does not exceed 30 climatic scenarios, and interestingly the only sites which demonstrate climate suitability are those where the species is found today, apart from a site neighbouring the western-most outpost.   There is climate suitable on the neighbouring Caribbean islands of Cuba, Jamaica and Puerto Rico, but similarly these sites do not exceed 30 simulations, with many having just five or less, a common trait of many the predicted sites of occupation (Fig. 3.5.15).   This suggests that during last 120 thousand years of climatic change, there were no consistently suitable areas in the Caribbean for *L. megaplaga*.   Therefore the species either had to move between islands or, as discussed previously, there were small areas of Hispaniola with microclimates that remained relatively climatically stable which cannot be effectively modelled at this grid scale.
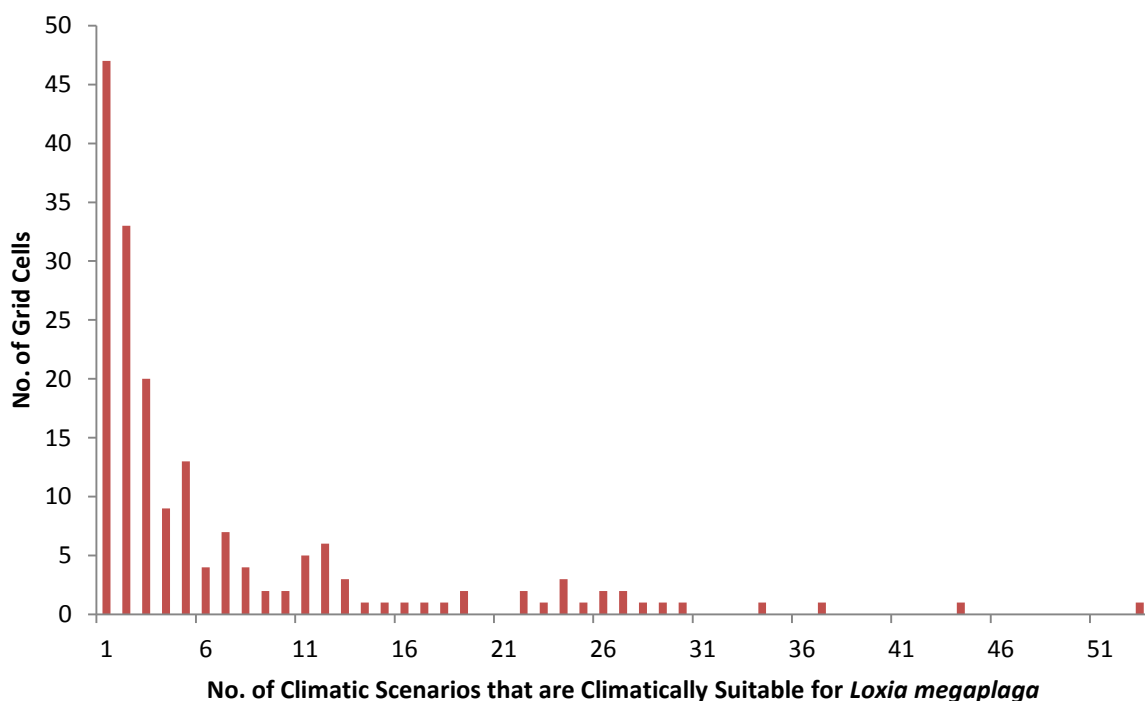
Figure 3.5.15:   The quantified durations of climatic suitability for *Loxia megaplaga*.   The number of 0.5° x 0.5° grid cells that have the same duration of occupation for *L. megaplaga*.   Duration of occupation is calculated as the number of scenarios the grid cell is predicted to have climatic conditions suitable for the species.

BLANK PAGE

Larix species

Larix species have four distinct regions of distribution at the previous interglacial, 120 thousand years ago, across Russia, in the Himalayas, across Canada and in Alaska (Fig. 3.5.16 A). The cooling climate of the stadial (Fig. 3.5.16 B) and glaciations (Fig. 3.5.16 C, D & E) sees a significant expansion in Russian range across much of northern Eurasia into Europe and during warmer periods of the glaciation, interstadials, southerly into regions of central Eurasia, resulting in there being a greater quantity of climatically suitable regions for *Larix* species during the glacial. The colder climate causes the Himalayan range to become inhospitable, instead southern regions such as Bhutan become more climatically suitable. In North America the Canadian population is significantly reduced before even the advancement of the Laurentide ice sheet, with the population restricted to the eastern regions of the USA during the glacial. However, the Alaskan population persists throughout the glacial and the lower sea-level results in the exposure and possible colonisation of the Bering Strait by *Larix*. As conditions warm post glaciation and heading into the Holocene (Fig. 3.5.16 F), European climates are simulated as inhospitable for *Larix* and restricting it to its present range in Russia, while in North America the receding Laurentide ice sheet means there is an expanse of climate available for *Larix* across Canada and the possibility at the beginning of the Holocene that the Alaskan and Canadian climate ranges may have overlapped, prior to splitting again to form the segregated species of *Larix* observed today (Fig. 3.4.17).

Larix species, unlike many of the other conifer species, has a climatic niche which would have resulted in a more expansive distribution, specifically in Eurasia, during the glaciation compared to the interglacials, such as the present-day conditions, probably due to a number of the species having a great tolerance for cold extreme. It is also interesting to note the suitability of climate in Europe during the glacial close to the present day range of *Larix deciduas*, which, although included in the initial model, is of significantly different climatic niche that it is not represented in simulations of present range. It could be that the population was established during these cooler glacial conditions and that the remaining population is a vestige of this past colonisation.
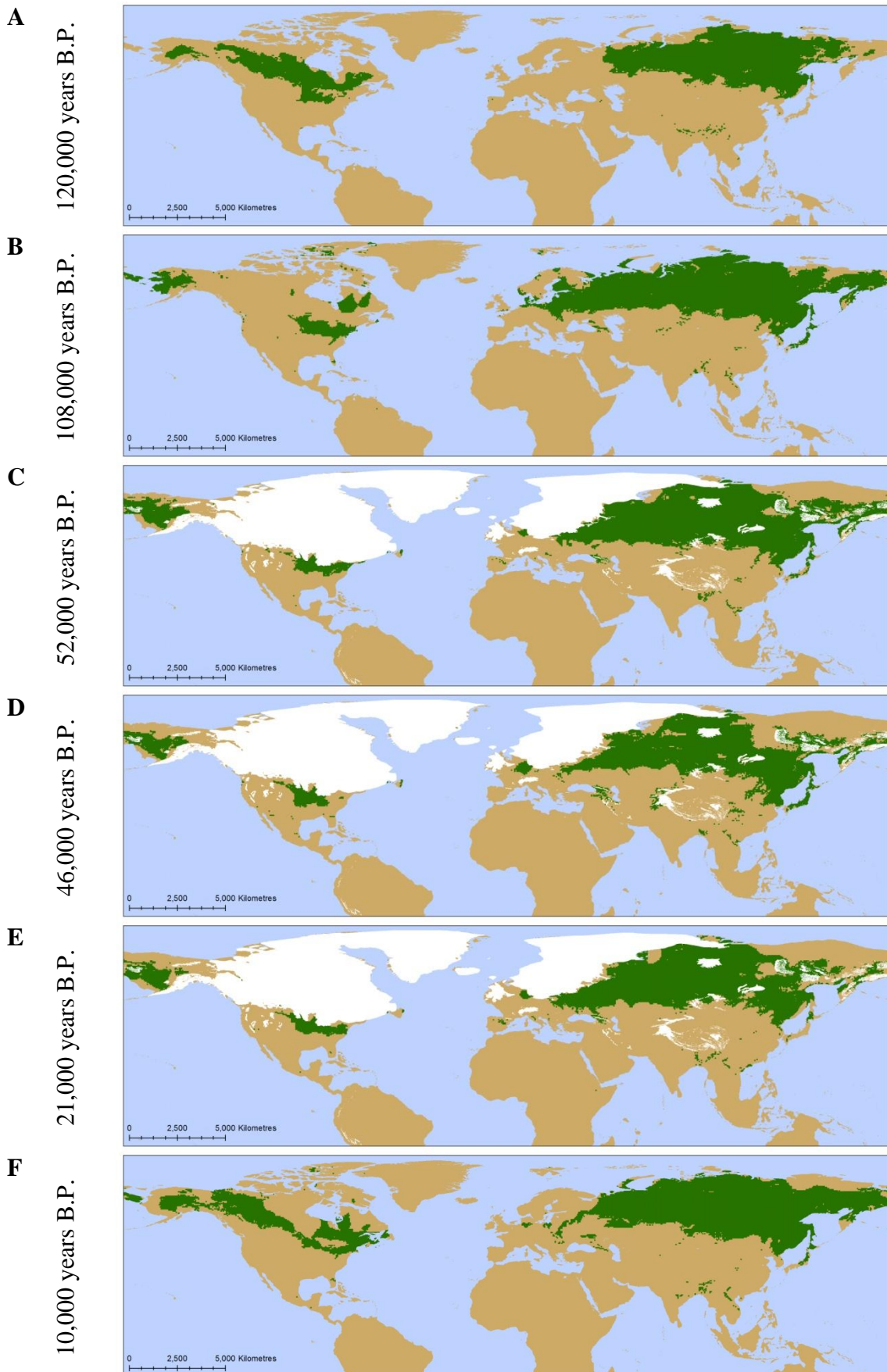
Figure 3.5.16: The simulated distribution of *Larix* spp. (green) during the Eemian interglacial (A); at the Meisley 1 stadial (B); during interstadial conditions (C); at Heinrich Event 5 (D); at the Last Glacial Maximum (E) and the beginning of the Holocene (F), all produced by the CRS model.
See Appendix: Results – *Larix* spp. for full descriptions of the simulated distributions.

Figure 3.5.17: The simulated duration of occupation for *Larix* spp., calculated as the number of palaeoclimate scenarios where presence is predicted by the CRS model.

For the modelled *Larix* genus there is the largest climatically stable region, numbering 5,540 grid cells which have climate that is suitable for at least 51 of the scenarios over the last 120 thousand years (Table. 3.5.1).   The majority of this climatically stable range is found in Russia, stretching as far east as the Kamchatka peninsula, north towards the coast of the Barents and Kara Seas of the Arctic Ocean and along the eastern coast as far south as northern Japan, northern China and neighbouring Mongolia (Fig. 3.5.17).   There are also locations in North America that remain relatively stable throughout the interglacial and glacial conditions; in eastern central Alaska and near the Great Lakes on the USA and Canadian border.   There are also locations in Quebec; however these sites were likely to have been covered by the expansive Laurentide ice sheet during the glacial so are unlikely to have sustained *Larix* populations despite the climate being suitable.

Surprisingly, unlike other species and genus modelled, the climatically stable regions account for just over a fifth (20.06%) of the total number of grid cells simulated, totalling to 27,612 grid cells (Table. 3.5.1).   And even more interestingly there are more grid cells that are simulated as having climate suitable for all 53 of the climate scenarios, nearly 3,500 grid cells, than any other frequency of scenario simulation (Fig. 3.5.18).

It is also interesting to note that much of the climatically stable range of *Larix* in Eurasia overlaps with that of *Loxia leucoptera*, the crossbill species which is most frequently associated with consuming this genus of conifer.   In North America, the stable locations around the Great Lakes for *Larix* species overlap with *Loxia leucoptera* and the smaller stable

Figure 3.5.18:   The quantified durations of climatic suitability for *Larix* species.   The number of 0.5° x 0.5° grid cells that have the same duration of occupation for *Larix* spp.   Duration of occupation is calculated as the number of scenarios the grid cell is predicted to have climatic conditions suitable for the species.

area in Alaska does coincide with *Loxia leucoptera* but is not as expansive as the crossbill's climatically suitable range.   However, overall this suggests that *Loxia leucoptera* and the *Larix* genus have had a close predator-prey relationship throughout the last 120 thousand years.

Also notably, many species of *Larix* maintained a stable niche in locations where they are presently observed, such as *L. kaempferi,* in Japan; *L. sibirica*, in Russia; and *L. gmelinii*, in Russia, Mongolia and northern China.   The *L. laricina* species in North America appears to have been split throughout the glaciation, producing two distinct stable locations in Alaska and the Great Lakes.   This interesting when one takes into account that the current range is mainly throughout Canada with a disjunct population in Alaska, and that in fact the climate of the area between Alaska and the rest of the Canadian population appears to have inhospitable throughout the last 120 thousand years, suggesting that this population in Alaska may have been isolated for this period.

BLANK PAGE

Picea species

120 thousand years ago, *Picea* species potential range based on the interglacial climatic conditions, was in northern Japan, southern and central Siberia and western Russia, as far east as Fennoscandia and the central Alps of Europe (Fig. 3.5.19 A). It also could be found throughout the central Asian mountain ranges and Caucasus Mountains, while in America its potential distribution was throughout southern and north-western Canada and Alaska. The cooling climate of the stadial (Fig. 3.5.19 B) from 108 thousand years ago and the glaciation (Fig. 3.5.19 C & E), from around 100 thousand years ago, resulted in a southern shift in climatic suitability in Eurasia, to central regions and a separation of climatically suitable regions in North America between Alaska and the central USA, climatically and physically by the formation of the Laurentide ice sheet. The lower sea-levels and exposure of the Bering Strait could have allowed the merging of climatically suitable ranges in the northern Pacific between Alaska and Siberia. During the dramatically cold Heinrich Event that occurred during the last glaciation (Fig. 3.5.19 D), the Eurasian *Picea* climate ranges were severely restricted; however, in North America there was an expansion of climatic suitable ranges south of the Laurentide ice sheet during these Events.

The initiation of warming and the melting of the glaciers into the beginning of the Holocene (Fig. 3.5.19 F) resulted in a relatively quick re-colonisation of the northern latitudes. Already by 10 thousand years ago, the climate is suitable for the Alaskan and Canadian ranges to have reconnected across northern North America to a distribution similar to that observed today (Fig. 3.4.20). Since the onset of the Holocene, climate in the north of Siberia that was once suitable is no longer, resulting in a southern shift in range suitability in this region to areas the present populations are observed in. A notable location of climatic suitability throughout the last 120 thousand years was the island of Newfoundland, where the bioclimatic is simulated as being suitable throughout the glacial and interglacials and where today there are both *Picea mariana* and *Picea glauca* as native species to this region, and the simulations suggest a spruce species such as these may have persisted in this isolated location.

In the case of the *Picea* species modelled, there are 2,631 grid cells which have climatic conditions which are suitable for 51 or more of the climatic scenarios, although this accounts for just 8.30% of the total number of simulated grid cells (Table 3.5.1). The stable climatic regions are in the central European mountains, the Alps, Dinaric Alps, Carpathians and Caucasus Mountains, throughout central Russia, and along the south-eastern coastline, into China and northern Japan (Fig. 3.5.20).
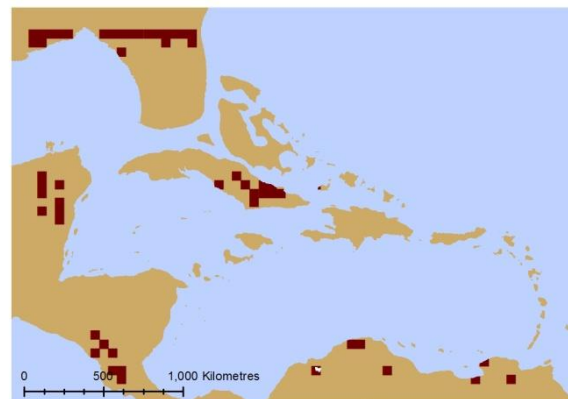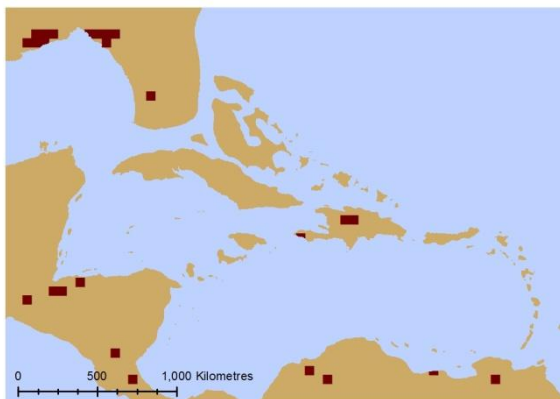
**A**

120,000 years B.P.

B

108,000 years B.P.

C

52,000 years B.P.

D

46,000 years B.P.

E

21,000 years B.P.

F

10,000 years B.P.
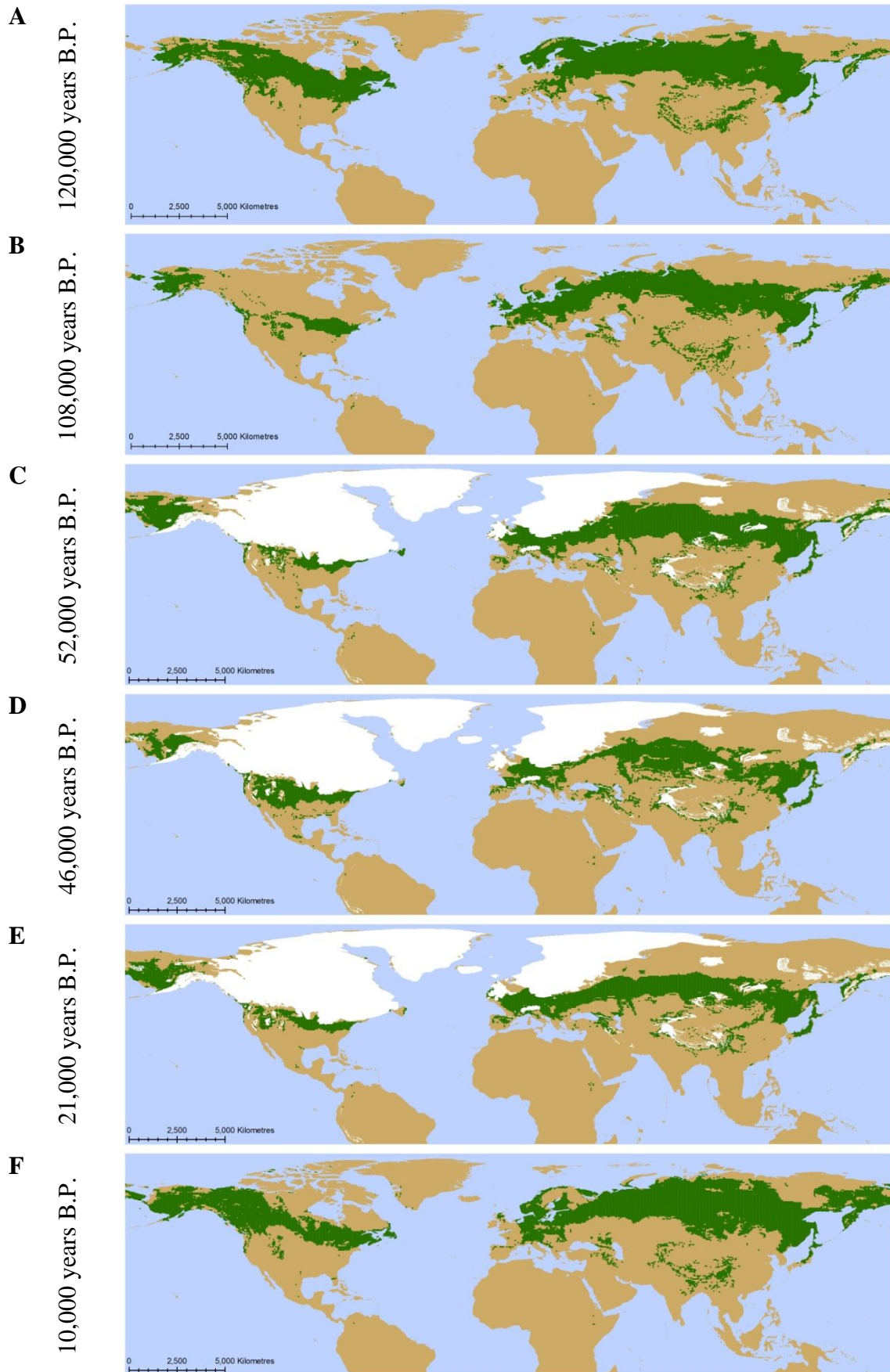
Figure 3.5.19: The simulated distribution of *Picea* spp. (green) during the Eemian interglacial (A); at the Meisley 1 stadial (B); during interstadial conditions (C); at Heinrich Event 5 (D); at the Last Glacial Maximum (E) and the beginning of the Holocene (F), all produced by the CRS model.
See Appendix: Results – *Picea* spp. for full descriptions of the simulated distributions.
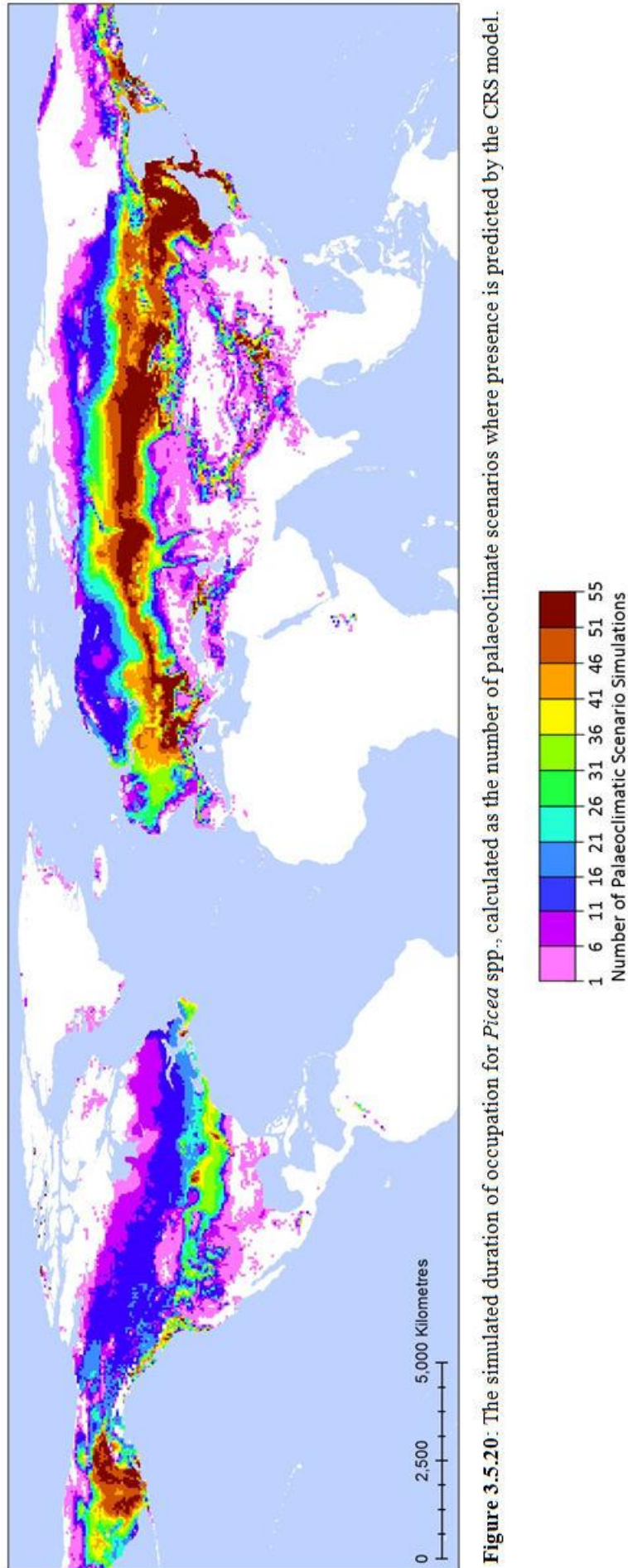
Figure 3.5.20: The simulated duration of occupation for *Picea* spp., calculated as the number of palaeoclimate scenarios where presence is predicted by the CRS model.
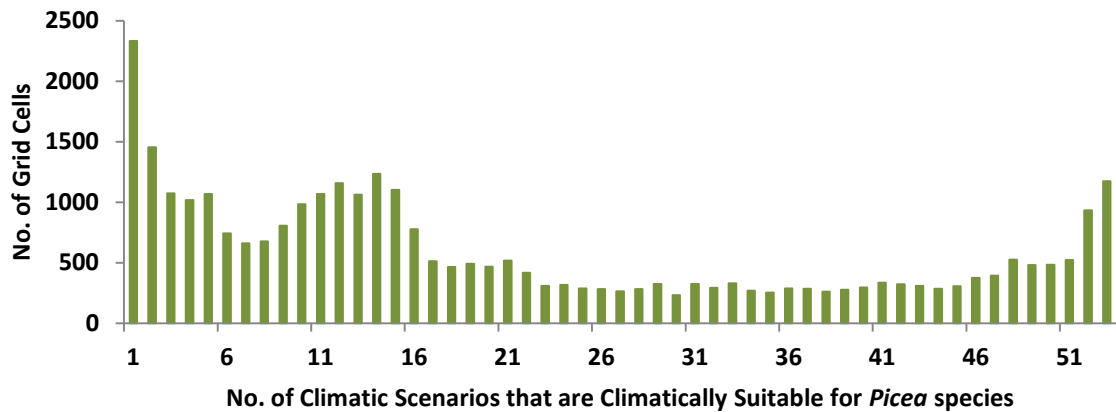
Figure 3.5.21:   The quantified durations of climatic suitability for *Picea* species.   The number of 0.5° x 0.5° grid cells that have the same duration of occupation for *Picea* spp.   Duration of occupation is calculated as the number of scenarios the grid cell is predicted to have climatic conditions suitable for the species.

The Siberian Kamchatka peninsula and the Himalayas also have locations that remain climatically suitable throughout the last 120 thousand years of climate scenarios.   In North America, there are fewer locations of stable climate; the majority are in Alaska, with some sporadic locations along the west coast of Canada, around the Great Lakes in north-eastern USA and in the east, in Newfoundland.

Many of the sites which are climatically suitable for at least one of the climate scenarios, particularly in North America, do not exceed 16 of the climatic scenarios being suitable (Fig. 3.5.21).   Over two thousand have just one scenario when climate is suitable, but 1,175 grid cells have climatic conditions which are suitable for all 53 of the climatic scenarios modelled.   It is also evident that the development of the vast Laurentide ice sheet in North America resulted in a more dramatic range shift and therefore limited stability in climate than Eurasia.

Loxia curvirostra is often considered a dietary specialist of *Picea* species, specifically in northern Eurasia, and comparing the duration simulations (Fig. 3.5.1 & 3.5.20) it is evident that the climatically stable region in Eurasia shares a significant overlapping range.   In North America this is not the case, however the native sub-species of *L. curvirostra* tend to consume *Pinus* species and this may have been specialism which was in some way driven by the climatic constraints on both conifer and crossbill species in North America.

Like *Larix*, many of the present day species of *Picea* have ranges which appear to have been maintainable, at least in part, throughout that last 120 thousand years, these include; *P. abies*, throughout central Europe and Russia; *P. alcoquiana, P. koraiensis* and *P. torano,* in Japan; *P. orientalis*, in the Caucasus Mountains; *P. mariana*, in Alaska and also Newfoundland; and around the Great Lakes as well as other smaller ranged species in the mountains of Asia.

Pinus species

Pinus species have a broad climatic niche today being found in boreal, steppe and tropical climates and this was similar during the Eemian glacial, 120 thousand years ago, with an expansive potential range throughout much of Europe, central Russia and as far east as Japan and in southern Asia, from the Himalayas and surrounding mountain ranges into southern Vietnam (Fig. 3.5.22 A).   In North America, the climatic range stretches across the central regions from east to west, north into southern Alaska and throughout the western mountain ranges into Mexico.   As the climate cools and becomes drier in the stadial (Fig. 3.5.22 B) the areas available for *Pinus* species become more restricted, reducing in size and fragmenting and with the colder glacial and interstadial conditions (Fig. 3.5.22 C & E) seeing a southerly shift in the ranges in northern Eurasia and North America.   The longitudinal changes in climate suitability differ on the two continents; with the northern Eurasian population separating between east and west populations, while the North American climate across the central regions, on the edge of the Laurentide ice sheet, is consistently suitable from east to west   Although central Africa is simulated as climatically suitable throughout the glacial, its geographic isolation from other populations of *Pinus* meant it is likely to have remained uncolonised.   The warming temperatures at the beginning of the Holocene (Fig. 3.5.22 F) result in an expansion of climate available to the north in Eurasia, and to the north east and west in North America and this continues with areas like Fennoscandia becoming more climatically suitable and forming the range observed today (Fig. 3.5.23).   The south Asian populations remain relatively stable throughout the interstadial and glacial conditions.

Notably the climatic conditions in Hispaniola, where *Pinus occidentalis* the feeding tree of *Loxia megaplaga* is currently found, remains suitable throughout the last 120 thousand years. Although this is simulated using the combined *Pinus* species niche, rather than one specific to the species, it does highlight that the distribution may not have altered significantly through the glacial.   Similarly, the Philippines is also simulated as remaining a relatively stable climatic niche for *Pinus*, where the species *Pinus kesiya* is found and is the primary food-plant of *L. curvirostra* population in this region, however it may have only become suitable since the beginning of this glacial, as simulations of the Eemian suggest it was not climatically suitable then.

A 120,000 years B.P.

B 108,000 years B.P.

C 52,000 years B.P.

D 46,000 years B.P.

E 21,000 years B.P.

F 10,000 years B.P.
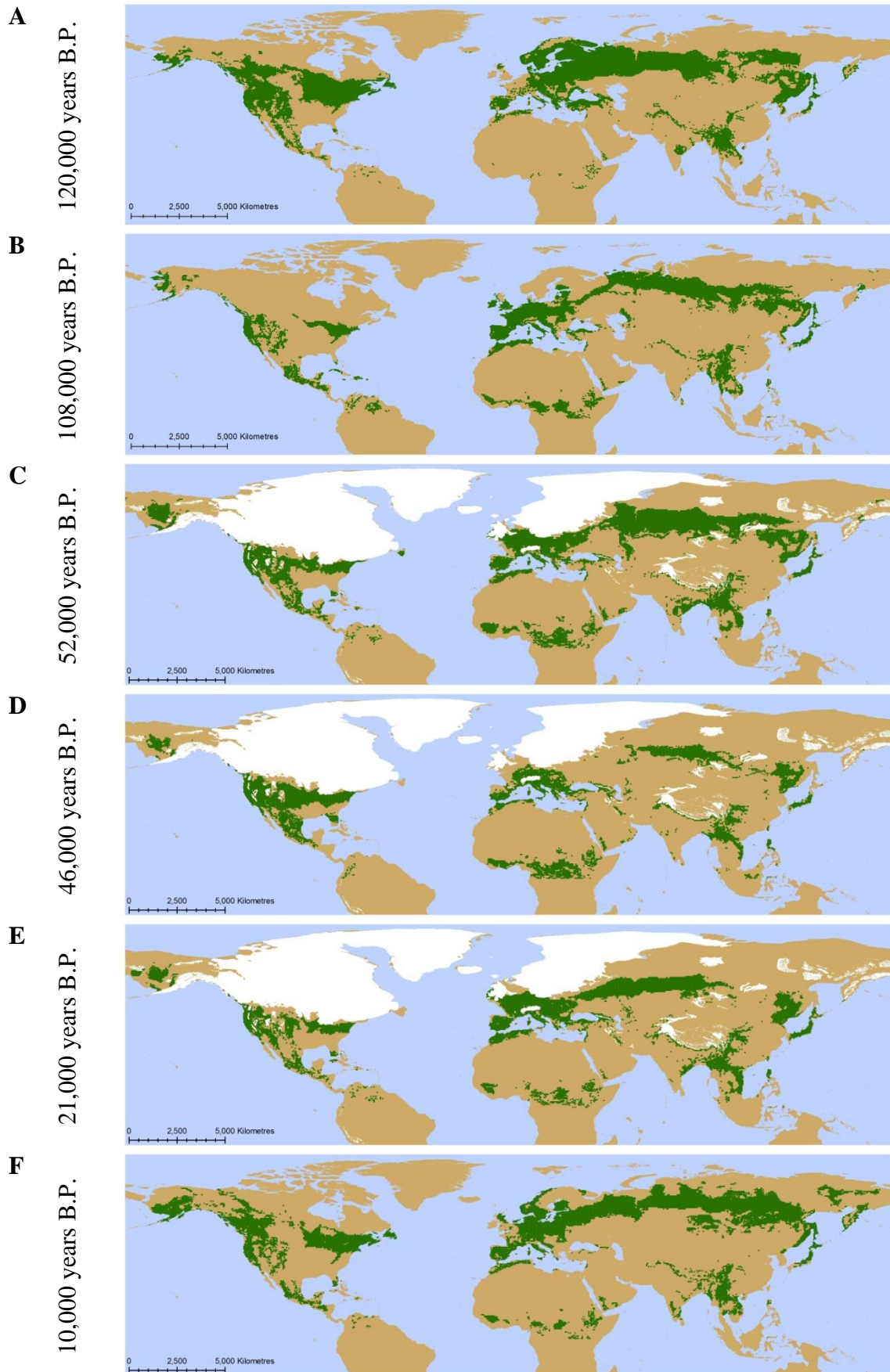
Figure 3.5.22: The simulated distribution of *Pinus* spp. (green) during the Eemian interglacial (A); at the Meisley 1 stadial (B); during interstadial conditions (C); at Heinrich Event 5 (D); at the Last Glacial Maximum (E) and the beginning of the Holocene (F), all produced by the CRS model.
See Appendix: Results – *Pinus* spp. for full descriptions of the simulated distributions.
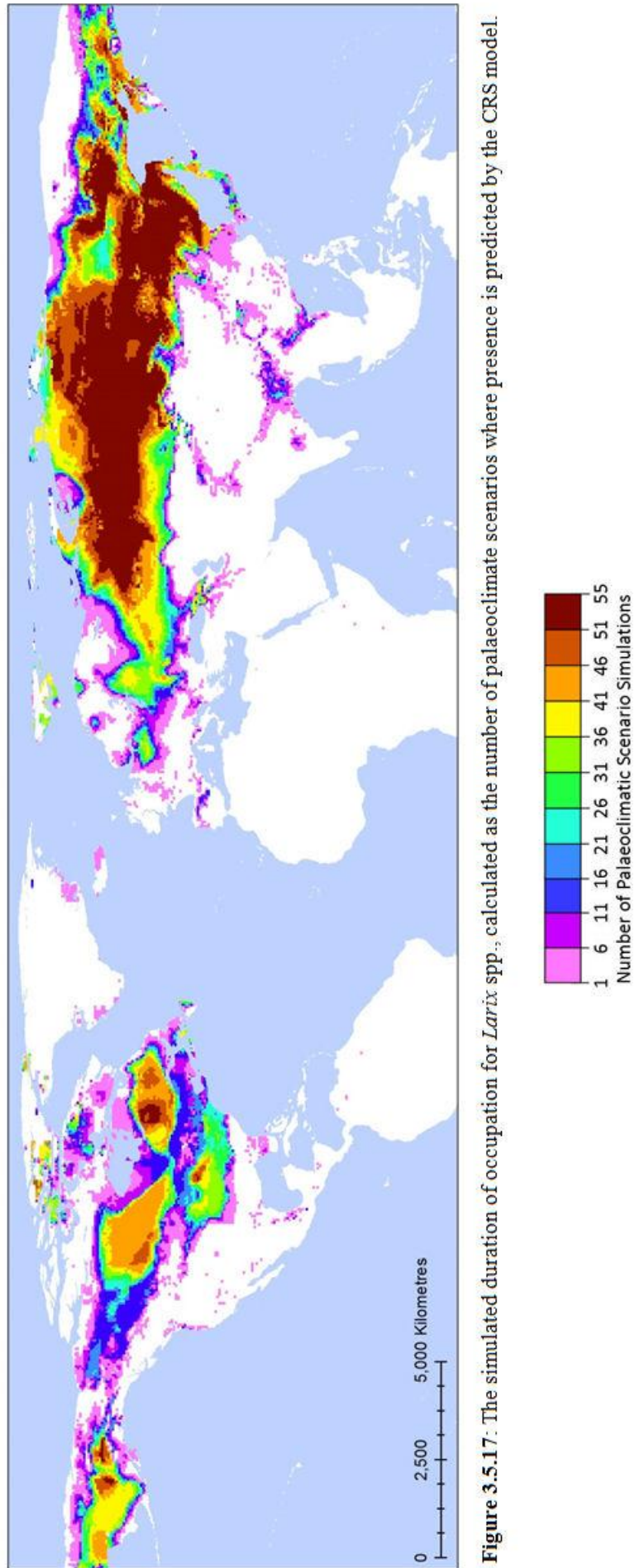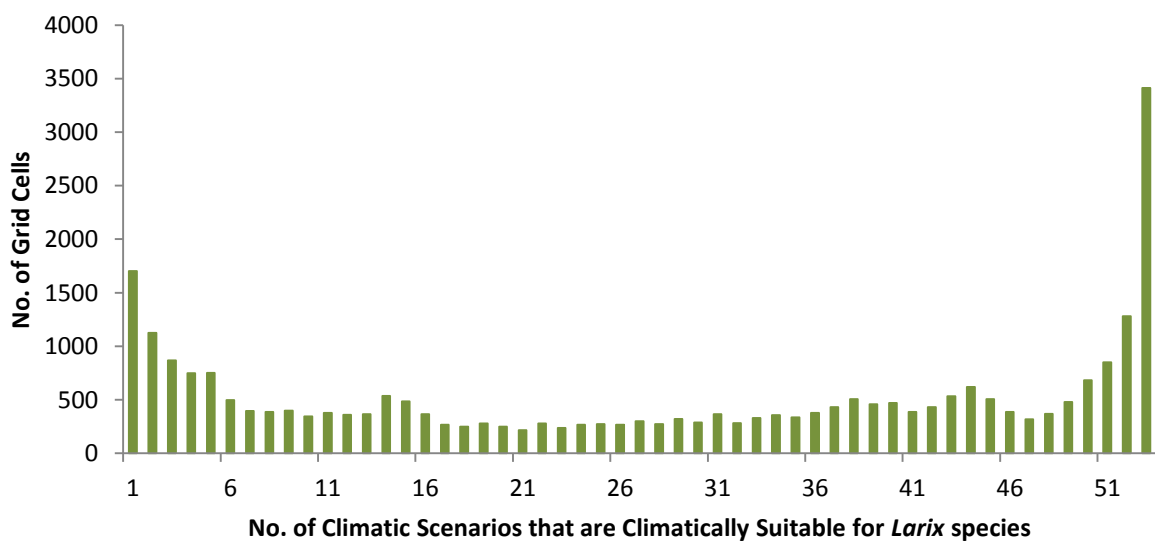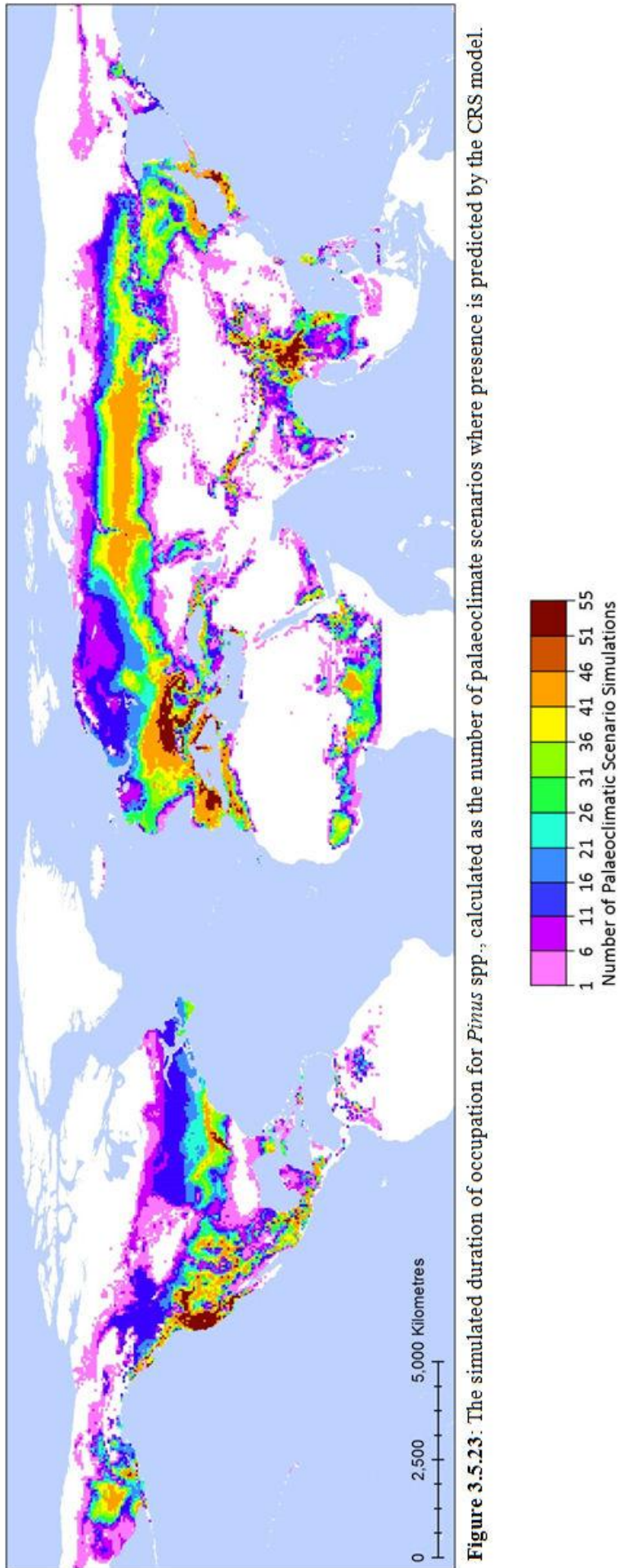
Figure 3.5.23: The simulated duration of occupation for *Pinus* spp., calculated as the number of palaeoclimate scenarios where presence is predicted by the CRS model.

Compared to the other wide-ranging conifer genera, the *Pinus* genus has a limited number of grid cells that have stable climate throughout the glacial and interglacial conditions, 864 grid cells that are simulated as being suitable in 51 or more scenarios, accounting for only 2.94% of the total number of grid cells which are suitable at least once (Table 3.5.1).   These areas of climate stability are found in Eurasia; north-eastern Africa, south-eastern Spain and the central mountain ranges of Europe, the Apennines, Alps, Dinaric Alps and Caucasus Mountains, south-eastern coastline of Siberia and Japan, the Himalayas, Myanmar and Vietnam (Fig. 3.5.23).   In North America, the stable areas of climate are the southern coastline of Alaska, along the western coast of North America, the western Rocky and eastern Appalachian Mountains, and as far south as the Mexican Sierra Madres.

Only 361 of the grid cells have climatic conditions which remain suitable throughout all 53 of the simulations, with a vast majority of the cells which have suitable at one time having 16 or fewer scenarios that are suitable, and over 2,500 having just one (Fig. 3.5.24).   This indicates that compared to the other broad ranging conifer genera of *Larix* and *Picea*, there has been significant climate range shifts for *Pinus* resulting in substantial changes in distribution throughout the last 120 thousand years not only in North America, as a result of the formation and expansion of the Laurentide ice sheet, but also in Eurasia.

As mentioned earlier, North American populations of *Loxia curvirostra* have specialised on the consumption of *Pinus* rather than *Picea* conifer species, and there is some observed overlap of the western regions of longer duration in *Pinus* with that of *L. curvirostra*, however the conifer genus is not as stable throughout the Rocky Mountains as the crossbill, but many locations are simulated for at least 36 of the 53 climatic scenarios.

Figure 3.5.24:   The quantified durations of climatic suitability for *Pinus* species.   The number of 0.5° x 0.5° grid cells that have the same duration of occupation for *Pinus* spp.   Duration of occupation is calculated as the number of scenarios the grid cell is predicted to have climatic conditions suitable for the species.

Another interesting association with *L. curvirostra* to note is that the climate in Vietnam remains stable throughout the last 120 thousand years for *Pinus*, as this area is where the sub-species *L. c. luzoniensis* is found today, consuming *P. kesiya*. Despite the duration of simulation for *L. curvirostra*'s modelled distributions not finding this area climatically stable, the evident stability for *Pinus* hints that this region may have still remained a crossbill outpost throughout the last 120 thousand years. While similarly *Pinus* is also simulated having a longer climatically suitable duration in the Philippines than *L. curvirostra*, this another area inhabited by *Pinus kesiya* and there is a resident sub-species, *L. c. meridionalis*. Other species of *Pinus* that have stable ranges, or parts of range, include; *P. contorta* and *P. strobiformes,* in the western USA; *P. kesiya* and *P. latteri*, in Myanmar and Vietnam; *P. halepensis,* in Mediterranean, North Africa and southern Europe; *P. sylvestris*, in the central Alps; *P. nigra*, in the Dinaric Alps; and many of the numerous Mexican pines.

Interestingly the climate in the Caribbean, at this coarse scale, and similarly to the individual model of *Pinus occidentalis*, is not climatically stable throughout the 120 thousand years despite there being two resident populations now, *P. occidentalis* and *P. caribaea*. Notably, the climate in Japan is found to be stable throughout the glacial and interglacials despite species from this region not being modelled, but there are *Pinus* species resident in Japan, *P. thunbergii* and *P. densiflora*.

BLANK PAGE

Pseudotsuga species

120 thousand years ago during the Eemian interglacial *Pseudotsuga* species had the potential to be found in the mountains of southern Asia, on the island of Japan and Taiwan, in southern Europe and around the Baltic coastline, and in western North America (Fig. 3.5.25 A).   The colder stadial (Fig. 3.5.25 B) leading into the widespread glaciation (Fig. 3.5.25 C, D & E) provided conditions with more climate suitability than the interglacials and results in a southerly extension of climate suitable in south Asia with areas such as Japan in the north become inhospitable, and a complete shift and expansion in Europe and occurrence in central Africa, while in North America, the west remains climatically suitable to the south of the extensive ice sheets, colonising more areas in Mexico and the Caribbean.

The warming climate at the onset of the Holocene (Fig. 3.5.25 F) and the retreating glaciers result in a northerly expansion of the western range in North America into Canada to a population similar to that observed today (Fig. 3.4.26).   It also becomes more climatically sparse in Europe and the central regions of the Himalayas become climatically unsuitable splitting the range, with the region to the south-east in southern China and northern Laos and Vietnam remaining relatively large, areas that are occupied by *Pseudotsuga* species. Compared to other conifer species, the changing climatic conditions of the last 120 thousand years have not resulted in significant alteration to the range of the south Asian and west North American population, remaining relatively stable, however, Japan's climate does become inhospitable during the glaciation, so whether the population observed there presently was able to persist is questionable.   Notably, despite there being climate suitable in Europe for the last 120 thousand years, it is unlikely that these regions were ever colonised, and certainly any such populations are extinct today.
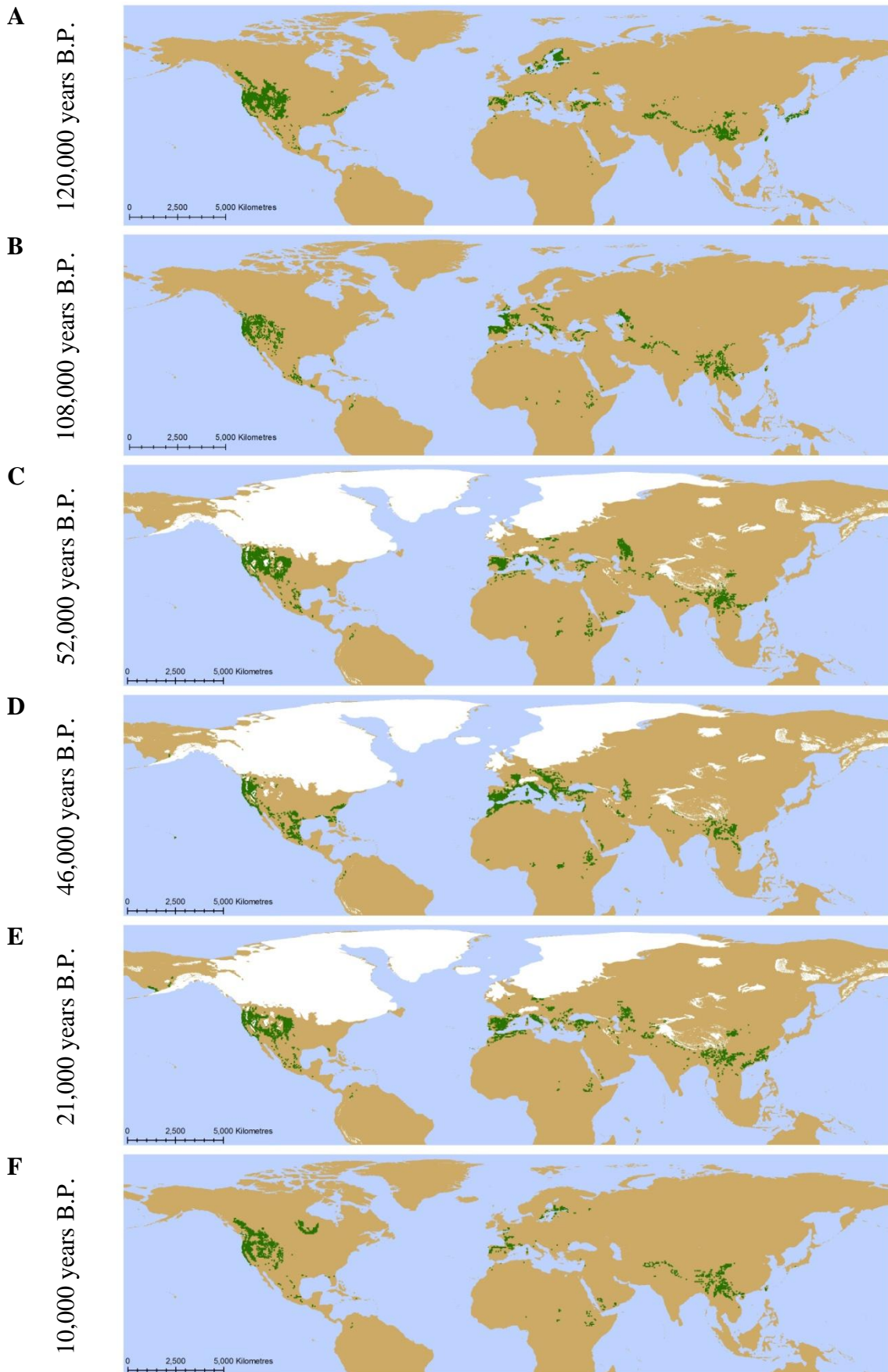
Figure 3.5.25: The simulated distribution of *Pseudotsuga* spp. (green) during the Eemian interglacial (A); at the Meisley 1 stadial (B); during interstadial conditions (C); at Heinrich Event 5 (D); at the Last Glacial Maximum (E) and the beginning of the Holocene (F), all produced by the CRS model.
See Appendix: Results – *Pseudotsuga* spp. for full descriptions of the simulated distributions.

Figure 3.5.26: The simulated duration of occupation for *Pseudotsuga* spp., calculated as the number of palaeoclimate scenarios where presence is predicted by the CRS model.

Figure 3.5.27:   The quantified durations of climatic suitability for *Pseudotsuga* species.   The number of
0.5° x 0.5° grid cells that have the same duration of occupation for *Pseudotsuga* spp.   Duration of occupation is
calculated as the number of scenarios the grid cell is predicted to have climatic conditions suitable for the species.

The genus of *Pseudotsuga* has just 86 grid cells which are simulated as having climatic
conditions which are suitable for 51 or more of the climate scenarios (Table. 3.5.1),
accounting for just 0.93% of the simulated grid cells for *Pseudotsuga* species' modelled
niche.   The regions with stable climate for *Pseudotsuga* are mainly in western North
America, where *P. menziesii* is found today, and a few locations in southern China, areas of
the current range for *P. sinensis* (Fig. 3.5.26).   Many of the areas have less than 6 different
modelled scenarios when the climate is suitable, with over 2,000 grid cells with only one valid
simulation 120 thousand years (Fig. 3.5.27).   However, many of these are found in Europe,
the Middle East and central Africa, which although climatically suitable, were unlikely to
have ever been colonised by *Pseudotsuga* due to their significant isolation from other ranges.

***Tsuga* species**

Similarly to *Pseudotsuga*, *Tsuga* species' climatic model simulates climate suitable in Europe throughout the last 120 thousand years, despite there being no records of it being there prior to the last glaciation. Discounting indications of these European populations, the larger distributions at the Eemian are throughout the Himalayas, into southern China, Japan and Korea; in south-eastern and along the western coast of North America (Fig. 3.5.28 A). The colder stadial conditions for Melisey 1 (Fig. 3.5.28 B) resulted in a reduction in climatically suitable range throughout the northern hemisphere for *Tsuga* species but most dramatically for the eastern range in North America, restricted it to the coast. During the glaciation (Fig. 3.5.28 C & E) there were some southerly shifts in the range of climate suitable in North America, but the eastern and western populations are maintained, and in south Asia there is little change in the overall range, although during the cooler Heinrich Event (Fig. 3.5.28 D), there is significantly more climate available in North America while there is a reduction in climate space in south Asia. As the climate warmed into the Holocene interglacial (Fig. 3.5.28 F), the *Tsuga* populations in North America could spread northwards, with the easterly range potentially increasing in range size to a distribution similar to present day (Fig. 3.4.29) while the populations in south Asia remain similar in overall extent from the end of the glacial throughout the Holocene to present day. Most interestingly, despite *Tsuga sieboldii*, the Japanese native Hemlock, being excluded from the model due to it not being a common food resource of *Loxia* species, the *Tsuga* niche model simulates that Japan remains a stable climatic niche throughout the interglacials and glacial, suggesting it has a long history here and that its climatic niche is shared with other Hemlock species.

A 120,000 years B.P.

B 108,000 years B.P.

C 52,000 years B.P.

D 46,000 years B.P.

E 21,000 years B.P.

F 10,000 years B.P.

Figure 3.5.28: The simulated distribution of *Tsuga* spp. (green) during the Eemian interglacial (A); at the Meisley 1 stadial (B); during interstadial conditions (C); at Heinrich Event 5 (D); at the Last Glacial Maximum (E) and the beginning of the Holocene (F), all produced by the CRS model.
See Appendix: Results – *Tsuga* spp. for full descriptions of the simulated distributions.
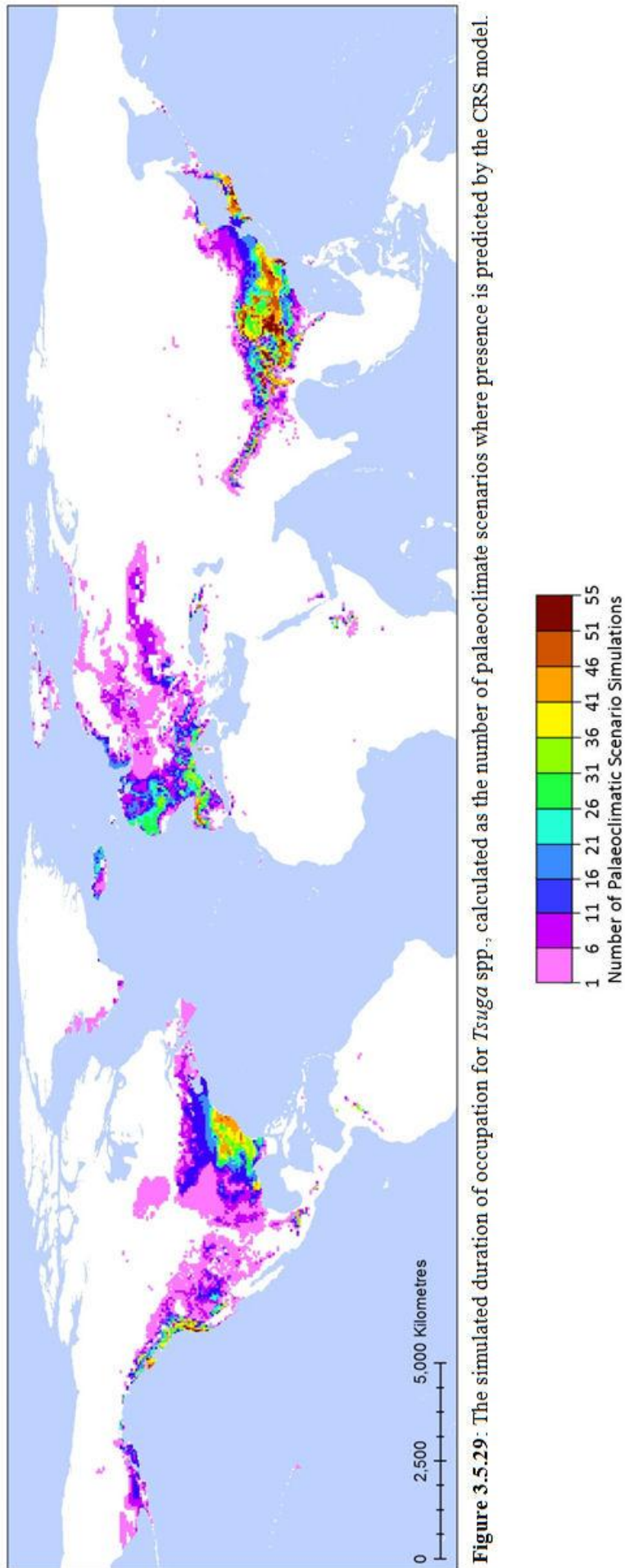
Figure 3.5.29: The simulated duration of occupation for *Tsuga* spp., calculated as the number of palaeoclimate scenarios where presence is predicted by the CRS model.
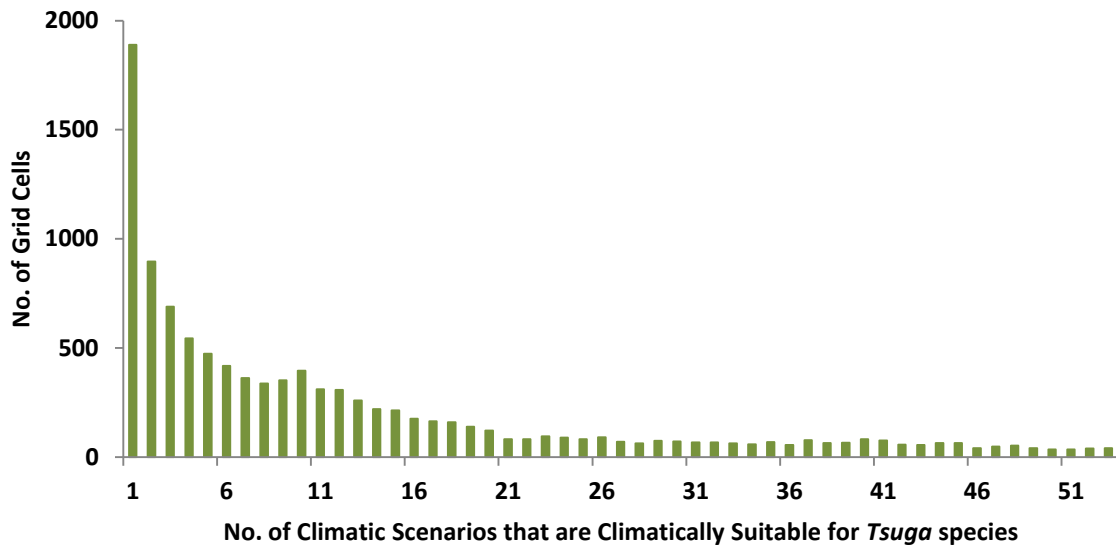
Figure 3.5.30: The quantified durations of climatic suitability for *Tsuga* species. The number of 0.5° x 0.5° grid cells that have the same duration of occupation for *Tsuga* spp. Duration of occupation is calculated as the number of scenarios the grid cell is predicted to have climatic conditions suitable for the species.

The climatically stable range for *Tsuga* species where the climate is suitable for 51 or more of the scenarios covers 118 grid cells (Table 3.5.1), just 1.11% of the simulated grid cells. The areas that have the most stability for *Tsuga* are in eastern and western coastline of North America, the Himalayas, southern China, Taiwan and southern Japan (Fig. 3.5.29). Many of these areas coincide with regions where *Tsuga* species are found today, *T. canadensis* in eastern USA; *T. heterophylla,* along the western coast of North America; *T. dumosa* in the Himalayas; and Myanmar and *T. chinensis,* in southern China and Taiwan. Notably there is also a population in southern Japan, *T. sieboldii*, although this is not included in the model.

There are substantial areas which do not have stable climatic conditions, the majority of these having less than 11 scenarios when the climate is suitable (Fig. 3.5.30) with over 2,000 grid cells having conditions only one simulation. There are extensive periods of suitable climate simulated in Europe, however, these areas, as with *Pseudotsuga*, are significantly isolated from their ranges today and so were unlikely to ever have been utilised over the last 120 thousand years.

Picea abies

The interglacial warm, wet conditions of the Eemian result in *Picea abies* having a potential distribution from eastern European mountains throughout central Russia to the south-eastern coast of Siberia (Fig. 3.5.31 A).   The colder stadial (Fig. 3.5.31 B) results in greater climatic suitability in western Europe and further east in Siberia, and a restriction to the north in eastern Russia and south in western Russia.

The glacial conditions see a more southerly shift in range in Europe and Russia (Fig. 3.5.31 E), with warmer conditions of the interstadial (Fig. 3.5.31 C) providing conditions in higher latitudes suitable for *Picea abies* and the colder Heinrich Events (Fig. 3.5.31 D) result in fragmentation and a patchier range, specifically with eastern Europe becoming inhospitable.   As the conditions warm into the Holocene, the onset (Fig. 3.5.31 F) has highly favourable climate situated in the north of Russia and areas of southern Fennoscandia, becoming more suitable into the north of Fennoscandia and restricted to central Russia during still changing conditions of the Holocene to the range observed today (Fig. 3.4.32).
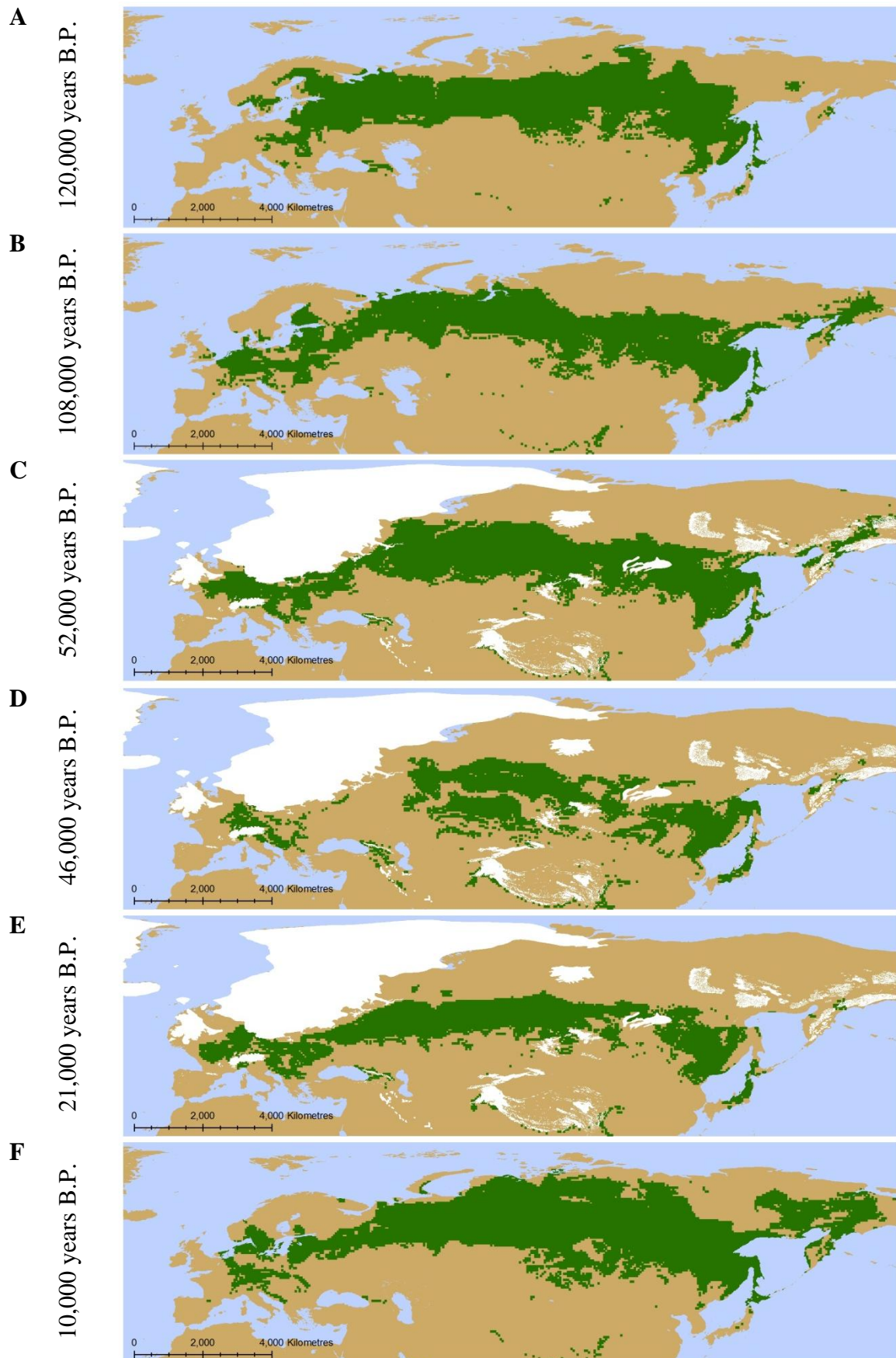
Figure 3.5.31: The simulated distribution of *Picea abies*. (green) during the Eemian interglacial (A); at the Meisley 1 stadial (B); during interstadial conditions (C); at Heinrich Event 5 (D); at the Last Glacial Maximum (E) and the beginning of the Holocene (F), all produced by the CRS model.
See Appendix: Results – *Picea abies* for full descriptions of the simulated distributions.
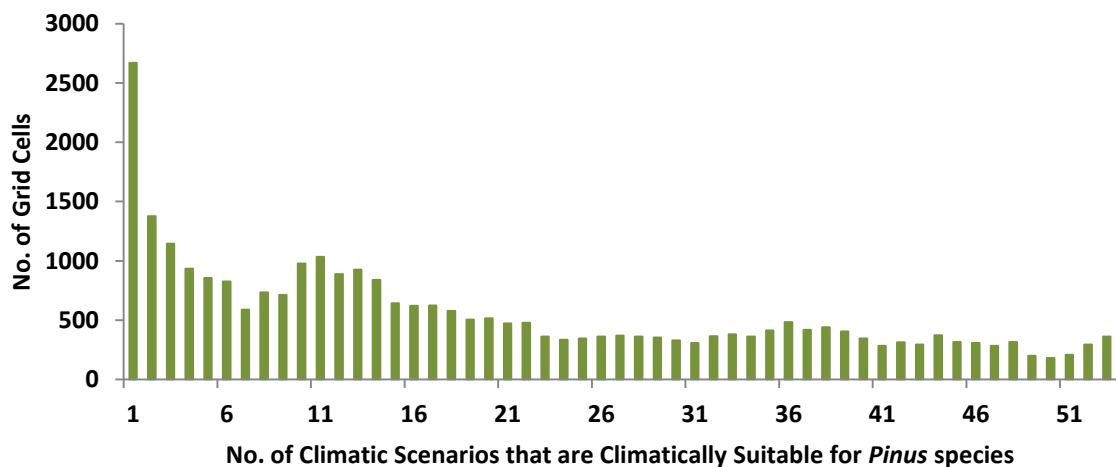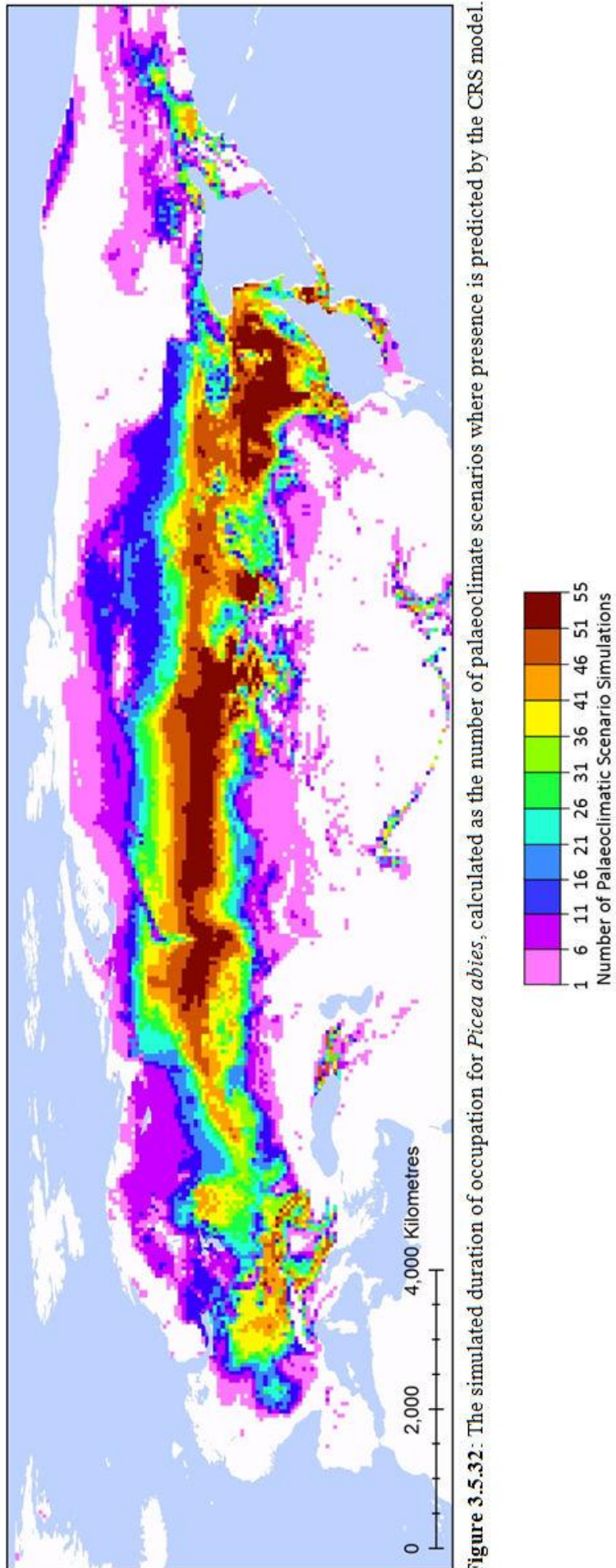
Figure 3.5.32: The simulated duration of occupation for *Picea abies*, calculated as the number of palaeoclimate scenarios where presence is predicted by the CRS model.
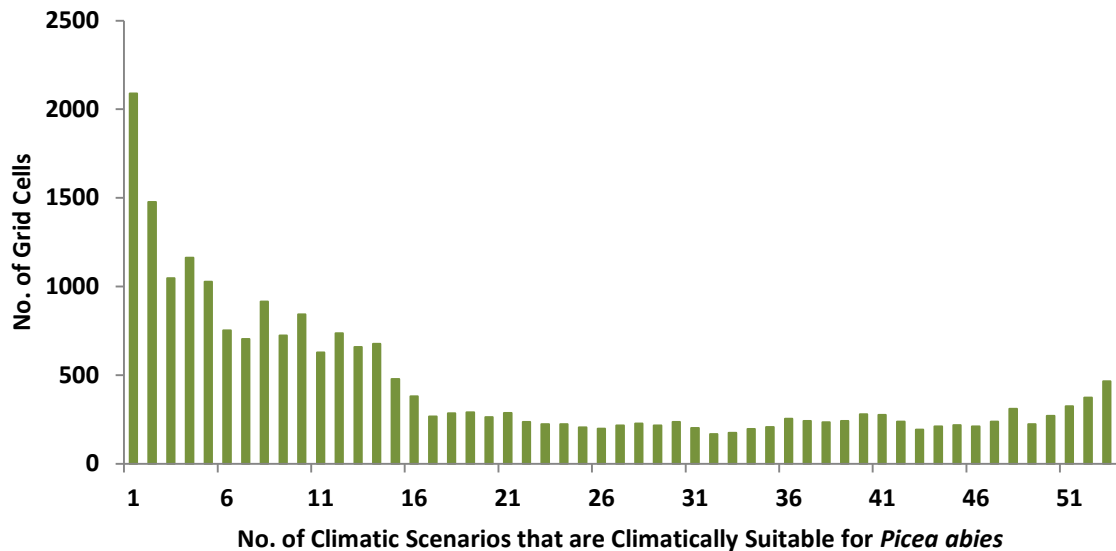
Figure 3.5.33:   The quantified durations of climatic suitability for *Picea abies*.   The number of 0.5° x 0.5° grid cells that have the same duration of occupation for *P. abies*.   Duration of occupation is calculated as the number of scenarios the grid cell is predicted to have climatic conditions suitable for the species.

Picea abies has a broad stable climate range through central Russia, the Sayan Mountains and Siberia, south-east into northern China and Japan as well as some isolated location in the Alps (Fig. 3.5.32), totalling 1,165 grid cells which have climate suitable for *Picea abies* for 51 or more scenarios (Table 3.5.1).   The stable climate range accounts for 4.96% of the simulated grid cells, with a majority of grid cells having less than 16 scenarios where climate is adequate for the modelled niche (Fig. 3.5.33).

The range of the climate stability for *Picea abies* indicates that the present day range in Russia remained consistent over the last 120 thousand years, with potential latitudinal expansion when the climate was more favourable, and overlaps with the areas of stability modelled for its predator, *L. curvirostra*.   On the other hand, in Europe the climatic range of *Picea abies* was subject to more changes, likely as a result of the expansion of the Weichselian ice sheet which made Fennoscandia, where the species is abundant today, inhospitable during the glacial.

Pinus sylvestris

Similar to *Picea abies*, *Pinus sylvestris* has a climatically suitable range from northern China and Japan throughout central Russia, although patchier in the east, into central Europe, southern Fennoscandia, stretching further south west than *Picea abies* into Spain and isolated climate suitable in Scotland (Fig. 3.5.34 A).   The cooler stadial (Fig. 3.5.34 B), 108 thousand years ago, resulted in northern regions of Europe become inhospitable, restricting the climatic suitability to central and southern Europe, while, in Russia, the distribution in the west became more restricted to the north, and in the east was constrained by inhospitably both to the north and south of the range.   This southerly restriction in Europe was maintained throughout the glacial that began 100 thousand years before present and at the glacial maximum (Fig. 3.5.34 E) the Russian range was restricted southerly and fragmented to the west and east of its previous interglacial range.   During the warmer conditions of the interglacials (Fig. 3.5.34 C) the climate became consistently more suitable throughout Russia and there was a northern expansion in potential range but the colder Heinrich Events (Fig. 3.5.34 D), resulted in further fragmentation of populations, with the inhospitability of eastern and western Europe isolating the climatically suitable range to the mountain ranges. The interglacial conditions at the beginning of the Holocene (Fig. 3.5.34 F) result in a shift of climate suitable in the north of Russia and into southern Fennoscandia, with further expansion into these regions during the warming that followed to present day (Fig. 3.4.35).

Like *Picea abies*, the Caucasus Mountains and the Himalayas are simulated as having regions suitable throughout the interglacials and glacial, however the significant isolation and presence of other competitive species, such as *Pinus orientalis* in the Caucasus Mountains, has meant that they are unlikely to have ever been colonised by the specific *Pinus sylvestris*. However, during the interglacials, Scotland has climate suitable for *Pinus sylvestris* and during the glacial, although much of Scotland is inhospitable due to the Devensian ice sheet, areas to the west of the ice sheet on the Scottish islands and in Ireland are simulated as having a potential bioclimate that is within the modelled niche.
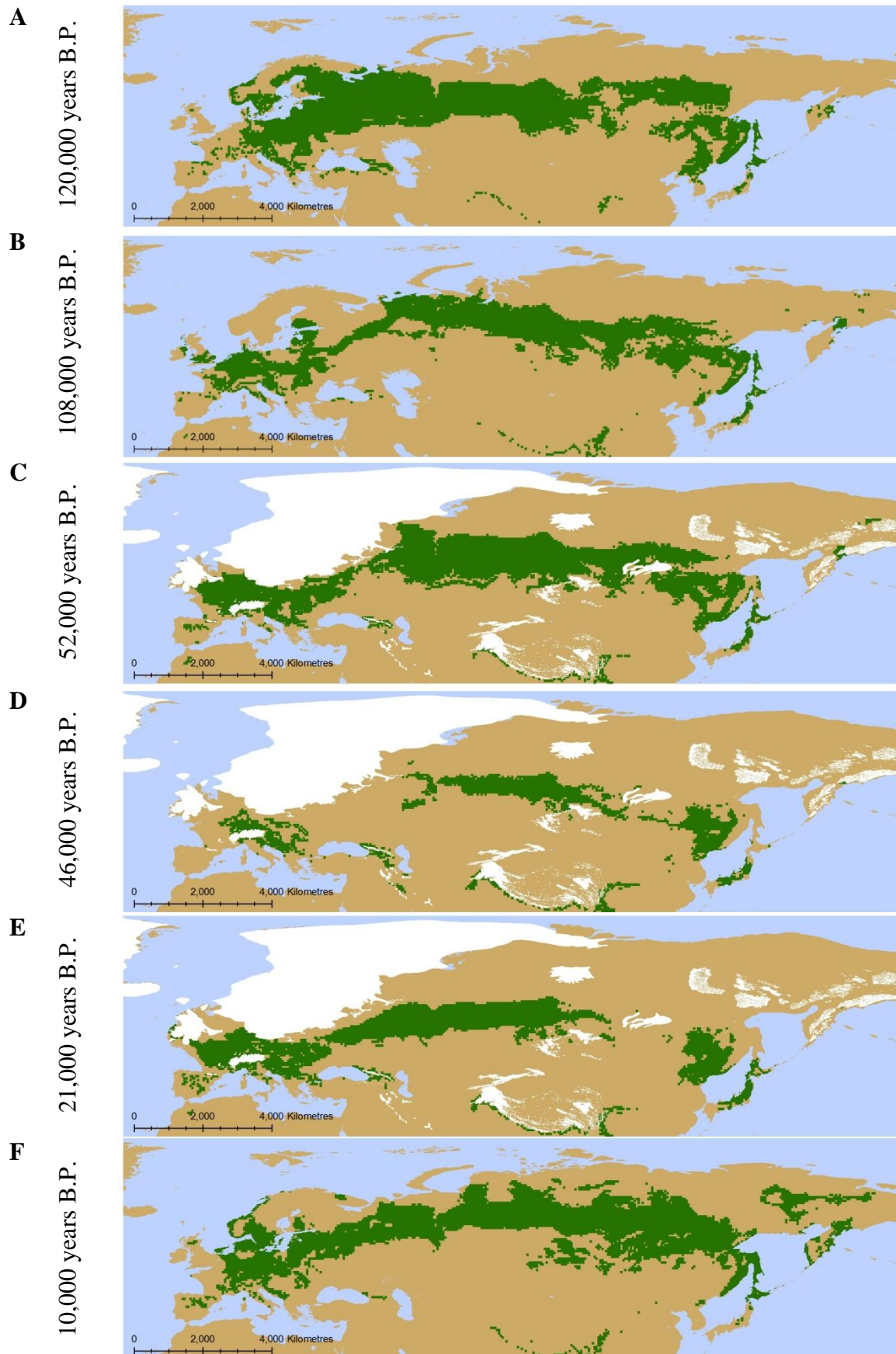
Figure 3.5.34: The simulated distribution of *Pinus sylvestris*. (green) during the Eemian interglacial (A); at the Meisley 1 stadial (B); during interstadial conditions (C); at Heinrich Event 5 (D); at the Last Glacial Maximum (E) and the beginning of the Holocene (F), all produced by the CRS model.
See Appendix: Results – *Pinus sylvestris* for full descriptions of the simulated distributions.
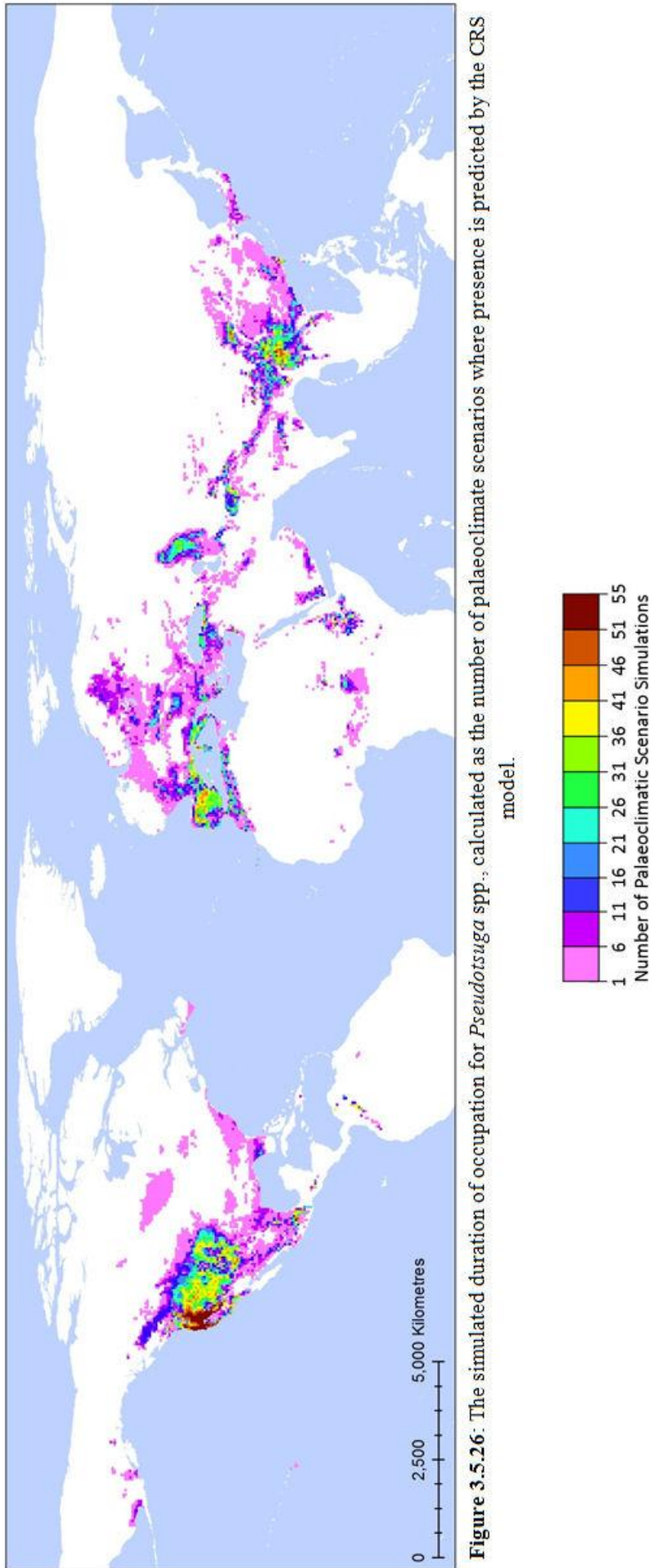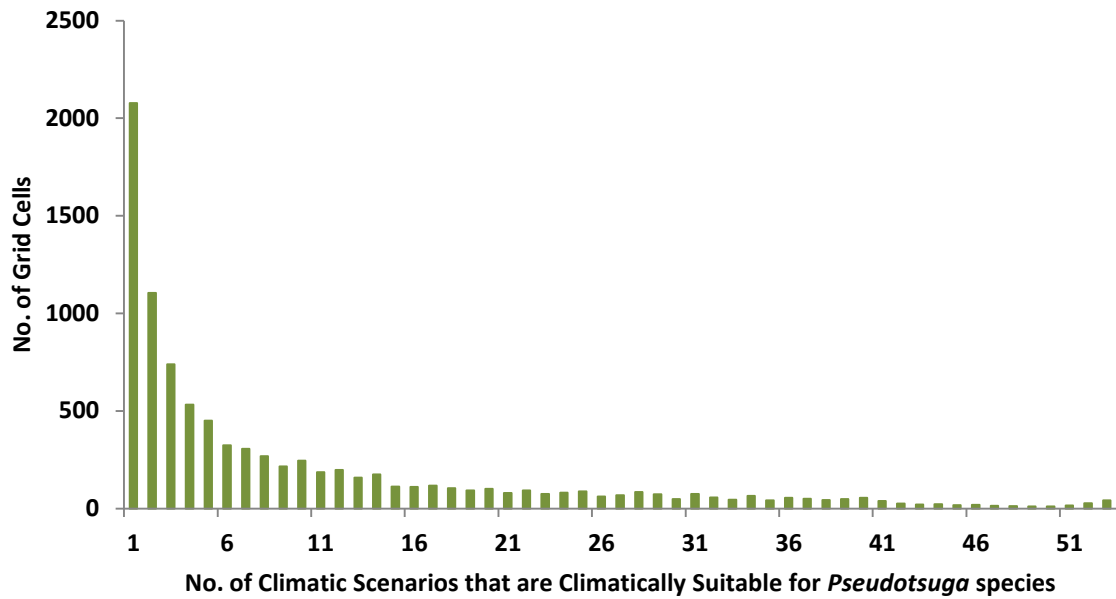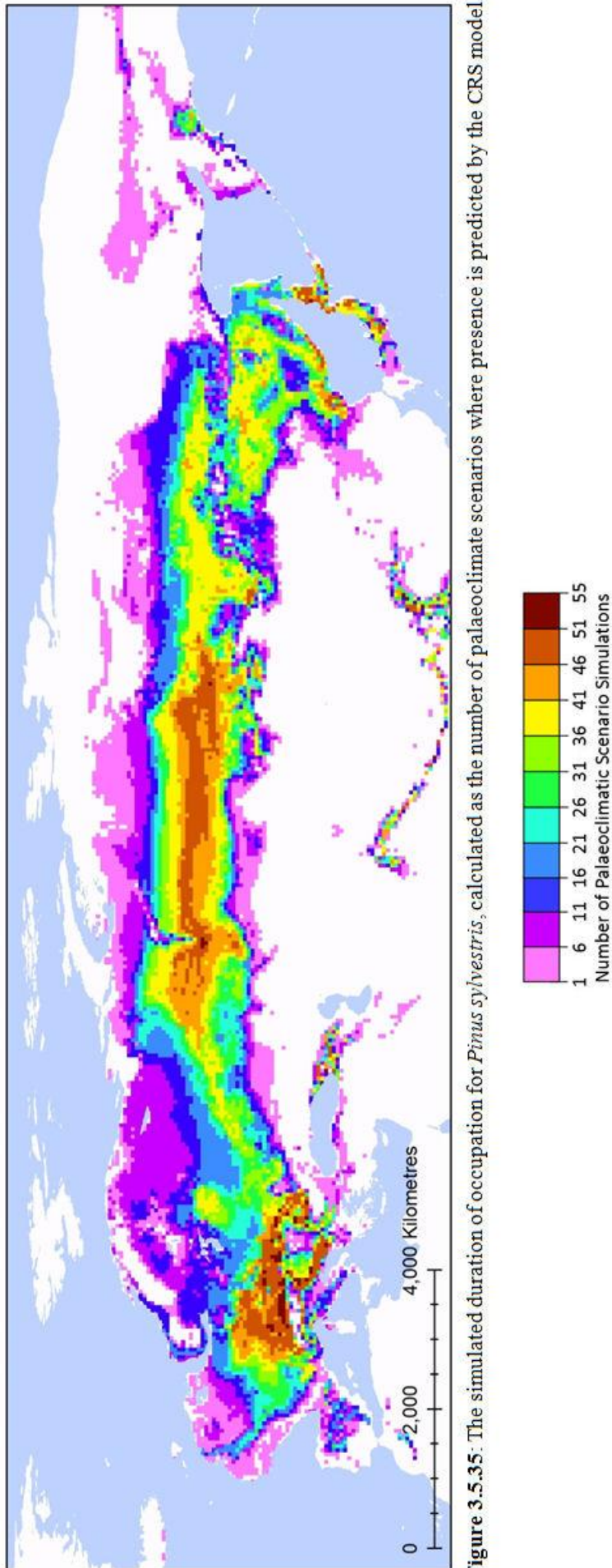
Figure 3.5.35: The simulated duration of occupation for *Pinus sylvestris*, calculated as the number of palaeoclimate scenarios where presence is predicted by the CRS model.
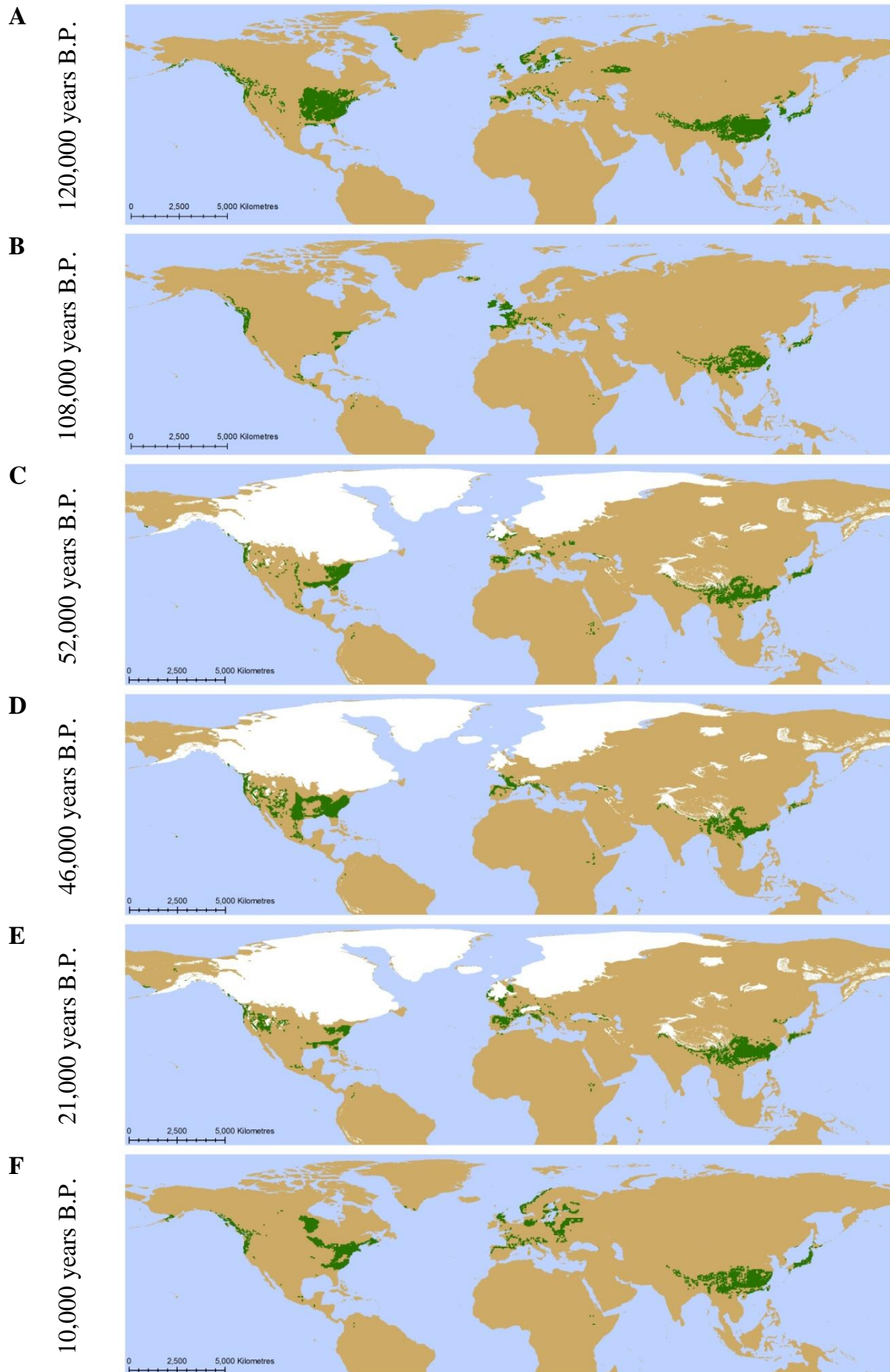
Although *Pinus sylvestris* has a broad range across northern Eurasia like *Picea abies*, it does not have as much modelled climatic stability, with just 65 grid cells having climate which is suitable for 51 or more of the scenarios modelled (Table 3.5.1) which accounts for just 0.33% of the simulated grid cells (19,688). This area sparse climatic stability for *Pinus sylvestris* is located in central Europe, the Alps, Dinaric Alps and the Carpathian Mountains, and locations in central Russia (Fig. 3.5.35). The majority of sites are climatically suitable for fewer than 16 of the 53 scenarios simulated, with only 6 sites actually being suitable for every one of the scenarios (Fig. 3.5.36). This highlights that as a species, *Pinus sylvestris'* present-day climatic niche varied its range in Eurasia significantly meaning that it is probable there have been substantial range shifts over the last 120 thousand years.

Interestingly the areas of stable climate in central Europe overlap with the areas where *L. pytyopsittacus*, a *P. sylvestris* dietary specialist, could have climatically persisted through the glacial conditions. The other population of crossbills, *L. scotica*, which is also a specialist of *P. sylvestris*, is simulated as having a non-stable climate range that fluctuates across Ireland and Scotland over the last 120 thousand years, and it is notable that these are areas where *Pinus sylvestris*, although not temporally stable, have climate which is suitable too.
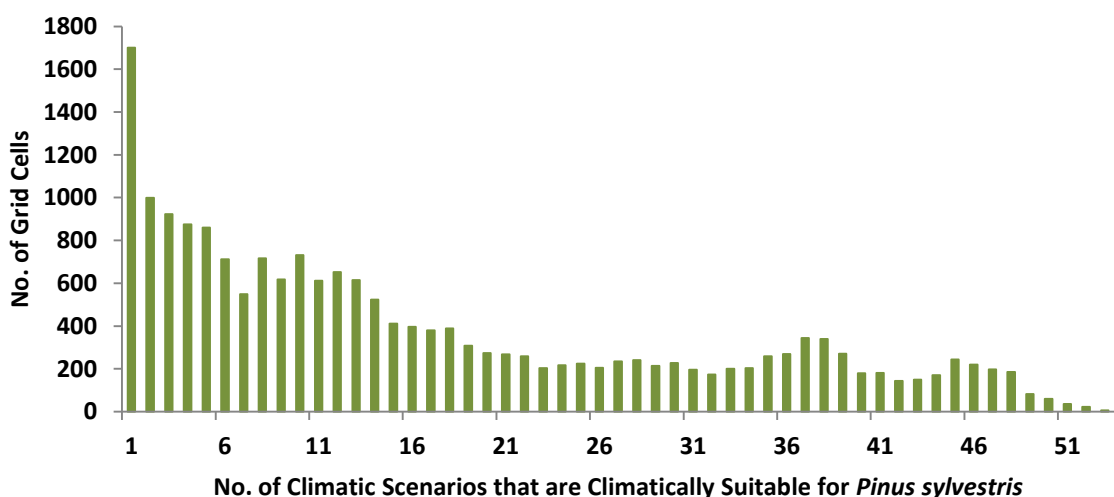
Figure 3.5.36: The quantified durations of climatic suitability for *Pinus sylvestris*. The number of 0.5° x 0.5° grid cells that have the same duration of occupation for *P. sylvestris*. Duration of occupation is calculated as the number of scenarios the grid cell is predicted to have climatic conditions suitable for the species.

3.5.35

Pinus occidentalis

The Caribbean islands of Hispaniola, Cuba and Jamaica had climate suitable for *Pinus occidentalis* during the Eemian interglacial (Fig. 3.5.37 A) however the colder stadial (Fig. 3.5.37 B) conditions limited this range to western Hispaniola.   Throughout the glacial there was climate in the Caribbean which was within the modelled niche of *P. occidentalis*; however it did not remain on any single island for the longevity of the glacial.   During warmer conditions of the interstadials (Fig. 3.5.37 C) Hispaniola, Puerto Rico and northern Cuba had numerous locations of climatic suitability, while the colder Heinrich Events (Fig. 3.5.37 D) resulted in southern areas of the Caribbean being unsuitable, with Cuba and more northerly locations having climate more suited to *P. occidentalis* but by the LGM (Fig. 3.5.37 E), with less cold extremes than the Heinrich Events, the more southerly island of western Hispaniola and Puerto Rico are again climatically suitable.   By the onset of the Holocene (Fig. 3.5.37 F), there is cli4ate in the east of Hispaniola which is suitable, and in the neighbouring island of eastern Cuba which is still present today (Fig. 3.4.38) although since the beginning of the Holocene, the climate has become more suitable in the central mountains of Hispaniola.

Throughout the glacial and interglacial scenarios there are conditions in Cuba and Hispaniola, where it is found today, which are suitable for *P. occidentalis*, however they shift regularly between climatic scenarios.   This may be due to their actual ranges being at a significantly smaller regional scale, in small niches of climate suitable which are lost at this coarse model resolution.   In addition to the ranges in the Caribbean, the surrounding mainland also has a number of climatically suitable locations, which are mainly to the south, in Central and South America during the interglacial, expanding into North American coastline of the Mexican Gulf during the glacial conditions, but it is unlikely the species ever colonised these regions due to their significant isolation from the present day range and the presence of other competitive *Pinus* species in these areas, such as *Pinus caribaea* which is found in the Bahamas, Belize, Cuba, Guatemala, Mexico and Nicaragua.

A 120,000 years B.P.
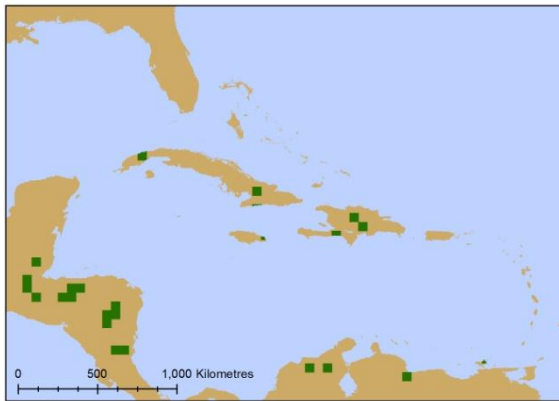
B 108,000 years B.P.
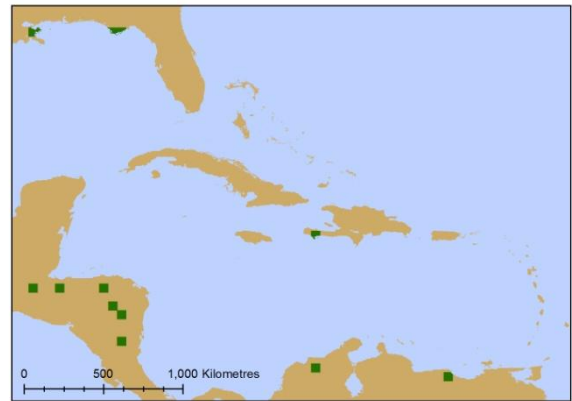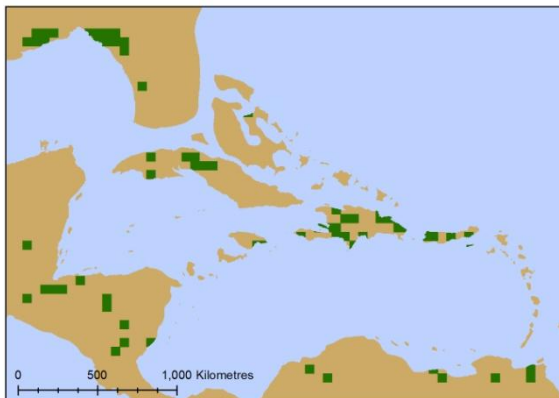
C 52,000 years B.P.
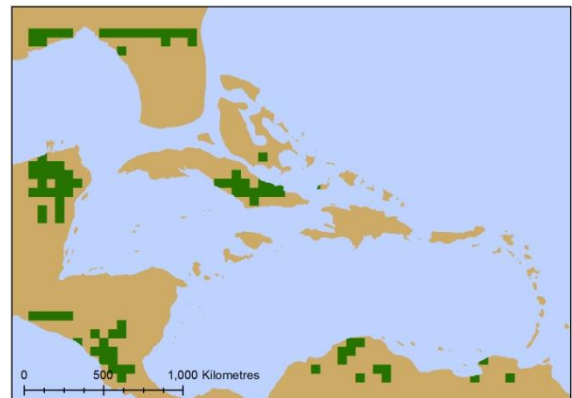
D 46,000 years B.P.

**E** 21,000 years B.P.

F 10,000 years B.P.

Figure 3.5.37: The simulated distribution of *Pinus occidentalis* (green) during the Eemian interglacial (A); at the Meisley 1 stadial (B); during interstadial conditions (C); at Heinrich Event 5 (D); at the Last Glacial Maximum (E) and the beginning of the Holocene (F), all produced by the CRS model.
See Appendix: Results – *Pinus occidentalis* for full descriptions of the simulated distributions.
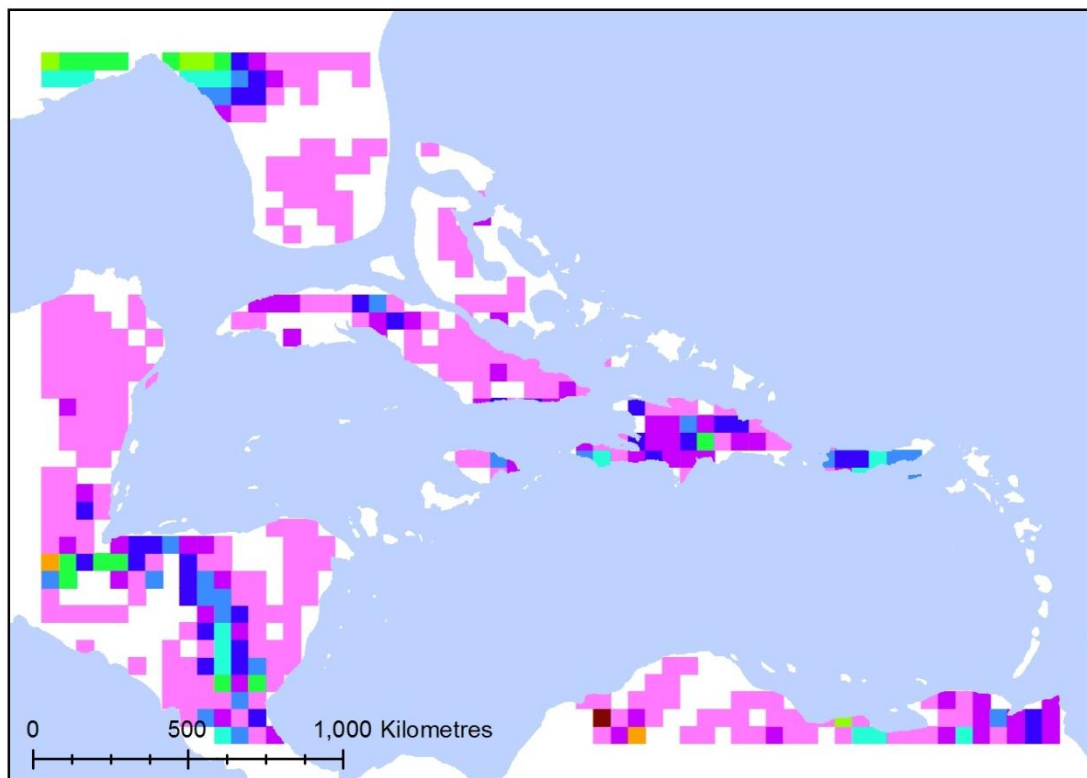
Figure 3.5.38:   The simulated duration of occupation for *Pinus occidentalis*, calculated as the number of
palaeoclimate scenarios where presence is predicted by the CRS model.

Number of Palaeoclimatic Scenario Simulations
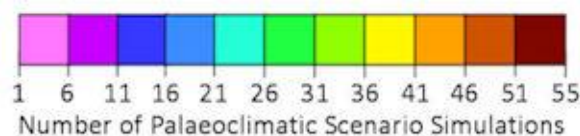
This *Pinus* species is the primary food source for *L. megaplaga*, and it, too, has a single site
which has a frequency of simulations exceeding 51 scenarios (Table. 3.5.1, Fig. 3.5.38) which
is located in precisely the same location in northern Colombia as the site of *L. megaplaga*
(Fig. 3.5.14).   In total there are 430 grid cells, many more than *L. megaplaga*, that are
climatically suitable for *Pinus occidentalis*, many of these are only suitable for less than 6
scenarios (Fig. 3.5.39).   There are numerous sites distributed on the mainland, with areas in
Nicaragua, Honduras and northern Florida having some of the greater frequencies of climatic
suitability.

Within the Caribbean islands, Hispaniola and southern Cuba, where the species is native
today, suitable climatic scenarios do not exceed 30 climate scenarios.   But, unlike
L. megaplaga, there is a greater abundance of sites throughout the Caribbean; elsewhere in
Cuba, Jamaica, Puerto Rico and the Bahamas which are suitable for *Pinus occidentalis*.
Although there are only short periods of climate suitable in many of the locations, the species
had the potential to survive elsewhere in the Caribbean, or, like *L. megaplaga*, it may have
been sustainable in smaller climatically suitable regions resulting from the varying
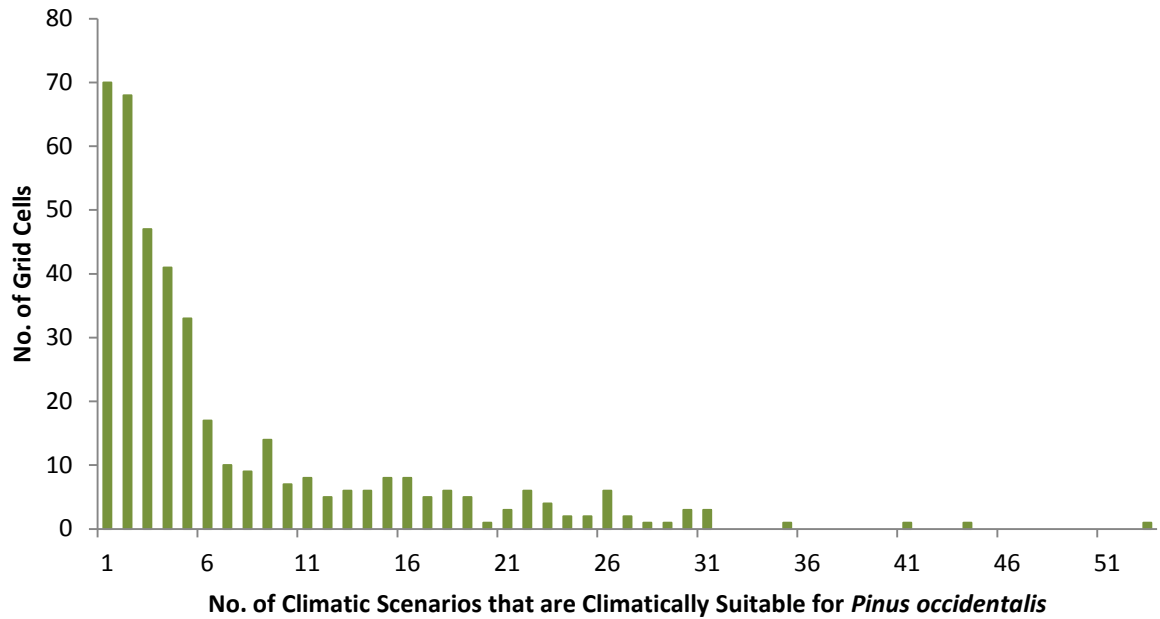
Figure 3.5.39:   The quantified durations of climatic suitability for *Pinus occidentalis*.   The number of 0.5° x 0.5° grid cells that have the same duration of occupation for *P. occidentalis*.   Duration of occupation is calculated as the number of scenarios the grid cell is predicted to have climatic conditions suitable for the species.

topography of the islands which is lost at this coarse scale.   Interestingly, many of the sites in Hispaniola where both the *Pinus occidentalis* and *L. megaplaga* are simulated, have a similar frequency in simulations, suggesting overlapping simulated scenarios, despite the more expansive climatic niche of *Pinus occidentalis*.

CHAPTER 4 – Discussions & Conclusions

Section 4.1

Evaluation of Species' Distribution Models

Comparing the observed distribution with the present day simulations produced by the three modelling methods; maximum entropy (Maxent), climate response surface (CRS) and generalised additive models (GAM), allowed the evaluation of the 'goodness of fit' measures (Section 3.1), maximum κ and AUC values (Table 3.1.1-3), which indicated that the CRS model performed the best. The CRS has the highest values of 'goodness of fit' across all species and genera modelled, for all grid extents, better than both Maxent and GAM. Tests for robustness (Table 3.1.4-6) also demonstrate that the CRS model performs well, achieving the highest average maximum κ and AUC values in all but four of the robustness tests undertaken. Despite initial assumptions that CRS's tendency to over-fit would result in a poor robustness, in 21 out of 33 of the standard deviations for robustness 'goodness of fit' measures were lowest for CRS. Any degradation in performance of CRS was associated with the smaller grid extents used to model the more regionally restricted species. GAM out-performed both CRS and Maxent on several occasions, particularly on the smallest, Caribbean grid achieving the best robustness values for *Pinus occidentalis*, both AUC and maximum κ values.

It is widely discussed in the literature that robustness tests on limited distributions, like that of *P. occidentalis* (recorded in just 23 cells) and *L. megaplaga* (just 10 grid cells), often produce unsatisfactory results due to their small sampling size (Guisan & Zimmermann, 2000). However, the CRS model was the only one to produce 'goodness of fit' values for both *L. megaplaga* and *P. occidentalis*, when modelled with the complete distribution, that were considered to be a 'good' model performance, with the other two modelling techniques producing 'poor' simulations. This therefore affirms the selection of the CRS models as the modelling technique primarily described and explored in this study.

In the climate-based distribution predictions produced by the three modelling techniques (Section 3.2), in general there is extensive overlapping between the models' simulated distributions of climatic suitability (grey, Fig. 3.2.1-7, Table. 3.2.1). CRS often simulates many unique locations (red) which the other two models do not, but may be correct; for example the persistent simulation of *L.* curvirostra in south-eastern regions of Asia and Mexico where they do presently reside. A large number of sites simulated by CRS are also shared with GAM simulations (orange), suggesting that Maxent is a more conservative model,

possibly due to restrictions in its potential of simulating into non-analogous climates particularly during colder periods such as the Heinrich and stadial conditions (Fig. 3.1.4 & 3.1.6). Nevertheless, there are numerous locations were just GAM and Maxent simulate suitability (green), not CRS. However, most of these are on the periphery of areas where the CRS model does simulate areas of climate suitability. The fact the GAM results often overlaps with the two other models, and produces very few unique model predictions, is probably due to the previously discussed manner in which it extrapolates into novel climates, with its method an intermediate between CRS and Maxent's approaches, resulting in it identifying regions which CRS and Maxent individually simulate too. The differences between model outputs highlight the importance that model selection may have on the resulting distributions, but in many cases the simulations do not excessively diverge from the patterns of restriction; such as increases in range more southerly observed during colder and drier and more northerly expansions of climate suitability in warmer and wetter conditions.

There were a number of similarities amongst the range size predictions for species/genera generated by the three different modelling techniques (Section 3.3). In 8 out 13 of the species/genera modelled, the three modelling techniques CRS, Maxent and GAM produce very similar relative changes in range size, these include: *Loxia curvirostra*, *L. pytyopsittacus*, *Larix*, *Picea*, *Pinus*, *Tsuga*, *Picea abies* and *Pinus sylvestris*.

Species/Genera	Difference Between the Largest and Smallest Simulated Range Size (Calculated as a Ratio of No. of Grid Cells Recorded in the Observed)		
	CRS	Maxent	GAM
Loxia curvirostra	<u>0.512</u>	**0.845**	0.597
L. leucoptera	0.825	**1.001**	<u>0.706</u>
L. pytyopsittacus	1.029	<u>0.993</u>	**1.211**
L. scotica	2.696	<u>1.304</u>	**3.478**
L. megaplaga	**4.900**	1.600	<u>1.000</u>
Pinus occidentalis	3.478	<u>3.261</u>	**7.304**
Larix species	<u>0.652</u>	0.664	**0.881**
Picea spp.	0.758	**0.873**	<u>0.706</u>
Pinus spp.	0.863	**0.972**	<u>0.812</u>
Pseudotsuga spp.	**1.203**	1.011	<u>0.788</u>
Tsuga spp.	<u>1.061</u>	**2.261**	1.617
Picea abies	<u>0.998</u>	**1.379**	1.069
Pinus sylvestris	<u>1.252</u>	**1.393**	1.252

Table 4.1.1: The variance of the simulated range sizes produced by the species' distribution models, climate response surface (CRS), maximum entropy (Maxent) and generalised additive model (GAM). This calculated as the difference between the largest and smallest simulated range size, a ratio of the number of grids in the simulated range in relation to the observed range, generated by the species' distribution model for each of the species or genera.
Values in bold represent the BIGGEST difference in predicted range size.
<u>Values underlined represent the SMALLEST difference in predicted range size.</u>

Across all the species/genera models there are differences in the cumulative totals of sites identified as suitable at each scenario by the different modelling techniques. GAM simulations are frequently the most 'optimistic' identifying the greatest number of suitable sites for a species/ genera during both the warmer Holocene (6 out of 13) and cooler glacial conditions (8 out 13) (Fig. 3.3.1-13). Maxent tends to produce the more restricted estimates of range size during both the Holocene (7 out of 13) and glacial (11 out of 13), whilst CRS's simulations of range size often lie between these two models. Variance in predicted range size across the 53 scenarios simulated was more often highest for GAM (5 out of 13) and Maxent (6 out of 13) models (Table 4.1.1). CRS often had variance in between the two modelling techniques, although it did have the least variance in 5 out of 13 of the models. Interestingly the cases when Maxent had the smallest variance of predicted range size, compared to the other models, were those modelled on smaller grid extents in the Caribbean and Europe (3 out of 4) while GAM had the higher variance, confirming a relationship between background grid extent and the performances of these bioclimatic niche models. However, the consistency of the CRS model, as a conservative predictor, both by simulating range sizes that often lie between the two other models predictions and showing less variation in amplitude of potential range, highlights it as the most favourable of the models to be used when modelling species' climatic niches.

It is interesting to note that across all the species, there were predictions from Maxent, GAM, and frequently CRS too, that the Heinrich Events resulted in significantly less climatically suitable regions for the species and genera modelled compared to conditions preceding and succeeding these events, the only exception being the boreal dominating genus *Larix*. *Larix* species was, in fact, the only genera to show an increase in range size during the glacial universally across all the modelling techniques used. The broad ranging genera of *Pinus* and *Picea*, as well as the more limited *Tsuga*, and the tree species *Pinus sylvestris* and *Picea abies*, all show significant declines in the range availability during the glacial period across all three of the modelling techniques. The similarly wide ranging *Loxia curvirostra* and *L. leucoptera* also show this decline in climate availability during the colder glacial conditions. In addition to these the presently Fennoscandia restricted species *L. pytyopsittacus* also demonstrates an even greater decline relative to its present size, probably as a results of its restriction to more southerly regions of Europe due to the formation of Weichselian glacier.

A comparison of these three modelling techniques has not been conducted before and this study suggests the CRS is the most effective species' distribution model to use when

simulating species' range, in relation to bioclimatic parameters, with the best performance at re-simulating present range compared to the observed.   However, it must be noted that both Maxent and GAM have additional modelling facilities which were not utilised in this study which may have improved their overall performance.   Despite the differences in the models' methods of fitting the species' relationship to climate, many of the outputs showed significant areas of overlap, highlighting that there is a consistency across the models in identifying similar locations including relative longitudinal and latitudinal shifts in distributions according to the changes in climate.   In addition to this, the differing nature of the outputs and performance accentuates the need for studies to consider doing multiple investigations using different species' distribution modelling techniques before selecting the best model output.

Section 4.2

Comparison of Crossbill Simulations with the Fossil Record

Comparing the crossbill simulations with the known fossil record is an effective way of confirming whether the distributions predicted by the species' climatic niche are potentially correct. Unfortunately, as previously discussed (Section 1.3), the avian fossil record is sparse and analysed samples are mainly limited to central Europe (Fig. 1.3.1) and vary in date from present to 20 million years ago (Table. 1.3.1). Despite the limited records, there are some interesting comparisons with the simulated distributions of both *Loxia curvirostra* and *L. pytyopsittacus* and their fossil records.

When the fossil records for *L. curvirostra* are overlaid with the simulated duration, a measure of the number of scenarios where the climate is suitable in a grid cell for the species (Fig. 3.7.1), there are some notable concurrences (Fig. 4.2.1). All of the fossil records are at sites where *L. curvirostra* is simulated as being present for at least one of the climatic scenarios. The fossil records that span the last 120 thousand years (black) have varying simulation duration at their sites, from 30 to 51 simulated scenarios. Although *L. curvirostra* is observed at many of these sites today (Fig. 3.4.2), the longevity of climate
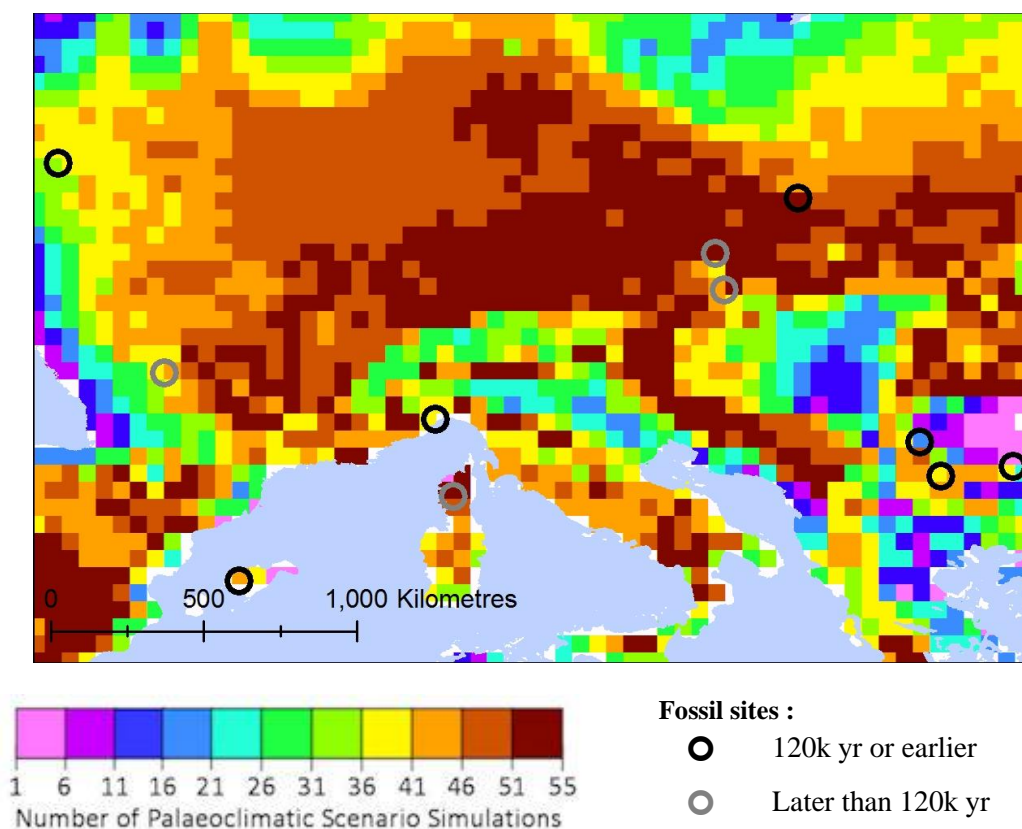
Figure 4.2.1: Fossil sites (circles) and the simulated duration produced by the CRS model for *Loxia curvirostra*. Black circles represent fossils dating from 120 thousand years ago to today; grey circles represent fossil sites older than 120 thousand years (Table. 1.3.1).

suitable throughout the glacial suggests that the models are indeed predicting feasible distributions which corroborate with the fossil record. There are also a number of older fossils, dating from 900 to 200 thousand years ago (grey), in the Alps and Corsica, sites which have climate that is suitable for more than 51 of the scenarios modelled. As the conditions over this time period have seen similar glacial and interglacial conditions, it is likely that these locations would have been similarly likely to have had climate suitable at these earlier times. The corroboration of the fossil record with the CRS model's *L. curvirostra* simulations confirms to some extent their significance in being used to explore past distributions.

L. pytyopsittacus is a different case from *L. curvirostra*, as its present day range (Fig. 3.4.8) is not found in central Europe where the fossils have been found. Thus the discovery of *L. pytyopsittacus*' fossils around the Mediterranean has motive many hypotheses of this species residing in more southerly locations during the glacial conditions (Tyrberg, 1991). When the duration simulation for *L. pytyopsittacus* (Fig. 3.5.8) is overlaid with the observed fossil records (Fig. 4.2.2), all three locations where the fossil was dated earlier than 120 thousand years (black), from 13,400 to 28,000 years ago, were sites situated on the fringes of the simulated range of *L. pytyopsittacus*, that were suitable during the glacial period. The
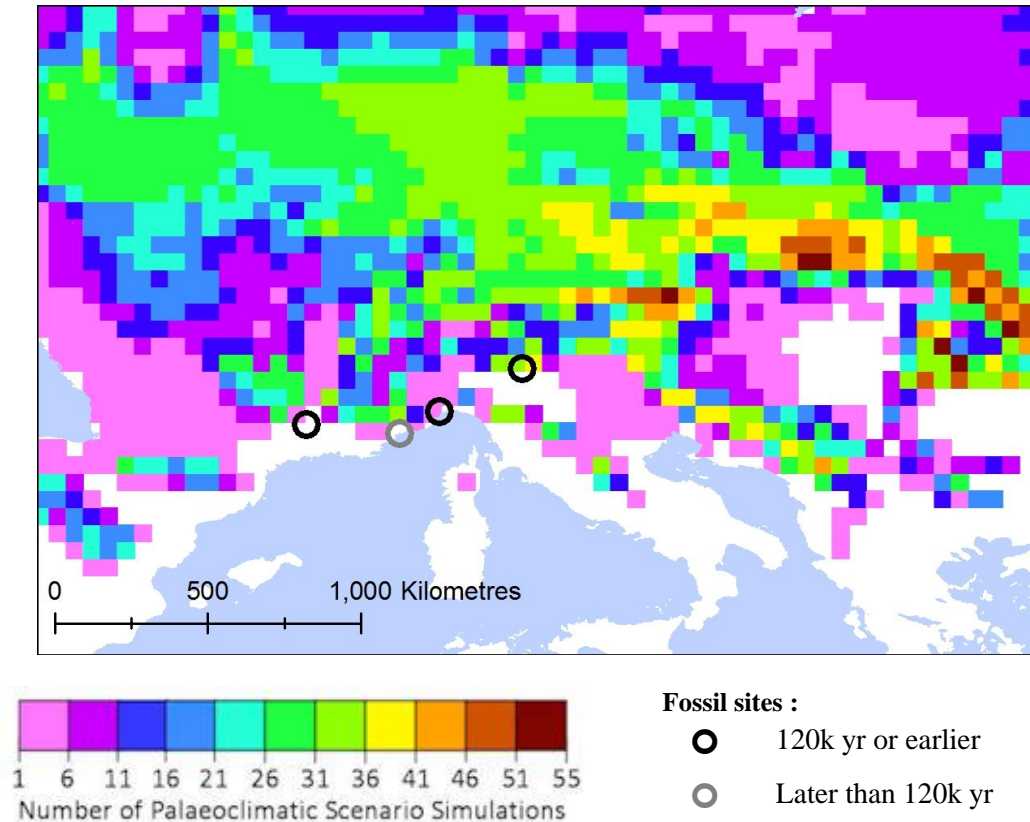
Figure 4.2.2:   Fossil sites (circles) and the simulated duration produced by the CRS model for *Loxia pytyopsittacus*.   Black circles represent fossils dating from 120 thousand years ago to today; grey circles represent fossil sites older than 120 thousand years (Table. 1.3.1).

fossil sites dated to be older (grey), between 125 and 150 thousand years ago, is not simulated by the model as being climatically suitable during the last 120 thousand years for *L. pytyopsittacus* although sites neighbouring are.   It may be that the climate became more favourable at an earlier date.   The fact southern fringes of the simulated distributions of *L. pytyopsittacus* around the Mediterranean correlate with fossil records of the species not only provides further support that the model is simulating 'sensible' range limits but also corroborates with previous hypotheses of *L. pytyopsittacus* residing in Southern Europe (Tyrberg, 1991)

Although the fossil record is limited, the correlation of simulations with the fossils is valuable support in ascertaining the effectiveness of the models.   It will be interesting to note whether further fossil discoveries in the future also correlate with the predicted distributions of *Loxia* species.   If the fossil record was more complete, reconstructions could be made according to these, but difficulties in dating, bias in fossil site selection and preservation would still restrict the distribution predictions. The corroboration with the species' distribution climatic response surface model highlights that is could be an effective method to determine the potential range of the species during the changing palaeoclimatic conditions on a more temporally consistent basis than a fossil record could achieve.

o

Section 4.3

Comparison of Conifer Simulations with Pollen Records and Palaeovegetation Models

To ascertain the potential validity of the simulations produced by the species' distribution models for the conifers, comparisons can be made with the fossil pollen records and also palaeovegetation models.

Pollen Records

There are numerous studies into the historical pollen record as it can be used to determine regional variations in climate according the vegetation compositions and can supplement many palaeoclimate reconstructs.   Many of these records have been consolidated into openly accessible international databases such as European Pollen Database (EPD: http://www.europeanpollendatabase.com), as well as the more expansive Global Pollen Database (GPD: http://www.ncdc.noaa.gov/paleo/gpd.html) and global Neotoma Palaeoecology Database (http://www.neotomadb.org/index.php/data).   In this study, pollen records from the EPD (Last accessed on 1st December 2011) were compared with the Eurasian predicted ranges, while a consolidated pollen record study undertaken in North America by Williams *et al.* (2004) was used to determine the validity of the North American range simulations for the conifer genera modelled.

In general the pollen fossil record for the northern hemisphere is mainly dated from post-glacial maximum as the glacial formation affected the stratigraphy of samples and thus their dating accuracy.   The Holocene has an abundant fossil pollen record, and thus simulations at 5 and 10 thousand years ago of conifer genera potential distributions were compared to the individual pollen records for these dates from EPD (Fig 4.3.x A & B) and the consolidated mapped pollen abundances produced by Williams *et al*. (2004) (Fig. 4.3.x C & D) for North America.   Pollen records were selected from the EPD for each genera which were within 1,000 years of the date of simulation (Appendix: Tables 2-4), for instance the 5 thousand years ago simulation was compared to pollen records from 4,000-6,000 years ago.   For each site a single record was taken which was closest in date to the simulation and mapped using ArcGis (ESRI, 1998).

Larix/Pseudotsuga **species**

Larix pollen is poorly preserved in the fossil record, often found in close vicinity to *Larix* macrofossils and therefore records are not far dispersed from the location of origin (Godwin, 1934).   It is also exceedingly similar to *Pseudotsuga* pollen grains and thus many of the identifications are done to a grouped class including both of these genera (Weber, 1998).   However, relative location and extant species often provide a method by which genus can be resolved.   The simulated distributions of *Larix* in Eurasia were compared to the EPD records (Fig. 4.3.1 A & B) but *Pseudotsuga* was excluded as the pollen records were from Russia and Europe while *Pseudotsuga* is a native species to southern Eurasia so although there were climate suitable areas in Europe during the Holocene (Fig. 3.5.25 F) these were unlikely to have been colonised.   A few of the pollen records in

A.   5,000 years B.P.

B.   10,000 years B.P.

Key: ●   *Larix* pollen   ●   *Larix/Pseudotsuga* pollen   ●   *Larix* stomata

Figure 4.3.1 A & B   Simulated distribution of *Larix* species at 5,000 (A) and 10,000 (B) years before present (B.P.) produced by the CRS model.   Pollen and stomata fossil record locations selected as sites where presence was dated from 4-6,000 years B.P. (A) and 9-11,000 years B.P (B) data sourced from European Pollen Database (EPD: http://www.europeanpollendatabase.com, Appendix: Table 2)

central Russia and eastern Europe correlate with the predicted range based on climate for both 5 and 10 thousand years ago produced by the CRS model.   However there are far greater number of fossil pollen and stomata records in the mountainous regions of Europe, the Alps and Caucasus Mountains, which do not have correlation with the relevant simulated distributions.   These sites are most likely to be ancestral populations of the present day *Larix decidua* found in these mountain ranges today, however simulations even of present day distributions did not correctly predict this range despite its inclusion in the initial dataset for the model.

As previously discussed (Section 3.4), the climatic niche for *Larix decidua* populations is evidently significantly different from the larger ranges in northern Eurasia and America.   In fact is may be more similar to the climatic niche of the closely related *Pseudotsuga*, as the CRS models of this genera predict climate suitability in central Europe in present day

C. 5,000 years B.P.   **D. 10,000 years B.P.**

Percentages

| 0 to 1 | 1 to 5 | 5 to 10 | 10 to 100 |
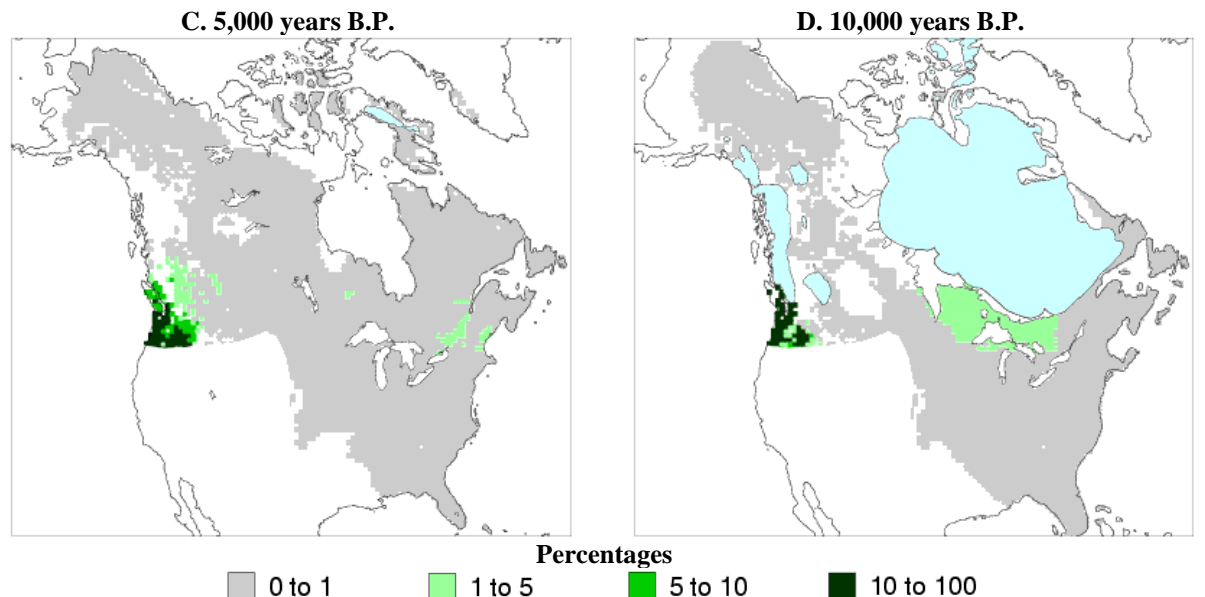
Figure 4.3.1 C & D: Maps of interpolated pollen percentages of *Larix/Pseudotsuga* species for 5,000(C) and 10,000 (D) years B.P. produced from aggregated pollen records and published by Williams *et al*. (2004).

E. 5,000 years B.P.   **F. 10,000 years B.P.**
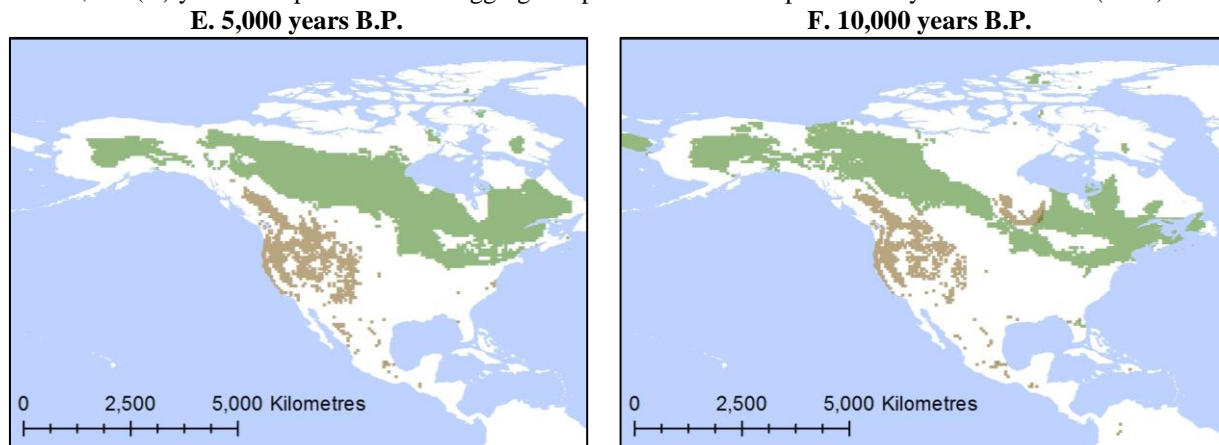
Figure 4.3.1 E & F: Simulated distribution of *Larix* species and *Pseudotsuga* species at 5,000 (E) and 10,000 (F) years B.P. produced by the CRS model.

(Fig. 3.4.27) and throughout the palaeoclimatic scenarios (Fig. 3.5.25). Pollen records indicate that *Larix decidua* was a resident of the Alps throughout the Holocene (Huntley & Birks, 1983, Tinner *et al.*, 1996). Despite the evident bias in fossil pollen record analysis, with many more sites in Europe analysed compared to elsewhere in Asia, these results do highlight the disadvantage of aggregating species into genera for distribution modelling. In such cases, where a species' niche is significantly different from the genus, independent modelling would be advisable for further investigation work.

In North America, both the conifer genera *Larix* and *Pseudotsuga* are natively found in present day. The consolidated fossil pollen abundance for these two genera (Fig. 4.3.1 C & D), although sparse, show significant similarity with the regions that are simulated as suitable for *Larix* and *Pseudotsuga* species (Fig. 4.3.1 E & F). The regions of greatest pollen abundance, located on the west coast at both 5 thousand (C) and 10 thousand (D) years ago, shows significant overlap with the northern limits of simulated range of *Pseudotsuga* species in North America (E & F) and potentially identifies this pollen as being from the *Pseudotsuga* genus. Lower percentages of abundance, but presences nonetheless of *Larix/Pseudotsuga* type pollen, on the eastern coast of North America at 5 thousand years ago and the south of Hudson Bay 10 thousand years, correspond adequately with the respective simulations produced. The fossil pollen record of *Larix/Pseudotsuga* may be scarce nevertheless the overlapping with the simulated distributions produced by the CRS model suggests that the model is not producing unfeasible distribution reconstructions for these two genera.

Picea species

Picea fossil pollen records are much more abundant than the *Larix/Pseudotsuga* type, however similarly there are far great numbers of sites analysed in Europe than elsewhere in the Eurasia (Fig. 4.3.2 A & B).   The simulated distribution of *Picea* species for the climatic conditions 5 thousand years ago (Fig. 4.3.2 A) demonstrates an overlap with over 40 sites which have been identified as having pollen dated from approximately the same era.   The major discrepancies being *Picea* pollen being present further west in France and southerly in eastern Europe than the simulations suggest from the climatic conditions.

Similarly the fossil pollen records correlate with the predicted distribution at the beginning of the Holocene (Fig. 4.3.2 B), 10 thousand years ago, with sites of pollen evidence being more southerly restricted in Europe with areas of Fennoscandia not being suitable, which were suitable in later warmer conditions (Fig. 4.3.2 A).   Notably pollen dated to *circa* 10 thousand

A.   5,000 years B.P.
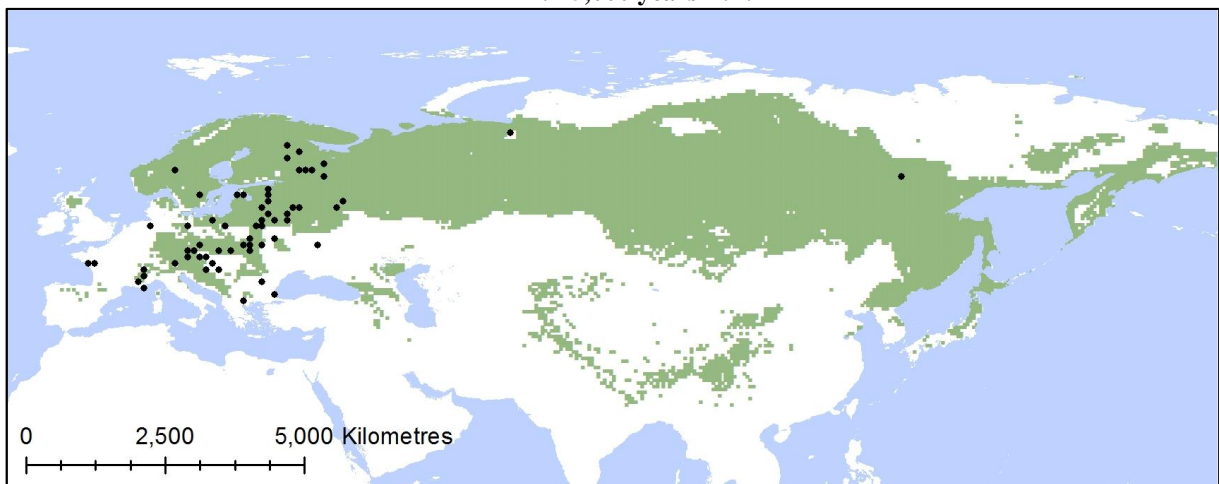
B.   10,000 years B.P.
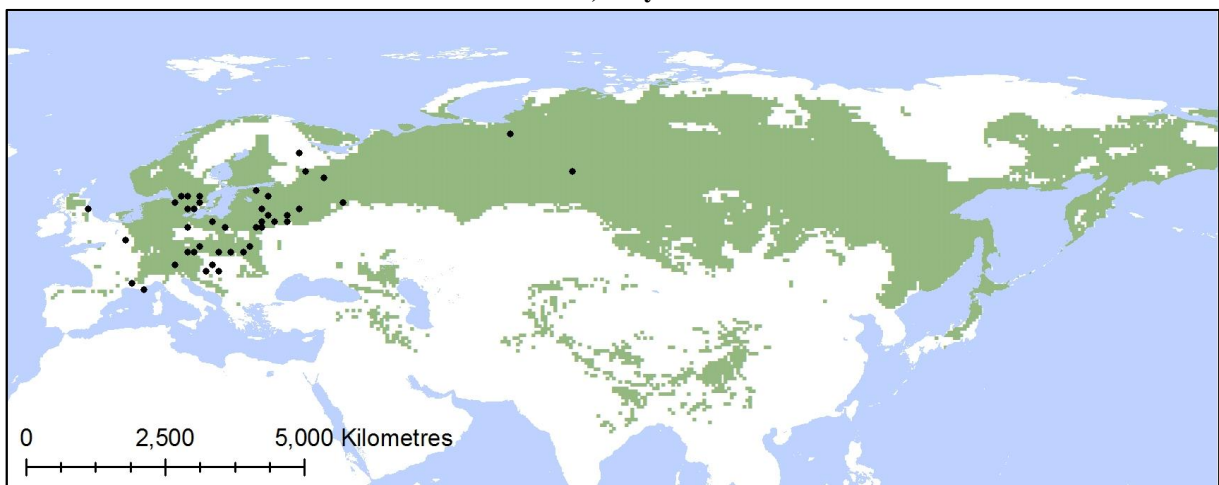
Key: ●   *Picea* pollen

Figure 4.3.2 A & B   Simulated distribution of *Picea* species at 5,000 (A) and 10,000 (B) years before present (B.P.) produced by the CRS model.   Pollen fossil record locations selected as sites where presence was dated from 4- 6,000 years B.P. (A) and 9-11,000 years B.P (B) data sourced from European Pollen Database (EPD: http://www.europeanpollendatabase.com, Appendix: Table 3)

years ago is found on the east coast of Scotland, where simulations also suggest in these climatic conditions *Picea* species could have resided here.

The North American pollen abundance for *Picea* species (Fig. 4.3.2 C & D) show extensive correlation with the respective simulations generated in this study (Fig. 4.3.2 E & F). Particularly of note is the fact the longitudinal extent of the simulated distribution produced for the *Picea* genera in this study for 5 thousand years ago (E) is of great similarity to the pollen abundance (C); also the simulations suggest greater southerly range extent than pollen records.   While the 10 thousand years ago simulation (F) and pollen abundance map (D) both suggest that there was a restriction in climate available in southern-central Canada at the beginning of the Holocene.   The pollen data for both Eurasia and North America validates many of the simulated sites as being correct and thus helps to confirm the effectiveness of these simulations.
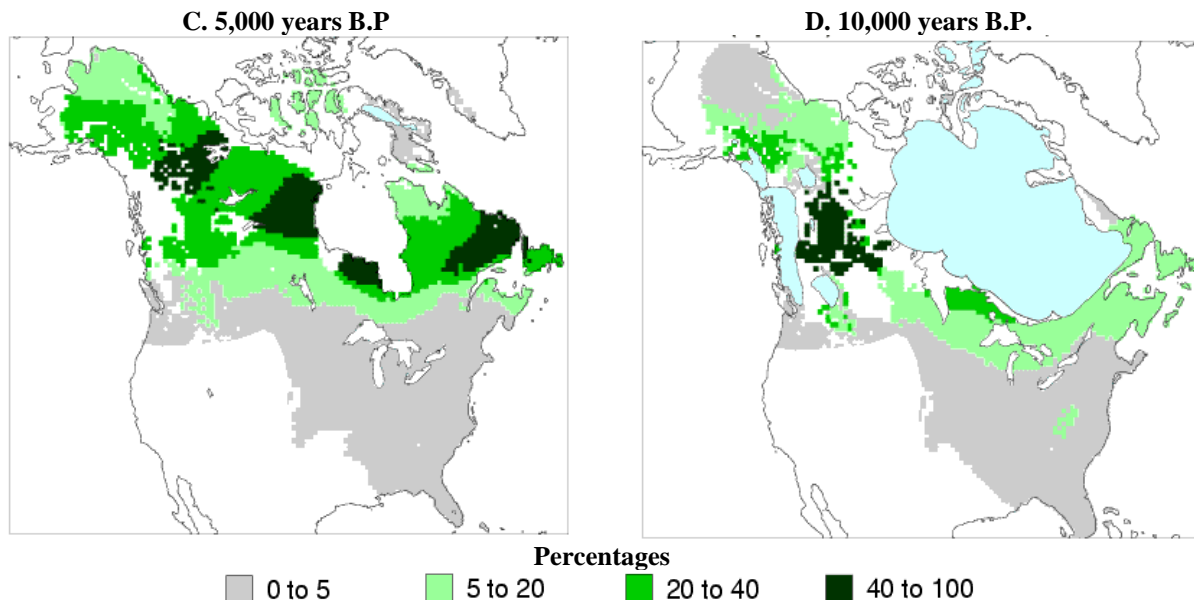
Figure 4.3.2 C & D: Maps of interpolated pollen percentages of *Picea* species for 5,000(C) and 10,000 (D) year before present (B.P) produced from aggregated pollen records and published by Williams *et al*. (2004).
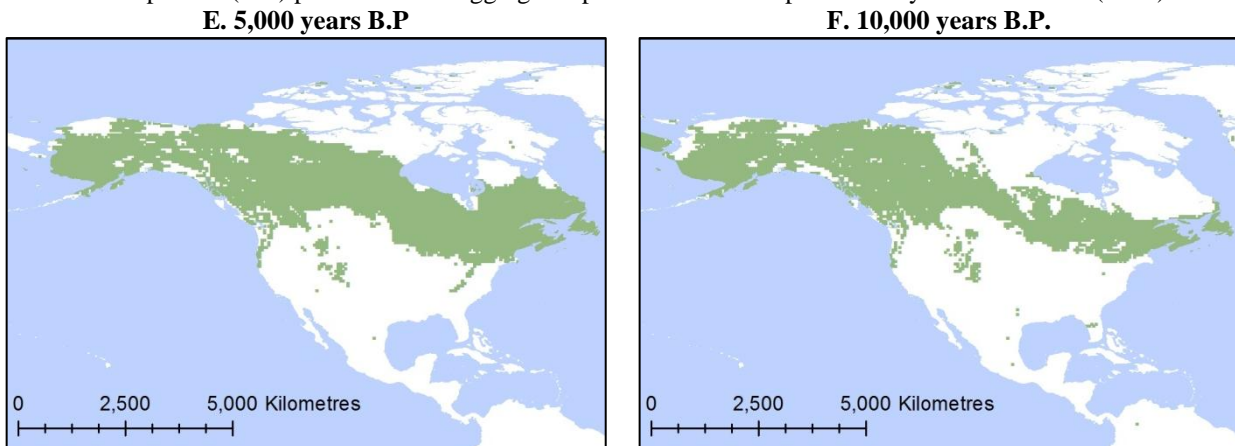
Figure 4.3.2 E & F: Simulated distribution of *Picea* species at 5,000 (E) and 10,000 (F) years B.P. produced by the CRS model.

Pinus species

Pinus species, like *Picea*, has similarly abundant fossil pollen records in Europe, however it is very easily transported long distances from its origin and thus can be misinterpreted as presence of the genus when in fact it may be from a distant population (Hjelmroos & Franzén, 1994).   Despite this, there is evident overlap with the fossil pollen records and the simulated distributions of *Pinus* species based on the CRS model for both those representing 5 and 10 thousand years ago (Fig. 4.3.3 A & B).   Discrepancies occur with sites in western France, southern England and Ireland being identified as having pollen but the simulations not predicting climate suitable in these regions.   However the pollen sites for *Pinus* species are more southerly restricted, like the simulations, at the beginning of the Holocene compared to the later warmer conditions.

A. 5,000 years B.P.

B. 10,000 years B.P.

Key: ●   *Pinus* pollen
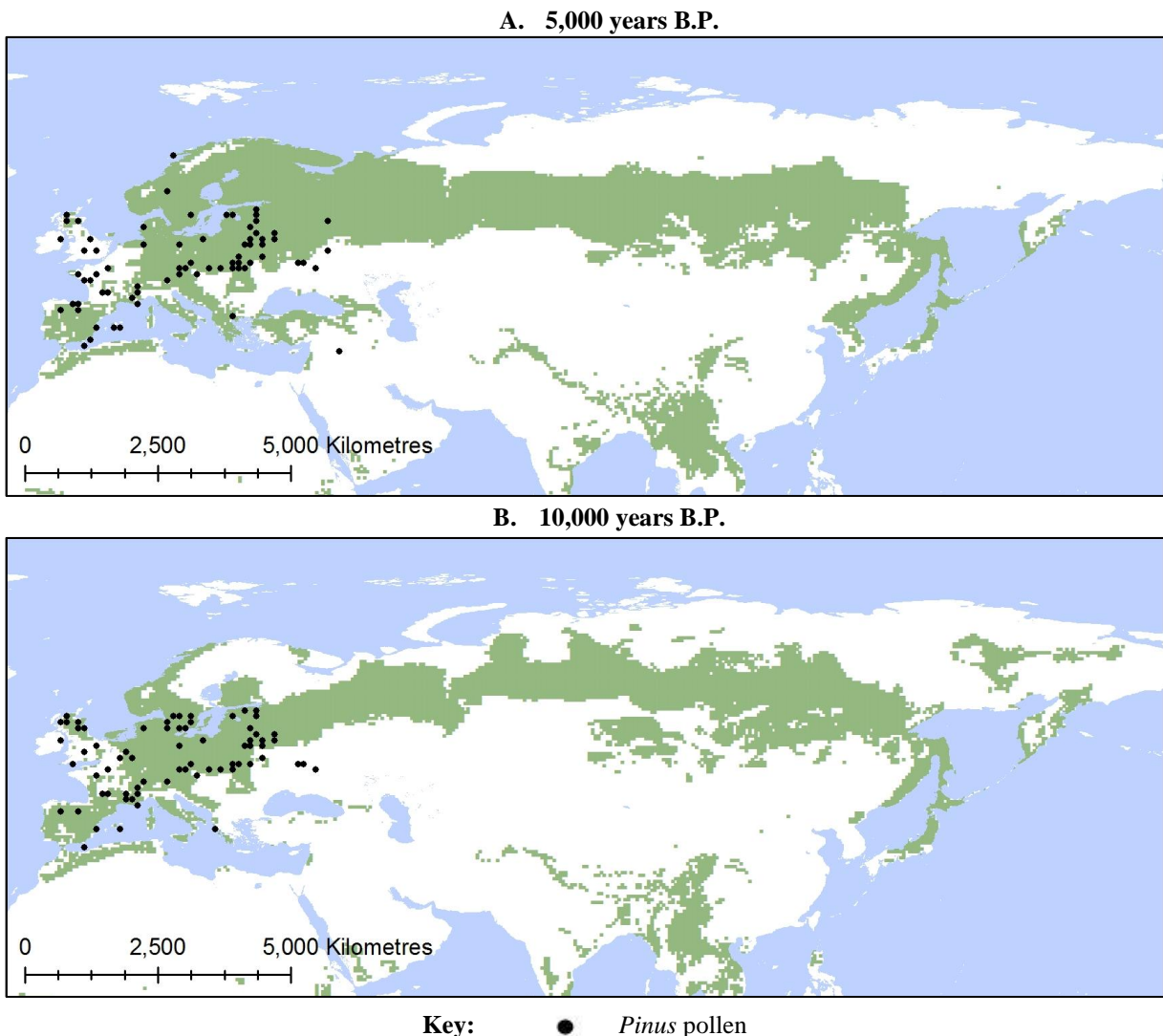
Figure 4.3.3 A & B   Simulated distribution of *Pinus* species at 5,000 (A) and 10,000 (A) years before present (B.P.) produced by the CRS model.   Pollen fossil record locations selected as sites where presence was dated from 4- 6,000 years B.P. (A) and 9-11,000 years B.P (B) data sourced from European Pollen Database (EPD: http://www.europeanpollendatabase.com, Appendix: Table 4)

In North America, the pollen abundance maps (Fig. 4.3.3 C & D) show significant overlap with the respective *Pinus* species simulations (Fig. 4.3.3 E & F); however unlike the other conifer genera, the pollen abundance records suggest a wider distribution of *Pinus* species than the predicted distribution.   This is unsurprising on account of the dispersal distances *Pinus* pollen is known travel and its relatively good preservation in the fossil record, but areas of high percentage pollen abundance do correlate with the regions where there are simulated occurrences.   Most notably the presence of fossil pollen records in south-eastern USA, although there are no *Pinus* species residing there in present day conditions the simulated distributions suggest that the climate in Florida was suitable for *Pinus*, affirming the likelihood of occupation.   In the case of *Pinus*, the climate-based simulations of distributions actually suggest potential constraints on the populations which investigation based on the pollen record along may miss due to its transportation and deposition in sites where *Pinus* may not have been found.

C. 5,000 years B.P   **D. 10,000 years B.P.**

Percentages

☐ 0 to 5   ☐ 5 to 20   ☐ 20 to 40   ■ 40 to 100
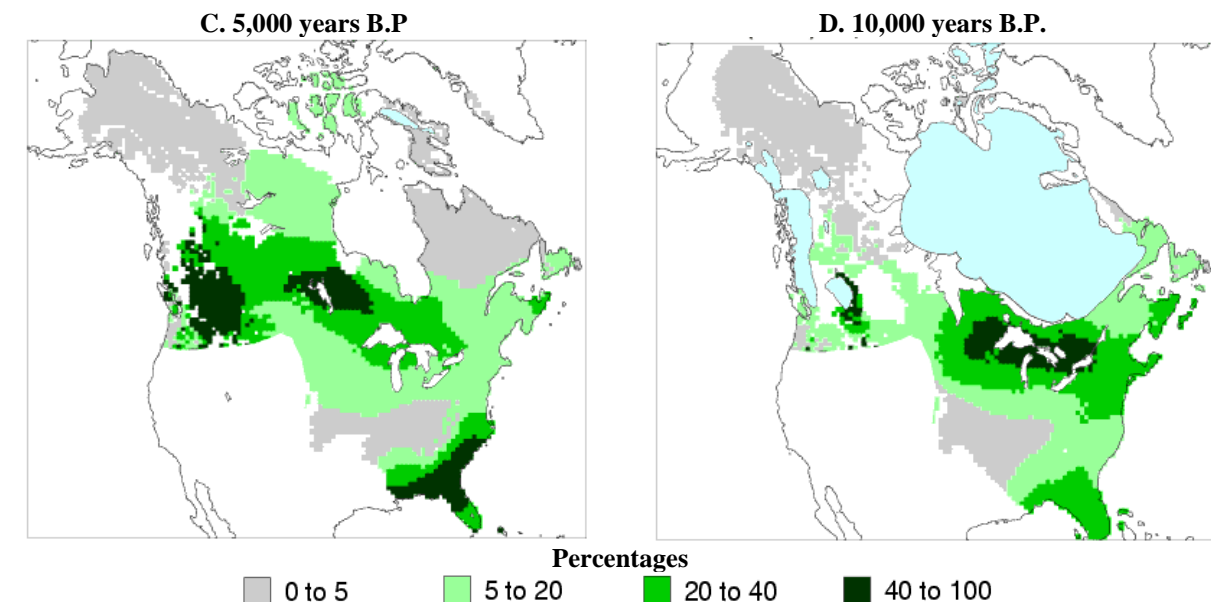
Figure 4.3.3 C & D: Maps of interpolated pollen percentages of *Pinus* species for 5,000(C) and 10,000 (D) year before present (B.P) produced from aggregated pollen records and published by Williams *et al*. (2004).

E. 5,000 years B.P   **F. 10,000 years B.P.**
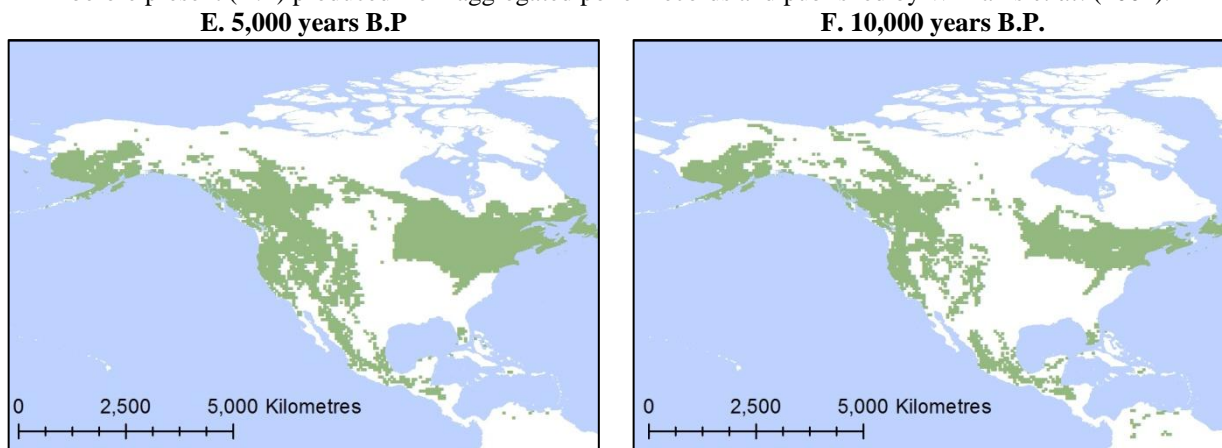
Figure 4.3.3 E & F: Simulated distribution of *Pinus* species at 5,000 (E) and 10,000 (F) years B.P. produced by the CRS model.

Tsuga **species**

Tsuga species are not found in Europe or northern Eurasia; however there are species of this genus native to both the western and eastern regions of North America (Fig. 3.4.29). The pollen abundance record for *Tsuga* species (Fig. 4.3.4 A & B) correlates with the simulated distribution of *Tsuga* species produced based on the climatic conditions (Fig. 4.3.4 C & D). The pollen sites which have been analysed on the west coast do not extend as far south as the *Tsuga* species are simulated as occurring, but as the northern sites correlate with the simulated distribution, it demonstrates that such models as these may have the potential of extrapolating potential distributions into un-sampled regions. On the east coast the simulated range at 10 thousand years ago has similar northern and southern limits (D) to the pollen record (B) however the pollen record does not extend as far easterly as the simulations suggest. In the case of the simulation for 5,000 years before present, the southern limit potential extends much further than the pollen records indicate.

A. 5,000 years B.P.   **B. 10,000 years B.P.**

Percentages

| 0 to 1 | 1 to 5 | 5 to 10 | 10 to 100 |
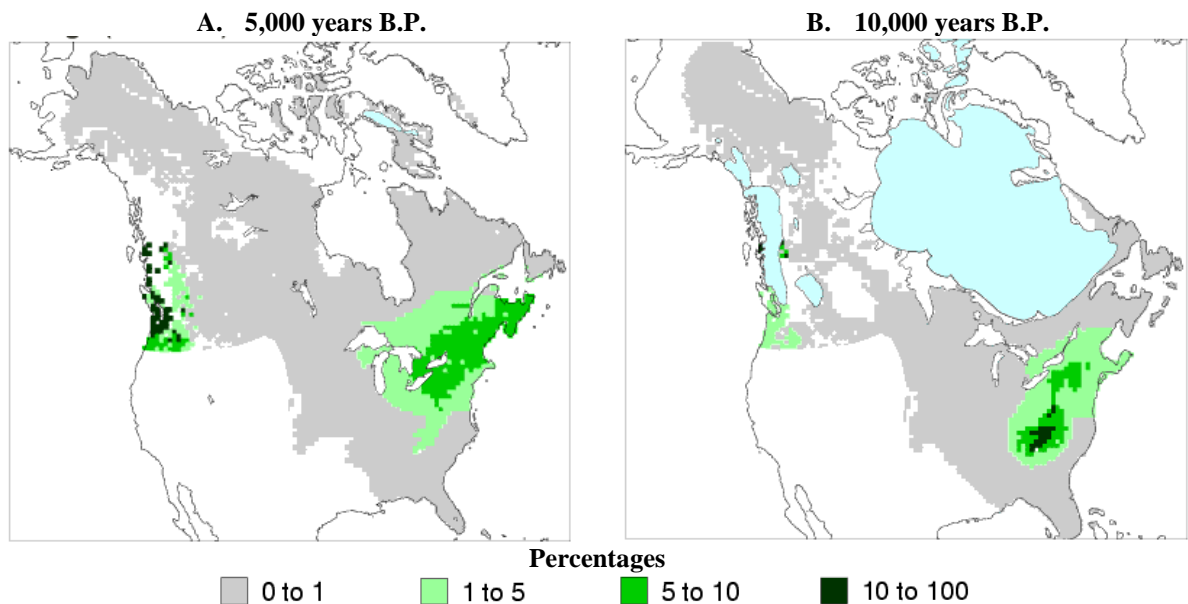
Figure 4.3.4 A & B: Maps of interpolated pollen percentages of *Tsuga* species for 5,000(A) and 10,000 (B) year before present (B.P) produced from aggregated pollen records and published by Williams *et al*. (2004).

C. 5,000 years B.P.   **D. 10,000 years B.P.**
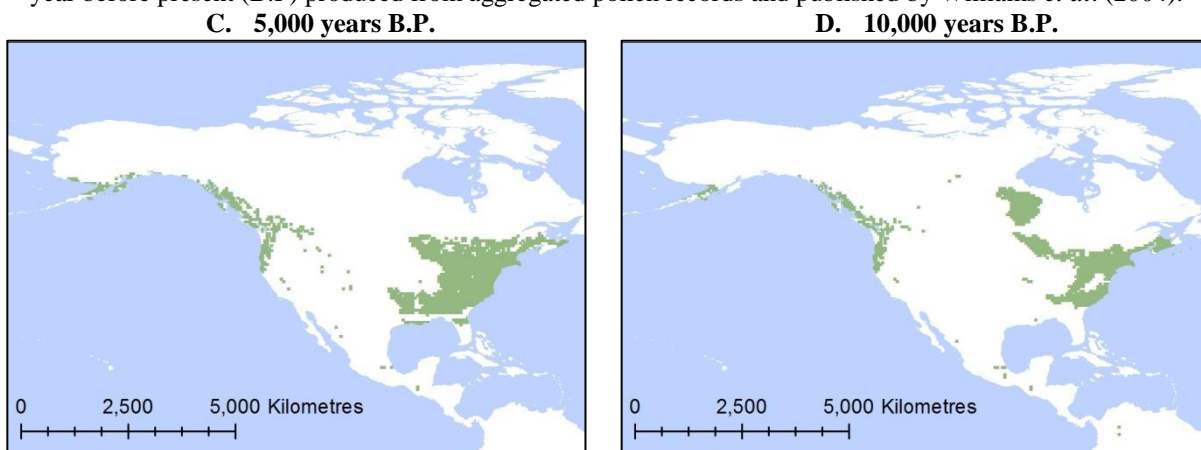
Figure 4.3.4 C & D: Simulated distribution of *Tsuga* species at 5,000 (C) and 10,000 (D) years B.P. produced by the CRS model.

Nevertheless, caution must be taken when interrupting the pollen fossil record as there are potentially a lot of discrepancies in dating the records and there is a plethora of research developing methods to improving temporal uncertainty in constructs (Parnell *et al.*, 2008, Blois *et al.*, 2011). In addition collaborative databases, like the EPD, have different contributors and error in data input, although not intentional, may occur as well as differences in data input information.

Overall the pollen records provide some genuine evidence of validity among the simulations generated as well as in some cases identifying improvements; such as modelling some of the species separately due to their distinctive climatic niche. By combining the available pollen records with palaeoclimatic simulations such as those produced here, it may be possible for a more complete history of spatial distribution, filling in gaps where pollen samples are not available or yet to be analysed such as observed with the *Tsuga* species, and temporally, going further back in time than the limited preservation of pollen records may allow.

Palaeovegetation Models

Most palaeovegetation assessments are made from plant pollen and macrofossil data, however as discussed above these can often be misleading. More recently, as a supplement to this data, independent modelling techniques have been developed to look at the dynamics of vegetation. One such technique has been coined LPJ-Guess (Smith *et al.*, 2001) and combines a model of growth and competition among individual plants and a 'dynamic global vegetation model' simulating plant functional types responses (PFT) in relation to atmospheric, climatic and soil conditions. It has been utilised for a number of studies including projecting the future impacts of climatic changes on vegetation composition in the Mediterranean (Gritti *et al.*, 2006), Sweden (Koca *et al.*, 2006), northern Europe (Wolf *et al.*, 2008) and further localities across Europe (Morales *et al.*, 2005, Morales *et al.*, 2007) However more relevant to this study, it has been applied historically for an exploration of the bioclimatic controls during the Holocene on Fennoscandian vegetation composition (Miller *et al.*, 2008) and a wider study of the vegetation and its related productivity in northern Eurasia from 42 to 10 thousand years ago (Allen *et al.*, 2010). The latter of these studies was conducted using the same palaeoclimatic data (Singarayer & Valdes, 2010) and Allan *et al* conducted simulations of productivity at the same intervals as in this study, although not all have been published. Here a comparison is made between the simulated above-ground net primary productivity (ANPP) and the distributions simulated in this study for *Larix* species, *Picea abies* and *Pinus sylvestris*.

Larix **species**

Similarly to the simulations produced in this study for *Larix* species (Fig 3.5.16), the simulated ANPP of *Larix* species is throughout the 120 thousand years modelled, highest in
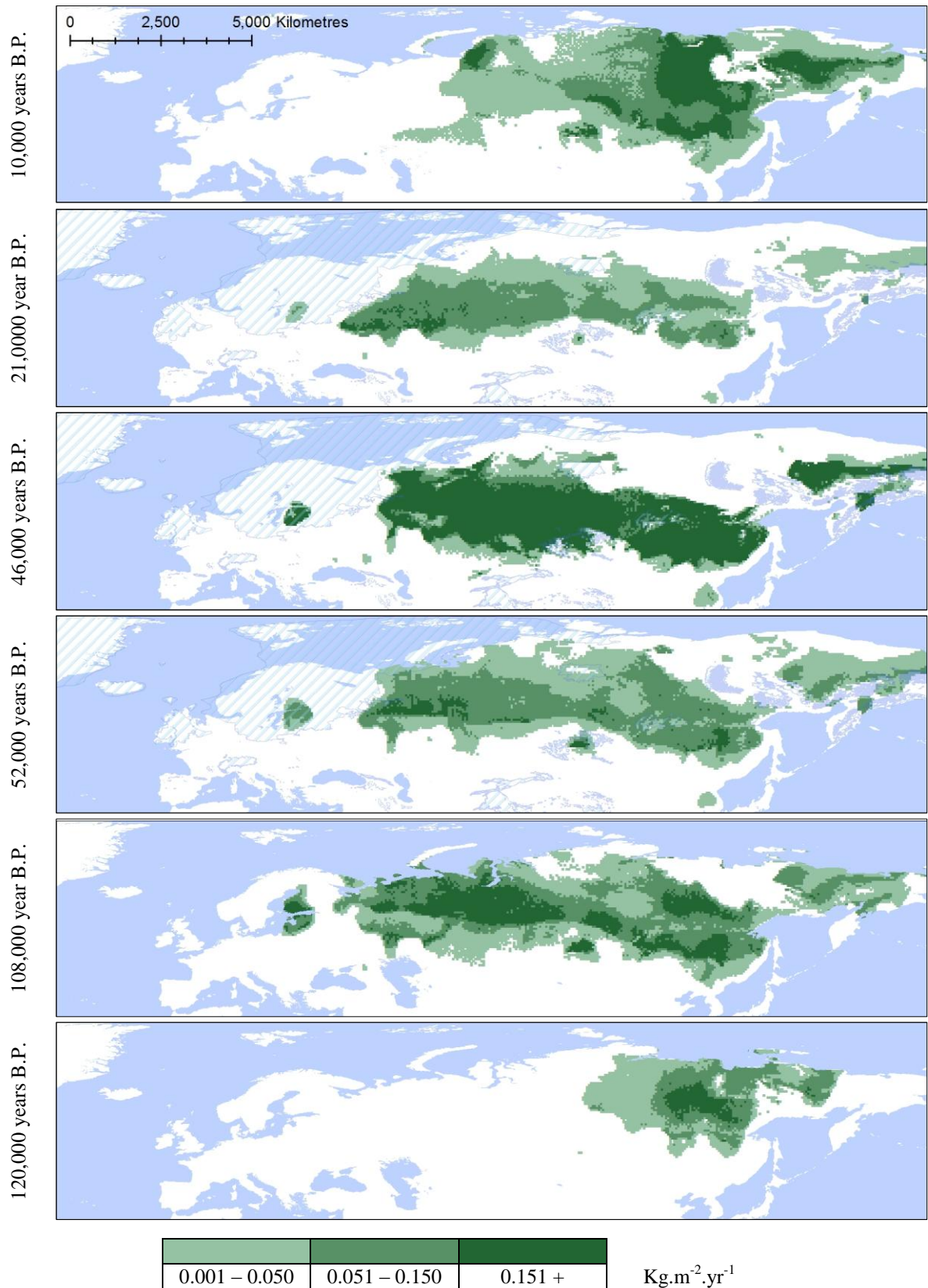
Figure 4.3.5: Simulated above-ground net primary productivity (ANPP, Kg.m^{-2}.yr^{-1}) for *Larix* species generated for a series of palaeoclimatic scenarios, dates in years before present (B.P.) (Allen *et al.*, 2010)

Russia (Fig. 4.3.5) with an absence of productivity in Europe despite the evidence of *Larix decidua* as a native species of this genus in central Europe post-glacial. The productivity does not directly overlap with the simulated distributions, for example the simulated ANPP at 21 thousand years before present does not extend as far north as the climatically suitable range suggests *Larix* could be found (Fig. 3.5.16 E). Despite this, the trend in climatic response appears similar between the two models, with *Larix* species having the highest productivity during the colder conditions of the glacial, 21, 46, 52 thousand years ago and the stadial, 108 thousand years ago, than warmer the interglacial 10 and 120 thousand years ago (Fig. 4.3.5) correlating with the greater abundance of climatically suitable locations during the glacial (Fig. 3.3.7) produced by the climatic response surface model. It is evident that although sites are simulated as climatically suitable for *Larix*, the productivity of the site can vary, for example the western regions of the CRS simulated Eemian distribution, 120 thousand years ago (Fig. 3.5.16 A), having no simulated ANPP despite the climate being suitable (Fig. 4.3.5) while the eastern populations had the potential to be very productive.

This confirms the likelihood that in fact *Larix* species had a larger range size and greater productivity during the colder conditions of the last 120 thousand years. Both of these theories would be hard to validate using the limited pollen records of *Larix* and so modelling such as this may be an effective way of establishing a better understanding of historical range limits and productivity of vegetation.

Picea abies

The palaeo-simulated mapped ANPP for *Picea abies* (Fig. 4.3.6) has many similarities with the climatically suitable ranges generated by the CRS model in this study (Fig. 3.5.31) with productivity and climatically suitable range more southerly distributed during the glacial conditions. The greatest numbers of locations that are productive are during the warmer interglacial conditions, 10 and 120 thousand years ago, and similarly the greatest quantity of climatically suitable grid cells is also found at these palaeoclimatic scenarios (Fig. 3.3.12). Interestingly both models suggest that areas of Japan are both climatically suitable and more productive that other locations in northern Eurasia, despite this there is no recorded presence of *Picea abies* in Japan presently, rather other *Picea* species are noted to reside here, and suggesting *Picea abies* shares a similar climatic niche to these close relatives.

During the glacial, 21 to 52 thousand years ago, the ANPP simulations suggest that in the west *Picea abies* is most productive in central Europe than elsewhere, and actually at its highest productivity during the cold conditions of the Heinrich Event 5, 46,000 years ago
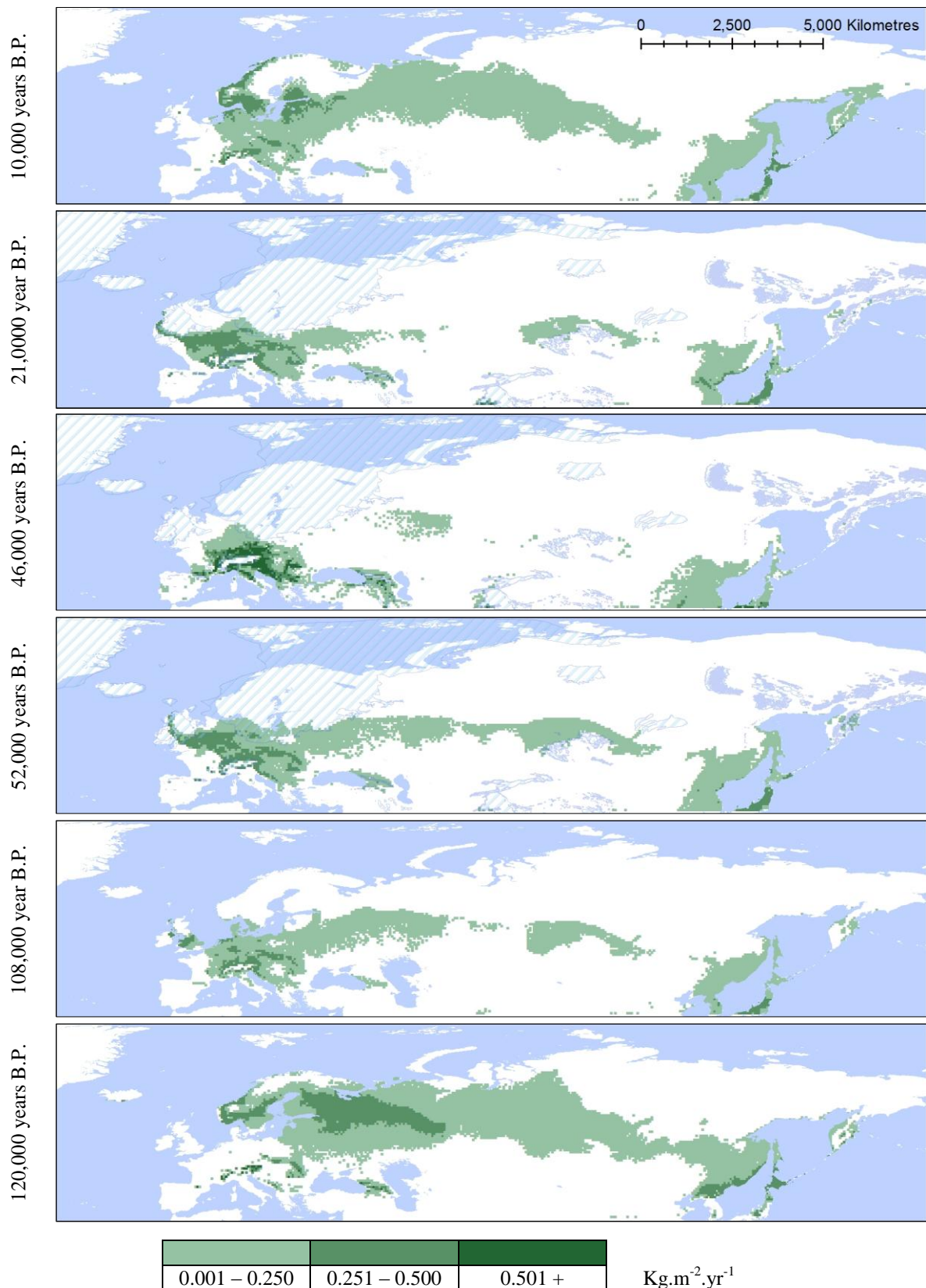
Figure 4.3.6: Simulated above-ground net primary productivity (ANPP, Kg.m^{-2}.yr^{-1}) for *Picea abies* generated for a series of palaeoclimatic scenarios, dates in years before present (B.P.) (Allen *et al.*, 2010)

before present.   This differs somewhat from the climatically suitable range modelled (Fig. 3.5.31 D), which predicts that there was a more limited climatic range for *Picea abies* in central Europe than the ANPP model would suggest.   However, there are similar fragmentations of the climatically suitable range and regions of productivity between Europe, southern Russia and the south eastern Eurasian coastline.   As well as this both models demonstrate a similar western expansion of climate suitability and productivity into southern England, during the cooler conditions of 21 (Fig. 3.5.31 E), 56 (Fig. 3.5.31 C) and 108 (Fig. 3.5.31 B) thousand years ago.   Many of the patterns of change in range of productivity or climate suitability are similar for the two models, but discrepancies do arise.   More constrained productivity ranges highlight areas where, although the climate is simulated as suitable, reproduction and growth may be more limited.   More abundant productivity ranges than the climatic suitability model predict, accentuate that the over-fitting of the climatic response model to observed data, and its non-assuming method of extrapolation, may have resulted in it producing more 'pessimistic' range predictions.

Pinus sylvestris

The resemblance of ANPP simulations for *Pinus sylvestris* (Fig. 4.3.7) compared to the simulated climatic range (Fig. 3.5.34) is not as consistent as the previously discussed genus and species; however there are still many similarities including the fragmentation and more southerly range potential in Russia during the cold glacial conditions (21, 46, 52 thousand years ago) compared to the warmer interglacials.   In Europe, the predicted ANPP indicates a greater range of localities of productivity throughout the modelled palaeoclimatic simulations than the climatic response surface suggests are suitable climate conditions.   Nonetheless many of the areas with the greatest productivity do overlap with the climatically suitable range predictions, for example in northern Spain and the western coast of Ireland at the LGM, 21 thousand years ago (Fig. 3.5.34 E).   In fact these regions and southern fringes of the Weichselian ice sheet are most productive during glacial conditions, while during interglacial, Scotland, Fennoscandia, northern Spain and northern Russia have the areas of higher productivity, areas which corroborate with regions where *Pinus sylvestris* CRS mode suggests are climatically suitable.

The most evident discrepancy is that productivity for *Pinus sylvestris* is suggested as being abundant in areas of central Eurasia, northern China and central Asian mountain ranges, specifically during the glacial conditions (Fig. 4.3.7) which does not occur as prolifically in the climate suitability simulations produced by CRS.   In this case, the species' climatic niche model is likely to be producing a more realistic prediction of range in these past scenarios by

not simulating in these areas.   This is not to say that the ANPP simulations are completely incorrect, for there are other species of *Pinus* which are native to southern Asia (Fig. 3.3.35) which may share a similar climatic niche to *Pinus sylvestris* and could have colonised these
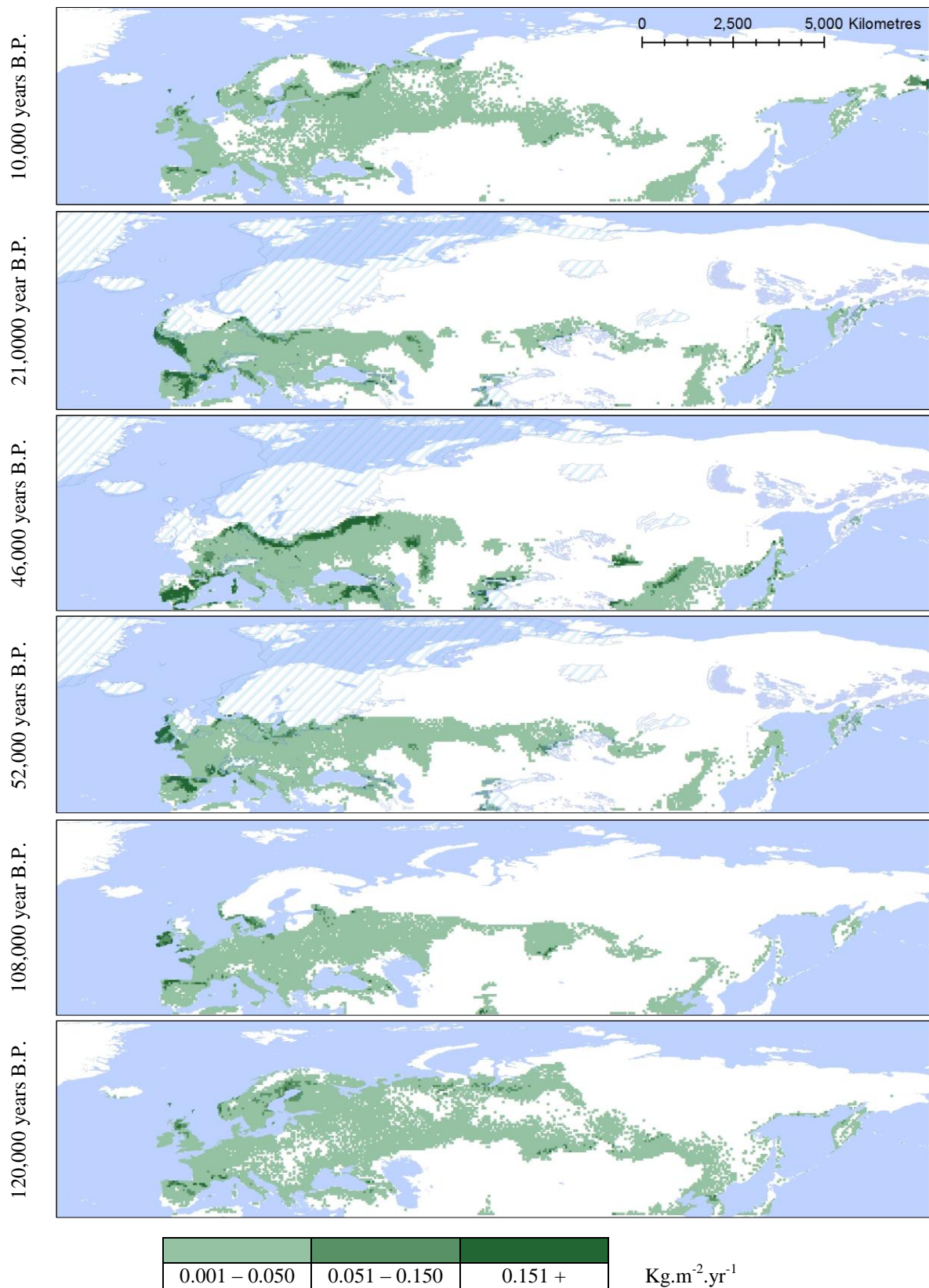
Figure 4.3.7 :Simulated above-ground net primary productivity (ANPP, Kg.m^{-2}.yr^{-1}) for *Pinus sylvestris* for a series of palaeoclimatic scenarios, dates in years before present (B.P.) (Allen *et al.*, 2010)

areas noted as having higher productivity potential.   In fact the CRS simulations of the genus *Pinus* during the glacial (Fig. 3.5.34), do indicate a more northerly climatically suitable range for these southern Asia pines.

Overall the comparison with the ANPP simulations of *Larix* species, *Picea abies* and *Pinus sylvestris* produced by LPJ-Guess with the simulated climatically suitable ranges produced using the CRS model; demonstrate many similarities despite their different approaches to modelling the potential range of the tree taxa.   The use of identical raw data and consistency in simulated scenario dates enables direct evaluations to be made between simulated outputs. In some cases the ANPP simulations indicate areas within the range of climatic suitability which had conditions more favourable for growth and reproduction than other areas were populations may have persisted but not necessarily thrived.   Other examples show regions where productivity is simulated but the climatic niche is not identified, either highlighting the climatic niche models limitations in extrapolation in non-analogous climates or on the other hand the productivity simulations identifying sites of high productivity which are not specific to the species, rather predicting productivity in areas occupied by closely related species. Future studies combining these two modelling techniques, productivity and climatic niche modelling, with existing pollen records and macro-fossil have the potential to greatly further our understanding of vegetational dynamics through the changing historical climate as well as the ecosystems associated with these tree species.

Section 4.4

Comparison of Crossbill Simulated Ranges with their Simulated Feeding Tree Range

The close association of crossbill with particular conifer feeding trees observed today is a relationship which is generally assumed to have occurred for many thousands of years. However, there are limited methods of confirming how long the particular predator-prey relationships between crossbill and conifer species have persisted. The fossil record is very limited and the pollen records do not extend much further than into the late glacial, so simulations such as these, where the feeding trees and *Loxia* species are independently modelled, may provide some further insight into whether these associations could have occurred over the last 120 thousand years.

Also, it has already been noted that the *Loxia* species range may in fact be restricted by the distribution of their feeding trees (Section 1.5) more so than climate, so modelling the feeding tree distributions may in fact supplement the understanding further in several ways. Firstly, it can highlight regions where although *Loxia* species are simulated at present, the climate is not suitable for their feeding trees and so colonisation is less likely. Secondly, the inverse, of highlighting areas of feeding tree abundance which although *Loxia* species are not simulated, may have been utilised in the past. Thirdly, the change in conifer ranges may have impacted upon the divergence of diet observed in crossbill populations.

Loxia curvirostra & their feeding trees

Loxia curvirostra is the most wide-spread and consider the most dietary generalist of the crossbills, consuming *Picea*, *Pinus*, *Pseudotsuga* and *Tsuga* (Table 1.1.2).   Although there are records of *L. curvirostra* consuming *Larix*, this has either be in plantations, artificial established populations (Marquiss & Rae, 1994, Edelaar *et al.*, 2008), or suggestions put forward for feeding trees from surveyed areas in crossbill population localities where other feeding trees of more widely consumed genera are present, rather than direct observation (Edelaar, 2008).   Frequently the palaeoclimatic simulations of *L. curvirostra* distributions coincide with the sites simulated as climatically suitable for one or more of the conifer genera. These corroborations in the range of *L. curvirostra* with the conifer genera are simulated during both the colder and drier extreme conditions of Heinrich Event 5 mid glacial, 52 thousand years ago, (Fig. 4.4.1) and the warmer wetter conditions of the previous interglacial (Fig. 4.4.2), 120 thousand years ago.

However, there are areas in central Asia where *L. curvirostra* is indicated as being potentially found in both the interglacial and more widely during the Heinrich Event, but there are no feeding tree genera predicted to have resided there, although they are found to the south in the mountain ranges of Asia and more northerly boreal regions of Russia.   The fact that these areas were not suitable for any of the feed tree genera suggest that despite the climatic suitability of these locations for *L. curvirostra,* they may not have been colonised.   Also, it is evident from the simulations that *L. curvirostra* populations could not have persisted on a single genus of conifer like some of the other species may, for example Eurasia populations show most overlap with *Picea* species, while in North America western population persist on *Pinus* (Siepielski & Benkman, 2004).   This divergence in diet to different genera has probably contributed to their expansive range and also the great variety of subspecies (Table. 1.1.1) with individual conifer species specialisms (Benkman, 1999).
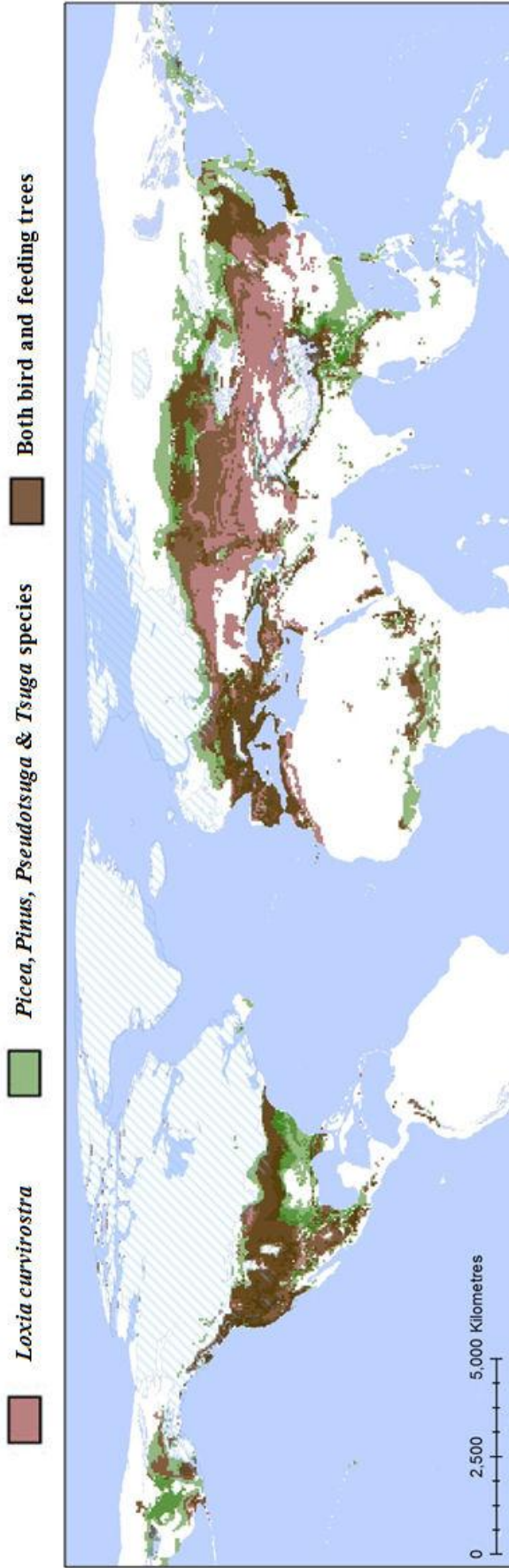
Figure 4.4.1: The simulated distribution of *Loxia curvirostra* and feeding tree genera, *Picea*, *Pinus*, *Pseudotsuga* and *Tsuga*, at the Heinrich Event 5, 46 thousand years ago produced by the CRS model. The darker the shade of green or brown the greater the number of feeding tree genera simulated as present.
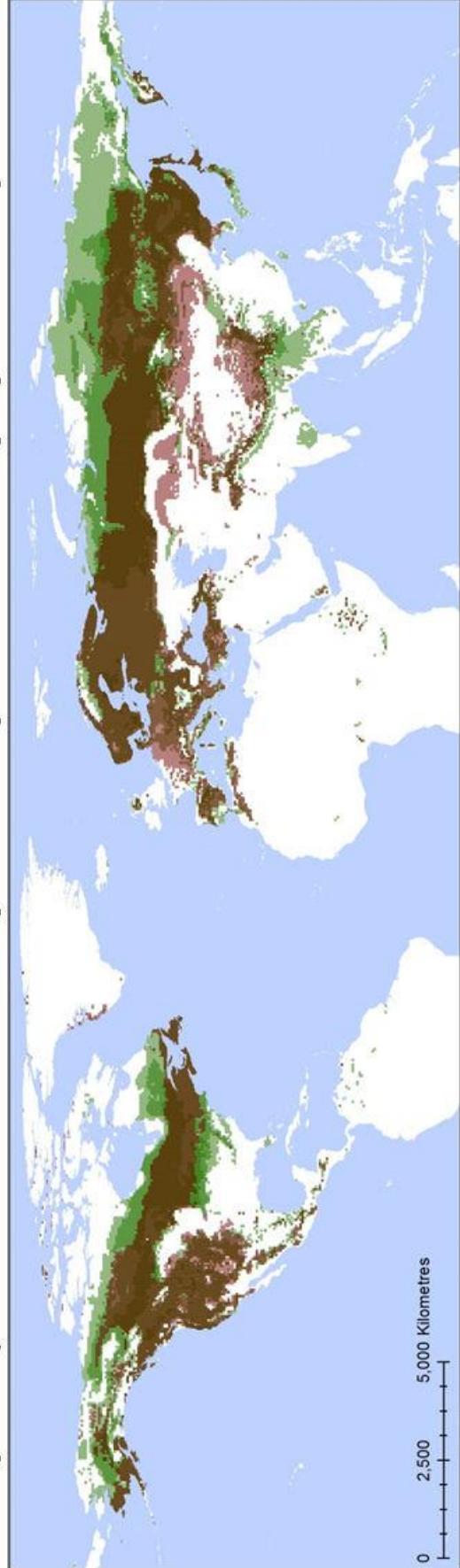
Figure 4.4.2: The simulated distribution of *Loxia curvirostra* and feeding tree genera, *Picea*, *Pinus*, *Pseudotsuga* and *Tsuga*, at the Eemian interglacial, 120 thousand years ago produced by the CRS model. The darker the shade of green or brown the greater the number of feeding tree genera simulated as present.

Legend:
- *Loxia curvirostra*
- *Picea, Pinus, Pseudotsuga & Tsuga* species
- Both bird and feeding trees

Scale: 0   2,500   5,000 Kilometres

Loxia leucoptera and *Larix* species

The Two-Barred Crossbill, *L. leucoptera* is most associated with *Larix* species (Danilov *et al.*, 1984, Cramp *et al.*, 1995), however it will consume other soft cones species of *Picea* and *Abies* genus (Table 1.1.3).   Nevertheless comparisons of *Loxia leucoptera* with just the simulations of *Larix* show a vast amount of overlap, not just in Eurasia but also in North America, through both colder dry conditions (Fig. 4.4.3) and warm wet (Fig. 4.4.4).   There are a few areas simulated where the climate is suitable for *Loxia leucoptera* but not *Larix,* both during the glacial Heinrich Event of 46 thousand years ago, in central and southern Europe and the mountains of western North America (Fig. 4.4.3), and at the Eemian interglacial in similar regions of North America 120 thousand years ago and more northerly in southern Fennoscandia (Fig. 4.4.4).

Loxia leucoptera is not able to exploit all of the simulated *Larix* climate range, but this is primarily because *Larix* has a greater tolerance of lower extremes of temperature (Fig. 3.4.16) than *Loxia leucoptera* (Fig. 3.4.4), and present day ranges of *L. leucoptera* have wintering ranges outside the southern limits of *Larix* ranges where they are likely to utilise other conifer species (Fig. 1.1.2).   However, the absence of *Larix* in Europe in the past, apart from temporally sporadic small outcrops of climate suitability, may well explain why *Loxia leucoptera* is not an established European resident, despite climate being suitable presently in Europe and breeding occurring occasionally (Fischer *et al.*, 1992).   Its strong dependence on *Larix* may well have restricted *Loxia leucoptera* distribution in both Eurasia and North America to the present day ranges, and the simulations suggest this relationship between *Loxia leucoptera* and *Larix* has been maintained throughout the last 120 thousand years.
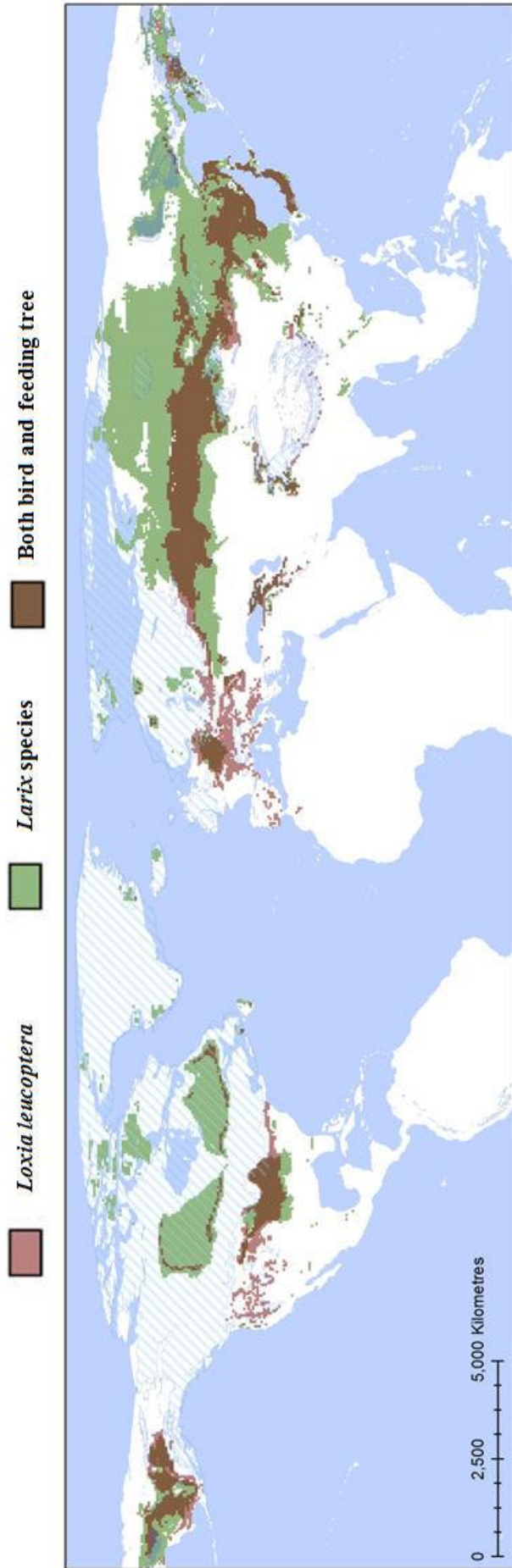
Figure 4.4.3: The simulated distribution of *Loxia leucoptera* and *Larix* species at the Heinrich Event 5, 46 thousand years ago produced by the CRS model.

Figure 4.4.4: The simulated distribution of *Loxia leucoptera* and *Larix* species at the Eemian interglacial, 120 thousand years ago produced by the CRS model.
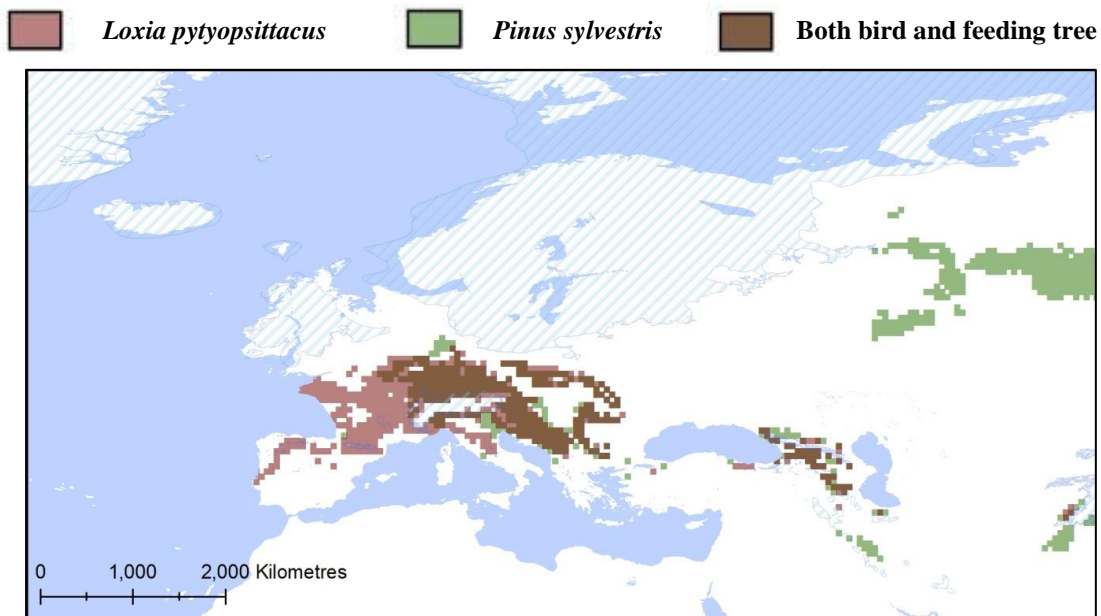
Figure 4.4.5: The simulated distribution of *Loxia pytyopsittacus* and *Pinus sylvestris* at the Heinrich Event 5, 46 thousand years ago produced by the CRS model.
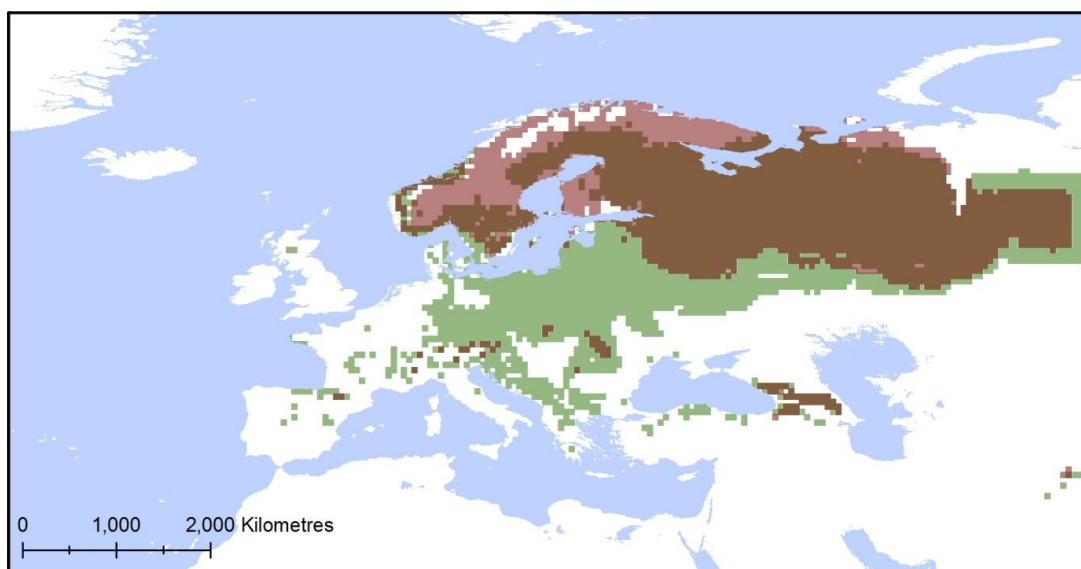
Figure 4.4.6: The simulated distribution of *Loxia pytyopsittacus* and *Pinus sylvestris* at the Eemian interglacial, 120 thousand years ago produced by the CRS model.

Loxia pytyopsittacus, *Loxia scotica* and *Pinus sylvestris*

Loxia pytyopsittacus and *L. scotica* are both considered to be specialists of *Pinus sylvestris* (Summers & Buckland, 2010).   Simulations suggest that this association with this particular pine species and *L. pytyopsittacus* could have occurred throughout the last 120 thousand years.   During the cold Heinrich Event 5 (Fig. 4.4.5) predictions indicate *P. sylvestris* was more southerly restricted than present day, limited to mountains of Europe, the Alps, Dinaric Alps, Caucasus, Carpathian and Balkan Mountains, where *L. pytyopsittacus* is predicted as present in this range.   However, there is further climate to the west where *L. pytyopsittacus*

could have persisted but with no simulations of *P. sylvestris* this establishment is more doubtful.   In the case of *L. scotica*, there is no locations of climatic suitability for the species at all during the Heinrich Events, but the later LGM simulations, which were warmer than the Heinrich extremes, suggest that *L. scotica* could have resided on the west coast of Ireland on the edge of the Devensian ice sheet alongside *Pinus sylvestris* (Fig. 4.4.7) and maintained this throughout milder glacial conditions.

The warmer interglacial, of 120 thousand years ago, results in both *L. pytyopsittacus* and *L. scotica* having overlapping predicted distributions with *P. sylvestris* (Fig. 4.4.6 & 4.4.8). However in both cases the simulations of the *Loxia* species are more expansive than the *P. sylvestris*, having a tolerance of more northerly conditions than *P. sylvestris*.   Despite these discrepancies in overlap, the fact there are many consistent corroborations between *L. pytyopsittacus* and *L. scotica* with *P.* sylvestris, even though its range extends much further east than these species are found and thus has a significantly different climatic niche model, indicates that it may have been the primary food plant for these *Loxia* species throughout the glacial conditions.   It is interesting to note, however, the absence of both *L. scotica,* during Heinrich Event conditions, and *P. sylvestris* limited distribution to central Europe, far from the areas where *L. scotica* may have been able to live during the glacial conditions (Fig. 4.4.7).   This suggests that *L. scotica* may not have existed as the species recognised today through the glaciation, despite the climate and tree species being present pre-glaciation in similar regions as observed today (Fig. 4.4.8) (Further explored: Section 4.6).

🟥 *Loxia scotica*	🟩 *Pinus sylvestris*	🟫 **Both bird and feeding tree**
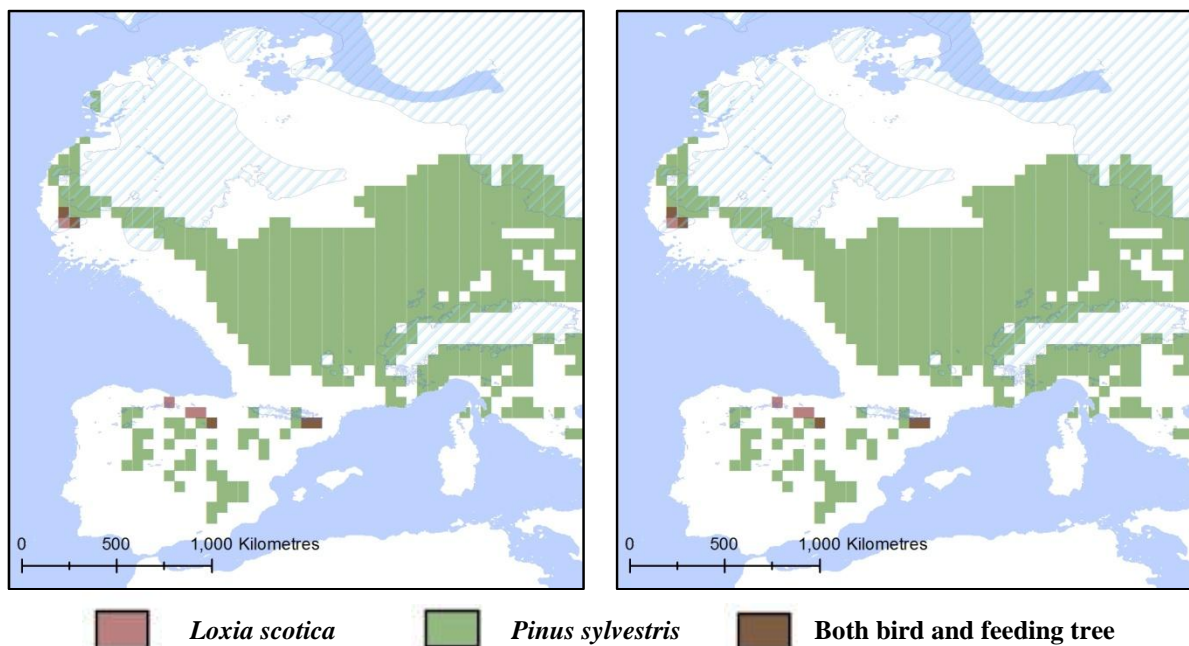
Figure 4.4.7: The simulated distribution of *Loxia scotica* and *Pinus sylvestris* at the last glacial maximum, 21 thousand years ago produced by the CRS model.

Figure 4.4.8: The simulated distribution of *Loxia scotica* and *Pinus sylvestris* at the Eemian interglacial, 120 thousand years ago produced by the CRS model.

Loxia megaplaga and *Pinus occidentalis*

The Hispaniolan Crossbill, *L. megaplaga*, is widely consider to be dependent on the seeds of *Pinus occidentalis* (Table 1.1.6, Benkman, 1994), a species limited to the Caribbean islands of Hispaniola and southern Cuba. Unsurprisingly, as these species share a very similar climatic, niche there is a frequently overlap between them, in both the cold, dry Heinrich Event 5 conditions (Fig. 4.4.9) and warm, wet conditions of the previous interglacial (Fig. 4.4.10), both in the Caribbean and on the surrounding mainland, although these areas are unlikely to have been colonised. Simulations suggest that the colder conditions of the glacial would have made Cuba more suitable while the warmer interglacial of 120 thousand years ago and present day, the Hispaniolan Island was more suited to the *L. megaplaga*. In the case of *L. megaplaga*, the distributions of their feeding tree may actually be a better representative of their past ranges, primarily as the species is noted to already be in decline (IUCN, 2011) and observations have been made of it on neighbouring island in the past (Dod, 1978) but since these populations have become extinct.

Previous theories have suggested the uniformity of climate in the Cuban population of *Pinus occidentalis*; have resulted in a seasonality in cone crops which means that there is not the temporal variance in cone cropping like that observed on the Hispaniolan Island, which can support *L. megaplaga* population throughout the year (Benkman, 1994). Nevertheless, in the past the climate may have fluctuated seasonally and regionally enough that populations were
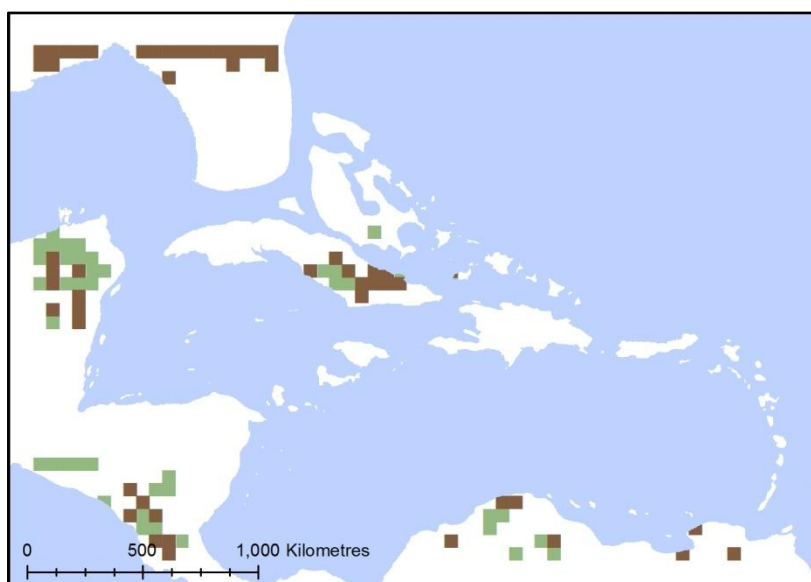
Figure 4.4.9: The simulated distribution of *Loxia megaplaga* and *Pinus occidentalis* at the Heinrich Event 5, 46 thousand years ago produced by the CRS model.

| | *Loxia megaplaga* | | *Pinus occidentalis* | | **Both bird and feeding tree** |
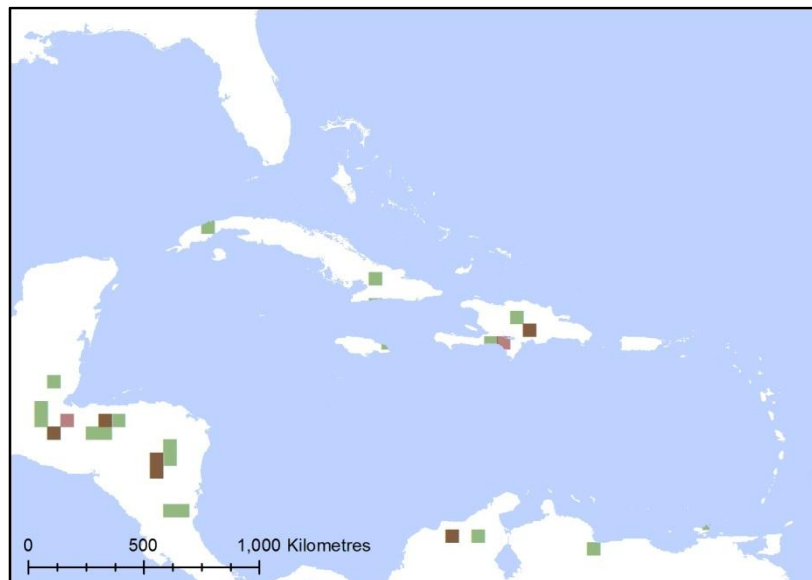
Figure 4.4.10: The simulated distribution of *Loxia megaplaga* and *Pinus occidentalis* at the Eemian interglacial, 120 thousand years ago produced by the CRS model.

🟥 *Loxia megaplaga*	🟩 *Pinus occidentalis*	🟫 **Both bird and feeding tree**

sustainable on Cuba which have only recently become extinct and so the tree distributions may provide us with a more accurate, and potentially larger range that *L. megaplaga* had during the last 120 thousand years, shifting between neighbouring islands in the Caribbean.

Overall the comparison of the *Loxia* species with their respective feeding trees provides further insight into the history of these relationships, as well as whether the birds' past distribution could have been constrained as a result of the feeding trees range, such is the probably case *L. leucoptera*, or more extensive, such as the potential outposts for *L. megaplaga* in Cuba. It highlights that although species' distribution models do successfully simulate the climatic range associated with the habitat the species is found in, species and their prey do not often utilise identical ranges and thus difference in their particular climatic niche resulting in variation in their response to changing climatic conditions. Modelling species' response to changing climate in isolation may overlook restrictions or increases in their potential as a result of prey or predator range change. Having modelled the trees, comparisons can also be made with the pollen records (Section 4.3), as well as the *Loxia* species with the available fossil record (Section 4.2).

Section 4.5

Dispersal Distances of Crossbills

Although many of the simulated range shifts for the *Loxia* species are gradual, with overlap predicted between chronologically adjacent simulations of range, there are scenarios where the climate can change dramatically in a short period of time, such as Heinrich Events, where the regions climatically suitable for a species may alter significantly in spatial distribution and in overall size (Section 3.3). At these times, it may be that both colonisation and the persistence of the population were dependent on the species' ability to move or migrate a substantial distance rather than just a gradual expansion of range over many consecutive years. Dispersal distances of crossbill species may provide us with a valuable insight into ability of the species to cope with more rapid changes in climate. Unfortunately the dispersal distances of crossbills have not been extensively studied but ringing records provide some insight into the distances crossbills can travel in a lifetime.

There are a number of ringing projects, primarily conducted in Europe and in this case Atlas records published for Britain and Ireland (Wernham *et al.*, 2002) and Norway (Bakken *et al.*, 2006) were obtained (Table 4.5.1). In the case of *L. curvirostra* the most widely distributed crossbill species, the maximum distance it has been recorded to travel from the Britain is approximately 1,100 km and from Norway, 1,248 km. Consultation with the primary Crossbill research lab in the USA, supervised by Professor Craig Benkman, also suggested that *L. curvirostra* in the North America may also migrate over 1,000 km and certainly there are records to indicate that they have travelled at least 640 km from initial capture sites. Due to *L. leucoptera*'s scarcity in Europe there are no ringing records in Britain and Ireland and only 151 ringed individual in Norway, of which the two which were recovered were still within Norway, having travelled a maximum of 219 km. However, it is likely *L. leucoptera* have the potential to disperse a lot further as the closest native range is approximately 1,000 km east from Norway in western Russia.

Loxia species	Maximum Distance	No. of Ringed Birds	No. of Recoveries	% Recovered within County Ringed in	Source
L. curvirostra	*Approx.* 1,100 km	3,566	29 (+1 foreign)	-	(Wernham *et al.*, 2002)
	1,248 km	2,711	10	37.5%	(Bakken *et al.*, 2006)
	640 km	-	-	-	Benkman Lab, USA
L. leucoptera	219 km	151	2	100%	(Bakken *et al.*, 2006)
L. pytyopsittacus	366 km	575	5	80%	(Bakken *et al.*, 2006)

Table 4.5.1: Ringing records for *Loxia* species. The maximum distance recorded for a ringed bird from the site it was ringed. If available the number of ringed birds and number of recoveries conducted by the study group and the percentage of these recoveries that where within the country the bird was ringing in as well as the source of the data.

There are no known records of *L. scotica* migrating outside Scotland and although *L. pytyopsittacus* is occasionally found in the UK, over 500 km from its nearest populations in Norway, there are no ringing records to confirm this.   The Norwegian ringing atlas has a maximum distance recorded of 366 km for *L. pytyopsittacus*; however this was the only recovery out of five to have travelled a significant distance, the other four remaining close to the site of initial ringing.   This suggests that unlike the wider-ranging species *L. curvirostra* and *L. leucoptera*, *L. pytyopsittacus* is a relatively sedentary species, not migrating large distances like its relatives.

No records of *L. megaplaga* migrating could be ascertained but this is unsurprising when the species is currently poorly studied and given its small size of the population.   It is likely this species occupies a small niche of habitat suitable in the mountainous regions, so successful dispersal is unlikely, especially given that its habitat is at risk of further decline resulting in the IUCN red listing (IUCN, 2011).

However, the ringing records are very limited with few recoveries of crossbills limiting the assumptions that can be made from these.   Due to this sparseness of ringing and migration data, the general movements of *Loxia* species have also been deduced from population records of spatial and temporal patterns observed.   During years of poor *Picea* seed crops in Eurasia, irruptive populations of *L. curvirostra* are thought to travel longer distances of 4,000 km to find better feeding tree crops, such as the irruptions in the UK in 1990 (Marquiss & Rae, 1994), with mid-winter estimates suggesting there were half a million in Scotland and 40,000 alone in Kielder Forest, Northumberland (Wernham *et al.*, 2002).

So overall ringing records and observations of movements suggest the *L. curvirostra* and *L. leucoptera* more regularly disperse and greater distances than *L. pytyopsittacus* and the two endemic island populations of *L. scotica* and *L. megaplaga*.   In turn this may also indicate a greater ability to disperse in changing climatic conditions and may explain why these two species, *L. curvirostra* and *L. leucoptera*, have significantly broader distributions than the more sedentary species due to this great capacity to colonise new areas when they become available.

Section 4.6

Insights into Crossbill Evolution

The palaeoclimate simulations of range potential for *Loxia* species provide a chronological prediction of their palaeobiogeography (Fig. 3.5.1,4,7,10,13) which is a valuable tool in understanding the complex evolutionary history of the genus *Loxia,* as many speciations occur through segregations of populations which could be driven by climate.   These simulations can be supplemented by a fossil record (Section 4.2) but this has already been utilised to investigate the genus evolution (Tyrberg, 1991) and it is unfortunately very sparse. However, the strong relationship the genus has with particular feeding trees means that simulations of feeding tree climatic range shifts (Section 4.4), fossil pollen records and other palaeovegetation models (Section 4.3) can all be used to enhance the understanding of crossbill palaeobiogeography and potentially verify existing or establish new hypotheses for relatively recent crossbill evolution.

Loxia curvirostra

Loxia curvirostra, the conifer generalist of the genus, has the most prolific climatically suitable range of all the crossbill species throughout the 120 thousand years simulated.   In northern Eurasia, the species is often considered a *Picea* specialist and simulations suggest that this association could have persisted from the previous interglacial, but it does also utilise *Pseudotsuga, Pinus* and *Tsuga* especially in more southerly regions of Eurasia.   However, in North America it is considered more of a *Pinus* specialist, with a number of subspecies recognised specialising on particular pine species (Groth, 1993a, Benkman *et al.*, 2009). This closer association with *Pinus* is unsurprising when the past simulations are considered; as there is a far greater abundance of climate suitable for *Pinus* species south of the Laurentide ice sheet, along the western coastline, during the glacial conditions showing greater overlap with the *L. curvirostra* simulated distributions than the more limited *Picea* species.   Many of the subspecies, however, are most likely to have developed as a results of a co-evolutionary process between the particular *Pinus* species and specific populations that predate on them (Smith & Benkman, 2007) rather than geographic isolation.   The exception to this may be the subspecies, *L. c sitkensis*, currently found in Alaska where climate is simulated as being suitable throughout the glacial and *Picea sitchensis*, its food plant, could have persisted too according to *Picea* species climatic niche model, west of the Laurentide ice sheet.

Several of the subspecies recognised in Eurasia; such as *L. c. japonica,* in Japan, south-eastern Russia and northern China, *L. c. balearica*, central and southern Spain, *L. c. poliogyna,* in Morocco, northern Algeria, Tunisia and southern Italy and the isolated race *L. c. corsicana*, in Corsica all have recurrent simulated climatic suitability throughout the last 120 thousand years (Fig. 3.5.2) suggesting that these subspecies may be very well established having been resident in their respective locations for many thousands of years.

Interestingly the relatively well studied *L. c. luzoniensis* of the Philippines and its nearest *L. curvirostra* species, *L. c. meridionalis* in Vietnam, are not simulated as having stable climatic niches in the localities they are found today although the nearby *L. c. himalayensis* population does.   However, simulations of *Pinus* do show long durations of climate suitable in Vietnam and the Philippines, likely colonised by *P. kesiya*, throughout the 120 thousand year period simulated suggesting that both species do have a long history of occupation in south east Asia as suggested by Clouet & Goar (1999, 2001).   Similarly, *Picea* species are simulated as having climatic suitability in Newfoundland from Eemian interglacial throughout the glacial to the present Holocene in the locality of heavier-billed subspecies *L. c. percna* and its feeding tree *Picea mariana*, which has a notable co-evolutionary relationship (Benkman, 1989b) but the modelled climatic niche for *L. curvirostra* is not as stable but with the presence of the feeding tree populations could have persisted.

Loxia leucoptera

Although very little is known about the evolutionary history of *Loxia leucoptera*, the simulations in this study suggest that the species has been around throughout the last 120 thousand years although it had substantial range shifts.   *Larix*, its most often utilised feeding tree, also showed similar patterns of climatic suitability range change and thus it is likely that this dependence on *Larix* has been a historically long association, and may in fact be a specialism which resulted in its speciation from an ancient crossbill ancestor.   Certainly *Loxia leucoptera*'s bill morphology is adapted for the soft cones archetypal of the *Larix* genus.

In North America the populations of *Loxia leucoptera* during the glacial are split between central and north-western regions by the Laurentide ice sheet, with the potential of mixing between the Alaskan and eastern Russian populations during this time across the Bering Strait.   Therefore there may be genetic distinctions between the populations which resided in Alaska during the glaciations compared to those in central North America; however phylogenetics studies are still in their infancy for *Loxia* species.   Future studies may

compliment and further our understanding of whether this isolation had any genetic effect on the populations observed today.

Notably though, the lack of climatic suitability of *Larix* genus in Europe simulated in this study and the limited productivity (Fig. 4.4.5) also modelled may provide an explanation for the absence of *Loxia leucoptera* in Europe despite climate suitability and the presence of a *Larix* species, *Larix decidua*. However *Larix decidua* is persistently excluded from simulations of both productivity and climatic range of the *Larix* genus, suggesting it has a unique Alpine climatic niche which is not similar to other *Larix* species and is also not favourable for *Loxia leucoptera*.

Loxia pytyopsittacus

The Fennoscandian distribution of *Loxia pytyopsittacus* observed today was completely inhospitable during the glacial conditions mainly as is was covered by the Weichselian ice sheet, so the glacial distribution was constrained to central and southern Europe as far as west as the coast of Ireland.   Its primary feeding tree, *Pinus sylvestris*, also has a similar southerly range during the glaciations (Fig. 3.5.35 C, D & E), indicating that their association is likely to have been established prior to the 120 thousand years ago modelled in this study. Although there is a substantial range shift for *L. pytyopsittacus*, the change is gradual with successive temporal simulations showing overlap in simulated distribution with previous, rather than a rapid change.   This shift to the central and southern Europe by *L. pytyopsittacus* also corroborates with fossil evidence, which suggests that it was found around the Mediterranean.

This study suggests that this heavier-billed crossbill species has had a long history in Europe being a specialist of *Pinus sylvestris*. It potentially persisted alongside the smaller-billed species *L. curvirostra*, which predated on the softer-cones of *Picea* species in Europe and on more southerly distributed Mediterranean *Pinus* species as it does today.   This is evidence that discounts previous theories that a single but variable crossbill population dominated the glacial and then split during the interglacial conditions (Tyrberg, 1991), rather it suggests a longer evolutionary history for *L. pytyopsittacus* as it could have resided as it does today, in Fennoscandia, during the previous interglacial 120 thousand years ago.

Loxia scotica

The biggest insight provided by the simulations is that of the origins of the Scottish Crossbill, *Loxia scotica*. It has long been considered a descendant of the *L. pytyopsittacus* (Knox, 1990) primarily as they both feed on *Pinus sylvestris.* The CRS simulations of the climate suitability suggest that *L. scotica* was limited to the west coast of Ireland or Spain during the glacial, however it is likely that the Irish locality is a more reasonable assumption as there are successive simulations of climatic suitability shifting from the Eemian in Scotland through to Ireland in the glacial and back into Scotland for the Holocene (CD ROM Appendix: *Loxia scotica -* CRS). *Pinus sylvestris* is also simulated as having the potential of being along the west coast of Ireland during the glacial, and this corroborates with pollen records that suggest *P. sylvestris* was native to Ireland at the beginning of the Holocene (Birks, 1989). So these initial investigations suggest that *L. scotica* could have been in Scotland as early as 120 thousand years ago alongside populations of *P. sylvestris* (Huntley *et al.*, In Press).

However, Heinrich Event conditions are completely inhospitable for the *L. scotica* (Fig. 3.5.10 D) and *P. sylvestris* is simulated as also finding the conditions during this significantly colder period unsuitable along the western coast of Europe, with a more limited
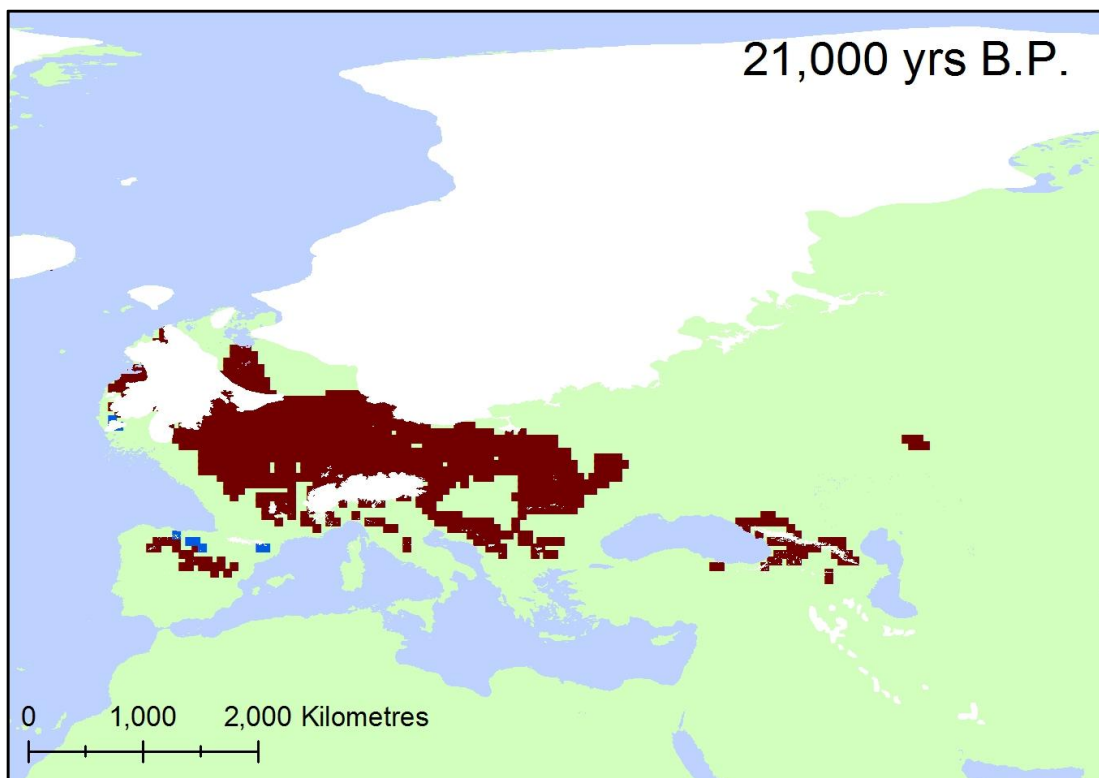
Figure: 4.6.1: The simulated distribution of *Loxia scotica* and *Loxia pytyopsittacus* at the last glacial maximum, 21,000 years before present (B.P.) produced by the CRS model.

range in central and southern Europe.   This throws into question whether *L. scotica* could have survived throughout the glacial on the western coast of Ireland.

Another explanation is that the species is a relatively new descendent of *L. pytyopsittacus*, as the two crossbill species are simulated as being alongside each other at the glacial maximum on the west coast of Ireland (Fig 4.6.1).   At this time it is possible that *L. pytyopsittacus* populations could have been isolated on the west of the Devensian ice sheet and been the ancestral origins of the present day species *L. scotica.*   This seems even more likely given that the simulated productivity of *Pinus sylvestris* was greatest along this west coastline (Fig. 4.4.7).   The better cone cropping and growth of *Pinus sylvestris* in this region during the glacial conditions would have provided more favourable conditions for *L. pytyopsittacus* increasing its likelihood of being found on the western coast of Ireland.   In addition *Pinus sylvestris* in Scotland has been found to be genetically distinct from the population on mainland Europe (Kinloch *et al.*, 1986), indicating that it may too have been isolated and genetically diverged in western Ireland.   Similarly simulations conducted in another study of the Willow Ptarmigan, *Lagopus lagopus* (Huntley *et al.*, In Press), demonstrate a similar climatic suitability and potential isolated populations of this species, which may be the origins of the present day race of Red Grouse, *Lagopus lagopus scotica,* which does not turn white like its mainland close relative.

There are a numerous scenarios where *L. curvirostra* is simulated as being near or in fact overlapping with *L. scotica* (Fig. 3.5.1 C & E), so one could assume that *L. scotica* is a descendent population of *L. curvirostra*.   However, unlike *L. pytyopsittacus*, there are presently populations of *L. curvirostra* that regularly breed alongside *L. scotica* in Scotland yet both appear to not interbreed (Summers *et al.*, 2007).   In addition to this, *L. curvirostra* irruptive behaviour in years of poor cone cropping (Newton, 2006) and longer dispersal distances (Section 4.5; Table 4.5.1) is likely to have resulted in numerous encounters between the *L. scotica* and *L. curvirostra* populations which would have limited the speciation potential of *L. scotica*.

The corroborating evidence suggests that *L. pytyopsittacus* became isolated on the edge of the Devensian ice sheet in Ireland during the glacial, sustained by a thriving population of *P. sylvestris*.   As the ice sheet melted, this population of *L. pytyopsittacus* did not reconnect with the mainland populations, rather it spread into Northern Ireland and across the Irish Sea along with *P. sylvestris* population into Scotland where it established the present day species *L. scotica*.

Loxia megaplaga

The simulations conducted in this study suggest that the regions with suitable climate for *Loxia megaplaga*, Hispaniolan Crossbill, and its feeding tree *Pinus occidentalis*, although consistently overlapping, varied greatly in distribution with different palaeoclimatic conditions, although at all times there is some climate suitable on at least one of the Caribbean islands.   The Hispaniolan Crossbill is considered a descendent of *L. leucoptera*; however conditions in the most recent glacial do not result in *L. leucoptera* being significantly closer, with the simulated populations being approximately 3,000 kilometres from Hispaniola at the LGM.   Thus the population may have been established in more extreme colder conditions prior to the most recent glacial such as the highly variable Beestonion Stage, or that *L. megaplaga* was a vagrant dispersing population that established in the Caribbean, as it is widely known crossbill can disperse vast distances in search of conifer crops (Section 4.5). However, the evidence of *Pinus* species in southern Florida both in the simulations throughout the glaciation and early Holocene (Fig. 3.5.22) and in the pollen record during the early Holocene (Fig. 4.3.4 E & F) suggests that there could have potentially been a passage of progression southerly into the Caribbean for Crossbills, however ancestral *L. megaplaga* must have diverged from the *Larix* specialism of *L. leucoptera* to that of *Pinus*.   It is interesting to note the *L. curvirostra* climatic niche could be found on Hispaniola during the glacial conditions (Fig. 3.5.1 C, D & E), precisely in the regions where present day *L. megaplaga* is found.   *L. curvirostra* also consume *Pinus* and their simulated past ranges are much closer to the Caribbean.   This evidence might suggest a *L. curvirostra* subspecies would as the primary candidate for colonisation of the Caribbean rather than the boreal *L. leucoptera*, but morphologically and genetically *L. megaplaga* is demonstrated to be most similar to *L. leucoptera* (Parchman *et al.*, 2006).

In the case of *L. megaplaga,* its origins still remain a mystery, although further phylogeny work may aid in unravelling its genetic divergence and could possibly provide a date of speciation (Carstens & Knowles, 2007).   The climatic conditions *L. megaplaga* is found in may not be modelled effectively at this scale, so more refined work, looking at the regional variations in its climatic niche, may highlight a niche more similar to *L. leucoptera* in the mountains of Hispaniola, and may improve our understanding of its palaeobiogeography and thus it origins.

Chapter 4.7
Conclusions

The species' distribution models in this study have provided valuable insights into further understanding the palaeobiogeography of *Loxia* species and their feeding plants. These climatic niche-based simulations demonstrate many similarities with the fossil records of both the *Loxia* spp. (Section 4.2) and conifer trees (Section 4.3) as well as other modelling studies, demonstrating their valid use in filling many gaps in our historical understanding of species' distributions.

By comparing the predicted ranges of *Loxia* with its feeding tree, some new hypotheses have been suggested for explaining the present day observed ranges, such as the absence of *L. leucoptera* in Europe. Most notably though is the simulated evidence that *L. scotica* may be a relatively new descendent of the heavier-billed *L. pytyopsittacus*. It is demonstrated here that a small population *L. pytyopsittacus* may have become isolated on the west coast of the Devensian ice sheet in Ireland during the glacial, alongside populations of their feeding tree *Pinus sylvestris* and remained disjunct from the rest of the mainland *L. pytyopsittacus* post-glacial, migrating into Scotland during the warmer Holocene conditions.

There is also evidence that many of the subspecies of *L. curvirostra* have had the potential for being regionally stable throughout the 120 thousand years modelled in this study, such as the *L. c. corsicana* in Corsica. Such a long duration of isolation is likely to have resulted in morphological and behavioural changes in these populations. It will be interesting to note if any further studies into the phylogeography and breeding status of these subspecies identify that significant divergence has occurred from the more broadly distributed range of *L. curvirostra*.

The predicted conifer distributions also provided some valuable insights into the vegetational changes during the glaciation, and may in fact be a valuable supplementary tool in combination with the existing pollen and macrofossils to understand biome shifts. Also, unlike pollen records which can often only be resolved to a genus level, such climatic distribution models can provide species' specific insights into movements and restrictions in range during the changing palaeoclimate.

This study also highlights the difficulties in modelling species' distributions of range restricted species. The Hispaniolan native species of crossbill, *Loxia megaplaga*, and its feeding tree, *Pinus occidentalis*, are primary examples of the problems that can arise,

producing models of lower performance and simulations which provide less robust insight into their past movements. The limited distributions combined with the relatively close mountains and maritime climates of these islands make it very difficult to effectively model the climatic niche at the grid scale chosen in this study. Certainly, further refinement of species' distribution models would not only improve the output in this study, but also other studies, especially since rare species are often of more interest, and effective simulations may help develop future conservation strategies.

Despite this investigation's focus on the past distributions of *Loxia* species, it does have some application in understanding their future. Climatic conditions are certain to continue changing into the future and it is widely understood that anthropogenic activities are probably affecting the amplitude and rate of change being observed. The response of *Loxia* species to these future predicted changes has already been investigated in Europe (Huntley *et al.*, 2007). The future projections for *L. scotica* are particularly bleak, indicating that climatic conditions in Scotland will potentially become inhospitable, with the only viable climate being in Iceland. However, this study indicates that *Loxia* species may be more constrained by conifer ranges than direct climate conditions, so conservation efforts focused on maintaining coniferous forests in Scotland may help to sustain populations, a much more optimistic prognosis for Britain's only endemic bird.

So, in addition to retrodicting species' distribution models providing an unequivocal valuable supplement to our understanding of past range movements and evolutionary history, they also may aid the understanding of future implications for the species. Species' distribution models are widely used with future climatic change as the main focus, but this study highlights that retrodiction may be a more effective way of confirming the validity of the predictions of models prior to their application to novel future scenarios. This study was also a significant opportunity to compare multiple modelling techniques, note their corroboration both with each other and with independent evidence of past occupation. Overall, this highlights the value of such palaeobiogeography studies in furthering ecologically modelling interpretation, understanding and their further development.

BLANK PAGE

Appendix Contents

Appendix

Table 1: The 'Goodness of Fit' measures for the *Loxia* species' feeding tree species.   The number of 0.5° by 0.5° grid cells the tree species is recorded in and the maximum κ and Area Under Curve (AUC) values obtained for the species modelled using climate response surface (CRS) model.

Species		No. of grid cells from which recorded	'Goodness of Fit' Measure	
			Maximum κ value	AUC Value
Larix	*decidua*	227	0.407	0.994
	gmelinii	5417	0.818	0.985
	griffithii	134	0.714	0.998
	kaempferi	22	0.368	0.996
	laricina	3728	0.545	0.867
	potaninii	191	0.456	0.993
	sibirica (*russica*)	3512	-	-
Picea	*abies*	8478	0.714	0.966
	alcoquiana	24	0.381	0.997
	asperata	168	0.497	0.992
	brachytyla	175	0.513	0.994
	glauca	4204	0.525	0.951
	glehnii	85	0.189	0.991
	jezoensis	867	0.355	0.953
	koraiensis	28	0.363	0.995
	likiangensis	108	0.584	0.998
	mariana	4306	0.522	0.951
	meyeri	181	0.672	0.993
	neoveitchii	131	0.453	0.994
	orientalis	87	0.456	0.989
	rubens	334	0.418	0.991
	schrenkiana	217	0.684	0.998
	sitchensis	388	0.456	0.914
	smithiana	245	0.580	0.985
	Picea spinulosa	36	0.637	0.999
	torana	54	0.285	0.996
Pinus	*ayacahuite*	71	0.620	0.998
	caribaea	88	0.359	0.965
	contorta	1221	0.530	0.962
	cooperi	37	0.676	0.998
	douglasiana	35	0.625	0.999
	durangensis	78	0.638	0.999
	engelmannii	119	0.568	0.994
	halepensis	364	0.605	0.994
	hartwegii	62	0.655	0.998
	kesiya	369	0.705	0.996
	latteri	499	0.646	0.994
	lawsonii	44	0.666	0.998
	leiophylla	182	0.581	0.998
	lumholtzii	85	0.662	0.997
	merkusii	101	0.213	0.989
	michoacana	97	0.666	0.999
	montezumae	95	0.643	0.998
	nigra	419	0.558	0.993
	occidentalis	23	0.264	0.997

Table 1 cont.: The 'Goodness of Fit' measures for the *Loxia* species' feeding tree species.

Species		No. of grid cells from which recorded	'Goodness of Fit' Measure	
			Maximum κ value	AUC Value
Pinus	*ponderosa*	869	0.634	0.990
	pseudostrobus	155	0.640	0.997
	strobus	1261	0.559	0.952
	strobiformes	161	0.552	0.993
	sylvestris	6723	0.675	0.964
	teocote	144	0.663	0.998
	yunnanensis	218	0.768	0.990
Pseudotsuga	*japonica*	29	0.285	0.998
	menziesii	922	0.596	0.985
	sinensis	379	0.527	0.993
Tsuga	*canadensis*	802	0.634	0.963
	chinensis	909	0.603	0.959
	dumosa	229	0.629	0.997
	heterophylla	510	0.470	0.934

Appendix

Table 2: *Larix* & *Pseudotsuga* species pollen records from European Pollen Database (EPD: http://www.europeanpollendatabase.com).   Pollen and stomata fossil record locations selected as sites where presence was dated from 4-6,000 years B.P. and 9-11,000 years B.P.   Used to produce Fig. 4.3.1 A & B.

Fossil Type	Date (yrs B.P.)	Latitude	Longitude
Larix Stomata	4109	46°52'11"N	10°28'47"E
Larix Stomata	5000	46°13'49"N	8°0'41"E
Larix Stomata	5011	46°10'36"N	7°5'37"E
Larix Stomata	5037	46°9'4"N	8°0'44"E
Larix Stomata	5051	46°13'56"N	8°0'51"E
Larix Stomata	5057	46°7'27"N	8°3'53"E
Larix Stomata	5144	46°9'57"N	7°30'14"E
Larix Stomata	5214	46°6'54"N	7°30'16"E
Larix Stomata	5303	46°26'38"N	8°31'1"E
Larix Stomata	5550	46°13'18"N	7°35'33"E
Larix Stomata	5667	46°13'29"N	8°0'53"E
Larix Stomata	5778	46°30'54"N	10°17'7"E
Larix Stomata	5902	46°8'25"N	7°12'10"E
Larix Stomata	9048	46°16'53"N	10°12'5"E
Larix Stomata	9116	46°47'1"N	10°18'38"E
Larix Stomata	9207	46°5'29"N	7°13'14"E
Larix Stomata	9264	46°15'33"N	7°50'35"E
Larix Stomata	9500	46°9'57"N	7°30'14"E
Larix Stomata	9500	46°13'49"N	8°0'41"E
Larix Stomata	10000	46°9'57"N	7°30'14"E
Larix Stomata	10111	46°9'4"N	8°0'44"E
Larix Stomata	10185	46°16'53"N	10°12'5"E
Larix Stomata	10280	46°52'11"N	10°28'47"E
Larix/Pseudotsuga Pollen	4060	61°4'0"N	36°3'0"E
Larix/Pseudotsuga Pollen	4108	53°38'20"N	18°21'30"E
Larix/Pseudotsuga Pollen	4185	46°23'1"N	10°0'44"E
Larix/Pseudotsuga Pollen	4400	64°34'0"N	30°32'0"E
Larix/Pseudotsuga Pollen	4420	49°32'0"N	21°42'0"E
Larix/Pseudotsuga Pollen	4520	47°10'0"N	13°54'0"E
Larix/Pseudotsuga Pollen	4623	49°2'30"N	19°40'40"E
Larix/Pseudotsuga Pollen	4647	52°19'10"N	17°21'48"E
Larix/Pseudotsuga Pollen	4671	46°25'14"N	10°2'48"E
Larix/Pseudotsuga Pollen	4794	44°8'50"N	7°14'20"E
Larix/Pseudotsuga Pollen	4800	46°26'38"N	8°31'1"E
Larix/Pseudotsuga Pollen	4810	47°10'0"N	13°52'0"E
Larix/Pseudotsuga Pollen	4811	44°14'0"N	7°8'0"E
Larix/Pseudotsuga Pollen	4840	48°47'30"N	16°23'15"E
Larix/Pseudotsuga Pollen	4876	62°19'0"N	33°51'0"E
Larix/Pseudotsuga Pollen	4877	44°25'12"N	6°20'11"E
Larix/Pseudotsuga Pollen	4901	46°9'57"N	7°30'14"E
Larix/Pseudotsuga Pollen	4903	47°17'30"N	10°58'35"E
Larix/Pseudotsuga Pollen	4910	62°2'0"N	32°46'0"E
Larix/Pseudotsuga Pollen	4911	46°9'4"N	8°0'44"E
Larix/Pseudotsuga Pollen	4916	49°3'0"N	18°18'0"E

Appendix

Fossil Type	Date (yrs B.P.)	Latitude	Longitude
Larix/Pseudotsuga Pollen	4918	46°39'58"N	11°27'30"E
Larix/Pseudotsuga Pollen	4920	47°12'57"N	17°15'18"E
Larix/Pseudotsuga Pollen	4924	47°6'0"N	11°0'0"E
Larix/Pseudotsuga Pollen	4933	46°13'51"N	7°35'25"E
Larix/Pseudotsuga Pollen	4944	46°15'33"N	7°50'35"E
Larix/Pseudotsuga Pollen	4959	44°59'51"N	6°38'0"E
Larix/Pseudotsuga Pollen	4963	46°16'53"N	10°12'5"E
Larix/Pseudotsuga Pollen	4966	46°8'25"N	7°12'10"E
Larix/Pseudotsuga Pollen	4982	44°46'3"N	6°32'13"E
Larix/Pseudotsuga Pollen	4982	58°15'0"N	85°10'0"E
Larix/Pseudotsuga Pollen	5000	47°3'45"N	11°18'12"E
Larix/Pseudotsuga Pollen	5000	47°1'48"N	11°27'10"E
Larix/Pseudotsuga Pollen	5000	46°38'24"N	11°27'32"E
Larix/Pseudotsuga Pollen	5000	47°21'10"N	11°52'48"E
Larix/Pseudotsuga Pollen	5000	44°8'50"N	7°14'20"E
Larix/Pseudotsuga Pollen	5000	46°12'52"N	7°34'30"E
Larix/Pseudotsuga Pollen	5000	46°13'49"N	7°35'2"E
Larix/Pseudotsuga Pollen	5000	46°13'29"N	8°0'53"E
Larix/Pseudotsuga Pollen	5005	46°13'18"N	7°35'33"E
Larix/Pseudotsuga Pollen	5011	46°10'36"N	7°5'37"E
Larix/Pseudotsuga Pollen	5020	47°28'17"N	12°21'30"E
Larix/Pseudotsuga Pollen	5037	46°9'4"N	8°0'44"E
Larix/Pseudotsuga Pollen	5051	46°13'56"N	8°0'51"E
Larix/Pseudotsuga Pollen	5057	44°3'28"N	7°27'0"E
Larix/Pseudotsuga Pollen	5057	46°7'27"N	8°3'53"E
Larix/Pseudotsuga Pollen	5071	46°6'54"N	7°30'16"E
Larix/Pseudotsuga Pollen	5085	46°47'1"N	10°18'38"E
Larix/Pseudotsuga Pollen	5111	46°30'54"N	10°17'7"E
Larix/Pseudotsuga Pollen	5133	46°12'10"N	7°35'34"E
Larix/Pseudotsuga Pollen	5189	45°41'5"N	7°45'40"E
Larix/Pseudotsuga Pollen	5222	46°23'41"N	10°7'25"E
Larix/Pseudotsuga Pollen	5289	44°3'28"N	7°26'41"E
Larix/Pseudotsuga Pollen	5324	62°12'0"N	33°48'0"E
Larix/Pseudotsuga Pollen	5401	47°14'35"N	12°8'20"E
Larix/Pseudotsuga Pollen	5525	44°30'30"N	5°58'59"E
Larix/Pseudotsuga Pollen	5642	44°16'0"N	7°6'0"E
Larix/Pseudotsuga Pollen	5758	58°20'0"N	88°10'0"E
Larix/Pseudotsuga Pollen	5816	68°51'0"N	66°54'0"E
Larix/Pseudotsuga Pollen	9071	44°8'50"N	7°14'20"E
Larix/Pseudotsuga Pollen	9491	46°26'38"N	8°31'1"E
Larix/Pseudotsuga Pollen	9551	46°15'33"N	7°50'35"E
Larix/Pseudotsuga Pollen	9667	50°51'0"N	20°50'0"E
Larix/Pseudotsuga Pollen	9668	56°46'0"N	60°45'0"E
Larix/Pseudotsuga Pollen	9711	49°2'30"N	19°40'40"E
Larix/Pseudotsuga Pollen	9736	44°14'0"N	7°8'0"E
Larix/Pseudotsuga Pollen	9842	46°13'18"N	7°35'33"
Larix/Pseudotsuga Pollen	9898	46°9'4"N	8°0'44"E

Appendix

Fossil Type	Date (yrs B.P.)	Latitude	Longitude
Larix/Pseudotsuga Pollen	9931	47°36'45"N	12°10'15"E
Larix/Pseudotsuga Pollen	9973	49°3'0"N	18°18'0"E
Larix/Pseudotsuga Pollen	9989	46°38'24"N	11°27'32"E
Larix/Pseudotsuga Pollen	10000	52°33'0"N	20°40'0"E
Larix/Pseudotsuga Pollen	10000	50°47'0"N	21°17'0"E
Larix/Pseudotsuga Pollen	10000	44°8'50"N	7°14'20"E
Larix/Pseudotsuga Pollen	10000	46°9'57"N	7°30'14"E
Larix/Pseudotsuga Pollen	10000	46°12'10"N	7°35'34"E
Larix/Pseudotsuga Pollen	10005	49°47'0"N	21°28'0"E
Larix/Pseudotsuga Pollen	10010	47°4'35"N	11°24'40"E
Larix/Pseudotsuga Pollen	10030	58°15'0"N	85°10'0"E
Larix/Pseudotsuga Pollen	10036	46°8'25"N	7°12'10"E
Larix/Pseudotsuga Pollen	10047	47°14'25"N	11°25'15"E
Larix/Pseudotsuga Pollen	10062	46°16'53"N	10°12'5"E
Larix/Pseudotsuga Pollen	10062	49°22'22"N	21°53'13"E
Larix/Pseudotsuga Pollen	10072	42°13'0"N	6°46'0"E
Larix/Pseudotsuga Pollen	10072	45°41'5"N	7°45'40"E
Larix/Pseudotsuga Pollen	10076	47°17'30"N	10°58'35"E
Larix/Pseudotsuga Pollen	10086	47°28'26"N	12°22'38"E
Larix/Pseudotsuga Pollen	10087	47°10'0"N	13°54'0"E
Larix/Pseudotsuga Pollen	10092	46°47'1"N	10°18'38"E
Larix/Pseudotsuga Pollen	10097	49°26'45"N	19°34'0"E
Larix/Pseudotsuga Pollen	10136	46°39'58"N	11°27'30"E
Larix/Pseudotsuga Pollen	10146	47°14'35"N	12°8'20"E
Larix/Pseudotsuga Pollen	10155	46°56'15"N	11°0'55"E
Larix/Pseudotsuga Pollen	10156	55°51'0"N	30°0'0"E
Larix/Pseudotsuga Pollen	10160	47°7'0"N	13°54'0"E
Larix/Pseudotsuga Pollen	10194	46°30'54"N	10°17'7"E
Larix/Pseudotsuga Pollen	10209	54°16'0"N	22°49'0"E
Larix/Pseudotsuga Pollen	10280	46°46'28"N	17°10'13"E
Larix/Pseudotsuga Pollen	10300	47°12'57"N	17°15'18"E
Larix/Pseudotsuga Pollen	10370	46°9'4"N	8°0'44"E
Larix/Pseudotsuga Pollen	10504	42°59'11"N	10°53'0"E
Larix Pollen	5005	61°18'0"N	129°33'0"E
Larix Pollen	5015	57°2'0"N	124°7'0"E
Larix Pollen	5076	44°57'50"N	6°35'39"E
Larix Pollen	5093	66°42'0"N	79°44'0"E
Larix Pollen	5110	63°49'12"N	121°37'12"E
Larix Pollen	5143	63°40'0"N	123°15'0"E
Larix Pollen	5165	64°50'0"N	120°58'0"E
Larix Pollen	5192	61°59'0"N	129°22'0"E
Larix Pollen	5220	57°3'0"N	123°51'0"E
Larix Pollen	9227	66°42'0"N	79°44'0"E
Larix Pollen	9695	63°40'0"N	123°15'0"E
Larix Pollen	10000	61°59'0"N	129°22'0"E
Larix Pollen	10031	63°49'12"N	121°37'12"E
Larix Pollen	10191	57°3'0"N	123°51'0"E

Appendix

Fossil Type	Date (yrs B.P.)	Latitude	Longitude
Larix Pollen	10259	57°2'0"N	124°7'0"E

Appendix

Table 3: *Picea* species pollen records from European Pollen Database (EPD: http://www.europeanpollendatabase.com).
Pollen fossil record locations selected as sites where presence was dated from 4-6,000 years B.P. and 9-11,000 years B.P.
Used to produce Fig. 4.3.2 A & B.

Fossil Type	Date (yrs B.P.)	Latitude	Longitude
Picea Pollen	5256	47°1'8"N	1°53'35"W
Picea Pollen	4875	62°33'0"N	12°10'0"E
Picea Pollen	5000	47°39'0"N	12°18'0"E
Picea Pollen	4996	61°59'0"N	129°22'0"E
Picea Pollen	5005	61°18'0"N	129°33'0"E
Picea Pollen	5195	49°50'0"N	14°19'50"E
Picea Pollen	5036	53°50'0"N	14°40'0"E
Picea Pollen	5067	53°55'0"N	14°40'0"E
Picea Pollen	20	48°50'0"N	14°50'0"E
Picea Pollen	5089	49°13'0"N	14°54'0"E
Picea Pollen	5027	49°15'0"N	14°7'0"E
Picea Pollen	5046	49°13'50"N	15°22'15"E
Picea Pollen	5158	49°19'30"N	15°30'10"E
Picea Pollen	5147	50°6'0"N	16°15'0"E
Picea Pollen	4840	48°47'30"N	16°23'15"E
Picea Pollen	5052	58°1'0"N	16°4'0"E
Picea Pollen	5192	48°50'0"N	17°10'0"E
Picea Pollen	5346	48°58'40"N	17°12'10"E
Picea Pollen	5035	46°49'6"N	17°44'6"E
Picea Pollen	5249	54°42'0"N	18°10'0"E
Picea Pollen	5000	47°0'6"N	18°6'15"E
Picea Pollen	4858	54°43'0"N	18°7'0"E
Picea Pollen	5137	49°2'30"N	19°40'40"E
Picea Pollen	5208	46°21'41"N	19°59'39"E
Picea Pollen	5400	47°14'25"N	2°0'0"W
Picea Pollen	5060	53°45'0"N	20°12'0"E
Picea Pollen	4890	53°45'0"N	20°12'0"E
Picea Pollen	4960	49°22'22"N	21°53'13"E
Picea Pollen	5096	58°30'0"N	22°20'0"E
Picea Pollen	4852	41°42'0"N	23°2'0"E
Picea Pollen	4902	41°43'0"N	23°40'0"E
Picea Pollen	4960	50°20'0"N	23°57'0"E
Picea Pollen	5051	58°22'0"N	23°58'0"E
Picea Pollen	5300	49°55'0"N	24°1'0"E
Picea Pollen	4960	50°25'0"N	24°10'0"E
Picea Pollen	5020	50°58'0"N	24°13'0"E
Picea Pollen	4960	49°48'0"N	24°14'0"E
Picea Pollen	5408	51°6'0"N	24°20'0"E
Picea Pollen	5193	50°23'0"N	24°38'0"E
Picea Pollen	4960	50°16'0"N	24°45'0"E
Picea Pollen	4960	50°13'0"N	24°50'0"E
Picea Pollen	4960	50°20'0"N	24°7'0"E
Picea Pollen	4950	53°26'0"N	25°55'0"E
Picea Pollen	5132	56°46'0"N	26°11'0"E

Appendix

Fossil Type	Date (yrs B.P.)	Latitude	Longitude
Picea Pollen	4800	54°57'0"N	26°25'0"E
Picea Pollen	5020	53°25'0"N	26°26'0"E
Picea Pollen	5098	53°16'0"N	26°4'0"E
Picea Pollen	4960	50°16'0"N	26°50'0"E
Picea Pollen	5012	44°7'1"N	26°57'0"E
Picea Pollen	4963	58°24'0"N	27°14'0"E
Picea Pollen	5109	57°41'0"N	27°15'0"E
Picea Pollen	4955	59°13'0"N	27°35'0"E
Picea Pollen	5160	55°38'0"N	27°46'0"E
Picea Pollen	4591	51°12'0"N	28°0'0"E
Picea Pollen	5495	51°12'0"N	28°0'0"E
Picea Pollen	4800	54°11'0"N	28°12'0"E
Picea Pollen	4640	42°4'3"N	28°53'20"E
Picea Pollen	5007	54°2'0"N	28°6'0"E
Picea Pollen	4800	55°51'0"N	30°0'0"E
Picea Pollen	5233	54°13'0"N	30°0'1"E
Picea Pollen	4880	64°34'0"N	30°32'0"E
Picea Pollen	5002	66°21'0"N	30°34'0"E
Picea Pollen	5359	66°21'0"N	30°34'0"E
Picea Pollen	5165	66°22'0"N	30°42'0"E
Picea Pollen	882	64°34'0"N	30°50'0"E
Picea Pollen	4965	56°0'0"N	31°59'0"E
Picea Pollen	5020	56°12'0"N	32°0'0"E
Picea Pollen	5096	65°7'0"N	32°38'0"E
Picea Pollen	4979	65°7'0"N	32°38'0"E
Picea Pollen	4910	62°2'0"N	32°46'0"E
Picea Pollen	4918	62°49'0"N	33°34'40"E
Picea Pollen	4925	62°17'0"N	33°39'0"E
Picea Pollen	5078	62°12'0"N	33°48'0"E
Picea Pollen	4876	62°19'0"N	33°51'0"E
Picea Pollen	5075	62°45'0"N	34°35'0"E
Picea Pollen	4960	50°54'0"N	35°13'0"E
Picea Pollen	4915	63°54'0"N	36°15'0"E
Picea Pollen	4997	61°4'0"N	36°3'0"E
Picea Pollen	4838	56°49'0"N	38°46'0"E
Picea Pollen	5000	57°11'0"N	39°27'5"E
Picea Pollen	4970	44°14'30"N	6°42'8"E
Picea Pollen	5185	68°51'0"N	66°54'0"E
Picea Pollen	5044	46°38'45"N	7°32'36"E
Picea Pollen	4947	46°43'30"N	7°34'30"E
Picea Pollen	5189	45°41'5"N	7°45'40"E
Picea Pollen	5189	45°41'5"N	7°45'40"E
Picea Pollen	4909	46°10'36"N	7°5'37"E
Picea Pollen	4876	43°48'0"N	7°6'0"E
Picea Pollen	4940	53°36'54"N	8°44'13"E
Picea Pollen	9180	49°15'0"N	14°7'0"E
Picea Pollen	9603	44°21'0"N	5°14'0"E

Appendix

Fossil Type	Date (yrs B.P.)	Latitude	Longitude
Picea Pollen	9684	56°12'0"N	32°0'0"E
Picea Pollen	9842	55°38'0"N	27°46'0"E
Picea Pollen	9915	53°45'0"N	20°12'0"E
Picea Pollen	9937	49°13'0"N	14°54'0"E
Picea Pollen	9945	53°45'0"N	20°12'0"E
Picea Pollen	9982	49°43'0"N	21°35'0"E
Picea Pollen	9993	58°17'0"N	14°14'0"E
Picea Pollen	10000	49°13'0"N	14°54'0"E
Picea Pollen	10000	49°13'50"N	15°22'15"E
Picea Pollen	10000	47°0'6"N	18°6'15"E
Picea Pollen	10000	49°55'0"N	23°46'0"E
Picea Pollen	10003	56°13'0"N	15°13'0"E
Picea Pollen	10006	49°43'0"N	21°35'0"E
Picea Pollen	10011	54°42'0"N	18°10'0"E
Picea Pollen	10011	49°22'22"N	21°53'13"E
Picea Pollen	10012	53°26'0"N	25°55'0"E
Picea Pollen	10016	50°6'0"N	16°15'0"E
Picea Pollen	10016	54°2'0"N	28°6'0"E
Picea Pollen	10029	56°14'0"N	15°19'0"E
Picea Pollen	10035	49°2'30"N	15°11'30"E
Picea Pollen	10038	49°2'30"N	19°40'40"E
Picea Pollen	10040	43°48'0"N	7°6'0"E
Picea Pollen	10043	57°42'20"N	12°23'35"E
Picea Pollen	10044	51°33'15"N	4°46'10"E
Picea Pollen	10046	62°12'0"N	33°48'0"E
Picea Pollen	10052	58°1'0"N	16°4'0"E
Picea Pollen	10067	54°13'0"N	30°0'1"E
Picea Pollen	10070	46°49'6"N	17°44'6"E
Picea Pollen	10072	46°44'40"N	17°24'3"E
Picea Pollen	10072	62°0'0"N	76°40'0"E
Picea Pollen	10076	53°25'0"N	26°26'0"E
Picea Pollen	10078	46°21'41"N	19°59'39"E
Picea Pollen	10090	53°55'0"N	14°40'0"E
Picea Pollen	10094	62°49'0"N	33°34'40"E
Picea Pollen	10119	49°19'30"N	15°30'10"E
Picea Pollen	10123	59°26'0"N	25°0'0"E
Picea Pollen	10124	62°17'0"N	33°39'0"E
Picea Pollen	10125	57°45'6"N	12°51'40"E
Picea Pollen	10136	47°39'0"N	12°18'0"E
Picea Pollen	10154	54°11'0"N	28°12'0"E
Picea Pollen	10156	55°51'0"N	30°0'0"E
Picea Pollen	10163	56°18'0"N	14°59'0"E
Picea Pollen	10165	50°58'0"N	24°13'0"E
Picea Pollen	10173	62°19'0"N	33°51'0"E
Picea Pollen	10190	53°16'0"N	26°4'0"E
Picea Pollen	10200	54°57'0"N	26°25'0"E
Picea Pollen	10224	61°4'0"N	36°3'0"E

Appendix

Fossil Type	Date (yrs B.P.)	Latitude	Longitude
Picea Pollen	10267	57°11'0"N	39°27'5"E
Picea Pollen	10274	54°43'0"N	18°7'0"E
Picea Pollen	10292	58°24'0"N	27°14'0"E
Picea Pollen	10303	56°46'0"N	26°11'0"E
Picea Pollen	10400	65°7'0"N	32°38'0"E
Picea Pollen	10517	56°24'0"N	2°54'0"
Picea Pollen	10520	68°51'0"N	66°54'0"
Picea Pollen	10594	58°25'0"N	13°50'0"
Picea Pollen	10724	57°10'0"N	16°9'0"

Appendix

Table 4:   *Pinus* species pollen records from European Pollen Database (EPD: http://www.europeanpollendatabase.com).
Pollen fossil record locations selected as sites where presence was dated from 4-6,000 years B.P. and 9-11,000 years B.P.
Used to produce Fig. 4.3.3 A & B.

Fossil Type	Date (yrs B.P.)	Latitude	Longitude
Pinus Pollen	5188	48°32'54"N	0°15'30"W
Pinus Pollen	5020	39°6'0"N	0°41'0"W
Pinus Pollen	4503	52°35'0"N	0°5'0"E
Pinus Pollen	5000	54°43'0"N	1°18'0"W
Pinus Pollen	4942	45°50'59"N	1°38'45"E
Pinus Pollen	5012	47°16'7"N	1°45'0"W
Pinus Pollen	5023	47°15'40"N	1°46'50"W
Pinus Pollen	4896	37°12'30"N	1°49'25"W
Pinus Pollen	5005	47°11'10"N	1°51'29"W
Pinus Pollen	4983	47°1'8"N	1°53'35"W
Pinus Pollen	5063	47°18'28"N	1°57'55"W
Pinus Pollen	4975	62°33'0"N	12°10'0"E
Pinus Pollen	5000	47°39'0"N	12°18'0"E
Pinus Pollen	5021	68°8'0"N	13°35'0"E
Pinus Pollen	5195	49°50'0"N	14°19'50"E
Pinus Pollen	5036	53°50'0"N	14°40'0"E
Pinus Pollen	5067	53°55'0"N	14°40'0"E
Pinus Pollen	5020	48°50'0"N	14°50'0"E
Pinus Pollen	5089	49°13'0"N	14°54'0"E
Pinus Pollen	5027	49°15'0"N	14°7'0"E
Pinus Pollen	5046	49°13'50"N	15°22'15"E
Pinus Pollen	5158	49°19'30"N	15°30'10"E
Pinus Pollen	5147	50°6'0"N	16°15'0"E
Pinus Pollen	5052	58°1'0"N	16°4'0"E
Pinus Pollen	4844	48°50'0"N	17°10'0"E
Pinus Pollen	5346	48°58'40"N	17°12'10"E
Pinus Pollen	4936	54°42'0"N	18°10'0"E
Pinus Pollen	5005	54°43'0"N	18°7'0"E
Pinus Pollen	4960	49°2'30"N	19°40'40"E
Pinus Pollen	4800	47°14'25"N	2°0'0"W
Pinus Pollen	5062	47°15'54"N	2°1'0"W
Pinus Pollen	5009	36°47'40"N	2°35'20"W
Pinus Pollen	5009	36°46'25"N	2°36'5"W
Pinus Pollen	4941	49°27'45"N	2°41'28"E
Pinus Pollen	5045	45°31'0"N	2°49'0"E
Pinus Pollen	5145	45°8'22"N	2°51'33"E
Pinus Pollen	5015	52°48'30"N	2°6'30"W
Pinus Pollen	4922	47°14'18"N	2°9'0"W
Pinus Pollen	4960	49°22'22"N	21°53'13"E
Pinus Pollen	5096	58°30'0"N	22°20'0"E
Pinus Pollen	4852	41°42'0"N	23°2'0"E
Pinus Pollen	5000	49°55'0"N	23°46'0"E
Pinus Pollen	4700	49°40'0"N	23°56'0"E
Pinus Pollen	4960	50°20'0"N	23°57'0"E

Appendix

Fossil Type	Date (yrs B.P.)	Latitude	Longitude
Pinus Pollen	5051	58°22'0"N	23°58'0"E
Pinus Pollen	5300	49°55'0"N	24°1'0"E
Pinus Pollen	4960	50°25'0"N	24°10'0"E
Pinus Pollen	5020	50°58'0"N	24°13'0"E
Pinus Pollen	4960	49°48'0"N	24°14'0"E
Pinus Pollen	4992	51°6'0"N	24°20'0"E
Pinus Pollen	4960	50°16'0"N	24°45'0"E
Pinus Pollen	4960	50°13'0"N	24°50'0"E
Pinus Pollen	4960	50°20'0"N	24°7'0"E
Pinus Pollen	5180	49°45'0"N	25°27'0"E
Pinus Pollen	4950	53°26'0"N	25°55'0"E
Pinus Pollen	5132	56°46'0"N	26°11'0"E
Pinus Pollen	4800	54°57'0"N	26°25'0"E
Pinus Pollen	5020	53°25'0"N	26°26'0"E
Pinus Pollen	5098	53°16'0"N	26°4'0"E
Pinus Pollen	5210	54°49'0"N	26°45'0"E
Pinus Pollen	4960	50°16'0"N	26°50'0"E
Pinus Pollen	4963	58°24'0"N	27°14'0"E
Pinus Pollen	5109	57°41'0"N	27°15'0"E
Pinus Pollen	5066	59°13'0"N	27°35'0"E
Pinus Pollen	4800	55°38'0"N	27°46'0"E
Pinus Pollen	4650	51°12'0"N	28°0'0"E
Pinus Pollen	5333	51°12'0"N	28°0'0"E
Pinus Pollen	4569	51°12'0"N	28°0'0"E
Pinus Pollen	4800	54°11'0"N	28°12'0"E
Pinus Pollen	5400	53°33'0"N	28°36'0"E
Pinus Pollen	5007	54°2'0"N	28°6'0"E
Pinus Pollen	4878	42°2'0"N	3°1'0"W
Pinus Pollen	4951	57°0'0"N	3°26'0"W
Pinus Pollen	4965	48°25'0"N	3°40'0"W
Pinus Pollen	5020	43°7'17"N	3°42'2"W
Pinus Pollen	5146	39°56'13"N	3°57'54"E
Pinus Pollen	4974	39°47'34"N	3°7'9"E
Pinus Pollen	4800	55°51'0"N	30°0'0"E
Pinus Pollen	4867	54°13'0"N	30°0'1"E
Pinus Pollen	4700	50°25'0"N	34°0'0"E
Pinus Pollen	4960	50°33'0"N	34°30'0"E
Pinus Pollen	5250	50°25'0"N	35°24'0"E
Pinus Pollen	5250	49°44'0"N	37°40'0"E
Pinus Pollen	4995	57°11'0"N	39°27'5"E
Pinus Pollen	4763	52°15'0"N	39°50'0"E
Pinus Pollen	4867	39°55'29"N	4°1'38"E
Pinus Pollen	5033	43°7'0"N	4°21'51"W
Pinus Pollen	4590	43°12'56"N	4°26'10"W
Pinus Pollen	5000	39°52'30"N	4°7'35"E
Pinus Pollen	4994	39°52'14"N	4°7'53"E
Pinus Pollen	4983	35°14'0"N	41°11'0"E

Appendix

Fossil Type	Date (yrs B.P.)	Latitude	Longitude
Pinus Pollen	5073	58°3'38"N	5°10'30"W
Pinus Pollen	5125	57°34'6"N	5°19'40"W
Pinus Pollen	5058	57°33'32"N	5°20'37"W
Pinus Pollen	5014	54°56'0"N	6°18'0"W
Pinus Pollen	4970	44°14'30"N	6°42'8"E
Pinus Pollen	5026	42°13'0"N	6°46'0"W
Pinus Pollen	5044	46°38'45"N	7°32'36"E
Pinus Pollen	4947	46°43'30"N	7°34'30"E
Pinus Pollen	5189	45°41'5"N	7°45'40"E
Pinus Pollen	5100	43°48'0"N	7°6'0"E
Pinus Pollen	5160	56°8'0"N	8°38'0"E
Pinus Pollen	4940	53°36'54"N	8°44'13"E
Pinus Pollen	5036	53°40'0"N	8°45'50"E
Pinus Pollen	9000	50°20'0"N	24¡7'0"E
Pinus Pollen	9000	50°16'0"N	26¡50'0"E
Pinus Pollen	9408	59°13'0"N	27¡35'0"E
Pinus Pollen	9671	39°6'0"N	0¡41'0"W
Pinus Pollen	9704	44°14'30"N	6¡42'8"E
Pinus Pollen	9785	51°12'0"N	28¡0'0"E
Pinus Pollen	9788	56°8'0"N	8¡38'0"E
Pinus Pollen	9800	39°55'29"N	4¡1'38"E
Pinus Pollen	9842	54°49'0"N	26¡45'0"E
Pinus Pollen	9842	55°38'0"N	27¡46'0"E
Pinus Pollen	9890	39°39'0"N	20¡55'0"E
Pinus Pollen	9892	58°22'0"N	23¡58'0"E
Pinus Pollen	9894	47°39'0"N	12¡18'0"E
Pinus Pollen	9900	57°45'6"N	12¡51'40"E
Pinus Pollen	9907	49°19'30"N	15¡30'10"E
Pinus Pollen	9916	57°27'0"N	6¡12'0"W
Pinus Pollen	9928	45°28'24"N	5¡25'0"E
Pinus Pollen	9930	42°2'0"N	3¡1'0"W
Pinus Pollen	9934	48°58'40"N	17¡12'10"E
Pinus Pollen	9938	50°58'0"N	24¡13'0"E
Pinus Pollen	9941	57°0'0"N	3¡26'0"W
Pinus Pollen	9947	53°55'0"N	14¡40'0"E
Pinus Pollen	9947	58°5'0"N	5¡0'0"W
Pinus Pollen	9957	56°24'0"N	2¡54'0"W
Pinus Pollen	9958	52°48'30"N	2¡6'30"W
Pinus Pollen	9962	54°43'0"N	18¡7'0"E
Pinus Pollen	9971	57°42'20"N	12¡23'35"E
Pinus Pollen	9980	36°46'25"N	2¡36'5"W
Pinus Pollen	9981	56°23'0"N	3¡5'0"W
Pinus Pollen	9987	49°27'45"N	2¡41'28"E
Pinus Pollen	9991	58°24'0"N	27¡14'0"E
Pinus Pollen	9993	58°17'0"N	14¡14'0"E
Pinus Pollen	9993	52°14'13"N	5¡45'43"E
Pinus Pollen	9999	47°4'32"N	8¡19'32"E

Appendix

Fossil Type	Date (yrs B.P.)	Latitude	Longitude
Pinus Pollen	10000	49°13'0"N	14¡54'0"E
Pinus Pollen	10000	49°13'50"	15¡22'15"E
Pinus Pollen	10000	49°55'0"	23¡46'0"E
Pinus Pollen	10000	50°20'0"	23¡57'0"E
Pinus Pollen	10000	50°25'0"	24¡10'0"E
Pinus Pollen	10000	50°16'0"	24¡45'0"E
Pinus Pollen	10000	50°25'0"	34¡0'0"E
Pinus Pollen	10000	50°25'0"	35¡24'0"E
Pinus Pollen	10000	49°44'0"	37¡40'0"E
Pinus Pollen	10000	44°21'0"	5¡14'0"E
Pinus Pollen	10000	43°48'0"	7¡6'0"E
Pinus Pollen	10003	56°13'0"	15¡13'0"E
Pinus Pollen	10007	53°44'0"	0¡4'0"W
Pinus Pollen	10008	56°46'0"	26¡11'0"E
Pinus Pollen	10008	54°56'0"	6¡18'0"W
Pinus Pollen	10010	46°38'45"	7¡32'36"E
Pinus Pollen	10011	54°42'0"	18¡10'0"E
Pinus Pollen	10011	49°22'22"	21¡53'13"E
Pinus Pollen	10012	53°26'0"	25¡55'0"E
Pinus Pollen	10016	50°6'0"	16¡15'0"E
Pinus Pollen	10016	54°2'0"	28¡6'0"E
Pinus Pollen	10019	45°50'59"	1¡38'45"E
Pinus Pollen	10021	58°3'38"	5¡10'30"W
Pinus Pollen	10023	57°10'0"	16¡9'0"E
Pinus Pollen	10029	56°14'0"	15¡19'0"E
Pinus Pollen	10029	57°11'0"	6¡18'0"W
Pinus Pollen	10035	49°2'30"	15¡11'30"E
Pinus Pollen	10038	49°2'30"	19¡40'40"E
Pinus Pollen	10044	51°33'15"	4¡46'10"E
Pinus Pollen	10045	45°16'28"	2¡40'45"E
Pinus Pollen	10047	56°32'0"	14¡33'20"E
Pinus Pollen	10050	56°17'0"	12¡31'0"E
Pinus Pollen	10052	58°1'0"	16¡4'0"E
Pinus Pollen	10065	56°18'0"	14¡59'0"E
Pinus Pollen	10067	54°13'0"	30¡0'1"E
Pinus Pollen	10068	58°25'0"	13¡50'0"E
Pinus Pollen	10072	42°13'0"	6¡46'0"W
Pinus Pollen	10072	45°41'5"	7¡45'40"E
Pinus Pollen	10076	53°25'0"	26¡26'0"E
Pinus Pollen	10080	46°43'30"	7¡34'30"E
Pinus Pollen	10100	48°32'54"	0¡15'30"W
Pinus Pollen	10110	57°33'32"	5¡20'37"W
Pinus Pollen	10123	57°5'0"	12¡32'0"E
Pinus Pollen	10123	59°26'0"	25¡0'0"E
Pinus Pollen	10124	45°22'38"	2¡54'17"E
Pinus Pollen	10154	54°11'0"	28¡12'0"E
Pinus Pollen	10156	55°51'0"	30¡0'0"E

Appendix

Fossil Type	Date (yrs B.P.)	Latitude	Longitude
Pinus Pollen	10190	53°16'0"	26¡4'0"E
Pinus Pollen	10200	54°57'0"	26¡25'0"E
Pinus Pollen	10273	56°16'0"N	15¡1'0"E
Pinus Pollen	10417	56°19'0"N	15¡23'0"E
Pinus Pollen	10417	53°33'0"N	28¡36'0"E
Pinus Pollen	10670	51°34'43"N	6¡5'41"E
Pinus Pollen	10814	50°32'0"N	4¡36'0"W

Fossil Type	Date (yrs B.P.)	Latitude	Longitude

Maxent:

The user-friendly java-based interface provided with the freely downloadable Maxent package (ver. 3.3.3e) (Phillips & Schapire, 2005) required the input of two separate tabular datasets in a comma delimited format (.csv). The niche-model building dataset was a presence only data table where each row represented a grid cell with the species present and was denoted by a species ID followed by longitude, latitude, the three present bioclimatic variable values attributed to that location.

Example of species distribution input:

```
Loxia_curvirostra,longitude,latitude,GDD5,MTCO,AETPET
Loxia_curvirostra,108.25,11.25,7489,23.4,0.854
Loxia_curvirostra,108.75,11.25,7638,23.7,0.862
Loxia_curvirostra,107.75,11.75,6740,21.5,0.827
Loxia_curvirostra,108.25,11.75,6244,20.3,0.868
Loxia_curvirostra,108.75,11.75,6802,21.5,0.871
Loxia_curvirostra,107.75,12.25,6762,21.5,0.827
Loxia_curvirostra,108.25,12.25,6333,20.3,0.867
Loxia_curvirostra,108.75,12.25,6178,19.6,0.878
Loxia_curvirostra,-86.75,12.75,7684,25,0.649
Loxia_curvirostra,-86.25,12.75,7143,23.3,0.647
Loxia_curvirostra,-85.75,12.75,6614,21.5,0.704
…
```

The 'background' datasets, again with column headings, comprised of all gridded present or palaeo bioclimatic variables assigned to their relevant longitudes and latitudes, with a separate data set for each scenario.

Example of bioclimate grid:

```
background,longitude,latitude,GDD5,MTCO,AETPET
background,-80.25,0.25,7034,23.4,0.899
background,-79.75,0.25,7131,23.8,0.992
background,-79.25,0.25,7208,24.1,1
background,-78.75,0.25,5049,18.5,1
background,-78.25,0.25,3060,13,0.986
background,-77.75,0.25,3595,14.3,1
background,-77.25,0.25,6703,22.6,1
background,-76.75,0.25,7451,24.4,1
background,-76.25,0.25,7584,24.6,1
background,-75.75,0.25,7606,24.6,1
background,-75.25,0.25,7609,24.6,1
background,-74.75,0.25,7596,24.5,1
background,-74.25,0.25,7618,24.7,1
background,-73.75,0.25,7508,24.4,1
background,-73.25,0.25,7557,24.4,1
background,-72.75,0.25,7624,24.7,1
background,-72.25,0.25,7597,24.6,1
…
```

Having produced the species specific niche-model using the fitting function features, Maxent then applies this to the bioclimatic background to produce for each grid cell, identified by its longitude and latitude, a probability of occurrence between 1.0 and 0.0, 1.0 being complete certainty of presence and 0.0 being complete certainty of absence.

Example of output:

```
longitude,latitude,curvi2 logistic values
-80.25,0.25,0.03945493
-79.75,0.25,0.034194473
-79.25,0.25,0.019460367
-78.75,0.25,0.20792145
-78.25,0.25,0.5268079
-77.75,0.25,0.4557937
-77.25,0.25,0.049431145
-76.75,0.25,0.016430307
-76.25,0.25,0.015004969
-75.75,0.25,0.014717531
-75.25,0.25,0.014678706
-74.75,0.25,0.014662265
-74.25,0.25,0.014746845
-73.75,0.25,0.015638009
-73.25,0.25,0.014983322
-72.75,0.25,0.014669027
-72.25,0.25,0.014834542
...
```

In this way, Maxent produces simulated ranges for the species of interest based on environmental suitability for both present and for each of the past scenarios.

Appendix
GAM:

The input dataset for forming the fitted GAMs comprised of all the available present-day bioclimatic values for the gridded background, a row for each grid cell which is identified by its longitude and latitude followed by the three bioclimatic values attributed to it, and lastly the occurrence of the species, 1.0 for presence or 0.0 for absence.   This tabular dataset had column headings for referencing during the modelling process and was saved in a comma delimited format (.csv)

Example of input dataset:

```
LONG,LAT,GDD5,MTCO,APET,PRESENCE
-80.25,0.25,7034,23.4,0.899,0
-79.75,0.25,7131,23.8,0.992,0
-79.25,0.25,7208,24.1,1,0
-78.75,0.25,5049,18.5,1,0
-78.25,0.25,3060,13,0.986,0
-77.75,0.25,3595,14.3,1,0
-77.25,0.25,6703,22.6,1,0
-76.75,0.25,7451,24.4,1,0
-76.25,0.25,7584,24.6,1,0
-75.75,0.25,7606,24.6,1,0
-75.25,0.25,7609,24.6,1,0
-74.75,0.25,7596,24.5,1,0
-74.25,0.25,7618,24.7,1,0
-73.75,0.25,7508,24.4,1,0
-73.25,0.25,7557,24.4,1,0
-72.75,0.25,7624,24.7,1,0
-72.25,0.25,7597,24.6,1,0
...
```

In R, using the mgcv package, the fitted GAM was created by using the command "gam" and specifying, using the column headings, firstly the response variable, the presence/absence of the species, and then the covariates, the bioclimatic value columns, followed by the probability distribution family and the source of the data table within R.

Example of Model Run:

```
curvi <- read.csv("curvi.csv", header=TRUE , sep = ",")

curvimod <- gam(PRESENCE~s(GDD5)+s(MTCO)+s(APET), family="binomial", data = curvi)
```

Having produced the fitted GAM for the species' bioclimatic niche, the predicted distributions for the present and past were produced by combining this model with separate 'background' bioclimatic datasets, containing just longitudes, latitudes and the three relevant bioclimatic variables and specifying that the output should be a 'response', an automatic transformation of the linear predictors as described.

Example of the background data set: 1k_bioclimate.csv

```
LONG,LAT,GDD5,MTCO,APET
-80.25,0.25,6985,23.3,0.883
-79.75,0.25,7082,23.6,0.975
-79.25,0.25,7159,23.9,1
-78.75,0.25,5001,18.3,1
-78.25,0.25,3014,12.8,0.978
-77.75,0.25,3552,14.1,1
-77.25,0.25,6663,22.4,1
-76.75,0.25,7415,24.2,1
-76.25,0.25,7552,24.4,1
-75.75,0.25,7576,24.5,1
-75.25,0.25,7582,24.5,1
-74.75,0.25,7571,24.4,1
-74.25,0.25,7594,24.6,1
-73.75,0.25,7485,24.3,1
-73.25,0.25,7532,24.4,1
-72.75,0.25,7599,24.6,1
-72.25,0.25,7570,24.6,1
...
```

Example of the simulation run:

```
onek <- read.csv("1k_bioclimate.csv", header=TRUE , sep = ",")

curvi_onek<- predict(curvimod, newdata = onek, type = "response")
```

Appendix

The output from the 'predict' function was a probability of presence assigned to each of the grid cells, labelled by a grid ID corresponding to the order in the background dataset and this was exported as a comma delimited table.

Example of output:

```
"","x"
"1",0.0312244259371005
"2",0.0212770684885095
"3",0.0150670358332323
"4",0.162415930741516
"5",0.671763710471596
"6",0.598894314109012
"7",0.0459054117474095
"8",0.00980435279599011
"9",0.0082063242907866
"10",0.00800097274706333
"11",0.00794173980905715
"12",0.0080123814899209
"13",0.00786293600549903
"14",0.00891927073010157
"15",0.00841963362802929
"16",0.00781513004780271
"17",0.00809952192411836
"18",0.00943138260565394
...
```

R also facilitates the merging of multiple prediction datasets, using a 'merge' function, as well as the renaming of column headings to relevant names from the default "x" attributed to the probability prediction column.

Example of a **simple** merge command:

```
Onek_all <- data.frame(curvi_Onek,larix_Onek,leuco_Onek,...)
names(Onek_all) <- c("curvi","larix","leuco",...)
write.csv(Onek_all, file="H5_allspecies.csv")
```

Example of output:

```
,curvi,larix,leuco
1,0.061395264,3.34E-10,2.22E-16
2,0.065494837,7.69E-10,2.22E-16
3,0.033655966,1.33E-09,2.22E-16
4,0.180350638,0.121792161,1.50E-09
5,0.609581867,0.083793073,6.46E-06
6,0.491607914,0.146599637,1.82E-06
7,0.125366912,2.08E-07,9.13E-13
8,0.031166067,1.52E-10,2.22E-16
9,0.037211526,3.26E-11,2.22E-16
10,0.039612987,4.85E-11,2.22E-16
11,0.027806271,4.64E-11,2.22E-16
12,0.019841149,6.44E-11,2.22E-16
13,0.018024862,6.86E-12,2.22E-16
14,0.02863052,1.51E-11,2.22E-16
15,0.02642343,2.84E-12,2.22E-16
...
```

CRS:

CRS required the input of a dataset containing values for presence (1), absence (0) and no data (-9) saved in a space-delimited format (.asc) and grid IDs as well as longitudes and latitudes which corresponded to those in the bioclimatic dataset (.biocli) which had the three bioclimatic variables; absences of bioclimatic data were represented by -9999 for GDD5, -99.9.

Example of .asc file:

```
      0-179.750    0.250 ...      0   0   0
      1-179.250    0.250 ...      0   0   0
      2-178.750    0.250 ...      0   0   0
      3-178.250    0.250 ...      0   0   0
...
```

Example of .biocli file:

```
      0-179.750    0.250 ... -9999.-9999.-99.9-99.9  -9.999
      1-179.250    0.250 ... -9999.-9999.-99.9-99.9  -9.999
      2-178.750    0.250 ... -9999.-9999.-99.9-99.9  -9.999
      3-178.250    0.250 ... -9999.-9999.-99.9-99.9  -9.999
...
```

This was defined by an information file (.inf) which also specified; the columns to be read in; the size of the columns; the maximum, minimum and no data values, and the nodal grid size.

Example of .inf file:

```
AFEGIS
curvi
present.biocli
curvi
1 5
pytyop      9.00      0.00      -1.0
GDDO   11050.00      0.00   -9999.0
GDD5    9225.00      0.00   -9999.0
MTCO      29.00    -53.00     -99.9
MTWA      37.00    -12.00     -99.9
AET/PET    1.00      0.00    -9.999
122400
(a6,87x,f2.0)
(a6,80x,2f6.0,2f5.1,f8.3)
0
curvi2
1 0.01 0 0 0 3 3 0.0 9600.0 600.0 64 4 -56.0 31.0 6.0 58 6 -0.0125
1.0125 0.0625 41
```

Appendix

The output from this was the fitted response surface given the file name '.fit' to be used in the later simulations.

Example of .fit file:

```
 1:Lox_curv      3:GDD5          4:MTCO          6:AET/PET
 1 440 1    75.000 -50.750   0.975   0.000  1  0.0000 197    0
 1 441 1    75.000 -50.750   1.000   0.000  1  0.0000 190    0
 1 540 1    75.000 -49.250   0.975   0.000  1  0.0000 254    0
 1 541 1    75.000 -49.250   1.000   0.000  1  0.0000 246    0
 1 640 1    75.000 -47.750   0.975   0.000  1  0.0000 271    0
...
```

Again, simulations of potential range were run in Unix using a Fortran based programme, which combined, using a similar .inf file, the fit with the bioclimatic dataset which the model was originally derived from to simulate the probabilities of occurrences based on the response surface generated.   The output from this is a space delimited file with the file notation of '.sim', with grid IDs relating to the locations and associated bioclimatic values in the covariate datasets.

Example of .sim file:

```
...
 194     -9999
 195     -9999
 196     -9999
 197     -9999
 198     -9999
 199         7
 200        10
 201         3
 202        96
 203         0
 204       113
...
```

Notably the probabilities of occurrence have already been transformed in the model from 1.0 to 0.0 decimal values to be integer values, through multiplication by 1000, to values between 1000 and 0.   In addition as the bioclimatic dataset also included absences of data, these were attributed the value -9999.

Maximum κ value:

These maximum κ values were generated using a Fortran programme, running in a Unix environment, which combined the simulated (.sim) probabilities of occurrence with the original species distribution dataset (.asc) using a small text file (.obi) to denote the locations of these files and also the columns to be read in.

Example of an obi:

```
curvi.asc
curvi_norm.sim
curvi.asc
curvi_norm
(a6,80x,6x,f3.0)
(a9,1x,i5)
1 -1.0 -999.9 1
```

The output file contained the results of all the 1000 interval runs and also a selection of summary statistics.

The simulated outputs for both GAMs and Maxent were also run through this same programme, rather than using inbuilt assessments, and evaluated in relation to the original driving presence/absence data used in the models, to get the 'goodness of fit' measures.   Note that both these models original outputs as decimals were not compatible with the expected input into the evaluation programme, therefore they were transformed in Microsoft Excel, to be values between 1000 and 0; simply put each value was rounded to 3 significant figures and multiplied by 1000 to get whole integers for evaluating.   This simple transformation had no effect on the thresholds or evaluation of the model's performance.   During this process, the files were also saved in a space delimited format to comply with the requirement of the programme.

Mapping:

For the CRS model this was relatively simple as the simulated probability values were outputted in a grid containing all grid IDs which directly related to the original 0.5º x 0.5º Arc grid used to intersect the polygons as well as all being integer values ranging between 0-1000.   The grid IDs were the numbered grid squares, notably beginning at 0 rather than 1, starting in the south-west corner (bottom-left) and numbered sequentially left to right through to the north-east corner (top-right).   The simulated probabilities were combined into a large data set, with the ID numbers followed by columns for each of the simulated scenario probability values saved in a comma delimited format.   Using Arc, firstly a template was established of the grid IDs with the attributed longitude and latitudes

Example .csv of longlats:

```
1,-31.099,39.697
2,-31.199,39.438
3,-28.699,38.583
4,-28.295,38.462
5,-28.046,38.663
6,-27.219,38.712
7,-28.052,39.05
8,-25.113,36.967
```

Example Arc commands:

```
Arc: generate template
      Generate: input longlats.csv
      Generate: points
      Generate: quit
Arc: build template point (creates the .pat file)
```

Then a lambert azimuthal equal-area projection was applied to this template using the "project coverage" commands.

Example of Arc commands:

```
Arc: project cover template template2
     Project: input template
     Project: projection geographic
     Project: units dd (decimal degrees)
     Project: parameters
     Project: output
     Project: projection lambert_azimuth
     Project: units meters
     Project: parameters (Take defaults)
     Project: end
```

Having defined the simulated dataset using an arc macro language (aml) file, which denotes the column headings and length of the numerical value in each column, copies of this template were then combined using the Arc 'joinitem' command with the simulated species datasets, merging the grid IDs, and thus the simulated values, with the longitudes and latitudes in the template.

Example .aml file:

```
tables
define curvi
templatecurvi-id
6
6
b
present
6
6
i
onek
6
i
```

Example Arc script:

```
Arc: &run simulated.aml
          Item Name: "Press Enter"
      Tables: add from curvi.csv
      Tables: quit

Arc: joinitem templatecurvi.pat curvi templatecurvi.pat templatecurvi-id
```

These files were then viewable in ArcMap either on any of the predefined maps or could be customised in varying manners.   An array of in-built symbology options allows the selection of markers to represent presence/absence to produce effective representative maps which can be exported in a variety of output formats, such as Portable Document Format (.pdf) and Joint Photographic Group (.jpg) as well as many others.

The probability thresholds can be applied before or after viewing in ArcMap, either during the original manipulation of the simulated datasets into the comma delimited fileusing a programme such as Microsoft Excel, where the values equal or above the threshold are replaced with 1 and absences, 0, using the IF function. Thresholds could also be established in ArcMap using the symbology to define the thresholds above or below which a symbol should be displayed.   However, the large datasets that were being dealt with in this study were not suited for such processing in ArcMap and so instead the former method of predefining the simulated presence or absence in Microsoft Excel was preferentially used for map production.

In the case of GAMs and Maxent, the mapping was slightly more complicated by the fact that the simulated probability values had no longitude or latitudes labels and were produced for datasets which only included grid cells that had bioclimatic variables associated.   This meant that many of the grid squares had been removed, yet a complete grid with all the IDs for all longitude and latitudes, including the sea for example, would be required to map effectively in Arc.   In Excel, the original bioclimatic files containing all present and absent data along with all the IDs were used firstly to label the simulated output attributed to the bioclimatic values using the relevant IDs and then to add the additional absent data.   The grid IDs were then sorted into a sequential order to mirror the template data.   Markedly, this process was further convoluted by the fact that each palaeoclimate scenario had different sea levels, affecting the exposure of the shelf and the size of the bioclimatic dataset available.   Bearing this in mind, each simulation had to be sorted in relation to its relevant bioclimatic dataset in order that the correct localities were attributed.   Thresholding, in this study, was conducted, as with CRS, in Microsoft Excel.

Appendix

Automapping:

For this process, an un-projected template of just longitudes and latitudes was combined with each of the species' simulated output datasets, compiled as described above, using the method already outlined. In addition, the changing sea-level overlays were generated as individual layers to be inputted during the automapping process. The automapping arc macro language programme, used in Grid, took the selected species simulations, mapping them with the symbol size and style as articulated in the script and combined them with the relevant sea level layer. This script could also handle pre-thresholded data as well as the thresholding of the datasets, depending on the requirements of the user. The outputs were Encapsulated Postscript files (.eps) which were then combined using a pdf generating programme with simple figure legends denoting the species, model type and year simulated.

Example of .aml:

```
&args sp_distn timeslice name1 name2
map distn_map
pageunits cm
pagesize 21.0 29.7
linecolor cmyk -1 -1 -1 100
mape curvi

shadeset colornames.shd

clearselect
markerset glyph
markersymbol 45
markersize 0.03
markercolor cmyk 100 100 -1 -1
reselect %sp_distn% point ( %timeslice% > 0 )
points %sp_distn%
clearselect
markersymbol 45
markersize 0.03
markercolor cmyk -1 5 100 -1
reselect %sp_distn% point ( %timeslice% = 0 )
points %sp_distn%
&if %timeslice% = 'PRES' &then polygonshades sea0_poly grid-code
&if %timeslice% = 'ONEK' &then polygonshades sea0_poly grid-code
&if %timeslice% = 'TWOK' &then polygonshades sea0_poly grid-code
....
clear maplimits
map end
hardcopy postscript %name1%_%name2%.eps 1 rot90.prm
plot distn_map
display 9999 1
killmap distn_map
```

Appendix

Results

Loxia curvirostra

The Eemian interglacial produces a simulated distribution of great resemblance to the present climatic simulation.   The core range spanning across central Eurasia from Japan to Spain, across Siberia and northerly into Fennoscandia and southerly into the Himalayas, Caucasus Mountains, Turkey, Morocco and Algeria (Fig. 3.5.1 A).   Similarly to the present simulation, there was climatic suitability in Scotland with additional simulations sporadically in central-western Africa, Yemen and the Russian Kamchatka Peninsula.   The North American simulated range is throughout Canada, from Newfoundland to the Northwest Territories and the northern USA and Alaska.   Southerly, the potential range of *L. curvirostra* extended through the Rocky Mountains into Mexico, becoming sparser into Guatemala and Honduras.   There were some sporadic simulations on the south-west coast of Greenland and the northern islands of the Canadian.   Overall, the range of climatic locations suitable for *L. curvirostra* is at its greatest extent in the Eemian interglacial, with 16,459 simulated grid cells.

The Melisey 1 stadial resulted in a similar range size to the warmer interstadial conditions of 13,794 grid cells, smaller than the observed range (Fig. 3.5.1 B).   *L. curvirostra* is simulated from Japan, southern and central Siberia and the Himalayas, into north-west Russia and the east coast of the Caspian Sea.   In Europe, the colder climes meant that much of Fennoscandia was inhospitable but central and southern Europe remained climatically suitable, including additional areas of southern England, Ireland and Iceland.   There were sporadic locations of climatic suitability in central Africa and in southern India, Myanmar and Taiwan.   In North America, although the Laurentide ice sheet has yet to form, the simulated range in Alaska for *L. curvirostra* had already become geographically isolated from the main range in southern Canada, northern and western coast of the USA, Rocky Mountains and Mexico.   There are simulated potential occurrences in Central and Southern America and again, there is a climatic suitable location on Hispaniola.

The interstadial provided *L. curvirostra* with the possibility of climatic expansion in range during the glacial period, with 13,637 grid cells simulated (Fig. 3.5.1 C).   The longitudinal range across central Eurasia was maintained similar to that of present-day observed, with the warmer climes allowing the potential colonisation of sites northerly in Russia to the eastern border of the Weichselian ice sheet and across central regions of Siberia, areas inhospitable during normal glacial conditions.   To the west, areas of British Isles not covered by the Devensian ice sheet and Spain are simulated as having localities favourable for *L. curvirostra*'s climatic niche.   There are patchy simulations of climate suitability in southern areas of Eurasia including central Africa, Yemen, Burma and Taiwan.   Markedly, the climate reconstruction does not have climate suitable for *L. curvirostra* in Vietnam and the Philippines where populations are found today.   In North America simulations are in similar regions to the LGM, across the southern edge of the Laurentide ice sheet, with an outpost easterly in Newfoundland and down the western coast line, the Rocky Mountains into the Mexican Sierra Madres.   There are some simulated locations in Central and northern South America, and yet again the possibility of *L. curvirostra* persisting in Hispaniola.   To the north-west, Alaska has simulations which extend across the Bering Strait into Siberia.

Heinrich Event 5 does not simulate a significant reduction in the total coverage of the predicted climatically suitable range for *L. curvirostra*, with 11,785 grid cells simulated, greater than the number at the LGM (Fig.

3.5.1 D). The core simulated range was throughout central Eurasia, from Japan through southern Siberia, northern China, Mongolia, the Himalayas, Kazakhstan and throughout central and southern Europe, west to the Spanish coastline and south into Morocco and northern Algeria. The Ukraine and the British Isles are simulated as being inhospitable for the species during this colder period. Southerly outcrops of climate suitability during Heinrich Events were more abundant in central Africa and also Yemen than at any other scenario. In South Asia, Myanmar and Vietnam had areas where were climatically suitable, as well as sporadic simulated occurrences southerly in Sri Lanka, Indonesia and the Philippines. In the Americas, *L. curvirostra's* distribution is mainly south of Laurentide ice sheet, in the USA and the west coast into Mexico, Guatemala and Honduras and as far south as north west Colombia. Eastern North America had suitable climatic areas in north Florida and more isolated in the Caribbean, where *L. megaplaga* is presently found. This colder climate does however limit the amount climate suitable for *L. curvirostra* in its most northerly climatic outpost in Alaska compared to glacial conditions before and after the Heinrich Events.

At the LGM (Fig. 3.5.1 E) much of northern Eurasia and Northern America was either covered in ice sheets or climatically inhospitable for *L. curvirostra*, although it maintained a distribution throughout Eurasia and Northern America. The core climatically suitable areas were more southerly than their present range, into central Asia, to the south and east of the Caspian Sea and Southern Korea. Despite this southerly shift, much of the south Asia and Africa was climatically unsuitable, although there was an abundance of locations climatically suitable in central Africa and northern Algeria and Morocco. Glaciers in the Himalayas result in a more sporadic distribution than during the later Holocene. Interestingly the climate is also simulated as being suitable in Vietnam and the Philippines where isolated populations are today. The Laurentide ice sheet constrains the population of *L. curvirostra* to regions of the USA and Mexico, with greater climate abundance in western USA. Alaska, also, was an ice free climatically suitable area for *L. curvirostra* but whether this region was colonised is open for debate primarily as, although presently climatically suitable, it is not utilised. The simulation also suggests climate was suitable for *L. curvirostra* in Hispaniola at the LGM, indicating that past climatic conditions on the island have been suitable for other *Loxia* species. The simulated range size for *L. curvirostra* is lower than later conditions, only 11,785 grid cells, indicating that the LGM climatic conditions were a constraint on habitat availability for *L. curvirostra.*

Simulations of the beginning of the Holocene (Fig. 3.5.1 F) suggest that the areas climatically suitable for *L. curvirostra* were very similar to the present day distributions throughout areas of northern and central Eurasia and northern and the west coast of Northern America. In Asia there were more climatically suitable habitats in northern Siberia and throughout the Himalayas. Turkey and northern Fennoscandia were not as climatically suitable as it is present day. The eastern UK and continental shelf exposed by the lower sea-levels, were climatically suitable. In eastern Northern American climatically suitable range was not as northerly as the present simulations, not being suitable around the Hudson Bay, although the actual observed range is not this far north either. Western Canada and Alaska are indicated as more climatically suitable as far north as the Arctic Ocean coastline, however there are similar present-day Alaskan simulations of climatic suitability which are not occupied, past colonisation is more uncertain. The range is more expansive, with 16,940 grid cells having suitable climate, compared to both the observed (14,963) and present simulated (15,476). The great number of similarities between the Holocene onset and current ranges, suggests that range has not significantly changed in the last 10 thousand years.

Loxia leucoptera

The Eemian interglacial climatic conditions generate a simulated range for *L. leucoptera* (Fig. 3.5.4 A) of great resemblance to the present-day simulation (Fig. 3.4.5). There is a broad potential distribution across Siberia from the east coast, Sakhalin Island, northern Japan and the Kamchatka peninsula to north-western Siberia and extending west into southern Fennoscandia, following the Baltic Sea coastline. In North America there is an expansive distribution across southern and central Canada from Newfoundland across into Alaska and some sporadic outposts in the northern Rocky Mountains. In fact the total number of grid cells possessing suitable climate totals 10,575 grid cells, noticeably similar to present observed range (10,548).

The Melisey 1 stadial resulted in a limited range with simulated distributions covering just 8,455 grid cells. In Eurasia the climatically suitable range spanned from northern central Europe, through Eastern Europe, northern Siberia and towards the eastern coast and Japan, the Kamchatka peninsula and Chukotka (Fig. 3.5.4 B). There are some localities in southern Fennoscandia which are climatically suitable but it remains mainly inhospitable, similar to the current range. There are sporadic isolated sites of climatic suitability mountainous regions such as the Alps, Dinaric Alps, the Caucasus Mountains and the Himalayas. In contrast, the distribution in North America is very limited and has already become segregated prior to the ice sheet formation. On the eastern coast the climatically suitable range is in the southern regions of the Canada and patchy sites in northern Quebec and Newfoundland. There are some sporadic simulations in the west in the Rocky Mountains and the Cascades; however the core range appears to be in Alaska where there is an abundance of suitable climate for *L. leucoptera*.

The warmer interstadial conditions provided a substantial amount of suitable climate specifically in Eurasia, where the northern limits of the range during the glacial period expanded in central Siberia and into the Kamchatka peninsula (Fig. 3.5.4 C). The shift in range limits more northerly, lead to a segregation of climate suitability in central Europe between areas to the east, Poland and Ukraine and to the west, the Netherlands and Denmark. The overall range size is larger than the colder LGM, with 8,718 grid cells simulated. In North America, this northerly shift in range was constrained by the Laurentide ice sheet in the USA, resulting in a narrowing of range along the glacier edge. However, the warmer climes resulted in an evident expansion in the potential of climatic range in Alaska, northwards and also westwards across the now exposed land-bridge Bering Strait. In addition to this, the Newfoundland outpost has greater climatic suitability than at later stages such as the LGM and Heinrich Event 5.

The Heinrich Event 5 was significantly constraining on range of *L. leucoptera* according to the CRS model, with only 5,729 grid cells simulated as suitable, nearly half that encompassed in the present range (Fig. 3.5.4 D). Although the breadth of the Eurasian distribution from Japan to France was maintained similar to other glacial scenarios, the latitudinal limits were more constrained leading to a visible narrowing of range into southern Siberia, the southern edge of the Weichselian ice sheet and central Europe with some sporadic suitability of occurrence in Spain, the Himalayas and the Caucasus mountains. In North America, *L. leucoptera* distribution was limited to a narrow region bordering the Laurentide ice sheet on the east coast and patchy occurrences in west. To the north-west of the ice, in southern Alaska, the species has a greater prediction of range suitability. There is also a simulated presence on the ice-free south-coast of Newfoundland and this is interesting given that populations are observed there today.

At the LGM there were some substantial differences in the regions available for *L. leucoptera* occupation compared to present day (Fig. 3.5.4 E).   In Eurasia the distribution of *L. leucoptera* was constrained to southern Siberia and climate was suitable as far west as central Europe, to areas such as the southern UK, and the adjoining continental shelf exposed and northern Spain.   Despite these colder climes, to the east of Eurasia the southern bound of climate suitability was no further south than in present day simulations, to northern North Korea.   In Eurasia, a consistent distribution spanning east to west was maintained even at these extreme conditions, however, in North America the Laurentide ice sheet split the climatically suitable regions between Alaska, were there was an abundance of climate suitable and a sparse climatically suitable range in northern USA, mainly on the eastern coast.   There are also a couple of locations that remain suitable for *L. leucoptera* on the eastern ice-free coast of Newfoundland.   This colder and drier climate resulted in a limited range for *L. leucoptera*, at the beginning of the Holocene and present conditions.   This surprisingly highlights the inhospitability of these glacial conditions for this species of Crossbill despite it being considered a boreal, cold-climate, species.

The beginning of the Holocene simulations of *L. leucoptera* indicate that the range in Eurasia was more northerly in Siberia than present day and the climate was more suitable in Chukotka and Kamchatka peninsula of eastern Russia (Fig. 3.5.4 F).   Much of Fennoscandia was unsuitable for the species at the beginning of the Holocene, barring sporadic locations of climate suitability in southern Norway and Sweden.   Interestingly this absence in northern Europe actually fits the present range better than the present climate simulations and may indicate that this early inhospitablity in Europe limited colonisation and resulting in the distribution observed today.   Both in Eurasia and North America, the species range did not extended as far south as present.   In North America, the eastern populations were further constrained, with northern regions of the Canadian states being climatically unsuitable.   Simulated presences in western North America, such as Alaska, were more hospitable at this time than later conditions.   The simulated range of *L. leucoptera* covered 11,777 grid cells, not significantly greater than the observed range (10,548, simulated present – 11,080), indicating that conditions at the beginning of the Holocene were just as suitable as present day and the changes in climate since then to present day have resulted in regional specific expansion and contractions of range limits rather than overall range size.

Loxia pytyopsittacus

The previous Eemian interglacial had climatic conditions which were in fact more climatically suitable for *L. pytyopsittacus* than observed (2,409), with 2,773 grid cell presence simulated (Fig. 3.5.7 A).   The simulated distribution is very similar to the observed, throughout Fennoscandia, however there is greater range potential easterly into Russia.   The Baltic States, presently populated regions, are not simulated as suitable during the Eemian.   Similar to the present simulation (Fig. 3.4.8), the model predicts suitable locations in the Alps, Pyrenees, Carpathian and Caucasus Mountain ranges at the previous interglacial which were unlikely to have been colonised due to their isolation from the core range in northern Europe.

The Melisey 1 stadial resulted in climatically suitable range similar to that generated throughout the glacial, with *L. pytyopsittacus* range being constrained to central Europe despite the absence of ice sheets (Fig. 3.5.7 B).   In continental Europe the northern limit of simulations is southern Demark while the southern are the mountain regions of the Pyrenees, Apennines and Dinaric Alps; east to west spanning from the Ukraine to northern France. The most northern distribution potential is eastern and western coastal fringes of Iceland.   There is also abundant climate suitability in the British Isles throughout England, Wales, the western Scottish and eastern Irish coastline.   The interglacial results in a lower sum of climatically suitable regions, similar to the glacial, with just 951 suitable grid cells.

The warmer interstadial conditions also do not provide plentiful conditions for *L. pytyopsittacus*, with only 925 grid cells simulated as suitable (Fig. 3.5.7 C).   The core climatically suitable range spanned from the east in Ukraine westerly to the Devensian ice sheets of the British Isles and northwards into Germany and Poland bordering the Weichselian ice sheet.   Southern Europe is not particularly suitable, compared to glacial conditions, with much of France inhospitable.   There are mountainous locations in the Pyrenees, Alps. Dinaric Alps, Urals and Caucasus Mountains which are simulated as hospitable for *L. pytyopsittacus* but some are significantly isolated from the core range.   There are also simulated isolated occurrences on the west of the Devensian ice sheet in northern Scotland.

During the Heinrich Events resulted in the most restricted climatic conditions for *L. pytyopsittacus* in Europe, with only 664 grid cells simulated as suitable in the example Heinrich Event 5 shown (Fig. 3.5.7 D).   This limited distribution was found mainly in central Europe, as far north as southern Germany, Czech Republic and Poland; during these events the edge of the Weichselian ice sheet is inhospitable for the species.   The British Isles, and the continental shelf around it, were also climatically unsuitable for *L. pytyopsittacus* despite being suitable at the later LGM.   Conditions in the west of Spain and French continental shelf are the western limits of the simulations and there were some more southerly locations in northern Italy and Turkey which were suitable.   Additional but isolated climatically suitable habitats were also available in the Caucasus Mountains and the mountains of Kazakhstan.

The LGM, with the extensive Weichselian ice sheet across Fennoscandia and the Devensian covering much of central and northern Britain and Ireland in ice, resulted in central Europe having the only climatically suitable regions for *L. pytyopsittacus* (Fig. 3.5.7 E).   The core range extends as far east as the Ukraine; west across the exposed continental shelf to southern England border of the Devensian ice sheets; and the Weichselian ice sheet being the northern limit.   There are also sporadic presence simulations in the Caucasus Mountains and the mountains of Kazakhstan.   The northern Mesata mountain plateau of Spain is the southerly limit of climatic

suitability, and further westerly, conditions along the coastline on the western side of the Devensian ice sheet are also simulated for *L. pytyopsittacus* in northern Ireland and Scotland. This colder climate and the advanced glaciation means that in Europe there were only 1,124 grid cells which have climate suitable for *L. pytyopsittacus*, less than half the quantity of climatic space available for the observed range (2,409).

At the beginning of the Holocene, *L. pytyopsittacus'* core climatically suitable range was throughout Norway, southern Sweden and southern Finland, the Baltic States, Denmark and the local continental shelf exposed by the lower sea-level and western Russia, however not as far east as the present climate range extends (Fig. 3.5.7 F). In addition to this are sporadic simulations in the mountainous regions of central Europe including the Alps, Dinaric Alps, Carpathians and Pyrenees. Interestingly several grid cells in Scotland are simulated as being suitable for *L. pytyopsittacus*, often consider the closest relative of the Scottish native *L. scotica*. These climatic conditions are simulated to limit the species to 1,432 grid cells, more constrained than the present range (2,406) with an evident expansion of climatically suitable conditions to the east and northwards since the beginning of the Holocene.

Most notably for this crossbill species, the conditions over the last 21 thousand years have seen a significant shift in the regions of climatically suitable habitat, so substantial in fact that there is no overlap between the current observed range and the areas of suitability at the LGM indicating that there were dramatic climate range shifts for *L. pytyopsittacus.*

Loxia scotica

The Eemian interglacial conditions were most suitable for *L. scotica* in Scotland where the present range is found (Fig. 3.5 10 A).   Only 2 of the 14 grid cells of suitable climate are outside this Scottish range, one on the western coast of Norway and the other, on the southern coast of Iceland.

The cooler stadial conditions produce a climatically suitable range for *L. scotica* which just spans 10 grid cells and can be found in western and northern Ireland and southern Outer Hebrides (Fig. 3.5.10 B).   This indicates that before the formation of the glaciers, the colder climes of the stadial potentially would have limited populations of *L. scotica* to the Irish coastline where they could have remained through the glaciation.

The warmer interstadial conditions generated just two climatically suitable grid cells, both of which are situated on the west coast of Ireland on the edge of the Devensian ice sheet (Fig. 3.5.10 C).   This indicates that *L. scotica* populations could have persisted in these climatically suitable areas in Ireland throughout the standard conditions of the glacial, including the LGM, as well as the warmer interstadials periods in Ireland but not the harsh Heinrich Events.

The Heinrich Event 5 was completely inhospitable for the *L. scotica*, with no regions simulated to be within the modelled climatic niche (Fig. 3.5.10 D).   This is in fact the case for all the Heinrich Events which were modelled, which occur between 46 (Heinrich Event 5) to 17 thousand years ago.   This throws into question whether the climatic niche of *L. scotica* was broader in the past to have survived such events, or whether there were smaller climatic pockets were the species persisted which are not modelled at this scale or if in fact the species, as has been classified, did not exist until post Heinrich Events.

The LGM resulted in a climatic suitability range for *L. scotica* (Fig. 3.5.10 E) more southerly than the present warmer conditions allow.   Out of the 10 grid cells that have climate within the *L. scotica*' present-day climatic niche, a number are in northern Spain and the Pyrenees but these are significantly isolated from the current range in Scotland.   Closer to the present range in Scotland, which at the LGM was mostly covered by the Devensian ice sheet, would have been the climatically suitable locations on the south-western coast of Ireland, although limited to just 3 grid cells, on the edge of the Devensian ice sheet.

At the beginning of the Holocene *L. scotica* was limited to a small climatically suitable region in western Scotland, where only three grid cells possess climate that is within the present-day species' climatic niche (Fig. 3.5.10 F), compared to the current more expansive observed range of 23.   This does indicate that the current range in Scotland could have been established as early as the beginning of the Holocene, 10 thousand years ago but it was more range restricted that present day populations.

Loxia megaplaga

The conditions at the previous interglacial suggest that the climate in central Hispaniola was suitable for *L. megaplaga* (Fig. 3.5.13 A).   There are additional grid cells of climate suitability in Honduras, Nicaragua and Colombia.   This suggests that *L. megaplaga* could have been a resident of Hispaniola prior to the most recent glacial expansion.

The Melisey 1 stadial resulted in just 16 climatically suitable grid cells and all of these are found outside the Caribbean (Fig. 3.5.13 B).   These sites range from north of the Caribbean, Florida; west in Guatemala, Honduras and Costa Rica; and southerly in Colombia.   The absence of climatic suitability in the Caribbean islands is similar to the later climatic scenarios at the LGM (Fig. 3.5.13 E) and the Holocene onset (Fig. 3.5.13 F), and as discussed above it may be as a result of model resolution, species' niche changing over time or later colonisation.

The warmer interstadial conditions generate 25 climatically suitable grid cells for *L. megaplaga* (Fig. 3.5.13 C). Most of these suitable locations, again, are distributed outside the Caribbean islands, similar locations to the Heinrich Event.   However at this scenario, some of these climatically suitable grid cells are simulated on central and western Hispaniola, in precisely the locations where the species populations are observed.   It is interesting to note that the interstadial conditions appear to have favoured *L. megaplaga* populations in Hispaniola, a contrast to the other crossbill species presently native to more northerly latitudes, whose simulations suggest that, in general, populations were restricted to more southerly ranges than of present even during these warmer temperatures.

Unlike most other species of *Loxia* modelled, the Heinrich Event 5 conditions produced the greatest quantity of potentially suitable grid cells for *L. megaplaga*, totalling 54 (Fig. 3.5.13 D).   Similarly to the later scenarios of the LGM and beginning of the Holocene, none of these are found on the island of Hispaniola with a great majority of locations distributed around the Caribbean in northern Florida, Mexico, Nicaragua, Coast Rica, Colombia and Venezuela.   However, most notably there are a significant number on the island of Cuba, just north of Hispaniola and the small neighbouring island of Great Inagua.

At the LGM (Fig. 3.5.13 E) the regions of suitable climate for *L. megaplaga*, which total 17 grid cells, are in northern Florida and on the exposed continental shelf, in Central American countries such as Guatemala, Honduras and Nicaragua, and in South America, northern Colombia and Venezuela.   The absence of climate suitability in the Caribbean is interesting, as it is either an indication that the model merely represents the present day distribution and that in the past the climatic niche exploited by *L. megaplaga* was significantly different, it persisted in climatic regions that are not successfully modelled at this scale, or it is a relatively new coloniser of Hispaniola.

At both the beginning of the Holocene (Fig. 3.4.9) and the LGM (Fig. 3.5.13 F), despite their differing climatic conditions, neither is a climatic scenario where there is climate on the Caribbean Island within the CRS modelled niche for *L. megaplaga*.   The warming temperature post-glaciation at the Holocene onset produces just five climatically suitable grid cells, the closest of which to Hispaniola, where the population is found today, was in Florida; the other sporadic occurrences of climate suitability being in Guatemala and Colombia.

Appendix

Larix species

At the Eemian (Fig. 3.5.16 A), the distribution resembles the present range (Fig. 3.4.17). _Larix_ species' simulated range is mainly in Russia but did not extend as far at the Bering Strait, with the climate in Europe being inhospitable, similar to the present simulated, barring some isolated occurrences in northern Spain. There was also climate suitable in the Himalayas for _Larix_ and a single grid cell of suitability in Vietnam. In North America the potential range spans across Canada from Quebec and Newfoundland on the east coast to the Northwest Territories with a population segregated in Alaska from the rest of this core range. The more restricted climatic range in Eurasia results in a lower quantity of available climatic space for _Larix_ species of just 11,155 grid cells.

The Melisey 1 stadial produced a potentially expansive range for _Larix_ species, covering 15,709 grid cells. The majority of this distribution is in northern Eurasia, stretching from the Baltic Sea, across Russia to Cape Dezhnez on the eastern coast of the Siberia, as far south as the southern Japan (Fig. 3.5.16 B). There were isolated locations of potential occupation, in south Asia; China, Bangladesh, Bhutan and Vietnam, the Middle East; Tian Shan and Caucasus Mountains and also in Europe; southern England, northern Norway and Svalbard. In North America, there were three distinct regions of climatic suitability for _Larix_; in Alaska extending as far west as the Cape Prince of Wales; in the North East USA and north-east Canada, Quebec and Newfoundland. There are smaller areas of predicted range as far south as Florida, Mexico and even Venezuela and north into Baffin Island, Ellesmere Island and Greenland.

During the warm interstadial, _Larix_'s climatic range could be found throughout northern Eurasia, from the eastern edge of Weichselian ice sheet across Russia and the Bering Strait into northern North America, connecting with simulated occurrences in Alaska and the western edge of the Laurentide ice sheet (Fig. 3.5.16 C). For the duration of the interstadial, Japan, northern Vietnam and southern Himalayas, such as Bhutan, are simulated as potential ranges. In Europe these warmer glacial conditions provided potential distributions in Germany, bordering the Weichselian ice sheet and mountains of northern Spain, Apennines the Dinaric Alps and the Caucasus Mountains. The Atlantic coastline of North America and the coastal edge of Newfound possessed climatic conditions within _Larix_'s climatic niche, and there was a range from the north-east USA to the Middle West along the Laurentide ice sheet. This expansive interstadial distribution for _Larix_ species in Eurasia and areas of North America produces a predicted range size of 15,910 grid cells.

The Heinrich Event 5 resulted in a shift in the climatic range of _Larix_ in Eurasia. Although simulations suggest it was still the larger of the ranges of _Larix_, it is distributed primarily in south and western Siberia, spreading west to the Russia borders and eastern Europe but not abutting the Weichselian ice sheet (Fig. 3.5.16 D). To the east, much of Japan is climatically suitable for _Larix_, and, to the south, the mountainous regions of Mongolia, China and Bhutan are also simulated as potential locations for _Larix_. In Europe, climatically suitable locations for _Larix_ are simulated to the west of the Weichselian ice sheet in Germany and northern France. The temperature decline resulted in the east coast of North America becoming climatically inhospitable for _Larix_, with the population south of Laurentide ice sheet being restricted the Middle West of the USA. There are some isolated locations on the east coast, notably in Newfoundland and northern Florida. To the west of the expansive ice sheet, the Alaskan climatic niche remained, although it is restricted to the southern and central regions with the range potentially connecting with eastern Siberia across the Bering Strait. Overall, despite the

Appendix

restriction on range size from those simulated at the LGM and through into the Holocene, 13,946 grid cells are simulated as suitable for *Larix* species, larger than the current observed range (13,202).

The LGM simulations also suggest a plethora of climatic conditions suitable for *Larix*, 15,391 grid cells with simulated presence and, like present day and the preceding Holocene, a vast majority of this climate suitability was in northern Eurasia, throughout Russia (Fig. 3.5.16 E).   Despite the colder climate, the northern extent of *Larix* is not significantly restricted in central Russia; in the north-eastern regions of Siberia, the climate has become unsuitable but to the west the *Larix* climatic range extends to Weichselian ice sheet edge.   The glacial made areas of Kazakhstan, in the Caucasus Mountains and eastern Europe favourable for *Larix* occupation as well as a regions west of the ice sheet in Germany and simulations in northern Spain, Apennines and the Dinaric Alps.   In south Asia, similar regions to the later Holocene onset were suitable for *Larix* in Bangladesh, Myanmar, Vietnam and southern China.   The northern island of Hokkaido and the southern Kyushu are the only Japanese regions that had climate suitable for *Larix* species.   The Laurentide ice sheet in the North America segregates the *Larix* climatic population, with the majority of simulations being in southern Alaska. In the USA the other climatically suitable region fringes the ice sheet from the north-east coast to the Middle West.   In addition to this there are simulations on the east coast of the Newfoundland, Florida, the Rocky Mountains and southern Mexico.

The onset of the Holocene had an abundance of climatic conditions that suited the climatic niche of *Larix* species, with 15,225 grid cells having climate suitable for the selection of species (Fig. 3.5.16 F).   The majority of this range is throughout Russia, with the only the extreme Arctic-coastline, northern regions of Sakha Republic and Chukotka not having climatic conditions suitable for *Larix*.   To the west, the range becomes patchier towards the Russian border but there some areas of climatic suitability in northern Germany and Poland and also the Caucasus Mountains.   In southern Asia, there is no climatic suitability in the Himalayas for *Larix* but there are some niches in India, Bangladesh, Bhutan, Myanmar and Vietnam.   Much of northern Japan is also climatically suitable for *Larix*, and the Siberian range extends as far east as the Bering Strait, which at this time period was almost connected with North America.   The climate suitability in North America is patchier than present day.   Although it extends across from Alaska throughout Canada, regions in central Canada were climatically inhospitable for *Larix*.   Interestingly to the south, there are simulations in Mexico and also in the southern state of Florida.

Appendix

***Picea* species**

For *Picea* species the interglacial provides the greatest abundance of suitable climate with 16,667 grid cells simulated.   The core range in Eurasia spanned from eastern Siberia, through Japan and Siberia throughout western Russia into Eastern Europe, Fennoscandia and Alpine regions (Fig. 3.5.19 A).   Mountainous regions such as the Himalayas, Tian Shan and Pamir Mountains, Caucasus Mountains, Pyrenees, Mesta and the Scottish Highlands were also localities of potential *Picea* populations.   North America had a range spanning from the east coast of Newfoundland throughout south-eastern and north-western Canada into Alaska and southerly into the Rocky Mountains.

The Melisey 1 stadial results in presence simulations of just 11,999 grid cells for *Picea*.   The climatically suitable range in Eurasia spans from Japan and south-east Siberia through into north-west Russia and into central Europe as far west as Ireland and northern Spain (Fig. 3.5.19 B).   Additional to this core range, the central Asian mountain ranges, Caucasus Mountains, regions north of the Caspian Sea and eastern Russia, also have climate suitable for *Picea* species.   In North America, the interjection of colder climate during the interglacial resulted in a split in simulated range between Alaska and central North America, where the majority of the potential range is on the east coast, while the Rocky Mountains and Cascades provided additional adequate locations in the west.

The warmer interstadial conditions favoured the modelled *Picea* climatic niche compared to the other glacial conditions such as the LGM and Heinrich Events, with 12,073 simulated grid cells.   In contrast to the colder events during the glacial, the warmer climate results in an expansion northerly of *Picea*'s range in Eurasia, into central Russia and south-westerly into Europe as far as the Devensian ice sheets and westerly to the Irish coast (Fig. 3.5.19 C).   Mountainous regions including the Asian mountain ranges and the Caucasus Mountains remained climatically suitable for *Picea* species even during this warmer period.   The exposed Bering Strait between Siberia and North America had regions of climatic suitability which connected with Alaska and its expansive range of climate suitability for *Picea* species to the edge of the Laurentide ice sheet.   South of this ice sheet, simulated presences can be found from the west to east coast and progressing most southerly through the Rocky Mountains.   The most eastern location of climatic suitability is on the exposed island of Newfoundland, where the whole island had suitable climate for *Picea* species.

The Heinrich Event 5 limited the climatically suitable range of *Picea* species to just 9,366 grid cells.   The most reduced distributions, compared to both interglacial and glacial conditions, are in Asia, where *Picea*'s simulations are constrained to southern Russia, Japan, northern China, Mongolia and Kazakhstan but it a maintained a presence in the central Asian mountain ranges (Fig. 3.5.19 D).   The inhospitablity of the northern regions of Siberia isolated the climatic niche found in the Kamchatka peninsula.   In the Middle East there was climate suitable from the Caucasus Mountains as far south as northern Iran and Iraq, while the eastern Russian distribution was limited by the Weichselian ice sheet.   To the south of this ice sheet, simulations are expansive in central Europe, into France, northern Spain, the Apennines and the Dinaric Alps.   In North America, the Alaskan climatic range was limited to central regions; while, in contrast, the predicted distributions of *Picea* species south of the Laurentide ice sheet stretch further southward that at the LGM into central USA.   Notably, there are simulations on the Newfoundland coast, similar to those at the LGM (Fig. 3.5.19 E).

The colder climate of the LGM resulted in much of northern Eurasia being unsuitable for *Picea* species (Fig. 3.5.19 E).   The Eurasian range was constrained to southern Russia, Mongolia, Kazakhstan and central Europe, from the southern England bordering the Devensian ice sheet to the west Pacific coastline, the Russian island of Sakhalin and Japan.   Despite the presence of glaciers in the central Asian mountain ranges, there is still suitable climate throughout the Himalayas, China and into Mongolia; in addition the Caucasus Mountains have simulated presences for *Picea* species.   There are simulations as easterly in Russian Kamchatka peninsula and across the exposed Bering Strait into Alaska, where the range could extend as far as the edge of the Laurentide ice sheet.   The other substantial area of climatic suitability in North America was along the southern limit of the Laurentide ice sheet, stretching from the west to east coast USA.   There was notably also climate suitable on the east coast of Newfoundland, where the presently *Picea mariana* is a native.   The LGM does constrain the quantity of climatically suitable regions, with just 9,539 grid cells possessing suitable climate for *Picea* species.

The commencement of the Holocene produces simulations that indicate the *Picea* species range may have been before expansive, with 17,730 grid cells having climate within the modelled niche.   In Eurasia the largest range spans from eastern France and Germany through Russia to the eastern Pacific coast, the Bering Strait coastline and Japan (Fig. 3.5.19 F).   Northern areas of Fennoscandia and north-eastern Siberia have climate which is unsuitable for the selection of species of the *Picea* genus modelled.   Compared with present-day distributions, the bioclimatic conditions in more northerly sites are suitable for Spruce.   In addition to this core range, there is also climatic suitability in Scotland, northern Spain, the Caucasus Mountains, throughout the Himalayas and surrounding mountain ranges such as Tian Shan.   North America has potential range coverage from south-east Canada through to the north-west and in Alaska as far as the coastline of the Bering Strait as well as southerly into the Rocky Mountains.   There are also some sporadic isolated locations of climatic suitability in Florida, Mexico and the south-west coast of Greenland.

Appendix

Pinus species

The Eemian interglacial scenario had a substantial climatically suitable range for _Pinus_ species, covering 13,397 grid cells, greater than the observed (11,405).   In Eurasia, this potential range spans from the Atlantic coast in Spain and southern Mediterranean coastline through the Alps into central Europe and Fennoscandia, south-easterly into Turkey and the Caucasus Mountain (Fig. 3.5.22 A).   From west Russia the range narrows into central regions and becoming more fragmented in its south-eastern Siberian distribution, but it simulated abundantly in northern China and Japan.   The Kamchatka peninsula and the Scottish Highlands are also simulated as being climatically suitable.   The South Asian simulations suggest a distribution in Vietnam, Thailand and Myanmar, the Himalayas eastern India and mountain ranges of China and Afghanistan, with isolated occurrences on the islands of Taiwan and Hainan.   Notably there is an absence of climate suitable in the Philippines at this previous interglacial.   The distribution simulated in North America is of great similarity to that simulated using present day climate (Fig. 3.4.23), simulated in the north-east; through southern Canada, northern USA, along the western coast and Rocky Mountains into Mexico as far south as Honduras and a segregated climatically suitable region in southern Alaska.   In additions to these expansive potential ranges, there are smaller isolated outposts in southern Florida, Hispaniola and northern South America.

Melisey 1 simulated distributions for _Pinus_ species throughout central and southern Europe, reaching as far south as the north-west coastline of Africa and north into England, Ireland and north-west Scotland (Fig. 3.5.22 B).   To the east the range narrows into north-western Russia, extending south-easterly to the Pacific coast and the islands of Sakhalin and Japan.   The Caucasus Mountains, Turkey and north-eastern Caspian Sea coastline are predicted occupation sites.   South Asia had a large range, spanning from the Himalayas, Thailand, Vietnam, the Bay of Bengal and Sri Lanka.   The south-east Asian islands of the Philippines and Celebes also had climatic conditions suited for _Pinus_ species.   Significantly isolated from these core Eurasian ranges, Central Africa and along the coast of the Arabian Sea are simulated to have potential occupation.   The North American climatic ranges are limited to three cores segregated regions, the north-east USA, the west USA and western Alaska.   There was an abundance of suitable sites in Mexico, Nicaragua; northern South America and the Caribbean islands of Cuba, Hispaniola, Jamaica Puerto Rico as well as the Florida peninsula.   In total there are 9,640 simulated grid cells for _Pinus_ species, fewer than available during warmer interglacial conditions.

The interstadial saw an expansion in range compared to the standard glacial conditions, with a broad climatically suitable distribution from Japan and northern China across southern Russia to the Weichselian ice sheet and south of this ice mass into central and southern Europe as far west as Spain, northern Africa and southern British Isles to the Devensian ice sheet, with climate also suitable to the west of the ice along the Irish coast (Fig. 3.5.22 C).   South Asia was also a climatic suitability hot-spot, with range potential in Vietnam, Myanmar, Thailand, eastern India, the Himalayas and east into the Philippines and Taiwan.   During the interstadial, central Africa and southern Middle East also exhibited multiple outposts of suitable climatic conditions for the genus.   North America had a potentially expansive range along the south edge of the Laurentide ice sheet and western USA into Mexico and as far south as Panama with sporadic occurrences in northern South America, Colombia and Venezuela.   The southern tip of Florida and the Caribbean islands of Cuba, Hispaniola and Jamaica also had suitable regions.   To the west of the Laurentide ice sheet, Alaska and to the east, the exposed island of Newfoundland had favourable simulated conditions.   Overall the warmer conditions of the interglacial resulted in an increase, compared to glacial, in available climatic range with 11,109 grid cells simulated.

Appendix

The Heinrich Event 5 severely restricted the cumulative climatically suitable range for *Pinus* species to just 7,161 grid cells.   In Eurasia the favourable regions were in central and southern Europe and also the southern Mediterranean coastline in northern Africa (Fig. 3.5.22 D).   The Caucasus Mountains and regions around Caspian Sea, in countries such as Iran, Kazakhstan and Turkmenistan are also areas with simulated potential range.   Other regions of simulated climatic suitability include; northern Eurasia - southern Russia, eastwards to south-eastern Siberia, north China and southern Japan; southern Asia - the Himalayas, Chinese mountains, Bhutan, Myanmar and Vietnam; and the south-east Asian islands - Philippines, Borneo, Taiwan and the Celebes, although many were landlocked at this time.   There is also an abundance of climate suitable in central Africa, Yemen and Oman.   The most widespread simulated range in North America is south of the Laurentide ice sheet, throughout Mexico and the USA, excluding some of the South East states but northern Florida is suitable. There are also simulations in Alaska and some isolated locations in South America, western Colombia. Overall, the Heinrich Event climatic conditions suggest that ranges in Eurasia were more fragmented and limited than during the rest of the glacial, while in North America, south of the glaciers, there was an expansion of range.

The LGM was a period of restricted climatic range for *Pinus* species, with just 8,316 grid cells simulated.   In Eurasia, the expansive ranges of the interglacials were segregated in the colder conditions, the larger range from north-west coast of Africa and the western coast of Europe throughout central Europe as far north as the Weichselian and Devensian ice sheet (and to the west of this ice in Ireland) spreading west into south-west Russia (Fig. 3.5.22 E).   The Black Sea coast and Caucasus Mountains are also simulated as having climate suitable.   The eastern limits of climatic range in Asia were in north-eastern China, south-east Siberia and throughout Japan.   South Asia had an abundance of climatic suitability as far south as the continental shelf exposed around Malaysia, and areas in Thailand, Vietnam, Myanmar, the Himalayas, China and Mongolia. The south-eastern Asian islands of the Philippines, Taiwan, although land-locked, Borneo, Celebes and Halmahera all have locations of climatic suitability for *Pinus* species.   The Laurentide ice sheet formed a physical barrier across North America, to the west, there are simulations in southern Alaska, however the core range was more southerly throughout the west and north east USA.   The simulations extend as far south as Central and northern South America; with further localities identified on the Florida coast continental shelf and the Caribbean islands of Cuba, Hispaniola and Puerto Rico.

10 thousand years ago, the warming temperatures post-glaciation resulted in a substantial quantity of climatic space which falls within the modelled niche for the selection of *Pinus* species modelled, with a total of 12,685 grid cells with suitable conditions.   The Eurasia simulations are from the west coastline of Europe in Spain (and north-western Africa) and Scotland through central and southern Europe and southern Fennoscandia into north-western Russia shifting southerly as it tracks easterly into south-eastern Siberia and as far east as the islands of Sakhalin and Japan (Fig. 3.5.22 F).   Further east there are simulations in eastern Siberia, Chukotka and Kamchatka Peninsula.   In south Asia climatically suitable locations were in Vietnam, Thailand and Myanmar stretching north into the Himalayas and westerly along the Bay of Bengal in India, Sri Lanka and isolated localities in the Philippines.   Central Africa and Yemen are also simulated as having a number of climatically suitable locations; however these were isolated from other *Pinus* populations.   In North America simulations for the eastern range stretch from Newfoundland through southern Canada and northern USA into the Middle West.   In western North America areas were favourable from southern Alaska through north-western Canada

Appendix

and western USA coast and the Rocky Mountains.   Mexico, southern Florida and the Caribbean islands, Cuba and Hispaniola, also possessed climatically suitable locations for *Pinus*.

Pseudotsuga species

The previous Eemian interglacial had more favourable climatic conditions for _Pseudotsuga_ species, with 2,018 grid cells simulated.   In south Asia, the potential range occurs as far east as southern Japan, Korea, Taiwan and the Chinese coastline (Fig. 3.5.25 A).   Throughout the Himalayas, Myanmar and China there was a connected range of climatic suitability extending as far west as the mountains in Afghanistan, Tajikistan and Kyrgyzstan. In southern Europe, Turkey, the Apennines, Pyrenees and northern Spain and the Baltic Sea coastline are also simulated as being potential ranges for the genus.   In North America the simulated range along the western coastline and mountain ranges, with sporadic locations in Mexico and some eastern areas of the USA.

The Melisey 1 had climatic conditions that are favourable in the southern Asian regions of northern Vietnam and Laos, Myanmar into the southern China, the eastern and western Himalayas and Afghanistan (Fig. 3.5.25 B). Further west along the eastern cost of the Caspian Sea, as well as isolated localities in Taiwan and eastern India, were also regions of Asia of potential occupation by _Pseudotsuga_ species.   In Europe there were patchy potential occurrences in Turkey, the Dinaric Alps, Italy, Ukraine, Poland, northern Spain, France and southern England, with Morocco, Algeria, central Africa and the Mediterranean islands of Corsica and Sardinia also having limited climatically suitable conditions.   The coastline and mountain ranges of western North America provide the most substantial regions of climatic suitability on this continent, with smaller distributions possible in southern Mexico, on the Florida peninsula and in South America.   In total the climatically suitable range covers 1,545 grid cells, not as large as the later glacial conditions.

The warmer interstadial condition also did not simulate much change in the overall potential range size for this genus, with 1,858 grid cells simulated.   Northern Vietnam, southern China, Myanmar and into the Himalayan Mountains of Nepal, Bhutan and Tibet were encompassed in primary south Asian simulated range with additional localities on the island of Taiwan and in central India (Fig. 3.5.25 C).   There were also regions with suitable conditions in central Asia - Kazahstan, the southern Middle East; Yemen; southern Europe - Greece, Turkey, Italy, Corsica, Sardinia and Spain and in Africa - east-central and north-western coastline.   In western North America, the potential distribution extended from south of the Laurentide ice sheet along the western coastline and mountain ranges and patchily into Mexico with some further localities in Florida and Colombia having conditions favourable.

The Heinrich Event 5, although significantly colder, did not result in a significant change in range size for _Pseudotsuga_ species with a sum of 1,846 grid cells, similar to other glacial scenarios, but it did result in a shift in distributions.   The south Asian regions of northern Vietnam and Laos, southern China, Bhutan, Nepal and sporadic localities in the Himalayas are simulated as being an area of climatic suitability (Fig. 3.5.25 D).   There were also potential localities in the northern Philippines and central India, as well as westerly in Iran, Kazahstan, the southern Middle East and areas of central Africa.   In Europe, the western shores of the Mediterranean, Turkey, southern France and Ukraine are simulated as having conditions which are within the modelled climatic niche for _Pseudotsuga_ species.   In North America the climate suitable range for this genus was south of the Laurentide ice sheet, along the west coast and patchy throughout Mexico, extending along the south-eastern coast into Florida, North and South Carolina.   Alaska and Colombia had a few additional climatically favourable locations.

Appendix

The LGM resulted in a greater quantity of climatically suitable areas than the interglacial periods, with 1,865 grid cells simulated for *Pseudotsuga* species.   Despite the ice sheets forming over much of the Asian mountain ranges, the ice-free mountainous areas possessed the climatic conditions suited for this genus, south into Nepal, Bhutan, Myanmar and southern China (Fig. 3.5.25 E).   To the west, areas surround the Caspian Sea, Turkey, the Dinaric Alps, Apennines, Spain and north-eastern Africa were all regions which had potential climatic conditions for the modelled *Pseudotsuga* species.   The west of Northern America had a large, but patchy, expanse of possible range and sporadic occurrences south in Mexico.   There are several additional isolated localities simulated in southern Alaska, Florida and Colombia.

The onset of the Holocene resulted in climatically suitable total range coverage of 1,360 grid cell similar in size to present range although the distribution of this climate is different.   The south Asian range spanned from northern Vietnam, Laos and southern China through Myanmar and into the Asian mountain ranges of the Himalayas in Nepal and Bhutan and westerly into Afghanistan (Fig. 3.5.25 F).   The islands of Taiwan and southern Japan, areas where populations are observed today, are climatically suitable.   There were also suitable localities in the southern Middle East, eastern central Africa and in Europe; northern Spain, west coast of France and around the Baltic Sea.   In North America, the west is the core potential range, along the coastline and the mountain ranges, such as the Rocky Mountains.   There were also favourable regions in Mexico and southern Canada.   There are isolated sites of climatic suitability in Florida, the Caribbean island of Hispaniola and in Colombia.

Tsuga species

The warm conditions of the Eemian are much more favourable than the stadial, with 4,224 grid cells simulated for _Tsuga_ species. These simulated ranges are located throughout southern China and westerly through the Himalayas; north in Japan and Korea. Southern Fennoscandia, Scotland, eastern Russia, the Caucasus Mountains and patchy areas of southern Europe also had the conditions suitable for _Tsuga_ species (Fig. 3.5.28 A). North America has a vast range of climate suitable in the east, stretching from southern Canada down the south-eastern coast to the states of Louisiana and Florida. There are also conditions suitable along the western coast of Canada and into the Rocky Mountains, as well as in southern Alaska and the south-west coast of Greenland.

Melisey 1 stadial climate scenario simulations for _Tsuga_ species are in southern Japan, South Korea, Taiwan and mainland southern China where is extends west into the Himalayas and Myanmar (Fig. 3.5.28 B). In Europe, the climatically favourable locations were in the Dinaric Alps through in the Alps, France, northern Spain, southern UK, Ireland and Iceland. The North American suitable ranges are greatly restricted, compared to glacial and interglacial, with isolated populations on the western and eastern coast and sporadic occurrences in Central America. Overall these colder stadial conditions results in total grid cell simulated coverage of just 1,802.

The warmer interstadial also results in a similarly limited climatic range of just 2,032 grid cells available for _Tsuga_ species' however there are differences in their distribution to those from the cooler Heinrich Event. The simulated distributions in south Asia were situated in the Himalayas, Myanmar, southern China, along the south-eastern coastline and southern Japan (Fig. 3.5.28 C). In Europe the climatically suitable range was around the edge of the Devensian ice sheet and patchy across southern Europe, Spain, France, Italy as far east as the Ukraine. Eastern North America had a substantial region with conditions that suited the modelled niche extending from the Laurentide ice sheet along the south-eastern coastline; with additional predictions in the Rocky Mountains; south in Mexico and Colombia; and along the western Canadian coast.

The Heinrich Event 5 resulted in a more limited climatic range than during other times of the glaciation and interglacials, with just 2,024 grid cells simulated for _Tsuga_ species. The Himalayas, Myanmar and southern borders of China were climatically suitable, but the eastern coastline between this range and further suitable conditions in southern Japan is inhospitable (Fig. 3.5.28 D). The colder climates in Europe resulted in the south-western regions of Spain, southern France and the Apennines being climatically suitable locations. In North America, there are locations suitable throughout the regions south of the Laurentide ice sheet, patchy in the west and more consistent in central and eastern areas, stretching south into Mexico.

At the LGM, despite the ice sheets in the higher altitudes for the Himalayas, lower altitudes remain climatically suitable and these favourable conditions expand south-easterly, into Myanmar, southern China and Japan (Fig. 3.5.28 E). In Europe, areas around the Devensian ice sheet covering the British Isles, the Alps and Apennines and Spain are simulated as potential ranges for _Tsuga_ species. North America had two core regions which possessed climate within the modelled niche of _Tsuga_ species, both south of the Laurentide ice sheet, one to the west along the coast and patchy through the Rocky Mountains, the other in the east along the south-eastern coastline and north-east USA. These colder conditions caused an overall restriction in climatic range from the interglacials, with just 2,132 grid cells simulated for _Tsuga_ species.

Appendix

The beginning of the Holocene generates simulations of climatically suitable areas in four core regions globally for *Tsuga* species' niche; in south Asia - the Himalayas and easterly into southern China and Japan; in Europe - central into eastern Russia and northern coastlines of Norway and Scotland; western North America - along the west-coastline of Canada, British Colombia and in the eastern North America- from the North East USA into Canada, south of the Hudson Bay (Fig. 3.5.28 F).   There were also isolated potential occurrences in southern Greenland and Alaska, Mexico and Colombia.   In total this scenario produced a range which covered 3,015 grid cells.

Picea abies

The Eemian interglacial resulted in simulated ranges for *Picea abies* in southern and eastern Fennoscandia and from the Carpathian Mountains, Dinaric Alps and Eastern Europe, throughout central Russia and the northern Japan (Fig. 3.5.31 A). Further to the east sporadic patches of potential climatic suitability can be found in Russian Magadan and Kamchatka peninsula. The overall simulated range for *Picea abies* covers 9,356 grid cells.

At the Melisey 1 stadial *Picea abies* climatically suitable range was from the south coast of England and eastern France through central Europe and southern Fennoscandia into north-western Russia and across to the south-eastern Siberian coastline, Kamchatka peninsula, island of Sakhalin and northern Japan (Fig. 3.5.31 B). There are also sporadic simulations elsewhere in Eurasia, including the Caucasus Mountains and the Himalayas, and the overall simulated range is 8,223 grid cells.

During the warmer interstadial conditions, there was an expansive suitable across central and southern latitudes of Siberia; from the eastern coastline and southern Japan, north to Chukotka and south-easterly across Russia to the Weichselian ice sheet edge throughout central Europe and the exposed continental shelf (Fig. 3.5.31 C). There were sporadic but isolated localities in the Caucasus Mountains and the Himalayas. Overall, these warmer wetter conditions are more favourable with 8,070 climatically suitable grid cells simulated.

The climatic conditions of Heinrich Event 5 resulted in a significant reduction in the total simulated range for *Picea abies* to just 5,556 grid cells compared to the later LGM. The main predicted range is throughout Russia to the south-eastern coast and Japan but there are many gaps in this range where the climate is inhospitable at this time (Fig. 3.5.31 D). A vast expanse of unsuitable climate to the east of the Weichselian ice sheet results in the segregation of the Russian range from favourable locations in Europe; the Alps, France, Germany and Dinaric Alps. There is additional climatic suitability in the Caucasus Mountains, the Himalayas and in the north-eastern Kamchatka peninsula.

The LGM conditions resulted in *Picea abies* being climatically restricted to southern Russia, easterly as far as Japan, and Kamchatka peninsula, and westerly to the edge of the Weichselian ice sheet into central Europe and on to the continental shelf exposed at this time (Fig. 3.5.31 E). Similar to earlier and later conditions, the climate in the Caucasus Mountains and the Himalayas is suitable for the species. Overall this more southerly restricted distribution covers a more limited total range extent of 5,556 grid cells.

The beginning of the Holocene simulated distributions for *Picea abies* indicate it may have had a range spanning across central Russia; north to the coastline of the Barents and Kara Sea and east to Sakhalin, northern Japan, Chukotka and the Kamchatka peninsula (Fig. 3.5.31 F). Northern Fennoscandia was climatically unsuitable, but southern regions of Sweden, the continental shelf exposed around Holland and the central and southern European mountain ranges of the Alps, Dinaric Alps and Carpathian Mountains also had climatic conditions suitable for *Picea abies*. Isolated mountainous regions with favourable conditions, such as the Caucasus Mountains and the Himalayas were unlikely to be colonised by this particular species. Across the whole northern hemisphere, there are more climatically suitable grid cells, 11,477, compared to the later present-day simulations, 10,162.

Appendix

Pinus sylvestris

The Eemian interglacial climatic conditions provided climatic conditions suitable for *P. sylvestris* from Japan, northern China and the south-eastern Russian coastline through central Russia into Europe and although patchier in the west; in France, the Iberian mountains and south; in Greece and northern Turkey (Fig. 3.5.34 A).   There are favourable sites in Scotland, similar to observed populations today, significantly isolated from the rest of the European range.   There are also sporadic locations simulated in the Himalayas and on the far eastern Kamchatka peninsula.   In total there are 8,575 grid cells simulated as suitable for *P. sylvestris*, a similar number to the later interglacial Holocene simulations.

The Melisey 1 resulted in a more restricted distribution than during the normal interglacial conditions, with a total of 5,619 grid cells simulated as suitable for *Pinus sylvestris*.   The simulated range spans from the south-eastern coast Russia and Japan, north-easterly to the northern Kara and Barents Sea coastline (Fig. 3.5.34 B). There was a restricted corridor of suitable climate through western Russia into Eastern Europe, where central Europe and the mountainous regions of the Pyrenees, Apennines and Dinaric Alps are the western limits. Southern England, north-western Ireland and the western coast of Scotland also had climatic conditions suitable for *Pinus sylvestris.*   In addition to this broad range, the climate in northern Turkey, the Caucasus Mountains, the Himalayas and Kamchatka peninsula were also potential localities for *Pinus* species.

The warmer interglacial conditions provide a greater number of climatically suitable locations than at other times during the glacial, with 6,320 grid cells simulated.   This potential range spans southern Russia, from the south-eastern coast, and neighbouring islands of Japan, to the western edge of the Weichselian ice sheet and along the southern edge of this ice mass into central and southern Europe as far west as the Iberian mountains and the Devensian ice sheet (Fig. 3.5.34 C).   There are also simulated presences to the north of this ice sheet, in north-western Scotland.   Again, like in the Heinrich Event 5 conditions, the Himalayas and Caucasus mountains were a climatically suitable location for *Pinus sylvestris.*

As a result of the cold conditions of the Heinrich Event 5, the total simulated range for *Pinus sylvestris* 3,209 grid cells, less than half the observed range (6,723).   *Pinus sylvestris'* climatic niche was found the European mountains; the Pyrenees, Alps, Dinaric Alps and Carpathian and Balkan Mountains as well as more distant regions in the Himalayas and Caucasus Mountains (Fig. 3.5.34 D).   Regions of southern Russia, northern China and Japan are also simulated as suitable.

At the LGM the simulations for *Pinus sylvestris* are split between western and central Eurasia; along the western and southern edge of the Devensian ice sheet and northern Spain, throughout central Europe and south-western Russia, and south-eastern Siberia, northern China and Japan (Fig. 3.5.34 E).   Similarly to the later Holocene simulations, there were climate niches in the Caucasus Mountains and Himalayas suitable for *Pinus sylvestris*, which are unlikely to have been occupied by this species, where other pine species are found today.   This fragmentation and smaller range size predictions results in a northern hemisphere total of just 4,309 grid cells simulated for *Pinus sylvestris.*

The onset of the Holocene resulted in a total climatic simulated range of 8,498 grid cells.   However, this includes simulations in regions significantly isolated from the core climatic range, which was potentially from northern Spain, through central Europe, southern Fennoscandia and into northern, central and the south-eastern

coastline of Russia, northern Japan and sporadically in eastern Siberia (Fig. 3.5.34 F).   The simulated presence of *Pinus sylvestris* in Scotland, where it is native today, suggests it has been a resident here since the early Holocene despite is geographic segregation from the core population.   Other isolated simulation in the Himalayas and Caucasus mountains, are unlikely to have ever been colonised.

Pinus occidentalis

The Eemian interglacial similar conditions to present day, provide just 25 grid cells of suitable climate, however unlike the colder conditions of the stadial, a great number are simulated in the Caribbean, on Hispaniola, Cuba and Jamaica (Fig. 3.5.37 A).   The rest of the climatically suitable locations can be found to the southern Guatemala, Honduras, Nicaragua, Colombia and Venezuela.

The Melisey 1 stadial resulted in just one location in the Caribbean being suitable for *Pinus occidentalis* on the south-western peninsula of Hispaniola (Fig. 3.5.37 B).   There were also locations around the West Indies which are within the modelled climatic niche, along the Mexico Gulf coastline, USA states of Florida and Louisiana, Honduras, Nicaragua and some isolated locations in Colombia and Venezuela.   These conditions provided just 21 grid cells climatically suitable for *Pinus occidentalis*.

The interglacial conditions were warmer with simulations suggesting that there were sporadic locations throughout Hispaniola, Puerto Rico, eastern Jamaica northern Cuba and the Bahamas climatically suitable for *Pinus occidentalis* (Fig. 3.5.37 C).   In addition to these, there are sites in western Florida - along the continental shelf exposed along the peninsula; Central American - Guatemala, Honduras and Nicaragua; and northern coastline of South America where climatic conditions are suitable for this species, summing to 68 simulated grid cells.

The Heinrich Event 5 climatic conditions resulted in numerous locations in eastern Cuba, surrounding areas of the Caribbean exposed by the lower sea level and the more easterly Great Inagua Island having had climatic conditions suited for *P. occidentalis* (Fig. 3.5.37 D).   Again there were many climatically suitable locations on the mainland; northern Florida, Mexico, Salvador, Nicaragua, northern Colombia and Venezuela.   In total there are 96 grid simulated as being within *Pinus occidentalis*' modelled niche.

At the LGM, despite the ice sheet being significantly north of the Caribbean, there was a southerly restriction of climatically suitable localities within the islands, only eastern Hispaniola and Puerto Rica having conditions favourable for *P. occidentalis* (Fig. 3.5.37 E).   Predictions on the mainland are both to the north, in northern Florida, and south in Honduras, Guatemala, Nicaragua and northern South America, similar areas to the later Holocene.   A sum of 48 grid cells around the Caribbean have climate which is within the modelled climatic niche of *P. occidentalis*.

At the beginning of the Holocene there are several locations in eastern Hispaniola, Cuba and Jamaica simulated as suitable for *Pinus occidentalis* (Fig. 3.5.37 F).   In addition to these, the mainland surrounding the Caribbean also has climatically suitable locations to the south, in Guatemala, Honduras, Nicaragua and northern Colombia and Venezuela.   In total there are 35 grid cells in the Caribbean region which were climatically suitable *P. occidentalis* at this scenario.

References

Allen, J. R. M., Brandt, U., Brauer, A., Hubberten, H.-W., Huntley, B., Keller, J., Kraml, M., Mackensen, A., Mingram, J., Negendank, J. F. W., Nowaczyk, N. R., Oberhänsli, H., Watts, W. A., Wulf, S. & Zolitschka, B. (1999). Rapid Environmental Changes in Southern Europe During the Last Glacial Period. *Nature*, **400** (6746):740-743.

Allen, J. R. M., Hickler, T., Singarayer, J. S., Sykes, M. T., Valdes, P. J. & Huntley, B. (2010). Last Glacial Vegetation of Northern Eurasia. *Quaternary Science Reviews*, **29** (19-20):2604-2618.

Alonso, D., Arizaga, J., Miranda, R. & Hernández, M. Á. (2006). Morphological Diversification of Common Crossbill *Loxia curvirostra* Populations within Iberia and the Balearics. *Ardea*, **94** (1):99-107.

Araújo, M. B. & Guisan, A. (2006). Five (or so) Challenges for Species Distribution Modelling. *Journal of Biogeography*, **33** (10):1677-1688.

Araújo, M. B., Pearson, R. G., Thuiller, W. & Erhard, M. (2005). Validation of Species-Climate Impact Models under Climate Change. *Global Change Biology*, **11** (9):1504-1513.

Arnaiz-Villena, A., Guillén, J., Ruiz-del-Valle, V., Lowy, E., Zamora, J., Varela, P., Stefani, D. & Allende, L. M. (2001). Phylogeography of Crossbills, Bullfinches, Grosbeaks, and Rosefinches. *Cellular and Molecular Life Sciences*, **58** (8):1159-1166.

Austin, M. (2007). Species Distribution Models and Ecological Theory: A Critical Assessment and Some Possible New Approaches. *Ecological Modelling*, **200** (1-2):1-19.

Austin, M. P. (1987). Models for the Analysis of Species' Response to Environmental Gradients. *Plant Ecology*, **69** (1):35-45.

Austin, M. P. (2002). Spatial Prediction of Species Distribution: An Interface Between Ecological Theory and Statistical Modelling. *Ecological Modelling*, **157** (2-3):101-118.

Avery, M. I. (1989). Effects of Upland Afforestation on Some Birds of the Adjacent Moorlands. *Journal of Applied Ecology*, **26** (3):957-966.

Avise , J. C. & Walker, D. (1998). Pleistocene Phylogeographic Effects on Avian Populations and the Speciation Process. *Proceedings of the Royal Society B: Biological Sciences*, **265** (1395):457-463.

Bakken, V., Runde, O. & Tjorve, E. (2006). "Norwegian Bird Ringing Atlas, Volume 2: Pigeons - Passerines " Stavanger Museum, Stavanger.

Bard, E., Hamelin, B. & Fairbanks, R. G. (1990). U-Th Ages Obtained By Mass-Spectrometry In Corals From Barbados - Sea-Level During The Past 130,000 Years. *Nature*, **346** (6283):456-458.

References

Bartolomei, G., Broglio, A., Cassoli, P. F., Cas-Telletti, L., Cattani, L., Cremaschi, M., Giacobini, G., Malerba, G., Maspero, A., Presani, M., Sarto-Relli, A. & Tagliacozzo, A. (1994). La Grotte de Fumane: Un Site Aurignacien au Pied des Alpes. *Preistoria Alpina*, **28**:131-179.

Beale, C. M., Lennon, J. J. & Gimona, A. (2008). Opening the Climate Envelope Reveals No Macroscale Associations with Climate in European Birds. *Proceedings of the National Academy of Sciences of the United States of America*, **105** (39):14908-14912.

Benkman, C. W. (1987). Crossbill Foraging Behaviour, Bill Structure, and Patterns of Food Profitability. *The Wilson Bulletin*, **99** (3):351-368.

Benkman, C. W. (1988). Seed Handling Ability, Bill Structure, and the Cost of Specialization for Crossbills. *The Auk*, **105** (4):715-719.

Benkman, C. W. (1989a). Intake Rate Maximization and the Foraging Behaviour of Crossbills. *Ornis Scandinavica*, **20** (1):65-68.

Benkman, C. W. (1989b). On the Evolution and Ecology of Island Populations of Crossbills. *Evolution*, **43** (6):1324-1330.

Benkman, C. W. (1993). Logging, Conifers, and the Conservation of Crossbills. *Conservation Biology*, **7** (3):473-479.

Benkman, C. W. (1994). Comments on the Ecology and Status of the Hispaniolan Crossbill (*Loxia leucoptera megaplaga*), with Recommendations for its Conservation. *Caribbean Journal of Science*, **30** (3-4):250-254.

Benkman, C. W. (1999). The Selection Mosaic and Diversifying Co-Evolution between Crossbills and Lodgepole Pine. *American Naturalist*, **153**:S77-S91.

Benkman, C. W. (2003). Divergent Selection Drives the Adaptive Radiation of Crossbills. *Evolution*, **57** (5):1176-1181.

Benkman, C. W. (2007). Red Crossbill Types in Colorado: Their Ecology, Evolution, and Distribution. *Colorado Birds*, **41** (3):153-163.

Benkman, C. W., Colquitt, J. S., Gould, W. R., Fetz, T., Keenan, P. C. & Santisteban, L. (2005). Can Selection by an Ectoparasite Drive a Population of Red Crossbills from its Adaptive Peak? *Evolution*, **59** (9):2025-2032.

Benkman, C. W. & Parchman, T. L. (2009). Coevolution between Crossbills and Black Pine: The Importance of Competitors, Forest Area and Resource Stability. *Journal of Evolutionary Biology*, **22** (5):942-953.

References

Benkman, C. W., Smith, J. W., Keenan, P. C., Parchman, T. L. & Santisteban, L. (2009). A New Species of the Red Crossbill (Fringillidae: *Loxia*) from Idaho. *The Condor*, **111** (1):169-176.

BirdLife International. (2010). IUCN Red List for Birds Downloaded from http://www.birdlife.org. Accessed on 22/11/2010.

Birks, H. J. B. (1989). Holocene Isochrones Maps and Patterns of Tree-Spreading in the British Isles. *Journal of Biogeography*, **16** (6):503-540.

Blois, J. L., Williams, J. W., Grimm, E. C., Jackson, S. T. & Graham, R. W. (2011). A Methodological Framework for Assessing and Reducing Temporal Uncertainty in Palaeovegetation Mapping from Late-Quaternary Pollen Records. *Quaternary Science Reviews*, **30** (15-16):1926-1939.

Bochenski, Z. (1982). "Excavation in the Bacho Kiro Cave (Bulgaria). Final Report." Kozlowski, J. K., (ed.). Panstwowe Wydanictwo Naukowe, Warsaw.

Boev, Z. (1999). Earliest Finds of Crossbills (Genus: *Loxia*)(Aves: Fringillidae) from Varshets (NW Bulgaria). *Geologica Balcanica*, **29** (3-4):51-57.

Boev, Z. (2000). Late Pleistocene Avifauna of the Razhishkata Cave, Western Bulgaria. *Historia Naturalis Bulgarica*, **10**:109-115.

Boev, Z. (2001). Late Pleistocene Birds from the Kozarnika Cave (Montana District: NW Bulgaria). *Proceedings First National Conference on Environment and Cultural Heritage in Karst*, **1**:133-128.

Boev, Z. (2002). "Neogene Avifauna of Bulgaria." *in* "Proceedings of the 5th Symposium of the Society of Avian Paleontology and Evolution." Zhou, Z. & Zhang, F., editors. Sciences Press, Beijing, China.

Boles, W. E. (1997). Fossil Songbirds (Passeriformes) from the Early Eocene of Australia. *Emu*, **97**:43-50.

Bond, J. (1948). Origin of the Bird Fauna of the West Indies. *The Wilson Bulletin*, **60** (4):207-229.

Burfield, I. & van Bommel, F. (2004). "Birds in Europe." Birdlife International.

Carstens, B. C. & Knowles, L. L. (2007). Shifting Distributions and Speciation: Species Divergence During Rapid Climate Change. *Molecular Ecology*, **16** (3):619-627.

Cassoli, P. F. (1980). L'avifauna del Pleistocene Superiore Delle Arene Candide (Liguria). *Memorie dell'Isituto Italiano di Paleontologia Umana Roma*, **3**:155-234.

References

Cassoli, P. F. & Tagliacozzo, A. (1994). Consideratzioni Paleontologiche, Paleoecologiche e Archozoologiche sui Macromammiferi e Gli Uccelli dei Livelli del Pleistocene Superiore del Riparo di Fumane. *Bollenti del Museo Civico de Storia Naturale di Verona*, **18**:349-445.

Cleveland, W. S. & Devlin, S. J. (1988). Locally Weighted Regression: An Approach to Regression Analysis by Local Fitting. *Journal of the American Statistical Association*, **83** (403):596-610.

Clouet, M. & Goar, J.-L. (1999). Vietnamese Crossbill *Loxia curvirostra meridionalis*. *Société d'Etudes Ornithologiques de France*, **67** (1):1-4.

Clouet, M. & Goar, J.-L. (2001). Note on the Philippine Crossbill *Loxia curvirostra luzoniensis*. *Alauda*, **69** (2):331-334.

Cohen, J. (1960). A Coefficient of Agreement for Nominal Scales. *Educational and Psychological Measurement*, **20** (1):37-46.

Cramer, W. P. & Prentice, I. C. (1988). Simulation of Soil Moisture Deficits on a European Scale. *Norsk Geografisk Tidskrift*, **42**:149-151.

Cramp, S., Perrins, C. M., Brooks, D. J., Dunn, E., Gillmor, R., Hall-Craggs, J., Hillcoat, B., Hollom, P. A. D., Nicholson, E. M., Roselaar, C. S., Seale, W. T. C., Sellar, P. J., Simmons, K. E. L., Snow, D. W., Vincent, D., Voous, K. H., Wallace, D. I. M. & Wilsom, M. G. (1995). "Handbook of the Birds of Europe the Middle East and North Africa: The Birds of the Western Palaearctic. Volume VIII: Crows to Finches." Oxford University Press, Oxford.

Critchfield, W. B. & Little, E. L., Jr.,. (1966). "Geographic Distribution of the Pines of the World." U.S. Department of Agriculture Miscellaneous Publication.

Danilov, N. N., Ryzhanovsky, V. N. & Ryabitsev, V. K. (1984). "The Birds of Yamal." Nauka, Moscow.

Dartmoor National Park Authority. (2010). "A Woodland Strategy for Dartmoor National Park."

Dávalos, L. M. & Brooks, T. (2001). Parc National la Visite, Haiti: A Last Refuge for the Country's Montane Birds. *Cotinga*, **16**:36-39.

Davis, M. B. (1983). Quaternary History of Deciduous Forests of Eastern North America and Europe. *Annals of the Missouri Botanical Garden*, **70** (3):550-563.

Davis, M. B. & Shaw, R. G. (2001). Range Shifts and Adaptive Responses to Quaternary Climate Change. *Science*, **292** (5517):673-679.

De'ath, G. & Fabricius, K. E. (2000). Classification and Regression Trees: A Powerful Yet Simple Technique for Ecological Data Analysis. *Ecology*, **81** (11):3178-3192.

References

Dietl, G. P. & Flessa, K. W. (2011). Conservation Paleobiology: Putting the Dead to Work. *Trends in Ecology & Evolution*, **26** (1):30-37.

Dod, A. S. (1978). "Aves de la República Dominicana." Museo Nacional de Historia Natural, Santo Domingo, Dominican Republic.

Dod, A. S. (1992). Endangered and Endemic Birds of the Dominican Republic. Cypress House, California.

Dullinger, S., Dirnböck, T., Köck, R., Hochbichler, E., Englisch, T., Sauberer, N. & Grabherr, G. (2005). Interactions Among Tree-Line Conifers: Differential Effects of Pine on Spruce and Larch. *Journal of Ecology*, **93** (5):948-957.

Eames, J. C. & Ericson, P. G. P. (1996). The Björkegren Expeditions to French Indochina: A Collection of Birds from Vietnam and Cambodia. *Natural History Bulletin of the Siam Society*, **44**:75-111.

Edelaar, P. (2008). Rediscovery of a Second Kind of Crossbill for the Himalayan Region, and the Hypothesis that Ecological Opportunity Drives Crossbill Diversification. *Ibis*, **150** (2):405-408.

Edelaar, P., Summers, R. & Iovchenko, N. (2003). The Ecology and Evolution of crossbills *Loxia* spp: The Need for a Fresh Look and an International Research Programme. *Avian Science*, **3**:1-9.

Edelaar, P. & Terpstra, K. (2004). Is the Nominate Subspecies of the Common Crossbill *Loxia c. curvirostra* Polytypic? I. Morphological Differences Among Years at a Single Site. *Ardea*, **92** (1):93-102.

Edelaar, P., Van Eerde, K. & Terpstra, K. (2008). Is the Nominate Subspecies of the Common Crossbill *Loxia c. curvirostra* Polytypic? II. Differentiation Among Vocal Types in Functional Traits. *Journal of Avian Biology*, **39** (1):108-115.

Edwards, S. V. & Boles, W. E. (2002). Out of Gondwana: The Origin of Passerine Birds. *Trends in Ecology & Evolution*, **17** (8):347-349.

Ehlers, J. & Gibbard, P. L. (2007). The Extent and Chronology of Cenozoic Global Glaciation. *Quaternary International*, **164-165** (0):6-20.

Elith, J., Phillips, S. J., Hastie, T., Miroslav, D., Chee, Y. E. & Yates, C. J. (2011). A Statistical Explanation of MaxEnt for Ecologists. *Diversity and Distributions*, **17** (1):43-57.

Ericson, P. G. P., Christidis, L., Cooper, A., Irestedt, M., Jackson, J., Johansson, U. S. & Norman, J. A. (2002). A Gondwanan Origin of Passerine Birds Supported by DNA Sequences of the Endemic New Zealand Wrens. *Proceedings of the Royal Society B: Biological Sciences*, **269** (1488):235-241.

References

ESRI. (1998). Arc/Info. Environmental Systems Research Institute Inc, Redlands, California.

EUFORGEN (2009). Distribution Maps; http://www.euforgen.org/distribution_maps.html. European Forest Genetic Resources Project. Last Accessed on 28/8/2011.

Fairbanks, R. G. (1989). A 17,000-Year Glacio-eustatic Sea Level Record: Influence of Glacial Melting Rates on the Younger Dryas Event and Deep-Ocean Circulation. *Nature*, **342** (6250):637-642.

Farjon, A. (1990). "Pinaceae." Koeltz Scientific Books, Koenigstein, Germany.

Fischer, S., Mauersberger, G., Schielzeth, H. & Witt, K. (1992). Erster Brutnachweis des Bindenkreuzschnabels (*Loxia leucoptera*) in Mitteleuropa. *Journal of Ornithology*, **133** (2):197-202.

Florit, X. & Alcover, J. A. (1987). Els Ocells del Pleistocè Superior de la Cova Nova (Capdepera, Mallorca). *Bolletí de la Societat d' Història Natural dels Balears*, **31**:7-32.

Gibbons, D. W., Reid, J. B. & Chapman, R. A. (1993). "The New Atlas of Breeding Birds in Britain and Ireland: 1988-1991." T. & A.D. Poyser, London.

Godwin, H. (1934). Pollen Analysis. An Outline of the Problems and Potentialities of the Method. *New Phytologist*, **33** (4):278-305.

Gordon, C., Cooper, C., Senior, C. A., Banks, H., Gregory, J. M., Johns, T. C., Mitchell, J. F. B. & Wood, R. A. (2000). The Simulation of SST, Sea Ice Extents and Ocean Heat Transports in a Version of the Hadley Centre Coupled Model without Flux Adjustments. *Climate Dynamics*, **16** (2-3):147-168.

Graham, R. W., Lundelius, E. L., Graham, M. A., Schroeder, E. K., Toomey, R. S., Anderson, E., Barnosky, A. D., Burns, J. A., Churcher, C. S., Grayson, D. K., Guthrie, R. D., Harington, C. R., Jefferson, G. T., Martin, L. D., McDonald, H. G., Morlan, R. E., Semken, H. A., Webb, S. D., Werdelin, L. & Wilson, M. C. (1996). Spatial Response of Mammals to Late Quaternary Environmental Fluctuations. *Science*, **272** (5268):1601-1606.

Grant, P. R. & Grant, B. R. (2009). The Secondary Contact Phase of Allopatric Speciation in Darwin's Finches. *Proceedings of the National Academy of Sciences of the United States of America*, **106** (48):20141-20148.

Grant, W. R. O. & Whitehead, J. (1898). XXI.—On the Nests and Eggs of Some Rare Philippine Birds. *Ibis*, **40** (2):231-247.

Griscom, L. (1937). A Monographic Study of the Red Crossbill. *Proceedings of the Boston Society of Natural History*, **41**:77-210.

References

Gritti, E. S., Smith, B. & Sykes, M. T. (2006). Vulnerability of Mediterranean Basin Ecosystems to Climate Change and Invasion by Exotic Plant Species. *Journal of Biogeography*, **33** (1):145-157.

Groth, J. G. (1993a). "Evolutionary Differentiation in Morphology, Vocalizations, and Allozymes Among Nomadic Sibling Species in the North American Red Crossbill (*Loxia curvirostra*) Complex." University of California Publication in Zoology, No. 127. Berkley, CA.

Groth, J. G. (1993b). Call Matching and Positive Assortative Mating in Red Crossbills. *The Auk*, **110** (2):398-401.

Guisan, A., Edwards, T. C. & Hastie, T. (2002). Generalized Linear and Generalized Additive Models in Studies of Species Distributions: Setting the Scene. *Ecological Modelling*, **157** (2-3):89-100.

Guisan, A. & Thuiller, W. (2005). Predicting Species Distribution: Offering More than Simple Habitat Models. *Ecology Letters*, **8** (9):993-1009.

Guisan, A. & Zimmermann, N. E. (2000). Predictive Habitat Distribution Models in Ecology. *Ecological Modelling*, **135** (2-3):147-186.

Hagemeijer, E. J. M. & Blair, M. J. (1997). "The EBCC Atlas of European Breeding Birds: Their distribution and abundance." A.D. Poyser, London.

Harrison, C. J. O. (1980). A Re-Examination of British Devensian and Earlier Holocene Bird Bones in the British Museum (Natural History). *Journal of Archaeological Science*, **7** (1):53-68.

Harrison, C. J. O. & Fisher, C. (1982). "An Atlas of the Birds of the Western Palaearctic." Princeton University Press, Princeton.

Harrison, S. P. & Prentice, I. C. (2003). Climate and CO_2 Controls on Global Vegetation Distribution at the Last Glacial Maximum: Analysis Based on Palaeovegetation Data, Biome Modelling and Palaeoclimate Simulations. *Global Change Biology*, **9** (7):983-1004.

Hastie, T. & Tibshirani, R. (1990). "Generalized Additive Models." *in* Chapman and Hall, London.

Heikkinen, R. K., Luoto, M., Virkkala, R., Pearson, R. G. & Körber, J.-H. (2007). Biotic Interactions Improve Prediction of Boreal Bird Distributions at Macro-Scales. *Global Ecology and Biogeography*, **16** (6):754-763.

Herold, N. D., Koeln, G. & Cunningham, D. (2003). Mapping Impervious Surfaces and Forest Canopy using Classification and Regression Tree (CART) Analysis. ASPRS 2003 Annual Conference Proceedings, Anchorage, Alaska.

Hewitt, G. M. (1996). Some Genetic Consequences of Ice Ages, and their Role, in Divergence and Speciation. *Biological Journal of the Linnean Society*, **58** (3):247-276.

Hewitt, G. M. (1999). Post-Glacial Re-Colonization of European Biota. *Biological Journal of the Linnean Society*, **68** (1-2):87-112.

Higgins, J. (1999). Túnel: A Case Study of Avian Zooarchaeology and Taphonomy. *Journal of Archaeological Science*, **26** (12):1449-1457.

Hjelmroos, M. & Franzén, L. G. (1994). Implications of Recent Long-Distance Pollen Transport Events for the Interpretation of Fossil Pollen Records in Fennoscandia. *Review of Palaeobotany and Palynology*, **82** (1-2):175-189.

Hofreiter, M. & Stewart, J. (2009). Ecological Change, Range Fluctuations and Population Dynamics during the Pleistocene. *Current Biology*, **19** (14):R584-R594.

Holliday, P. R. (2010). Potential Palaeogeographical Distributions of European Granivorous Birds and their Feeding Trees. University of Durham, Durham.

Holloway, S. (1996). "The Historical Atlas of Breeding Birds in Britain and Ireland 1875-1900." T. & A.D. Poyser Ltd., London.

Huntley, B. (1993). Species-Richness in North-Temperate Zone Forests. *Journal of Biogeography*, **20** (2):163-180.

Huntley, B. (1995). Plant Species' Response to Climate Change: Implications for Conservation of European Birds. *Ibis*, **136** (Supplement 1):127-138.

Huntley, B., Alfano, M. J., Allen, J. R. M., Pollard, D., Tzedakis, P. C., de Beaulieu, J.-L., Grüger, E. & Watter, B. (2003). European Vegetation during the Marine Oxygen Isotope Stage 3. *Quaternary Research*, **56** (2):195-212.

Huntley, B., Allen, J. R. M., Barnard, P., Collingham, Y. C. & Holliday, P. R. (In Press). Species' Distribution Models Indicate Contrasting Late-Quaternary Histories for Southern and Northern Hemisphere Bird Species. *Global Ecology and Biogeography*.

Huntley, B., Altwegg, R., Barnard, P., Collingham, Y. C. & Hole, D. G. (2012). Modelling Relationships Between Species Spatial Abundance Patterns and Climate. *Global Ecology and Biogeography*, **21** (6):668-681.

Huntley, B., Bartlein, P. J. & Prentice, I. C. (1989). Climatic Control of the Distribution and Abundance of Beech (Fagus L.) in Europe and North America. *Journal of Biogeography*, **16** (6):551-560.

Huntley, B., Berry, P. M., Cramer, W. P. & McDonald, A. P. (1995). Modelling Present and Potential Future Ranges of Some European Higher Plants Using Climate Response Surfaces. *Journal of Biogeography*, **22** (6):967-1001.

References

Huntley, B. & Birks, H. J. B. (1983). "An Atlas of Past and Present Pollen Maps of Europe: 0-13,000 Years Ago. ." Cambridge University Press, Cambridge.

Huntley, B., Collingham, Y. C., Green, R. E., Hilton, G. M., Rahbek, C. & Willis, S. G. (2006). Potential Impacts of Climatic Change upon Geographical Distributions of Birds. *Ibis*, **184** (s1):8-28.

Huntley, B., Collingham, Y. C., Willis, S. G. & Green, R. E. (2008). Potential Impacts of Climatic Change on European Breeding Birds. *PLoS ONE*, **3** (1):e1439.

Huntley, B., Green, R. E., Collingham, Y. C., Hill, J. K., Willis, S. G., Bartlein, P. J., Cramer, W., Hagemeijer, W. J. M. & Thomas, C. J. (2004). The Performance of Models Relating Species Geographical Distributions to Climate is Independent of Tropic Level. *Ecology Letters*, **7** (5):417-426.

Huntley, B., Green, R. E., Collingham, Y. C. & Willis, S. G. (2007). "A Climatic Atlas of European Breeding Birds." Lynx Edicions, Barcelona.

Hutchinson, M. F. (1989). "A New Objective Method for Spatial Interpolation of Meteorological Variables from Irregular Networks Applied to the Estimation of Month Mean Solar Radiation, Temperature, Precipitation and Windrun." *in* "Need for Climatic and Hydrologic Data in Agriculture in Southeast Asia, Proceedings of a United Nations University Workshop Held at the Canberra College of Advanced Education." CSIRO Division of Water Resources, Canberra, Australia: 95-104.

IOC, IHO & BODC. (2003). Centenary Edition of the GEBCO Digital Atlas, published on CD-ROM on behalf of the Intergovernmental Oceanographic Commission and the International Hydrogrpahic Organization as part of the General Bathymetric Chart of the Oceans. British Oceanographic Data Centre, Liverpool, UK.

Isaksson, E., Hermanson, M., Hicks, S., Igarashi, M., Kamiyama, K., Moore, J., Motoyama, H., Muir, D., Pohjola, V., Vaikmäe, R., van de Wal, R. S. W. & Watanabe, O. (2003). Ice Cores from Svalbard--Useful Archives of Past Climate and Pollution History. *Physics and Chemistry of the Earth, Parts A/B/C*, **28** (28-32):1217-1228.

IUCN. (2011). IUCN Red List of Threatened Species. Version 2011.2. www.iucnredlist.org. Accessed on Accessed on 22/11/2011.

Jackson, S. T. & Weng, C. (1999). Late Quaternary Extinction of a Tree Species in Eastern North America. *Proceedings of the National Academy of Sciences of the United States of America*, **96** (24):13847-13852.

Jánossy, D. (1972). "Die Mittelpleistozäne Vogelfauna der Stránská Skála." *in* "Stránská skála I." Musil, R., (ed.). Anthropos, Brno, 20: 35-36.

Jaynes, E. T. (1957). Information Theory and Statistical Mechanics. *Physical Review*, **106** (4):620-630.

Kinloch, B. B., Westfall, R. D. & Forrest, G. I. (1986). Caledonian Scots Pine: Origins and Genetic Structure. *New Phytologist*, **104** (4):703-729.

Klicka, J. & Zink, R. M. (1997). The Importance of Recent Ice Ages in Speciation: A Failed Paradigm *Science*, **277** (5332):1666-1669.

Knox, A. G. (1990). The Sympatric Breeding of Common and Scottish Crossbills *Loxia curvirostra* and *L. scotica* and the Evolution of crossbills. *Ibis*, **132** (3):454-466.

Koca, D., Smith, B. & Sykes, M. (2006). Modelling Regional Climate Change Effects On Potential Natural Ecosystems in Sweden. *Climatic Change*, **78** (2):381-406.

Koch, P. L. & Barnosky, A. D. (2006). Late Quaternary Extinctions: State of the Debate. *Annual Review of Ecology, Evolution, and Systematics*, **37** (1):215-250.

Kolar, C. S. & Lodge, D. M. (2002). Ecological Predictions and Risk Assessment for Alien Fishes in North America. *Science*, **298** (5596):1233-1236.

Kumar, S. & Stohlgren, T. J. (2009). Maxent Modeling for Predicting Suitable Habitat for Threatened and Endangered Tree *Canancomyrica monticola* in New Caledonia. *Journal of Ecology and Natural Environment*, **1** (4):94-98.

Kutzbach, J., Gallimore, R., Harrison, S., Behling, P., Selin, R. & Laarif, F. (1998). Climate and Biome Simulations for the Past 21,000 Years. *Quaternary Science Reviews*, **17** (6-7):473-506.

Latta, S. C., Sondreal, M. L. & Brown, C. R. (2000). A Hierarchical Analysis of Nesting and Foraging Habitat for the Conservation of the Hispaniolan White-Winged Crossbill (*Loxia leucoptera megaplaga*). *Biological Conservation*, **96** (2):139-150.

Latta, S. C., Sondreal, M. L. & Mejía, D. A. (2002). Breeding Behavior of the Endangered Hispaniolan Crossbill (*Loxia megaplaga*). *Ornitologia Neotropical*, **13** (3):225-234.

Lewis, R. J. (2000). An Introduction to Classification and Regression Tree (CART) Analysis. Annual Meeting of the Society for Academic Emergency Medicine, San Francisco, California.

Little, E. L. J. (1971). "Atlas of United States Trees, Volume 1, Conifers and Important Hardwoods." U.S. Department of Agriculture Miscellaneous Publication.

Loiselle, B. A., Howell, C. A., Graham, C. H., Goerck, J. M., Brooks, T., Smith, K. G. & Williams, P. H. (2003). Avoiding Pitfalls of Using Species Distribution Models in Conservation Planning

Evitando Dificultades Resultantes del Uso de Modelos de Distribución de Especies en Planeación de Conservación. *Conservation Biology*, **17** (6):1591-1600.

References

Loulergue, L., Schilt, A., Spahni, R., Masson-Delmotte, V., Blunier, T., Lemieux, B., Barnola, J.-M., Raynaud, D., Stocker, T. F. & Chappellaz, J. (2008). Orbital and Millennial-Scale Features of Atmospheric CH_4 over the Past 800,000 Years. *Nature*, **453** (7193):383-386.

Lowe, J. J., Rassmussen, S. O., Björck, J., Hoek, W. Z., Steffensen, J. P., Walker, M. J. C., Yu, Z. & the Intimate Group. (2008). Synchronisation of Palaeoenvironmental Events in the North Atlantic Region During the Last Termination: A Revised Protocol Recommended by the INTIMATE Group. *Quaternary Science Reviews*, **27** (1-2):6-17.

Manel, S., Williams, H. C. & Ormerod, S. J. (2001). Evaluating Presence–Absence Models in Ecology: The Need to Account for Prevalence. *Journal of Applied Ecology*, **38** (5):921-931.

Marco, A. S. (2004). Avian Zoogeographical Patterns during the Quaternary in the Mediterranean Region and Paleoclimatic Interpretation. *Ardeola*, **51** (1):91-132.

Marquiss, M. & Rae, R. (1994). Seasonal Trends in Abundance, Diet and Breeding of Common Crossbills (*Loxia curvirostra*) in an Area of Mixed Species Conifer Plantation Following the 1990 Crossbill 'Irruption' *Forestry*, **67** (1):31-47.

Marquiss, M. & Rae, R. (2002). Ecological Differentiation in Relation to Bill Size Amongst Sympatric, Genetically Undifferentiated Crossbills *Loxia* spp. *Ibis*, **144** (3):494.508.

Martinelli, N. (2004). Climate from Dendrochronology: Latest Developments and Results. *Global and Planetary Change*, **40** (1-2):129-139.

Maslin, M., Seidov, D. & Lowe, J. (2001). Synthesis of the Nature and Causes of Rapid Climate Transitions During the Quaternary. *Geophysical Monograph*, **126**:9-52.

Massa, B. (1987). Variations in Mediterranean Crossbills *Loxia curvirostra. Bulletin of the British Ornithological Club*, **107**:118-129.

McPherson, J. M., Jetz, W. & Rogers, D. J. (2004). The Effects of Species' Range Sizes on the Accuracy of Distribution Models: Ecological Phenomenon or Statistical Artefact? *Journal of Applied Ecology*, **41** (5):811-823.

Metz, C. E. (1978). Basic Principles of ROC Analysis. *Seminars in Nuclear Medicine*, **8** (4):283-298.

Mezquida, E. T. & Benkman, C. W. (2005). The Geographic Selection Mosaic for Squirrels, Crossbills and Aleppo Pine. *Journal of Evolutionary Biology*, **18** (2):348-357.

Miller, A. H. (1932). The Fossil Passerine Birds of the Pleistocene of Carpinteria, California. *University of California Press: Bulletin of the Department of Geological Sciences*, **21** (7):169-194.

References

Miller, P. A., Giesecke, T., Hickler, T., Bradshaw, R. H. W., Smither, B., Seppar, H., Valdes, P. J. & Sykes, M. T. (2008). Exploring Climatic and Biotic Controls on Holocene Vegetation Change in Fennoscandia. *Journal of Ecology*, **96** (2):247-259.

Mlíkovský, J. (2002). "Cenozoic Birds of the World Part 1: Europe." NINOX Press, Praha.

Mlíkovský, J. (2009). Middle Pleistocene Birds of Hundsheim, Austria. *Journal of the National Museum (Prague)*, **177** (7):62-82.

Monserud, R. A. (1990). "Methods for Comparing Global Vegetation Maps." International Institute for Applied Systems Analysis (IIASA), Laxenburg, Austria.

Monson, G. & Phillips, A. R. (1981). "The Races of Red Crossbill, *Loxia curvirostra*, in Arizona." *in* "Annotated checklist of the birds of Arizona 2nd Edition." University of Arizona Press, Tuscon: 223-230.

Morales, P., Hickler, T., Rowell, D. P., Smith, B. & Sykes, M. T. (2007). Changes in European Ecosystem Productivity and Carbon Balance Driven by Regional Climate Model Output. *Global Change Biology*, **13** (1):108-122.

Morales, P., Sykes, M. T., Prentice, I. C., Smith, P., Smith, B., Bugmann, H., Zierl, B., Friedlingstein, P., Viovy, N., Sabaté, S., Sánchez, A., Pla, E., Gracia, C. A., Sitch, S., Arneth, A. & Ogee, J. (2005). Comparing and Evaluating Process-Based Ecosystem Model Predictions of Carbon and Water Fluxes in Major European Forest Biomes. *Global Change Biology*, **11** (12):2211-2233.

Moss, D., Taylor, P. N. & Easterbee, N. (1979). The Effects on Song-Bird Populations of Upland Afforestation with Spruce. *Forestry*, **52** (2):129-150.

Mourer-Chauviré, C. (1975). Les Oiseaux du Pléistocène Moyen et Supérieur de France. *Documents du Laboratoire de Géologie de la Faulté de Sciences de Lyon*, **64**:1-624.

Mourer-Chauviré, C. (1995). Dynamics of the Avifauna During the Paleogene and the Early Neogene of France. Settling of the Recent Fauna. *Acta Zoologica Cracoviensia*, **38** (3):325-342.

Müller, M. J. (1982). "Selected Climatic Data for a Global Set of Standard Stations for Vegetation Science." Dr W. Junk Publishers, The Hague.

Nethersole-Thompson, D. (1975). "Pine Crossbills." T & A D Poyser, Berkhamsted.

New, M., Hulme, M. & Jones, P. D. (1999). Representing Twentieth-Century Space-Time Climate Variability. Part I: Development of a 1961-90 Mean Monthly Terrestrial Climatology. *Journal of Climate*, **12** (3):829-856.

New, M., Hulme, M. & Jones, P. D. (2003). CRU CL 1.0: http://www.cru.uea.ac.uk/~timm/grid/CRU_CL_1_0.html. Last Accessed on 28/8/2011.

Newton, I. (1972). "The Finches." Collins, London.

Newton, I. (1983). Birds and forestry. Centenary Conference on Forestry and Conservation, Royal Forestry Society of England, Wales and Northern Ireland, Tring.

Newton, I. (2006). Advances in the Study of Irruptive Migration. *Ardea*, **94** (3):433-460.

Nogués-Bravo, D., Rodríguez, J., Hortal, J., Bartra, P. & Araújo, M. B. (2008). Climate Change, Humans, and the Extinction of the Woolly Mammoth. *PLoS Biology*, **6** (4): e79.

Papeş, M. & Gaubert, P. (2007). Modelling Ecological Niches from Low Numbers of Occurrences: Assessment of the Conservation Status of Poorly Known Viverrids (Mammalia, Carnivora) Across Two Continents. *Diversity and Distributions*, **13** (6):890-902.

Parchman, T. L. & Benkman, C. W. (2002). Diversifying Coevolution Between Crossbills and Black Spruce on Newfoundland. *Evolution*, **56** (8):1663-1672.

Parchman, T. L. & Benkman, C. W. (2008). The Geographic Selection Mosaic for Pondersa Pine and Crossbills: A Tale of Two Squirrels. *Evolution*, **62** (2):348-360.

Parchman, T. L., Benkman, C. W. & Britch, S. C. (2006). Patterns of Genetic Variation in the Adaptive Radiation of New World Crossbills (Aves: *Loxia*). *Molecular Ecology*, **15** (7):1873-1887.

Parchman, T. L., Benkman, C. W. & Mezquida, E. T. (2007). Coevolution Between Hispaniolan Crossbills and Pine: Does More Time Allow for Greater Phenotypic Escalation at Lower Latitude? *Evolution*, **61** (9):2142-2153.

Parnell, A. C., Haslett, J., Allen, J. R. M., Buck, C. E. & Huntley, B. (2008). A Flexible Approach to Assessing Synchroneity of Past Events using Bayesian Reconstructions of Sedimentation History. *Quaternary Science Reviews*, **27** (19-20):1872-1885.

Payn, W. H. (1948). Notes from Tunisia and Eastern Algeria: February 1943 to April 1944. *Ibis*, **90** (1):1-21.

Payne, R. B. (1987). Populations and Type Specimens of a Nomadic Bird: Comments on the North American Crossbills *Loxia pusilla* Gloger 1834 and *Crucirostra minor* Brehm 1845. *Occasional Papers of the Museum of Zoology University of Michigan*, **714**.

Pearson, R. G. & Dawson, T. P. (2003). Predicting the Impacts of Climate Change on the Distribution of Species: Are Bioclimate Envelope Models Useful? *Global Ecology and Biogeography*, **12** (5):361-371.

References

Pearson, R. G., Thuiller, W., Araújo, M. B., Martinez-Meyer, E., Brotons, L., McClean, C., Miles, L., Segurado, P., Dawson, T. P. & Lees, D. C. (2006). Model-Based Uncertainty in Species Range Prediction. *Journal of Biogeography*, **33** (10):1704-1711.

Peterson, A. T., Martínez-Meyer, E. & González-Salazar, C. (2004). Reconstructing the Pleistocene Geography of the Aphelocoma Jays (Corvidae). *Diversity and Distributions*, **10** (4):237-246.

Peterson, A. T. & Papeş, M. (2006). Potential Geographic Distribution of the Bugun Liocichla *Liocichla bugunorum*, a Poorly-Known Species from North-Eastern India. *Indian Birds*, **2** (6):148-151.

Petit, J. R., Jouzel, J., Raynaud, D., Barkov, N. I., Barnola, J.-M., Basile, I., Bender, M., Chappellaz, J., Davis, M., Delaygue, G., Delmotte, M., Kotlyakov, V. M., Legrand, M., Lipenkov, V. Y., Lorius, C., Pépin, L., Ritz, C., Saltzman, E. & Stievenard, M. (1999). Climate and Atmospheric History of the Past 420,000 Years from the Vostok Ice Core, Antarctica. *Nature*, **399** (6735): 429-436.

Petit, S., Chamberlain, D., Haysom, K., Pywell, R., Vickery, J., Warman, L., Allen, D. & Firbank, L. (2003). Knowledge-Based Models for Predicting Species Occurrence in Arable Conditions. *Ecography*, **26** (5):626-640.

Phillips, S. J., Anderson, R. P. & Schapire, R. E. (2006). Maximum Entropy Modeling of Species Geographic Distributions. *Ecological Modelling*, **190** (3-4):231-259.

Phillips, S. J., Miroslav, D. & Schapire, R. E. (2004). A Maximum Entropy Approach to Species Distribution Modeling. *Proceedings of the Twenty-First International Conference of Machine Learning*, **69**:655-662.

Phillips, S. J. & Schapire, R. E. (2005). Maxent Software for Species Habitat Modeling: http://www.cs.princeton.edu/~schapire/maxent/ Version: 3.3.3e. Last Accessed on 28/8/2011.

Piertney, S. B., Marquiss, M. & Summers, R. W. (1998). Characterization of Tetranucleotide Microsatellite Markers in the Scottish Crossbill (*Loxia scotica*). *Molecular Ecology*, **7**:1261-1263.

Piertney, S. B., Summers, R. & Marquiss, M. (2001). Microsatellite and Mitochondrial DNA Homogeneity Among Phenotypically Diverse Crossbill Taxa in the UK. *Proceedings of the Royal Society of London Series B-Biological Sciences*, **268** (1475):1511-1517.

Pope, V. D., Gallani, M. L., Rowntree, P. R. & Stratton, R. A. (2000). The Impact of New Physical Parametrizations in the Hadley Centre Climate Model: HadAM3. *Climate Dynamics*, **16** (2):123-146.

Prentice, I. C., Cramer, W., Harrison, S. P., Leemans, R., Monserud, R. A. & Solomon, A. M. (1992). Special Paper: A Global Biome Model Based on Plant Physiology and Dominance, Soil Properties and Climate. *Journal of Biogeography*, **19** (2):117-134.

References

Priestley, C. H. B. & Taylor, R. J. (1972). On the Assessment of Surface Heat Flux and Evaporation Using Large-Scale Parameters. *Monthly Weather Review*, **100**:81-92.

Pulliainen, E. (1972). Summer Nutrition of Crossbills (*Loxia pytyopsittacus*, *L. curvirostra* and *L. leucoptera*) in Northeastern Lapland in 1971. *Annales Zoologici Fennici*, **8**:326-329.

Questiau, S., Gielly, L., Clouet, M. & Taberlet, P. (1999). Phylogeographical Evidence of Gene Flow Among Common Crossbill (*Loxia curvirostra*, Aves, Fringillidae) Populations at the Continental Level. *Heredity*, **83** (2):196-205.

R Development Core Team (2011). R: A language and environment for statistical computing: http://www.R-project.org/. R Foundation for Statistical Computing. Last Accessed on.

Salotti, M., Bellot-Gourlet, L., Courtois, J. Y., Dubois, J. N., Louchart, A., Mourer-Chauviré, C., Oberlin, C., Pereira, E., Poupeau, G. & Tramponi, P. (2000). La Fin du Pléistocène Supérieur et le Début de l'Holocène en Corse: Apports Paléontologique et Archéologique du Site de Castiglione (Oletta, Haute-Corse). *Quarternaire*, **11** (3-4):219-230.

Schultz, C. B. & Howard, E. B. (1935). The Fauna of Burnet Cave, Guadalupe Mountains, New Mexico. *Proceedings of the Academy of Natural Sciences of Philadelphia*, **87**:273-298.

Segurado, P. & Araújo, M. B. (2004). An Evaluation of Methods for Modelling Species Distributions. *Journal of Biogeography*, **31** (10):1555-1568.

Seppä, H. & Bennett, K. D. (2003). Quaternary Pollen Analysis: Recent Progress in Palaeoecology and Palaeoclimatology. *Progress in Physical Geography*, **27** (4):548-579.

Seppä, H., Birks, H. J. B., Odland, A., Poska, A. & Veski, S. (2004). A Modern Pollen–Climate Calibration Set from Northern Europe: Developing and Testing a Tool for Palaeoclimatological Reconstructions. *Journal of Biogeography*, **31** (2):251-267.

Settele, J., Kudrna, O., Harpke, A., Kühn, I., van Swaay, C., Verovnik, R., Warren, M., Weimers, M., Hanspach, J., Hickler, T., Kühn, E., van Halder, I., Veling, K., Vliengenthat, A., Wynhoof, I. & Schweiger, O. (2008). "Climatic Risk Atlas of European Butterflies." Pensoft Publishers, Moscow.

Sharrock, J. T. R. (1976). "The Atlas of Breeding Birds in Britain and Ireland." T & A.D. Poyser, London.

Siepielski, A. M. & Benkman, C. W. (2004). Interactions among Moths, Crossbills, Squirrels, and Lodgepole Pine in a Geographic Selection Mosaic. *Evolution*, **58** (1):95-101.

Singarayer, J. S. & Valdes, P. J. (2010). High-Latitude Climate Sensitivity to Ice-Sheet Forcing over the Last 120 kyr. *Quaternary Science Reviews*, **29** (1-2):43-55.

References

Smith, B., Prentice, I. C. & Sykes, M. T. (2001). Representation of Vegetation Dynamics in the Modelling of Terrestrial Ecosystems: Comparing Two Contrasting Approaches within European Climate Space. *Global Ecology and Biogeography*, **10** (6):621-637.

Smith, J. W. & Benkman, C. W. (2007). A Coevolutionary Arms Race Causes Ecological Speciation in Crossbills. *The American naturalist*, **169** (4):455-465.

Smith, K. D. (1965). On the Birds of Morocco. *Ibis*, **107** (4):493-526.

Snowberg, L. K. & Benkman, C. W. (2007). The Role of Marker Traits in the Assortative Mating within Red Crossbills, *Loxia curvirostra* complex. *Journal of Evolutionary Biology*, **20** (5):1924-1932.

Soberón, J. (2007). Grinnellian and Eltonian Niches and Geographic Distributions of Species. *Ecology Letters*, **10** (12):1115-1123.

Soberón, J. & Peterson, A. T. (2005). Interpretation of Models of Fundamental Ecological Niches and Species' Distributional Areas. *Biodiversity Informatics*, **2**:1-10.

Stewart, J. R. (2002). "The Evidence for the Timing of Speciation of Modern Continental Birds and the Taxonomic Ambiguity of the Quaternary Fossil Record." *in* "Proceedings of the 5th Symposium of the Society of Avian Paleontology and Evolution." Zhou, Z. & Zhang, F., editors. Science Press, Beijing, China: 261-282.

Stewart, J. R. (2004). "The Use of Modern Geographical Ranges in the Identification of Archaeological Bird Remains." *in* "Feathers, grit and symbolism. Birds and humans in the ancient Old and New Worlds." Grupe, G. & Peters, J., editors. Verlag Marie Leidorf GmbH, Rahden/Westfalen, Documenta Archaeobiologiae 3: 43-54.

Stewart, J. R. (2008). The Progressive Effect of the Individualistic Response of Species to Quaternary Climate Change: An Analysis of British Mammalian Faunas. *Quaternary Science Reviews*, **27** (27-28):2499-2508.

Stewart, J. R. & Lister, A. M. (2001). Cryptic Northern Refugia and the Origins of the Modern Biota. *Trends in Ecology & Evolution*, **16** (11):608-613.

Stockwell, D. R. B. & Peters, D. (1999). The GARP Modelling System: Problems and Solutions to Automated Spatial Prediction *International Journal of Geographical Information Science*, **13** (2):143-158.

Summers, R. W. (2002). Parrot Crossbills Breeding in Abernethy Forest, Highland. *British Birds*, **95**:4-11.

Summers, R. W. (2004). An Early Record of a Parrot Crossbill in Scotland. *Scottish Ornithologists' Club*, **24**:43-45.

References

Summers, R. W. & Buckland, S. T. (2010). A First Survey of the Global Population Size and Distribution of the Scottish Crossbill *Loxia scotica*. Bird Conservation International.

Summers, R. W., Dawson, R. J. G. & Phillips, R. E. (2007). Assortative Mating and Patterns of Inheritance Indicate that the Three Crossbill Taxa in Scotland are Species. *Journal of Avian Biology*, **38** (2):153-162.

Summers, R. W., Dawson, R. J. G. & Proctor, R. (2010). Temporal Variation in Breeding and Cone Size Selection by Three Species of Crossbills *Loxia* spp. in a Native Scots Pinewood. *Journal of Avian Biology*, **41** (3):219-228.

Summers, R. W., Jardine, D. C., Marquiss, M. & Rae, R. (2002). The Distribution and Habitats of Crossbills *Loxia* spp. in Britain, with Special Reference to the Scottish Crossbill *Loxia scotica*. *Ibis*, **144** (3):393-410.

Swets, J. (1988). Measuring the Accuracy of Diagnostic Systems. *Science*, **240** (4857):1285-1293.

Tchernov, E. (1979). "Quaternary Fauna. In Horowitz." *in* "The Quaternary of Israel." New York: 259-290.

Thorn, J. S., Nijman, V., Smith, D. & Nekaris, K. A. I. (2009). Ecological Niche Modelling as a Technique for Assessing Threats and Setting Conservation Priorities for Asian Slow Lorises (Primates: Nycticebus). *Diversity and Distributions*, **15** (2):289-298.

Thuiller, W. (2003). BIOMOD - Optimizing Predictions of Species Distributions and Projecting Potential Future Shifts under Global Change. . *Global Change Biology*, **9** (10):1353-1362.

Thuiller, W., Lavorel, S., Araújo, M. B., Sykes, M. T. & Prentice, I. C. (2005a). Climate Change Threats to Plant Diversity in Europe. *Proceedings of the National Academy of Sciences of the United States of America*, **102** (23):8245-8250.

Thuiller, W., Lavorel, S., Araújo, M. B., Sykes, M. T. & Prentice, I. C. (2005b). Climate Change Threats to Plant Diversity in Europe. *Proceedings of the National Academy of Sciences of the United States of America*, **102** (23):8245-8250.

Tinner, W., Ammann, B. & Germann, P. (1996). Treeline Fluctuations Recorded for 12,500 Years by Soil Profiles, Pollen, and Plant Macrofossils in the Central Swiss Alps. *Arctic and Alpine Research*, **28** (2):131-147.

Tomek, T. & Bocheński, Z. (2005). Weichselian and Holocene Bird Remains from Komarowa Cave, Central Poland. *Acta Zoologica Cracoviensia*, **48** (1-2):43-65.

Tuhkanen, S. (1984). A circumboreal system of climatic-phytogeographical regions. *Acta Botanica Fennica*, **127**:1-50.

References

Tyrberg, T. (1991). Crossbill (Genus *Loxia*) Evolution in the West Palearctic - A Look at the Fossil Evidence. *Ornis Svecica*, **1**:3-10.

Tyrberg, T. (1998). "Pleistocene Birds of the Palearctic: A Catalogue." Publication of the Nuttall Ornithology Club No.7, Cambridge.

USGS (2006). Digital Representations of Tree Species Range Maps from "Atlas of United States Trees" by Elbert L. Little, Jr. (and other publications): http://esp.cr.usgs.gov/data/atlas/little. United States Geological Survey. Last Accessed on 28/8/2011.

Vilette, P. (1983). Avifaunes du Pléistocène Final et de l'Holocène dans le Sud de la Fance et en Catalogne. *Antacina*, **11**:1-190.

Vilette, P. (1993). La Paléoavifaune du Pléistocène Moyen de la Grotte du Lazaret. *Bulletin du Musée d' Anthropologie Préhistorique de Monaco*, **36**:15-29.

Voous, K. H. (1960). "Atlas of European Birds." Thomas Nelson And Sons, London.

Walker, M. J. C., Björck, J., Lowe, J. J., Cwynar, L. C., Johnsen, S., Knudsen, K.-L., Wohlfarth, B. & the INTIMATE group. (1999). Isotopic 'Events' in the GRIP Ice Core: A Stratotype for the Late Pleistocene. *Quaternary Science Reviews*, **18** (10-11):1143-1150.

Watson, A., Marquiss, M. & Summers, R. W. (2009). Brief Report: Abundance of Crossbills, Siskins and Cone-Crops. *Ornis Fennica*, **86**:38-40.

Weber, R. W. (1998). Pollen Identification. *Annals of Allergy, Asthma & Immunology*, **80** (2):141-148.

Wernham, C., Toms, M., Marchant, J., Clark, J. A., Siriwardena, G. M. & Baillie, S. (2002). "The Migration Atlas: Movements of the Birds of Britain and Ireland." T. & A.D. Poyser, London.

Williams, J. W., Shuman, B. N., Webb, T., Bartlein, P. J. & Leduc, P. L. (2004). Late-Quaternary Vegetation Dynamics in North America: Scaling from Taxa to Biomes. *Ecological Monographs*, **74** (2):309-334.

Williams, J. W., Webb, T., Richard, P. H. & Newby, P. (2000). Late Quaternary Biomes of Canada and the Eastern United States. *Journal of Biogeography*, **27** (3):585-607.

Wolf, A., Callaghan, T. & Larson, K. (2008). Future Changes in Vegetation and Ecosystem Function of the Barents Region. *Climatic Change*, **87** (1):51-73.

Wolfe, J. A. (1978). A Paleobotanical Interpretation of Tertiary Climates in the Northern Hemisphere. *American Scientist*, **66** (6):694-703.

Wood, S. N. (2000). Modelling and Smoothing Parameter Estimation with Multiple Quadratic Penalties. *Journal of the Royal Statistical Society (B)*, **62** (2):413-428.

References

Wood, S. N. (2001). mgcv: GAMs and Generalize Ridge Regression in R. *R News*, **1** (2):20-25.

Wood, S. N. (2003). Thin-Plate Regression Splines. *Journal of the Royal Statistical Society (B)*, **65** (1):95-114.

Wood, S. N. (2006). "Generalized Additive Models: An Introduction with R." Chapman and Hall/CRC.

Wood, S. N. (2011). Fast Stable Restricted Maximum Likelihood and Marginal Likelihood Estimation of Semiparametric Generalized Linear Models. *Journal of the Royal Statistical Society (B)*, **73** (1):3-36.

Wood, S. N. & Augustin, N. H. (2002). GAMs with Integrated Model Selection Using Penalized Regression Splines and Applications to Environmental Modelling. *Ecological Modelling*, **157** (2):157-177.

Zech, W., Glaser, B., Abramowski, U., Dittmar, C. & Kubik, P. W. (2003). Reconstruction of the Late Quaternary Glaciation of the Macha Khola Valley (Gorkha Himal, Nepal) Using Relative and Absolute (^{14}C, ^{10}Be, Dendrochronology) Dating Techniques. *Quaternary Science Reviews*, **22** (21-22):2253-2265.

Zhang, J., Bala, J. W., Hadjarian, A. & Han, B. (2010). "Ranking Cases with Classification Rules." *in* "Preference Learning." Fürnkranz, J. & Hüllermeier, E., editors. Springer, Heidelberg, Dordrecht, London, New York: 155-177.